# Integrated Catchment Rainwater Harvesting Model Using GIS –Machine Learning Technique for Agricultural Use Under Climate Change

**Ban Hikmat Qasim AL-Hasani**

A thesis submitted in partial fulfilment of the requirements of Liverpool John Moores University for the degree of Doctor of Philosophy

February 2025

# ACKNOWLEDGEMENT

PhD is a rewarding but challenging journey, which would not be possible without the help of many people.

First and foremost, I would like to express my sincere gratitude to my supervisors, Dr. Mawada Abdellatif, Dr. Iacopo Carnacina and Dr. Clare Harris for their continuous support, advice, and guidance throughout my candidature. They have built and directed an environment that granted me an opportunity to learn and practice research skills, meet and collaborate with brilliant researchers, and transfer the long PhD journey to a great and lovely experience.

Special thanks go to all the administrative team in the faculty, they offered me guidance and how to use the electronic system and eDoc. Besides, I would like to thank my friends and colleagues at Liverpool John Moores University. It has been such a pleasure and a privilege to work with you all.

I would like to thank my family. The soul of my father who encouraged me to love science and supported me in chasing my dreams and following his steps in the engineering field, has always been my best model and a great inspiration to follow. For my beloved mother for all her love and encouragement and for being by my side and for all her sacrifices and support.

Finally, I would like to extend my heartfelt thanks to my two wonderful brothers who always supported me and encouraged me to follow my dreams and follow their steps in the engineering field.

## ABSTRACT

The impact of global climate change on water resources is a growing concern globally therefore, the transition to the approach of water resources management and water sustainability technologies such as rainwater harvesting (RWH) presents a promising solution to mitigate water challenges. This study aims to introduce a comprehensive new methodology that leverages various technologies and data sources by integrating multiple models and two climate change scenarios to identify suitable sites for RWH and the impact on crop water requirements for the near and far future. Two locations have been studied, the first one located in a semi-arid region, Iraq and the second one located in a humid environment, the UK. The integrated mathematical models first consist of downscaling of rainfall, minimum, maximum temperatures and sunshine hours on a small scale and were developed based on historical data. Then future climate projections under two greenhouse emissions SSP2-4.5 (intermediate) and SSP5-8.5 (very high) were generated. The second step is using remote sensing (RS) and geographic information systems (GIS) to collect and process geospatial data that were incorporated into Analytical Hierarchy Process (AHP) as a decision-making tool to assess and rank potential RWH locations based on multiple criteria, helping to prioritize the most suitable sites. To account for evaporation loss from the harvested water an artificial neural network model has been developed using the historical climate variables mentioned above. For assessing the impact of RWH on selected crops (wheat, barley, and sunflower) the irrigation water requirements have been estimated using CROPWAT 8.0 software. The integrated model showed a good performance as evidenced by low probability for the downscaling of future variables (P values range from 0.745-1.0 and the assessment was a good to perfect fit for all climatic variables) and high correlation of $R^2$ 95.5% - 96.8% for evaporation models.

The integrated model has been investigated using projections from the downscaling model and applied to the harvested rainwater, evaporation, and crop water requirements. The future outputs from these models for the periods (2031-2050, 2051-2070, 2071, 2090, and 2091-2100) were compared to the baseline period (1980-2010) to identify the climate change impacts. Based on results, the suitable site selection for RWH was divided into very high suitability, high, medium, and low.

For Kirkuk, the two scenarios experience some reduction comparing to historical results in RWH suitability area by 34.42, 23.5, 50.5, and 7.7% under SSP2-4.5 &

37.5%, 23.9%, 27.19, and 6.5% under SSP5-8.5. The average evaporation rate was increased by 57.2% and 85.9% under SSP2-4.5, and SSP5-8.5 respectively. Due to the condition above less water becomes available to the crops and all crops require more water to avoid the wilting point. Wheat experienced steady increases in crop water requirements under both scenarios of 13-16% by the later periods. Barley showed a rise in the early periods, with up to 21% Sunflower had the most dramatic increases, reaching 29%. For Oxfordshire, the decrease in RWH suitability area ranges; very high suitability: 11.7%, high suitability:15%, moderate suitability:23% and low suitability around 25.4%. The average evaporation rate was increased by 38 - 70 % and crop water requirements for wheat increased by 8-19% across different periods, with the largest increase under SSP5-8.5. Barley: Showed moderate increases ranging from 5-17% under SSP2-4.5 and SSP5-8.5. Sunflower: had the largest crop water increase, especially under SSP5-8.5, with more than 22%. The research's findings have significant implications for sustainable water resource management in the Kirkuk and Oxfordshire study area. As climate change exacerbates water scarcity, identifying suitable RWH locations becomes crucial for ensuring water availability. This study suggests a novel method for evaluating rainwater harvesting (RWH) while taking the effects of climate change into account to solve these complicated concerns, strive toward enhanced management of water, and ensure water's future sustainability and forecasting future of rainwater patterns under the climate change scenario to avoid future water sacristy risks in the near and far future.

The approach incorporates the use of remote sensing (RS) and the integration of Geographic Information System (GIS) technology in cooperation with LARS WG to identify suitable RWH sites under climate change scenarios and to forecast future precipitation patterns in the study region to make a better decision regarding future water resources management and to maintain suitable sustainable resolutions regarding water security and helping the managers and engineers in the region to work towards enhancing water resources management and water sustainability and implementing new water policies within the rapid effect of climate change.

This method is affordable and convenient to address the water scarcity; by anticipating the suitable sites selection for current and future projection and it can help the water resources engineers, mangers local authorities for better planning to choose best decisions for managing water resources by choosing best suitable sites for RWH with the high suitability and avoiding the low suitability places and planning to build suitable RWH structures, like small damns, barriers and tanks.

## Declaration

No portion of the work referred to in the thesis has been submitted in support of an application for another degree or qualification of this or any other university or other institute of learning.

# TABLE OF CONTENTS

## LIST OF FIGURES

## LIST OF TABLES

## ABBREVIATIONS

| | |
|---|---|
| ASARs | Arid and semi-arid regions |
| RWH | Rainwater Harvesting |
| GIS | Geographic Information System |
| RS | Remote Sensing |
| ANN | Artificial Neural Network |
| ˚**C** | Centigrade |
| IMSD | Integrated mission for sustainable development |
| MCDA | Multi Criteria Decision Analysis |
| AHP | Analytical Hierarchy Process |
| FAO | Food and Agriculture Organization |
| | |
| DEM | Digital Elevation Model |
| USGS | Unites States Geological Survey |
| CN | Curve Number |
| S | Potential maximum retention |
| P | Precipitation |
| HSG | Hydrologic Soil Group |
| LCLU | Land cover/Land Use |
| USDA | United States Department of Agriculture |
| IDW | The Inverse distance weighting algorithm |
| ESRI | An international supplier of geographic information system software, web GIS and geodatabase management applications. |
| SCS -CN | Conservation Service Curve Number |
| NRCSCN | Natural Resources Conservation Services Curve Number |
| Ia | Initial abstraction |
| CRI | Consistency Ratio |
| CR | Random consistency index |
| CI | Consistency Index |
| λmax | The principal eigenvalue |

| | |
|---|---|
| ArcMap | Is the main component of Esri's ArcGIS suite of geospatial processing programs, and is used primarily to view, edit, create, and analyze geospatial data. |
| GCMs | General Circulation Models |
| IPCC | Intergovernmental Panel on Climate Change |
| K-S | Kolmogorov-Smirnov |
| LARSE-WG | Long Ashton Research Station Weather Generator |
| SVM | Support Vector Machine |
| CRW | Crop Water Requirements |
| NIWR | Net Irrigation Water Requirement |
| USGS | United States Geological Survey |
| MLP | Multi-Layer Perception |

# Chapter One: Introduction

## 1.1 Overview

A rising world population, rapid urbanization, land development, and climate change exacerbate the global challenge of providing ample fresh water. These factors contribute to unsustainable watershed management practices, often resulting in diminished downstream flows, particularly during drought periods. Consequently, the imperative for sustainable water resource management has become increasingly urgent.

Among the solutions gaining extensive acceptance is the development of rainwater harvesting systems. While progress has been slow thus far, momentum is expected to surge soon (Orsini et al., 2013; Fatima, 2023). Water resources in various regions worldwide are facing mounting stress due to escalating demand. Notably, areas like the Southeast, Midlands, and eastern parts of England and Wales are already grappling with increasing pressure on water supply (Knox et al., 2010).

Rainwater harvesting (RWH) emerges as a multifaceted solution in various regions, mitigating drought risk, pollution, and sewer flooding. This versatile approach is increasingly garnering attention in the UK (Campisano et al., 2017). Water resources in many areas of the UK are strained due to rising demand. For example, the southeast and east of England are already experiencing growing pressure on their renewable water supplies. In certain regions, relying on this type of supply might become necessary to supplement demand management efforts and ensure long-term water security. Elsewhere, rainwater harvesting (RWH) can help mitigate drought risk and prevent sewer flooding (Fritish, 2017). Consequently, RWH is gaining more attention in the UK. The primary uses are for plant irrigation (such as gardening) and domestic purposes which can help reduce mains water consumption (Ward, 2010). In the UK, a significant amount of water is extracted from the environment for human consumption. The water demand is increasing due to population growth, evolving lifestyles, and the escalating effects of climate change (Mahmoud and Tang, 2015).

Several regions in the world have been facing changes in precipitation, increasing temperature, and severe drought, specifically in the Mideast part and less developed countries. Arid and semi-arid regions (ASARs) sprawl over 50 million km², encompassing 40% of the Earth's surface (Mekdaschi Studer and Liniger, 2013). There is evidence of climate change, and it has already been observed in many parts of the world (Shahid, 2012). These areas grapple with scarce, erratic rainfall patterns (Ibrhim et al., 2019).

The Middle East experience notably high aridity indices, with annual rainfall as low as 150-350 mm (Ouessar, 2007). Rainfall variability ranges from 350 to 700 mm annually in these regions, where a significant portion of the population relies on rain-fed agriculture and pastoralism for sustenance (Oweis and Hachum, 2006). Due to the dry and semi-arid conditions, the Mid-east is considered one of the regions most affected by global climate change, and water shortages would come from a significant rise in temperature and a decrease in precipitation according to Hassan and Niel, (2021). Iraq is considered one of the most vulnerable countries to a global warming and climate change. The country will be altered by severe environmental issues such as a decline in the amount of accessible water, and increasing the amount of population and due to hydrological projects in neighboring counties, climate change and bad water management inside Iraq will lead to more demand on water resources as well as an increase in temperature that can harm the ecosystem and even worsen the situation (Hassan and Niel, 2021). Food production and security in numerous developing nations, exemplified by Iraq, face persistent constraints stemming from various factors, including the availability of natural resources such as soil and water, climatic variability, and socioeconomic conditions. Climate change exacerbates these limitations, further straining agricultural systems and livelihoods. Addressing the looming challenges to food security necessitates proactive measures centered around innovative technologies and sustainable practices. Embracing such advancements becomes imperative to enhance agricultural resilience and adaptability. As highlighted by Cosgrove and Loucks (2015), advancing agricultural sustainability is paramount to bolstering the capacity and resilience of farming systems in the face of evolving environmental and socioeconomic dynamics.

## 1.2 Research prespective

In the new global development and within the constantly increasing population, freshwater sacristy has become a fundamental issue for sustainability development and as the expectation of water withdrawal is growing by 10- 12 % every 10 years to reach about

5, 240 $Km^3$ and water consumption will keep increasing by 2025 (UNESCO, 2008). Population growth has a direct influence on the water supply demand rates, for example, worldwide water demand increased six folds between 1990 and 1995 while the population only doubled, and the demand of the agricultural sector is almost 70% of the total demand and the rate of the growth in the urban area is about four times that of the rural areas (Cosgrove & Rijsberman, 2014).

Water scarcity is a major constraint that substantially impacts many areas, including established economies, developing countries, and the most underprivileged populations. It also significantly affects agriculture (Wu et al., 2018). One of the most important issues facing humanity in the twenty-first century is the availability of food (Hasan et al., 2020).

Around the globe, agricultural ecosystems are the primary producers of food as well as the primary users of water resources (Damkjaer and Taylor, 2017). Depending on the region's economic growth and climate, these ecosystems can utilize anywhere from 60 to 90 percent of the water that is available (Anzar et al, 2019). An annual growth rate of 1.3% is projected for the 275 million hectares of land worldwide devoted to irrigated agriculture. Although this makes up only 23% of the cultivated land, these kinds of crops provide 45% of the world's food production (Kopittkeet al, 2019).

Moreover, there is no denying the existence of climate change; experts predict that worldwide temperatures could rise by as much as 5 degrees Celsius in the following decades (Hoegh et al., 2018). Substantial climate occurrences, such as rising temperatures, droughts, floods, and other extreme weather events, serve as indicators of climate change. These advancements and modifications, especially in underprivileged areas, have led to water scarcity and a decline in agricultural production (Aznar et al., 2019). However, as climate change affects water supplies, rainwater harvesting (RWH), is becoming more and more significant. The main

requirements for RWH are a catchment area and a storage tank or reservoir. Uncertainty in rainfall both in frequency and quantity will affect groundwater recharge, raising the risk of floods and droughts and ultimately affecting groundwater levels in various locations. Decreased precipitation may limit net recharge and cause groundwater levels to drop. Overuse of subterranean aquifers is depleting water reserves that have built up over decades or even centuries. Our ecosystems will be impacted by population growth as a result of rising service needs, such as dependable and clean water (Mahmoud and Tang, 2015). A significant amount of water is extracted from the environment for human use. The growing population, shifting lifestyles, and growing significance of the effects of climate change are all contributing factors to the rising demand for water. For instant, in the UK There is less water in the southeast of England than in any other region of the country (Ward, 2010). The UK receives between 550 and 3,000 mm of rainfall a year, with the least-populated areas in the north and west of the nation receiving the most rainfall. Fewkes (2012) showed that the highest population areas have a precipitation density ranging from 600–800 mm annually. Moreover, there is regional variation in the UK's water consumption, with the places with the highest needs also having the lowest water availability. Rising sewage and water costs have contributed to the rise in RWH cases in recent years. Even though RWH has lately been utilized in well-known locations like the London Olympic Park Velodrome, the UK's continuous resurrection has trailed behind other nations like Germany, which is now the global leader in modern RWH. Germany is at the forefront of research and implementation of Rainwater Harvesting (RWH) systems. The idea of utilizing rainwater emerged between 1970 and 1975, driven by the need to address challenges related to water supply and sewage management (Fewkes 2012). During the 1980s, the focus shifted towards low-impact development technologies (García Soler et al. 2018), paving the way for more sustainable water management solutions. By the 1990s, the concept of integrating multiple decentralized rainwater management techniques had gained traction, becoming a fundamental component of Germany’s integrated stormwater management strategy (DWA 2016). According to German water law, rainwater must be retained on-site whenever feasible (Fletcher et al. 2015).

The widespread adoption of RWH systems in Germany is largely due to economic incentives. Urban drainage fees are determined by the amount of impermeable surface on a property, making it financially advantageous to disconnect roofs from the sewage

system (Herrmann and Schmida 2000). Approximately 75,000 RWH systems are installed annually, with two-thirds of newly constructed homes incorporating them. Property owners are only required to notify water supply companies of the installation, with no need for additional authorization.

Several regions in Germany provide financial support for RWH installations. In Bremen, subsidies cover up to one-third of the installation cost for residential systems. Thuringia offers loans of up to EUR 5,000 for residential property owners, while Saarland and Schleswig-Holstein also provide financial incentives for RWH installations (Schuetze 2013). Only 400 RWH systems are currently deployed annually in the UK. The United Kingdom authorities are currently advocating RWH under the sustainable home code.

Arid and semi-arid regions are areas where the amount, distribution, and/or unpredictability of rainfall is a problem (Ibrahim et al., 2019). The aridity index in some regions is quite high as they receive about 150-350 mm of rain per year (Ouessar, 2007), and the rain fall in these regions is also little, varying from 350 to 700 mm per year and the majority of the population in Arid and Semi-Arids ASARs depends on rain-fed agriculture and pastoralism for subsistence (Oweis et al., 2006). Global climate change presents an unprecedented challenge, as it disrupts annual precipitation patterns and contributes to escalating temperatures, exacerbating the overarching issue of global warming (Parchari et al., 2014). Regions such as the Middle East and less developed nations are particularly vulnerable due to shifting precipitation patterns, rising temperatures, and prolonged droughts. These unmistakable changes emphasize the urgency of addressing climate change (Shahid, 2012). Iraq, in particular, is highly vulnerable to climate change and global warming, grappling with multiple environmental challenges, including dwindling water supplies from lakes and rivers, a growing population, and escalating temperatures that further stress water resources and the local ecosystem (Hassan and Niel, 2021). Given these substantial challenges, rainwater harvesting (RWH) has gained prominence, particularly in water-constrained regions like semi-arid areas. RWH serves as a powerful strategy to enhance water accessibility and availability, addressing both domestic and agricultural needs (Abdulla et al., 2021). Rainfall is the central and critical variable in Rainwater Harvesting Systems (RWHS) and intensive rainfall in short duration of time as well as shift of rainfall season effects agriculture. with its temporal variability significantly influencing its efficiency (Silva et al., 2015). Numerous researchers have conducted

studies on suitable site selection for RWH, examining regions such as Dohuk Governate, Iraq (Ibrahim et al., 2019), semi-arid areas in India (Garg et al., 2022), the West Bank of Palestine (Shadeed et al., 2020), Pakistan (Khan et al., 2022), and Diyala province, Iraq (Nabit, Al-Anbari, and Alwan, 2023). These studies predominantly rely on historical climate data from the study locations for the analysis of suitable site selection for RWH. Melville-Shreeve et al, (2016) conducted a study regarding RWH in the UK but their research was limited to domestic use. Mahmoud and Tang (2015) focus in their research on locating RWH site selection in some parts of the UK but without considering the climate change effect and agricultural use. However, many of these studies focused primarily on identifying potentially suitable sites for RWH systems and structures, without specifically considering RWH for agricultural use, for both humid and semi-arid regions that face water poverty and scarcity.

As a result, further research is needed to identify suitable RWH locations for agricultural use under the impact of climate change scenarios. To address this research gap, an integrated methodology that combines GIS, RS, machine learning, and climate change techniques will be developed and applied in the UK and Iraq, a semi-arid country in the Middle East. The goal is to enhance water resources management and establish new policies for identifying suitable RWH sites under the impact of climate change.

Furthermore, the United Nation (UN) created in 2019 Sustainable Development Goals (SDGs) that aim to transform our world and ensure that all people enjoy health, justice, and prosperity by 2030. This involves targeting the most vulnerable, increasing basic resources and services, and supporting communities affected by conflict and climate-related disasters. The current study is working to achieve SDG 2 (aims to end hunger, achieve food security, and promote sustainable agriculture) and SDG 13 (Climate change exacerbates water scarcity and impacts agricultural productivity, especially in vulnerable regions. SDG 13 focuses on strengthening resilience and adaptive capacity to climate-related disasters and promotes climate-resilient water management strategies and agricultural systems to reduce vulnerabilities to climate impacts, such as droughts, floods, and unpredictable rainfall. Also, it encourages countries to integrate climate change measures into national policies, including water management and agricultural practices.

## 1.3 Aim and objectives of the research

The primary aim of this study is to identify and select optimal sites for rainwater harvesting (RWH), considering the impacts of climate change to address these complex challenges, improve water management, and ensure long-term water sustainability for sustainable agriculture in both semi-arid and humid regions. The approach integrates remote sensing (RS) with Geographic Information System (GIS) technology to identify suitable RWH locations. It also employs statistically downscaled models using the LARS WG stochastic weather generator to project future precipitation patterns, which are then combined with evaporation models to refine the final selection of RWH sites. The method proved effective in pinpointing ideal locations for RWH in both regions, offering valuable insights for water resource engineers and managers. These findings enable more cost-efficient planning and management of water resources for agriculture under climate change, while aiding in the selection of optimal locations for small barriers, ponds, or dams. Additionally, this approach can guide policymaking and the development of improved water management legislation for the future. The specific objectives for realizing the aim of the thesis as stated above are:

1. Identifying and selecting potentially suitable sites for RWH using GIS techniques based on current and future climate projections for two contrasting environments (Iraq as a semi-arid and the UK as a wet environment).
2. Develop a statically downscaling projection model for different climate variables e.g. (Min. and Max. temperature, rainfall, and sunshine hours) for appropriate climate change scenarios for near and far future.
3. To develop a rainfall-runoff model to estimate the overland flow incorporating the mentioned climate variables.

4. To predict the amount of evaporation losses from the RWH reservoir surface by using machine-learning technique and estimating the amount of net harvested water.
5. To provide an estimation of the irrigation water requirement for different crops and link it with the three developed models to create a decision support system for irrigation management.
6. To conduct uncertainty assessment by using different global climate change models and test the integrated models in the two studied regions.

### 1.4 Contribution to knowledge and research novelty

After conducting a preliminary literature review, it became apparent that there were not enough studies on integrated models of rainwater harvesting systems under climate change applied to the agricultural sector. Most of the studies conducted were focused on identifying the suitable sites of rainwater catchment areas in a specific region and there is a notable knowledge gap in implementing the idea of integrated models such as rainfall-runoff, evaporation, RWH, climate change projections, and different crops.

Therefore, the following three points explain the novelty of the proposed research:

1. Use of GIS to determine optimum RWH sites based on the current and future climates, as the existing methods use current climate only.
2. Integration of different models of GIS-hydrological model, evaporation, climate change, and optimizing different crops and areas using harvested water.
3. Investigate the ability to use Artificial Neural Network, a modified model to forecast and estimate the potential evaporation from RWH in two regions (Iraq semi-arid, and the UK as a wet environment) under climate change scenarios.

### 1.5 Thesis Organisation:

The overview, aim, objectives and novelty of the study have been discussed in the previous sections. The thesis chapters are organized as follows:

**Chapter 1**: This chapter includes, overview, research perspective, aims, contribution and thesis organization.

**Chapter 2:** The literature review presents different studies regarding rainwater harvesting systems and integrated modeling approaches of various models. This includes GIS models, rainfall-runoff, evaporation models, and crop water requirements models, and an overview of studies on climate change projections and their implications for water resources.

**Chapter 3:** This chapter focuses on the study areas, which offer essential issues regarding the location of the city, its weather, water resources, and climate for two different study areas. In addition, the chapter presents the data pre-processing technique that helps to prepare the data set before employing it in the integrated models.

**Chapter 4:** This chapter presents the steps for conducting the research methodology that includes the process and approaches that are used to simulate future climate factors under different scenarios, developing the integrated RWH models, rainfall-runoff models, and the estimation of evaporation and crop water requirements models.

**Chapter 5:** This chapter presents results and discussion, which show the development and validation of the proposed frameworks divided into four sections. 1) The calibration and validation of the downscaling model and the simulation of future climate variables and projections. 2)The suitability site selection of RWH by using GIS techniques. 3) The development of evaporation models. 4) The estimation of crop water requirements under the impact of climate change. This chapter also discusses the outcome of the results from the different experimental scenarios.

**Chapter 6:** The thesis conclusion contains the attained research aim and the contribution to fill the gap in this research field regarding the identifying suitable site selection of RWH for agriculture use considering climate change in two different regions. Moreover, this chapter shows the limitations that are found in this research and the essential recommendations for future work that should be considered to overcome these limitations.

**Appendices**: Detailed appendices that contain copies of additional figures and tables concerning this study are displayed at the end of the thesis. The organization of the thesis chapters is in Figure 1.1.

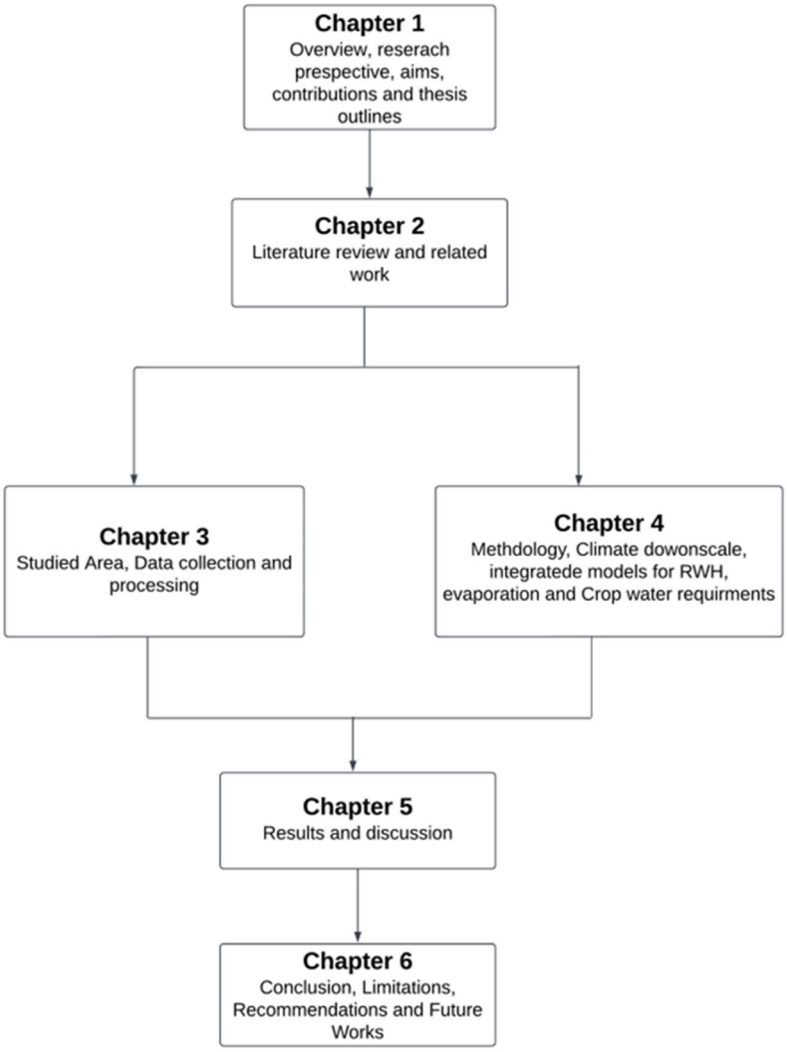


**Figure 1.1** The thesis organization

# Chapter Two: Literature Review

## 2.1 Introduction

This chapter highlights the importance of conducting a comprehensive literature review to understand the key principles, techniques, tools, and methods underpinning the proposed project's reliability and success. The project's primary goal is to identify potential sites suitable for rainwater harvesting (RWH) by integrating multiple models and leveraging advanced technologies. The methodologies employed include Geographic Information Systems (GIS), Remote Sensing (RS) data, and Artificial Neural Networks (ANN) to estimate critical factors such as evaporation and crop water requirements. The CROPWAT 8.0 model will be used for this purpose, applied in two contrasting regions: one being a semi-arid area and the other a humid region, both of which are affected by climate change across various greenhouse gas emission scenarios. The focus is on agricultural applications under these changing conditions.

## 2.2 Arid and Semi-Arid Regions: Iraq as a Case Study

Iraq, located in the Middle East, covers over 430,000 km² and had a population exceeding 36 million as of 2015. The country experiences an arid climate, with average annual precipitation ranging from ≤ 100 mm in the southeast to ≥ 400 mm in the northeast (Al-Obaidy et al, 2013). Until the 1970s, Iraq was considered to have rich water resources due to the Tigris and Euphrates Rivers. However, the impact of rainwater harvesting (RWH) on domestic use, agricultural production, and small settlements has always been limited. Most of the country's catchments lack efficient management tools or procedures for water harvesting. Human settlements and agricultural activities in Iraq have historically been concentrated in the Mesopotamian plain, where freshwater from the Tigris and Euphrates Rivers is accessible and can be used to irrigate flat areas with fertile and deep soil. RWH has primarily been used to secure drinking water for inhabitants and travellers in some remote areas (Al-Amri, 2021).

A few RWH systems are used in Iraq, including the ancient Kahariz technique, which is still in operation. Originating between 1300 and 600 BC, the Kahariz system is widespread in northern Iraq and can increase groundwater without the use of a pump. The faydah system is another type of RWH that can be applied in flat wadi areas where water collects. A faydah is particularly effective in collecting floodwater, especially if the site is improved by excavation (Al-Amri, 2021). The construction of dams in the upper reaches of the Tigris and Euphrates Rivers and their tributaries in Iran, Syria and Turkey has caused significant decreases in the flows of these rivers (Al-Ansari et al., 2021). Ersoy (2023) reported that the discharge from these two rivers would continue to decrease over time, potentially leading to complete drying by 2040. The amount of water available per person per year decreased from 5900 to 2400 $m^3$ between 1977 and 2009 (Giovanis and Ozdamar2024). Mismanagement of water resources and the effects of climate change are additional factors contributing to water shortages in Iraq. The ongoing water crisis has directly led to rising levels of food deprivation, displacement, and poverty in the country (Al-Ansari et al., 2023). Figure 2.1 illustrates the spatial distribution of the seasonal climatical water availability in Iraq (source: Salman et al., 2020).

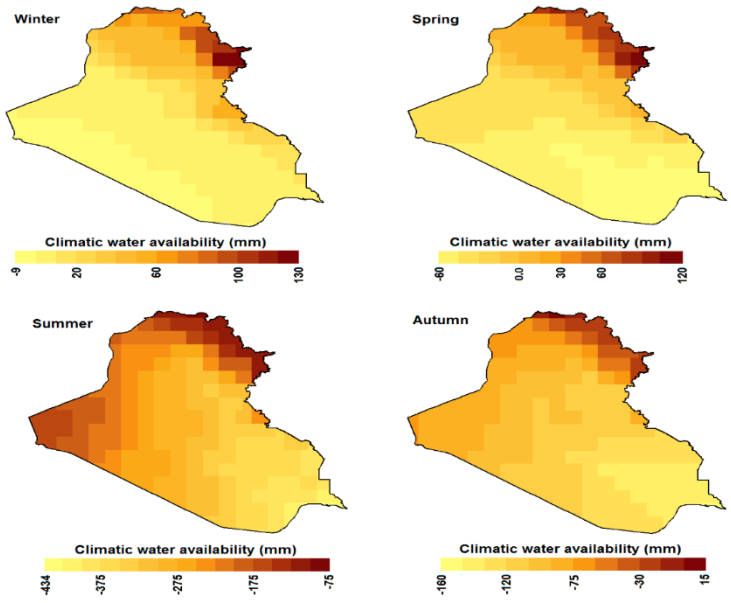


**Figure 2.1** Spatial Distribution for Seasonal Climatically Water Availability in Iraq (source: Salman et al, 2020).

## 2.3 The humid regions: The UK as a case study:

As shown (Fig. 2.2), the United Kingdom is in the mid-latitudes between 49°N and 60°N, on the western seaboard of Eurasia, the world's largest landmass. This geographical position facilitates the convergence of moist maritime and dry continental air. The wettest areas in the country are the mountainous regions of Wales, Scotland, the Pennines in Northern England, and the moors of Southwest England. In some of these locations, annual rainfall can reach up to 2,500 mm, making them some of the wettest places in Europe (Met Office UK, 2024). The wettest spot in the UK is Crib Goch in Snowdonia, which has averaged 3,000 mm of rain per year over the past 30 years. In contrast, the drier and densely populated parts of the UK receive significantly less rainfall. including the southeast of England, have an annual average of 550 mm.

Despite the amount of annual rainwater, the UK water sector faces increasing demand due to significant development and population growth. The UK population is projected to rise by approximately 10% over the next 25 years, driven by net migration and natural growth (Ward, 2010). For years, the water sector has employed a ‘twin track’ approach to water resources management, incorporating both demand management and resource development to achieve sustainable water management (SWM) (Ward, 2013). Following the implementation of the Water Framework Directive (WFD) in 2001, the Environment Agency (EA) in England and Wales introduced Catchment Abstraction Management Strategies (CAMS) to promote SWM and meet WFD objectives. Figures 2.2 illustrate the water consumption and demands in the UK (Kellagher and Maneiro Franco, 2005).

In the UK, three main sectors demand water resources: agricultural, industrial, and domestic. Agricultural water use is primarily for spray irrigation, which returns minimal water to the hydrological system due to evaporation and incorporation into crops (Kellagher and Maneiro Franco, 2005). Industrial users, typically metered, have an incentive to implement water-efficient processes to reduce overhead costs (Ward, 2010). However, the UK domestic sector is unique. Unlike many other countries, domestic water use is not widely metered and operates on a rateable value arrangement based on dwelling size. This system allows households to use unlimited water for a fixed charge to the water service provider (WSP) unless a meter is installed.

Consequently, without meters, there is no financial incentive for households to conserve water (Ward, 2010).

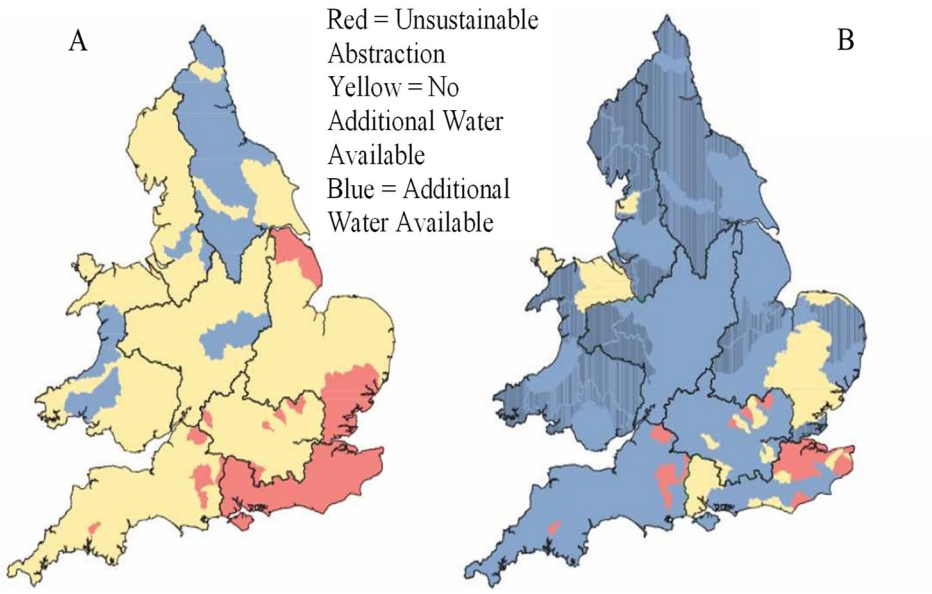


**Figure 2.2** Water Consumption and demand in England and Wales, Summer (A) and Winter (B)

## 2.4 Classifications of RWH

The classification of Rainwater Harvesting (RWH) techniques varies across regions, lacking standardized terminology at both regional and international levels, leading to different names for the same processes (Moges, 2009). Oweis (2004) defines RWH as the concentration of rainwater runoff into smaller target areas for beneficial use, while Kahinda et al. (2008) describe it as "The collection, storage, and use of rainwater for small-scale productive purposes." According to the Conservation World Overview of Approaches and Technologies database, RWH is characterized as "The collection and management of flood water or rainwater runoff to increase water availability for domestic and agricultural use as well as ecosystem sustenance" (Mekdaschi Studer and Liniger, 2013).

The primary objective of RWH typically revolves around augmenting accessible water by capturing rainwater for local consumption or redistribution to other areas. This approach not only reduces water loss but also enhances water resources within watersheds (Isioye et al., 2012)

### 2.4.1 Definition and Components of Rainwater Harvesting System

The water harvesting system term is the process of collecting and storing water from the area that has been treated to increase the precipitation runoff. A rainwater harvesting system is defined as the complete facility for collecting storing and treating system of precipitation runoff (Fernandes et al. 2015).

The following fundamental process diagram shows the rainwater harvesting system's components as demonstrated in Figure 2.3.

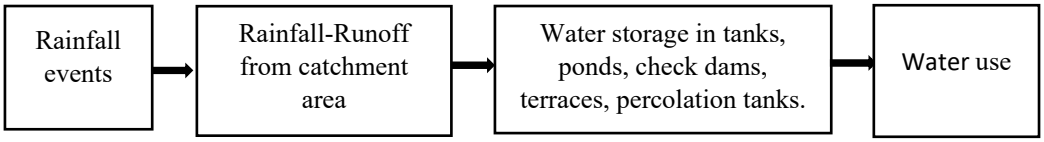


**Figure 2.3** Flow chart demonstrates fundamental rainwater harvesting system. (Modified from Dobrowsky et al. 2014)

According to Oweis (2004), rainwater harvesting systems consist of the following components:

1. Abatement Area: This is the runoff area where rainwater is harvested. It can include agricultural land, rocky surfaces, paved roads, or rooftops. The size of this catchment area can range from a few square meters to several square kilometers.

2. Storage Facility: This component refers to the area where harvested runoff water is stored until it is utilized. Storage facilities can include tanks, cisterns, reservoirs, or ponds, depending on the scale and purpose of the rainwater harvesting system.

3. Endpoint: This is the destination where the harvested water is used, either for domestic purposes such as drinking, cooking, or sanitation, or for agricultural purposes like crop irrigation and livestock watering.

These components collectively enable rainwater harvesting systems to capture, store, and utilize rainwater efficiently, contributing to water conservation and sustainable water management practices. Rainwater harvesting (RWH) is essential due to limited precipitation and unpredictable rain distribution.

This technique is employed to supplement water supply where rainfall alone cannot meet all water demands. The most common types of RWH structures include tanks (over-ground or underground tanks, ponds, check dams, terracing, percolation tanks, recharge aquifer and nala bunds).The Following points describe the multiple types of rainwater harvesting systems.

**Tanks: there are three calsssifications of Rainwater Harvesting Tanks:**

- Above-Ground Tanks: These are easy to install and maintain. Common materials include plastic, fiberglass, and metal.
- Underground Tanks: These save space and are protected from temperature fluctuations and UV light. They are typically made of concrete, plastic, or fiberglass.
- Modular Tanks: These can be configured to fit specific spaces and are often used in urban environments where space is limited.

The Following Figure 2.4 shows the schematic diagram of rainwater harvesting tanks for domestic use.

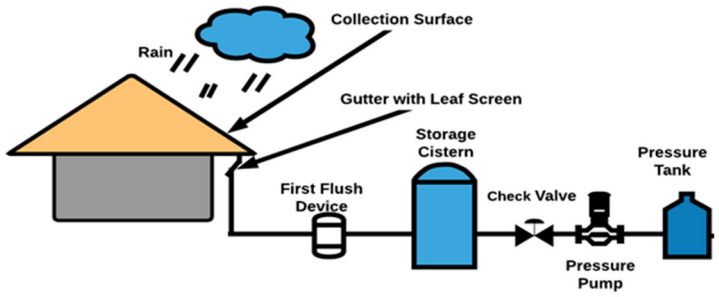


**Figure2.4** Schematic Diagram of Rainwater Harvesting System for Domestic Purposes (Modified from Hanson & Vogel, 2014)

**Ponds:** are among the most reliable and economical sources of water in arid and semi-arid regions. People in many parts of Jordan have utilized them for centuries. The harvested water from ponds serves various purposes:

- Irrigation (either fully or as a supplement)
- Domestic use
- Watering livestock
- Erosion control
- Stabilizing water channels

Farm ponds are suitable for water harvesting in farms and for agricultural use (Al-Adamat, 2008). These ponds are typically constructed on the higher parts of farms

to capture and store runoff rainwater. This is achieved by building an embankment across a watercourse, excavating a pit, or combining both methods (Oweis et al., 2012). Figure 2.5 illustrates the setup of farm ponds for RWH.

**Figure 2.5** Farm Pounds' source: (Al-Adamat.2008)

**Check dams**: are small dams built across water courses in narrow wadis with mild slopes. They are feasible in both hard-rock and alluvial formations (Arunima et al., 2015). While check dams are relatively inexpensive to construct, the availability of suitable sites is usually limited. Despite this, they are a very popular type of RWH. Check dams are particularly valuable not only for harvesting water but also for controlling soil erosion (Arunima et al., 2015). Figure 2.6 depicts the structure and setup of check dams.

**Figure 2.6** Check Dams' source: (Arunima et al., 2015)

**Terraces: s**erve as systems for both soil and water conservation. Constructed on steep slopes, terraces are formed by small retaining walls. Various terracing systems are practiced in Arabic regions, including weir terraces across narrow wadis, barrage terraces, linear dry-field terraces, and stair terraces (Ammar, 2017).

**Percolation tanks**: are artificially created surface water bodies designed to submerge land areas with adequate permeability, facilitating the percolation of impounded surface runoff to recharge groundwater. These multipurpose conservation structures store water for livestock and aid in groundwater recharge, depending on their location and size. Percolation tanks can be located across small streams by constructing low elevation check dams or on uncultivated land adjoining streams through excavation and connecting the tank to the stream with a delivery canal (Ammar, 2017).

**Nala bunds**: are embankments constructed across larger, second-order streams in areas with gentle slopes, functioning similarly to mini percolation tanks (Ammar, 2017). Figure 2.7 illustrates the structure of a percolation tank.

**Figure 2.7** Percolation Tank source: (Ammar, 2017)

### 2.4.2 Hydrological models for RWH

In addition to field measurements, the effects of Rainwater Harvesting (RWH) systems can be evaluated by modeling their hydrological characteristics (Darabi et al., 2007). Fewkes (2000) emphasized the need for a hydrological model to analyze RWH facilities. This hydrological analysis is akin to a long-term rainfall-runoff study within a watershed, assessing various components of hydrological circulation, such as

precipitation, evapotranspiration, infiltration, percolation, groundwater, and surface runoff (Jung et al., 2019). Several detailed models capable of simulating RWH system design and performance have been developed and published (Ward et al., 2010). For instance, Saha et al. (2021) utilized hydrological process to identify potential RWH locations in West Bengal, India. Similarly, Shadeed et al. (2020) employed the hydrological approach in combination with GIS and RS techniques to assess the suitability of sites for RWH in Palestine, specifically the West Bank. Aghaloo and Chiu (2020) utilized GIS, RS, and hydrological model to identify suitable site selection for RWH in Iran as a semi-arid region. Lupia et al., (2017) studied RWH for potential food production in Rome, Italy. While Preeti et al., (2022) utilized RS and hydrological model to identify suitable RWH site selection in Great |Western Sydney, Australia.

Dixon (2000) developed the Deterministic Rainfall-Runoff Hydrological Model (DRHM), a comprehensive mass-balance model incorporating stochastic elements to profile demand, thereby simulating the quantity, quality, and cost aspects of RWH systems. Vaes and Berlamont (2001) introduced the Rewaput model, a reservoir model that accounts for relationships among rainfall intensity, duration, and frequency using a triangular distribution to approximate the stochastic variability of storage volume and water consumption within a catchment.

Fewkes (2004) significantly advanced the field with the Rainwater Collection System Model (RCSM) model, providing a detailed analysis of time-interval variations and yield scenarios before and after spillage events in RWH systems. Kim et al, (2018) developed the RSR model, which was successfully applied in Korea. This model optimizes RWH system tank sizes to effectively manage stormwater and mitigate flooding risks. Additionally, Roebuck and Ashley (2008) created Rain Cycle, an Excel-based balance model incorporating a yield-after-spill algorithm and a comprehensive life cycle costing approach.

Mahmoud and Tang (2015) utilized GIS to identify RWH in the UK but in general process. On the other hand, Ward et al., (2013) developed a model for RWH for user's perception inside the UK. Numerous researchers have conducted studies on suitable site selection for RWH, examining regions such as Dohuk Governate, Iraq (Ibrahim et al., 2019), semi-arid areas in India (Garg et al., 2022), the West Bank of Palestine

(Sameer, Tariq, and Michel, 2020), Pakistan (Khan et al., 2022), and Diyala province, Iraq (Nabit, Al-Anbari, and Alwan, 2023).The digital revolution has spurred rapid advancements in hydrological modeling, introducing numerous improvements and the development of physically based watershed models, such as rainfall-runoff modeling systems. The Soil Conservation Service (SCS) method is widely utilized for estimating surface runoff in small catchments following precipitation events (Melenti et al., 2011). This method evaluates the relationship between land cover and hydrological soil group, collectively determining the Curve Number (*CN*) (Melenti et al., 2011). Many hydrological models incorporate the SCS-*CN* method to estimate storm runoff, including models like TOPMODEL and SWAT (Soil and Water Assessment Tool) (Ammar et al., 2016).

### 2.5 Criteria and techniques used for suitable RWH site selection.

The suitable selection of RWH sites depends on many criteria (Mahmoud & Alazba, 2015). There are two main criteria for identifying and selecting a suitable site, these are biophysical and socio-economic criteria. Since the early nineties of the last century, many studies focused on biophysical criteria that include, rainfall, soil texture, slope, drainages, land use, and land cover while many studies after the year 2000 have tried to make an integration between both biophysical and socio-economic criteria (Yalew et al., 2018). The Food and Agriculture Organization of the United Nations (FAO) has itemized six key criteria for selecting RWH sites as cited by Khudhair, Sayal, and Darama (2020), these are hydrology, topography, climate, soils, agronomy, and socio-economic. Table 2.1 shows the most common techniques and criteria that have been used to identify suitable selection sites for RWH. The most common methods that have been developed and used, ponds and pans, check dams, terracing, and percolation tanks are mentioned in Table 2.1.

It also lists the most common biophysical criteria that have been applied in planning and implementing these techniques (based on this review). For example, all five techniques are suitable in areas with rainfalls of 200-1000 mm per year, ponds are suitable for small flat areas with slopes less than 5%, percolation tanks and bunds are suitable on moderate slopes of 5-10% and terracing is suitable for steeper slopes of 5-30%.

The most suitable soil type, land use/cover, and catchment size for each RWH technique are also summarized in table 2.1. There are three commonly prescribed sets of criteria and guidelines for the selection of suitable sites for RWH. The first set was proposed by the integrated mission for sustainable development (IMSD, 1995) and included only biophysical criteria. The second set was proposed by Oweis (1998), who first included socioeconomic criteria. The third set was developed by the FAO (2003) and included more criteria in both domains. Most publications since 2000 followed or were derived from one of these sets of guidelines.

**Table 2.1** The most common techniques and criteria that have been used in the selection for RWH.

| RWH techniques | Rainfall (mm) | Slope (%) | Type of Soil | Land Cover/Use | Catchment Area (ha) | References, year and country |
|---|---|---|---|---|---|---|
| Check dams | <1000 | <15 | loam clay Sandy | Barren, shrub, and scrubland | N/A | Al-Daghastani (2010), Iraq Ziadat et al, (2012). Jordan Hameed (2013), Iraq |
| Ponds and pans | >200 | <5 | Clay loam sandy. and silty loam | Moderately cultivated, Shrub-land | < 2 | Al- Adamat et al, (2008) Al-Adamat et al, (2010) Jordan |
| Percolation tanks | <1000 | 5-10 | Clay loam and silt | Barren or scrubland | > 25 | Al-Adamat et al, (2012) Jordan |
| Terracing | 200-1000 | 5-30 | Sandy clay, clay loam and sandy loam | Bushland with scattered trees and shrub-land | N/A | Weerasinghe et al, (2011) Egypt |
| Check dams. | 200-500 | <5 | Sandy loam and sandy clay | Barren, shrubnd scrubland Arable land | N/A | Ammar (2017), Tunisia and Iraq |
| Ponds | >500 | <5 | Clay Clay loam Sandy clay loam | Vegetarian areas Agriculture areas | N/A | Mahmoud & Tang, 2015, UK |
| PVC. Tanks | >500 | <5 | N/A | Urban area | | Melville-Shreeve et al., 2016, UK |

The numerous criteria were more flexible in the IMSD (1995) guidelines than the other two guidelines. For instance, different soil textures were given for different RWH types, such as percolation tanks suited to sandy soils and ponds suited to clay soils. Slopes less than or equal 15% were considered suitable for some techniques. However, the land-use guidelines were restrictive and were recommended for land-use classes such as barren, scrubland, or bare soil. These land-use classes are rarely used for agriculture, and RWH in these areas are small and should be close to cultivated areas. The IMSD guidelines thus include suitable sites far from where the water is needed (Kadam et al., 2012). Additionally, the IMSD guidelines did not define socioeconomic criteria, which is a large limitation compared to the other two sets of guidelines.

The guidelines proposed by Oweis (1998) were more comprehensive than the IMSD guidelines. They considered RWH systems in difficult terrain and specified requirements specific to different types of agriculture, such as requirements for trees, field crops and rangeland. Moreover, criteria for the various types of RWH structures with values for each factor, such as soil texture, mean annual precipitation between 50-300 mm per year, soil depth less than 50 cm, slope less than 4% and vegetation have been determined as well (Al-Adamat, 2008; Ziadat et al., 2012). Socioeconomic criteria, however, were still limited and needed to be extended.

FAO (2003) guidelines are presently the most comprehensive for identifying potential RWH sites. They include more parameters and wider ranges relevant to RWH than the other guidelines and consider various socioeconomic criteria. The criteria for various RWH techniques have been determined, and the guidelines set suitable and ideal limits for factors such as water requirements for various crops, rainfall ranges, slope, and soil depth/texture. For example, the FAO (2003) guidelines consider medium-textured loamy soil the most suitable for agriculture. Mean annual precipitation of 150-750 mm per year is suitable for most RWH techniques. Slopes less than 5% are suitable for ponds, slopes less than 10% are suitable for percolation tanks, and slopes less than 15% are suitable for check dams (Krois and Schulte, 2014). These wide ranges and broad parameter definitions give more flexibility and reliability to the FAO guidelines for their accreditation by most researchers.

## 2.6 Tools and methods used for suitable sites selection for RWH.

Multiple methods and criteria can be integrated with specific tools that can be used to identify suitable RWH sites. These tools can apply to arid and semi-arid regions including the middle - east, are categorized as the following:

- GIS integrated with RS tools.
- Multi-criteria decision analysis method integrated with hydrological modeling, GIS, and RS tools.
- Multi-criteria decision analysis method integrated with GIS.

### 2.6.1 GIS Integrated with RS Tools

Recent advances in computing technology have contributed to numerous ways of identifying suitable sites for RWH. This included the use of GIS and RS tool packages that reduced cost and time effectively. Remote sensing (RS) can be used to develop precise information with a very high resolution. For instance, curve numbers (CNs) and land cover, which are needed to calculate the runoff, can be easily obtained by using GIS applications. This is helpful and useful, especially, in places where very little information and data are available specifically in developing countries (Mahmoud, 2014). GIS tools can also be used for collecting, storing, and analyzing spatial and non-spatial data in different layers applying the integration spatial analysis to identify suitable RWH sites (Mati et al, 2006). The integration use of GIS and RS tools for suitable site selection for RWH can offer an effective reasonable spatial analysis that employs the integrated tool in a rapid easy-to-read/use and gives a good opportunity to understand different patterns and produce information through maps. The accuracy of the GIS/RS tools depends on the resolution of the available data; therefore, it can be very useful and applicable to identify suitable sites for RWH in arid and semi-arid regions (Forzieri et al, 2008 ; Ziadat et al, 2006). Table 2.2 summarizes the rainwater harvesting types and the studies and criteria applied in the arid and semi-arid regions when using GIS and RS tools.

**Table 2. 2** Summary of RWH types and criteria that have been applied. by using GIS and RS tools.

| RWH types | Country and References |
|---|---|
| N/A | Syria, Oweis, Oberle,& Prinz (1998) |
| Cistern and pits contour | Jordan, Ziadat et al, (2006) |
| N/A | Syria, Bakir & Xingnan (2008) |
| Jessour and tabia | Tunisia, Ben Mechlia et al,(2009) |
| Dams and channels | Iraq, Al-Daghastani (2010) |
| N/A | Iraq, Kamel & Mohammed(2010) |
| Contour ridge and runoff strips | Jordan, Al-Shamiri & Ziadat (2012) |
| Reservoir | Iraq, Salih and Al-Tarif (2012) |
| Dams, ponds runoff and strips | Jordan, Ziadat et al, (2012) |
| N/A | UK, Mahmoud and Tang (2015) |
| PVC tanks | UK, Melville-Shreeve et al, (2015) |
| PVC tanks | UK, Ward et al., (2016) |
| N/A | Australia, Preeti et al, (2022) |
| PVC tanks | Rome, Italy, Lupia et al.,(2017) |
| Farm pounds, check damns and Nigarims | Pakistan, Khan et al,(2022) |

### 2.6.2 Multi-Criteria Decision Analysis Method Integrated with Hydrological Modelling, GIS, and RS Tools

Multi-criteria decision analysis (MCDA) is a generally used method for analyzing the combined data from different criteria. One of those methods is the analytical hierarchy process (AHP), an MCA method that has been applied extensively for identifying potential RWH sites (Krois and Schulte, 2014). One of the main procedures in the MCA method is the assessment of relative weight for each criterion, rather than assuming the same weight for all criteria and then comparing two or more alternatives. AHP is a multi-criteria decision-making method, providing a designed technique for organizing and analyzing composite decisions based on mathematics and expert knowledge (Saaty, 2008). The integration of the MCDA method with GIS and hydrological modeling is a good and widely used method for detecting suitable sites for RWH in arid and semi-arid regions.

Numerous studies in the middle east region have been applied this integrated method, taking benefit of the MCDA strengths together with those of hydrological modeling and GISs, as shown in Table 3. The table gives a summary of RWH types and criteria that have been applied using the integration of the MCA method with hydrological modeling and GIS/RS tools.

**Table 2.3** Summary of Integrated RWH, MCDA method with hydrological modelling and GIS/RS tools.

| RWH types | Country and References |
|---|---|
| Reservoir | Lebanon, Jabr & El-Awar,( 2005) |
| N/A | Egypt, Weerasinghe et al, (2011) |
| N/A | Egypt, Elewa et al, (2012) |
| Dams | Iraq, Hameed (2013) |
| N/A | UK, Mahmoud and Tang (2015) |
| Tanks | UK, Ward et al., (2016) |

### 2.6.3 Multi-criteria Decision Analysis Method Integrated with GIS

Multi-criteria analysis (MCDA) is a commonly wide used method of analysis that combines data from different criteria. One of those methods is the analytical hierarchy process (AHP, which is an MCA tool that has been applied extensively to identify potential RWH sites (Krois & Schulte, 2014). One of the main procedures in MCA is the assessment of relative weight for each criterion, rather than assuming the same weight for all criteria and then comparing two or more alternatives. AHP is a multi-criteria decision-making method, providing a designed technique for organizing and analyzing composite decisions based on mathematics and expert knowledge (Saaty, 2008). MCDA integrated with GIS is a good tool for detecting suitable sites for RWH and is widely used in arid and semi-arid regions. Numerous studies in the Middle East have applied this integrated approach, taking advantage of the strengths of MCA together with GIS techniques, as shown in Table 2.4. The table summarizes RWH types and by Integrating MCDA and GIS tools.

**Table 2.4** Summary of the RWH types by integrating MCDA and GIS tools.

| RWH types | Country and References |
|---|---|
| Ponds | Jordan, Al-Adamat (2008) |
| Micro and Macro catchments | Syria, Pauw et al, (2008) |
| Ponds | Jordan, Al-Adamat et al, (2010) |
| N/A | Jordan, Al-Adamat et al, (2012) |
| Groundwater recharge | Saudi Arabia, Mahmoud (2014 ) |
| In-situ | Saudi Arabia, Mahmoud & Alazba (2014) |
| N/A | UK, Mahmoud and Tang (2015) |
| Groundwater recharge | Iraq, AL- Shammari et al, (2021) |

## 2.7 Climate change

Climate change is a serious concern and has become a major global issue in recent years, especially in arid and semi-arid regions strongly affected by its impacts (Misra, 2013). Climate change refers to "any systematic change in the long-term statistics of climate elements (such as temperature, pressure, or winds) sustained over several decades or longer periods. In terms of hydrology, climate change can have a large impact on water resources by affecting the components of the hydrological cycle (Hassan et al, 2014). For instance, temperature and precipitation changes can directly impact evapotranspiration and the quantity and quality of runoff. The components of the water balance can consequently be strongly affected, which in turn influences sectors such as agriculture, industry, and urban development (Riedel and Weber, 2020).

The world faces an unprecedented challenge the adverse impact of global climate change on our invaluable water resources. This challenge manifests in altering annual precipitation patterns and escalating temperatures, contributing significantly to the overarching crisis of global warming (Parchari et al., 2014). The Middle East and less developed nations are especially vulnerable because of altering precipitation patterns, increasing temperatures, and protracted droughts. As seen changes have left an impact on diverse regions of the planet, there is no disputing the observable evidence of climate change (Shahid, 2012).

The Intergovernmental Panel on Climate Change (IPCC) and global climate models have made alarming forecasts that by the end of the twenty-first century, the mean temperature of the atmosphere may have increased by an incredible 2.6 to 4.8 degrees Celsius (IPCC, 2013).

This unsettling pattern is anticipated to generate reduced rainfall and increased evaporation rates, which could ultimately lead to a substantial decrease in surface runoff, with deficits in semi-arid regions of 10% to 30% (Hassan, 2020). Particularly in response to these substantial obstacles, rainwater harvesting (RWH) has become more popular throughout many water-constrained parts of the world, particularly in semi-arid regions. RWH stands as a powerful strategy to bolster water accessibility and availability, serving the needs of both domestic and agricultural sectors (Abdulla et al., 2021). Considering its dry and semi-arid conditions, the Middle East stands out as one of the region's most severely affected by global climate change. This vulnerability primarily stems from a significant rise in temperatures and a decrease in precipitation, as outlined in the study by Hassan and Niel in 2021. Iraq is one of the Middle Eastern countries that is most vulnerable to the effects of climate change and global warming.

Iraq is dealing with several environmental issues, including a sharp drop in the supply of water from lakes and rivers. The nation also must deal with an increasing population size, which puts further strain on its already scarce water supplies. Simultaneously, rising temperatures exacerbate the situation, posing threats to the local ecosystem and compounding the existing challenges (Hassan and Niel, 2021).

### 2.7.1 Downscaling Approaches

General Circulation Models (GCMs) are the primary tools used to project the impacts of emissions on future climates. They provide data at a scale of 100-500 kilometers per grid cell and on temporal scales of monthly averages or longer. This coarse resolution is often inadequate for planning and impact assessment for most decision makers.Various techniques have been employed to evaluate global climate simulations and downscale a range of global climate scenarios (derived from different emissions scenarios) to analyze their impact on hydrological systems. According to Daniels et al. (2012), these downscaling methods rely on several General Circulation Models (GCMs) and scenarios proposed by the Intergovernmental Panel on Climate Change (IPCC). There are two types of downscaling approach models:

- Dynamical Downscaling: This approach involves using a regional climate model (RCM) that operates on principles like those of General Circulation Models (GCMs) but at a much higher resolution, focusing on specific regions

of the globe. The RCM generates climate data with a spatial resolution of approximately 20 to 50 kilometers, utilizing large-scale atmospheric information produced by the GCM (Lee et al., 2023). However, the quality of the RCM outputs is contingent upon the quality of the GCM inputs, making the overall results dependent on the accuracy of the GCM model.

- Statistical Downscaling: This method involves developing statistical relationships between historical large-scale atmospheric data and local climate variables. Once these relationships are established and validated, the model can simulate future climate conditions at a site-specific level. However, this technique relies on the crucial assumption that the established relationship between local climate and large-scale atmospheric circulation will remain valid under future climate conditions. These methods can be categorized into two primary types, as illustrated in Figure 2.8.

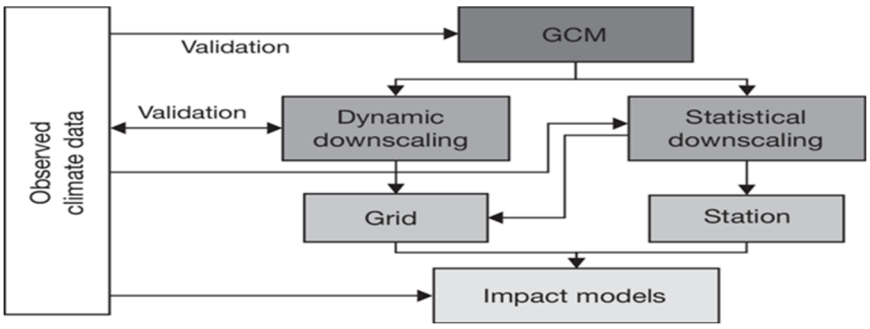


**Figure 2.8** Downscaling Methodologies Flow Chart

Downscaling techniques have been developed to generate climate change information at scales more relevant to stakeholders. These techniques offer spatial resolutions as fine as 20 kilometers or even specific locations, and can also provide temporal details, such as daily temperature sequences derived from monthly or seasonal averages (Trzaska and Schnarr, 2014).

Roy and Majumder (2016) highlight that the Intergovernmental Panel on Climate Change (IPCC) provides various climate change scenarios, which predict the effects of these changes on different natural phenomena. These scenarios consider factors such as pollution, land use dynamics, population growth, and the influence of climate change on these activities. The Working Group (WGI) assessed the climate response

to five illustrative scenarios based on Shared Socio-economic Pathways (SSPs)21 that cover the range of possible future development of anthropogenic drivers of climate change found in the literature. High and very high GHG emissions scenarios (SSP3-7.0 and SSP5-8.522) have CO2 emissions that roughly double from current levels by 2100 and 2050, respectively. The intermediate GHG emissions scenario (SSP2-4.5) has CO2 emissions remaining around current levels until the middle of the century. The very low and low GHG emissions scenarios (SSP1-1.9 and SSP1-2.6) have CO2 emissions declining to net zero around 2050 and 2070, respectively, followed by varying levels of net negative CO2 emissions (IPCC, 2023). The latest report from AR6 and IPCC6explained and describes the relationship of scenarios and modeled pathways considered across the AR6 working group and as shown in Figure 2.9.

| Category in WGIII | Category description | GHG emissions scenarios (SSPx-y*) in WGI & WGII | RCPy** in WGI & WGII |
|---|---|---|---|
| C1 | limit warming to 1.5°C (>50%) with no or limited overshoot*** | Very low (SSP1-1.9) | |
| C2 | return warming to 1.5°C (>50%) after a high overshoot*** | | |
| C3 | limit warming to 2°C (>67%) | Low (SSP1-2.6) | RCP2.6 |
| C4 | limit warming to 2°C (>50%) | | |
| C5 | limit warming to 2.5°C (>50%) | | |
| C6 | limit warming to 3°C (>50%) | Intermediate (SSP2-4.5) | RCP 4.5 |
| C7 | limit warming to 4°C (>50%) | High (SSP3-7.0) | |
| C8 | exceed warming of 4°C (>50%) | Very high (SSP5-8.5) | RCP 8.5 |

**Figure 2.9** The Relationship Between Scenarios and Modeled Pathways of the AR6 Working Group (IPCC, 2023)

Numerous studies have employed downscaling techniques to simulate future climate variables. These approaches enhance the resolution and accuracy of climate projections, facilitating more precise assessments of potential impacts and aiding in developing effective adaptation strategies. Räisänen (2016) employed 12 Regional Climate Model (RCM) simulations and baseline data from 1980 to 2010, focusing on monthly mean temperatures to investigate changes in snowfall in northern Europe. Similarly, Masanganise et al. (2014) utilized 10 RCMs along with monthly temperature and rainfall data to analyze Zimbabwe's climate changes for 2040-2070, relative to the 1980-2010 baseline. Daniels et al. (2012) highlighted that statistical downscaling methods offer several advantages, including efficiency, low computational cost, and the flexibility to accommodate various emissions scenarios and General Circulation Model (GCM) pairings. In contrast, dynamic downscaling methods require substantial computational resources, specialized expertise, and a large volume of data inputs.

The Long Ashton Research Station Weather Generator (LARS-WG) model considers one of the statistical downscaling methods that were used by several researchers in different areas. Osman et al. (2017) used the LARS-WG model with seven GCMs, the A2 scenario, and baseline data from 1980 to 2010 to examine the model's ability to replicate precipitation throughout three future periods in various parts of Iraq. Mekonnen and Disse, Fenta (2018) Utilize the LARS-WG version (5.5) to estimate the upper Blue Nile River basin's maximum and minimum temperatures as well as its rainfall to analyze future climate change. The outcome demonstrates the model's ability to replicate climatic parameters. Khalaf et al. (2022), employed LARS-WG, and CIMP5 with five GCMs to project precipitation and maximum temperature in the southern region of Iraq for the period (2021- 2100) and the models showed high performance in predicting climatic parameters. This study utilizes statistical downscaling techniques, specifically the LARS-WG weather generator, for several reasons. Statistical methods are chosen for their simplicity, requiring fewer computational resources and being more cost-effective compared to dynamic downscaling approaches.

The objective is to project future precipitation minimum and maximum temperatures in northern Iraq, Kirkuk governorate and southeast England in Oxfordshire. By using the latest version of LARS-WG-8.0, which incorporates scenarios from Phase 6 Coupled Model Intercomparison Project (CMIP6), the study aims to downscale Global Climate Model outputs to provide detailed climate predictions for both regions.

### 2.8 Evaporation

Evaporation plays a critical role in the hydrological cycle, where water transforms from liquid to vapor through the input of heat energy. Managing limited water resources sustainably, especially amidst rapid population growth, is increasingly crucial for agricultural production. In hot climates, evaporation significantly contributes to water loss from rivers, canals, and open-water bodies, consuming a substantial portion of available water supplies. Even in humid regions, evaporation remains significant, although it may be overshadowed by cumulative precipitation, particularly during rainy periods.

Understanding the magnitude and variability of evaporation losses is essential for designing and managing water resources effectively. Reliable models are necessary to

quantify these losses accurately, especially as water resources become scarcer. Water resource development projects and irrigation systems rely heavily on long-term average values of evaporation for their design and operation. Therefore, precise estimation of evaporation is fundamental for ensuring the efficient management and sustainability of water resources.

Evaporation rates are influenced by a range of meteorological variables including maximum and minimum temperatures, sunshine duration, wind speed, relative humidity, solar radiation, rainfall, and vapor pressure specific to each location. However, accurately, and continuously measuring pan evaporation is challenging. In such cases, the use of stochastic, neural network, multiple linear regression models etc. becomes essential as they can estimate pan evaporation using available climatic data, potentially yielding more accurate results than direct measurements (Al-Sudani and Salem, 2022).Researchers have developed various models for predicting pan evaporation across different locations in this globe. Many existing models for predicting evaporation rely on deterministic principles such as the combined energy balance-vapor transfer approach, or empirical relationships based on climatological variables. These approaches often require rigorous local calibration, which limits their applicability on a global scale (Hamza, 2024).To recognize these limitations, there is a growing need to enhance conventional modeling techniques to achieve better performance by adopting new and advanced methods.

Evaporation is a complex process characterized by non-linear behavior, making it suitable for modeling using Artificial Neural Networks (ANNs). ANNs can capture intricate relationships and patterns in data, which traditional methods may struggle to accommodate. By leveraging ANNs, researchers aim to improve the accuracy and robustness of evaporation predictions across diverse geographical and climatic conditions. In summary, the evolution towards advanced modeling techniques like ANNs is driven by the desire to overcome the limitations of existing models, enhance predictive accuracy, and enable more effective management of water resources impacted by evaporation.

Evaporation is influenced by various meteorological factors such as air temperature, sunshine hours, wind speed, relative humidity, solar radiation, evaporative power of the air, and vapor pressure deficit specific to a location (La Fuente et al., 2022).

However, accurately measuring evaporation is challenging. In such situations, it is beneficial to use formulas or statistical models that can estimate pan evaporation using available climatic data, potentially providing more accurate results than direct measurements. To address this need, numerous models have been proposed and developed by researchers for different locations in India and globally. These models are categorized into several types:

- General Evaporation Models: These models provide a broad framework for estimating evaporation based on general meteorological parameters.
- Linear Regression Evaporation Models: These models use linear regression techniques to establish relationships between evaporation and climatic variables, offering straightforward predictive capabilities.
- General Artificial Neural Network (ANN) Models: ANN models capture complex non-linear relationships between evaporation and meteorological variables. They are capable of learning from data and adapting to different conditions, potentially improving accuracy compared to traditional linear approaches.
- Artificial Neural Network Evaporation Models: Specifically tailored ANN models designed to predict evaporation, leveraging the network's ability to handle complex data patterns and nuances in meteorological inputs.

Each type of model aims to enhance the accuracy of evaporation estimates, contributing to better water resource management strategies. Researchers review and compare these models to identify the most effective approaches for specific geographic and climatic contexts. Several researchers utilized ANN models to estimate the evaporation in different regions.

Tan Shirgure and Rajput (2011) emphasized the significance of accurate evaporation rate estimation in water resource studies. Previous research has demonstrated that radiation-based models, mass transfer models, temperature-based models, and artificial neural network (ANN) models generally perform well in temperate climates. This study, however, evaluates the effectiveness of these models in estimating hourly and daily evaporation rates in an equatorial climate. The study found that, unlike in temperate regions, solar radiation strongly correlated with pan evaporation on both hourly and daily time scales in equatorial areas. On a daily time, scale, relative

humidity also emerged as a significant factor. Among the simplified models, only the radiation-based models were deemed suitable for modeling hourly and daily evaporation rates.

ANN models were found to be generally more accurate than simplified models, provided that an appropriate network architecture is selected, and a sufficient amount of data is used for training (Ghorbani et al., 2018).

ANN modeling becomes particularly relevant when both energy- and aerodynamics-driven mechanisms dominate, as radiation and mass transfer models fail to produce reliable evaporation estimates under such conditions.

Deswal and Mahesh Pal (2008) applied an ANN-based modeling technique to study the impact of various meteorological parameters on reservoir evaporation. They utilized a data set from a previously reported study and tested several input combinations to determine the importance of different parameters in predicting evaporation. Their findings indicated that the prediction accuracy of the ANN model was significantly influenced by the chosen input parameters.

In addition, the performance of the ANN was compared with that of linear regression for predicting evaporation. The comparison demonstrated the superior performance of the ANN over the linear regression approach (Abed et al., 2021).

The study revealed that considering all input parameters together, rather than individually, resulted in the most accurate predictions.

The highest correlation coefficient (0.960) and the lowest root mean square error (0.865) were obtained with the combination of air temperature, wind speed, sunshine hours, and mean relative humidity. A graph of actual versus predicted evaporation values suggested that most values fell within a ±15% scatter when using all input parameters. These findings underscore the usefulness of the ANN technique in accurately predicting evaporation.

Kumar and Tiwari (2012) utilized the ANN model to estimate evaporation in Nagar, India, based on four climatic factors (solar radiation, wind speed, relative humidity, and temperature) for nineteen years. The results show the efficiency of the model as the correlation coefficient value (0.923) and the mean square error (0.986). Benzaghta ( 2014) employed ANN to estimate evaporation in Iran as a semi-arid region for Amir

Kabir Dam as a reservoir case study, they used two layers with 8 neurons, and the results of correlation (0.90) and 0.0112 error which proves that ANN is an effective model. Another study by Srivastava et al. (2021) to predict and estimate evaporation in Jabalpur, India showed the effectiveness of utilizing the ANN model to estimate the evaporation they used two layers with seven input parameters and the correlation result (0.97).

In this study, ANN was utilized to estimate the evaporation for the two study regions by utilizing a neural network and support vector machine under the impact of climate change consideration and under two different scenarios SSP2-4.5 and SSP5.8. More details can be found in the methodology chapter.

### 2.9 Crop and Irrigation demands under climate change

Agriculture is the largest consumer of water, utilizing up to 70% of surface and groundwater resources for irrigation (FAO, 2003). The irrigation water requirements for specific crops are heavily influenced by climate conditions (Konzmann et al., 2013). The Food and Agriculture Organization's Figure 2.10 illustrates the global agriculture water withdrawal under climate change.

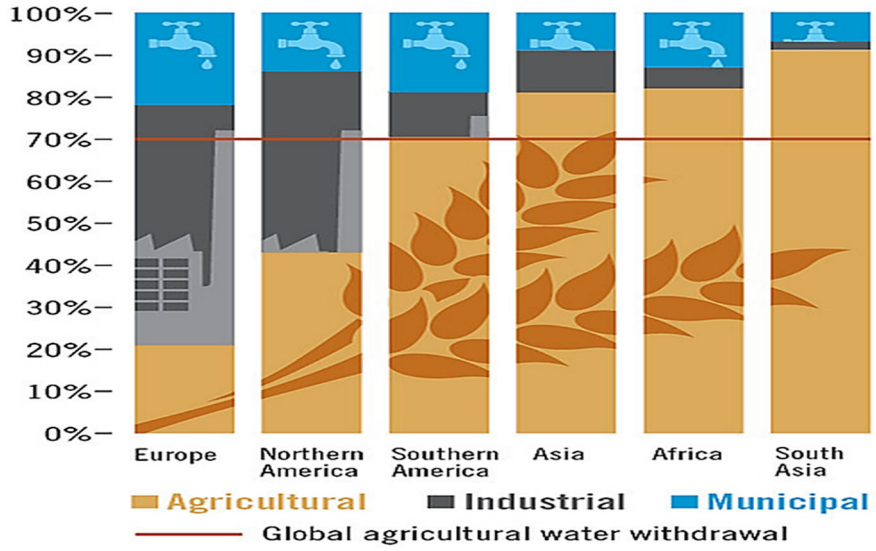


**Figure 2.10** Global Agriculture Water Withdrawal (Source: FAO, 2008)

Consequently, changes in climate patterns related to global warming play a crucial role in determining future agricultural water demand (Zhu et al., 2015; Gorguner and

Kavvas, 2020). Increased surface air temperatures due to climate change lead to higher evapotranspiration rates (Abtew and Melesse, 2013) and deplete soil moisture in the root zone (Huang et al, 2020).

Furthermore, plants tend to require more water to maintain their biomass under these conditions. In semi-arid regions, temperature is the most critical factor influencing irrigation water demand. As a result, the volume of water discharged to irrigated areas could change due to climate change (Pousa et al., 2019).

Agriculture is one of the most vulnerable sectors to climate change. Numerous researchers have investigated future water needs for irrigation considering climate change. Doria et al. (2012) evaluated daily crop water requirements in Southern Quebec, Canada by incorporating projected precipitation and temperature into the CROPWAT model. Compared with crop water requirements recorded in 1971-2000, these requirements are projected to increase by 8% by 2050 based on the HAD-MC3 climate model. Similarly, Diaz et al. (2007) forecasted future irrigation water requirements in the Guadalquivir River basin, in Spain by applying projected temperature and precipitation data to the CROPWAT model. Their results indicated an increase in irrigation water needs by 19.3% and 16.3% by 2050 under A2 and B2 climate change scenarios, respectively, due to increased evapotranspiration and a decline in spring rainfall. The study concluded that water resources will be under stress, and the irrigated area is expected to decrease. Zhu et al. (2015) examined agricultural water use for six crops cultivated in the semi-arid region of China under A2 and B2 climate change.

dium scenarios using the HadCM3 climate model. Climate variables extracted from the statistical downscaling model were processed using the FAO Penman-Monteith equation. The results showed that evapotranspiration is expected to increase by 4% to 7%. Different crops exhibited varying responses in terms of crop evapotranspiration increases. Moreover, crop irrigation water requirements are projected to increase (under A1-B2 scenarios) by 198-242 million cubic meters (MCM) for the period from 2041 to 2070 and by 342-456 MCM for the period from 2071 to 2099. Chowdhury et al. (2016) studied the potential impact of climate change on irrigation water needs by 2050 for various crops including wheat, maize, barley, tomato, potato, dates, citrus, and grapes planted in 112 thousand hectares located in the arid region of Al-Jouf, Saudi

Arabia. Data from the CROPWAT model projected an increase in irrigation requirements by 58 MCM (2.9%) with a 1°C increase in mean temperature, indicating a negative impact of climate change on irrigation water availability and the need for better water resource management. Cho et al. (2019) investigated future paddy water requirements in Korea under RCP 4.5 and RCP 8.5 climate change scenarios for the periods 2020-2059 and 2060-2100. The results showed an increase in irrigation demand despite a notable increase in effective rainfall, as the increased rainfall could not compensate for the decrease in soil moisture due to the significant rise in projected evapotranspiration rates. This suggests that water shortages are expected if current planting practices continue. Saeed et al. (2021) investigated future irrigation water demand in four reclaimed irrigation projects located in arid and semi-arid regions of Iraq by combining LARS-WG and CROPWAT-8.0 models. The study found that each of the 16 crops examined responded differently to climate change in terms of irrigation water demand. Additionally, irrigation water demand is projected to increase by 0.1% to 42.4% compared to the water utilized in the last three decades.

## 2.10 Summary

Climate change has adversely impacted water resources and agricultural water demand globally, therefore there is an important desire to investigate and mitigate practical solutions to face water scarcity and enhance the water sustainability concept. RWH system is considered one of the most effective and sustainable for water resources management that can help reduce water stress and promote water sustainability specifically in arid and semi-arid regions and even in humid climates that can be affected by climate change shortly. Many studies have focused on RWH for domestic use only and other studies discussed RWH site selection by integrating GIS, and MCDA with RS generally without considering the agricultural sector. While other studies only focused on climate change, evaporation, and crop water requirements.

Therefore, there is a real gap in combining and considering RWH suitable site selection considering climate factors for agricultural use in two different regions, one is a semi-arid region, and the other is a humid one. This study integrates multiple methodologies and techniques like, GIS, RS, MCDA, ANN, LARS-WG, and CROPWAT to achieve the research aim. In this chapter, the literature on identifying suitable sites for RWH by utilizing GIS, RS, and MCDA with the impacts of climate change and the approaches to downscaling future climate factors has been briefly summarized. Also, the prediction and estimation of evaporation are discussed, alongside an overview of different models by using ANN models and techniques that employ various inputs. Irrigation water demands have been discussed by utilizing CROPWAT to underscore the significant influence of climate variables on irrigation and crop water requirements.

# Chapter 3: Studied Areas, Data Collection and Processing

## 3.1 Introduction

This chapter presents an overview of the proposed methodology's study area, focusing on climate change's impact on rainwater in two regions: Kirkuk, Iraq, and Oxfordshire, UK. These catchments were strategically selected based on the contrasting scales of the cities—Kirkuk, a large governorate in northern Iraq as a semi-arid region, and Oxfordshire, a smaller rural county in southeast England as a humid region. This comparison allows for a nuanced analysis of climate change effects on rainwater demand for cultivation across different city scales.

The availability and reliability of long-term data were also critical factors in selecting these cities. Reliable data is essential for accurate forecasting models. The data for Kirkuk was sourced from the Iraqi Metrological Department, covering multiple metrological stations in the governorate, while the National Metrological Library obtained Oxfordshire's data in the UK. These datasets, provided by reputable organizations, consist of observed values, rather than calculated or estimated figures.

Before incorporating this data into the prediction model, several pre-processing techniques must be applied. One of these techniques is data normalization and correlation to prepare climate data. This chapter also explores key aspects of rainwater harvesting, including region location, climate, water resources, and climate in the study regions. Furthermore, it introduces monthly historical data on rainwater, along with five critical climate factors: maximum, mean, and minimum temperature, rainfall, and sunshine hours.

## 3.2 Study Areas

The Two selected regions for this work are described in more detail in the following sections:

### 3.2.1 Kirkuk, Iraq

Kirkuk governorate, situated in the northern part of Iraq, and bounded to the northeast by the Zagros Mountains and to the west by the Lower Zab and Tigres Rivers, which are recognized for their mild flow. Kirkuk is roughly 250 kilometers (155 miles) from Baghdad, Iraq's capital and biggest city. The location of the study area is 35° 28' N to

35° 47 latitudes and 44° 24' E to 44° 40' E longitude and elevation of 350 m. The north-eastern highlands of Iraq commence from the southern province of Kirkuk, extending to the borders of Turkey and Iran. Additionally, Kirkuk comprises three distinct neighborhoods: Daquq, Al-Hawiga, and Dibis. The study area is visually depicted in Figure 3.1, providing a detailed map representation. Despite its relatively small size, the governorate covers an expansive land area of around 9,679 square kilometers, which constitutes approximately 2.2% of Iraq's total landmass. Despite its modest dimensions, this governorate holds significant importance in agricultural land (Abdulrahman, 2018). According to Iraqi government estimates in 2007, the population of Kirkuk was approximately 902,019 people, accounting for roughly 3% of Iraq's total population.

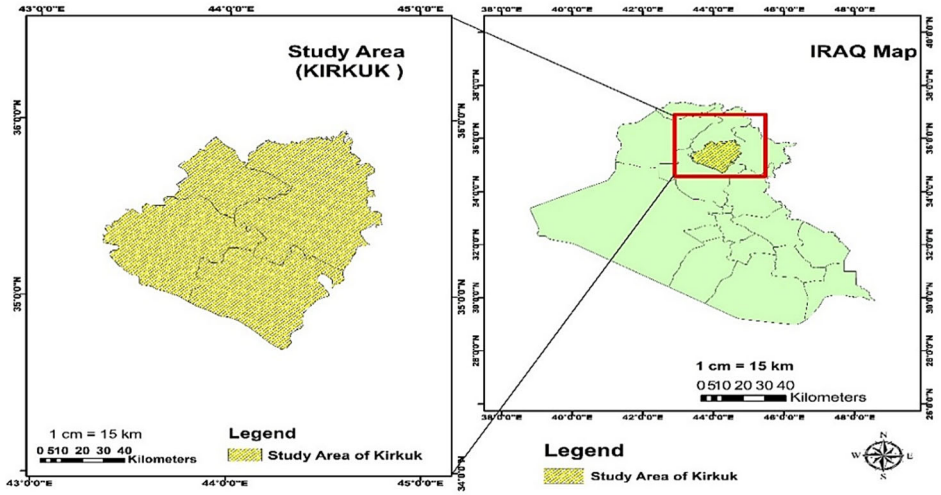


**Figure 3.1** Kirkuk Study Area

The weather in Kirkuk governorate varies from semi-arid to Mediterranean climate, which is warm in summer and cold and rainy in winter. There are four seasons in Kirkuk governorate: winter which lasts from December to the end of February band it is relatively mild to cool, and the average maximum temperature is between 10 °C to 15 °C but the temperature can drop near to freezing at night (Abdulrahman, 2018). The spring season lasts from March to May, and it is mild with average temperature ranging from 16 °C to 25 °C it is also one of the wetter seasons. While the summer season starts from June to September, it is hot and dry often with temperatures exceeding 40 C during the hottest months (July and August) and no rainfall during these months. The autumn in Kirkuk starts from October to November and is mild, and the temperature starts to drop down and rainfall begins to increase during this time. The rainfall season is mainly in winter through spring in Kirkuk governorate and the

average annual rainfall varies from 300-400 mm. Table 3.1 illustrates the average values for the four main climate factors (Min. temperature, Max. temperature, rainfall, and sunshine hours for the period 1980-2022).

**Table 3.1** Average values for four main climate factors for Kirkuk Area

| Months | Av. Tmax. ( °C) | Av. Tmin. ( °C) | Av. Rainfall (mm) | Av. SSH (hours) |
|---|---|---|---|---|
| J | 10.1 | 9.8 | 66 | 5.4 |
| F | 15.9 | 6 | 62.8 | 6.1 |
| M | 20.4 | 9.5 | 48.8 | 7.2 |
| A | 26.9 | 14.7 | 40 | 7.8 |
| M | 34 | 20.7 | 16.1 | 9.2 |
| J | 40.2 | 25.7 | 0.2 | 11.2 |
| J | 43.6 | 28.8 | 0 | 14.5 |
| A | 43.1 | 28.2 | 0 | 11.0 |
| S | 37.4 | 24.0 | 1 | 10.2 |
| O | 31.6 | 19.2 | 15.1 | 8.1 |
| N | 22.6 | 11.5 | 45.8 | 6.6 |
| D | 15.4 | 6.5 | 57.2 | 4.5 |

### 3.2.2 Oxfordshire, UK

Oxfordshire is a county located in Southeast England, bordering Warwickshire and Northamptonshire to the north, Buckinghamshire to the east, Berkshire to the south, Wiltshire to the southwest, and Gloucestershire to the west. Situated between the River Thames and the Cherwell River, its county town is Oxford. Oxfordshire covers an area of approximately 2,605 square kilometers and the approximate central coordinates of Oxfordshire are: Latitude: 51.75° N and Longitude: 1.25° W. Oxfordshire's temperate climate and fertile soil make it suitable for a variety of crops (City council, 2024). Agriculture plays a significant role in the county's rural areas and Oxfordshire has a long history of farming. The farming in the county includes both arable (crop production) and livestock farming, focusing on several key crops such as (Wheat, barley, corn, sunflower, and potatoes). The population as of recent estimates of Oxfordshire is around 725.000 people. Oxford City has a population of approximately 160. 000, while the rest of the population is spread across smaller towns and rural areas. Figure 3.2 shows the study region of Oxfordshire.

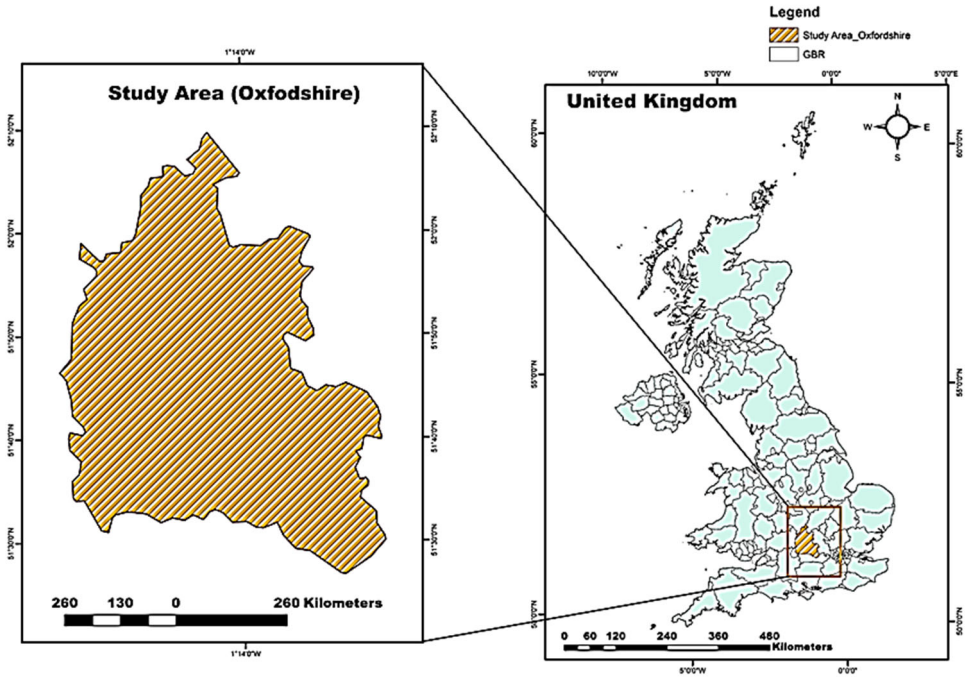


**Figure 3.2** Oxfordshire Study Area

The weather in Oxfordshire is classified as temperate maritime, typical of the UK. This means the county experiences mild winters, cool summers, and consistent yearly rainfall. Oxfordshire County has four seasons: winter lasts from December to February and the temperature varies from 0 °C to 7 °C and can drop below freezing during cold spells. The maximum average temperature ranges between 6 °C to 9 °C. The weather can be mild on some days, but cold spells may cause occasional dips in temperature, especially during January, the coldest month. This season has the fewest hours of daylight, with December having the shortest days. The spring season lasts from March to May with an average temperature varies from 8 °C to 15 °C. The weather starts to warm up after the winter months, though it can still be unpredictable, with occasional rain showers and cold snaps. Sunshine days gradually lengthen, and sunshine hours increase, especially in April and May. Summer season lasts from June to August with average temperature varying from 18 °C to 25°C and it can reach 30°C during heatwaves. The most sunshine hours occur during this season, with up to 16 hours of daylight in June.

Autumn starts from September to November and the average temperature varies from 7 °C to 15 °C Autumn is characterized by cooling temperatures. It's typically a wetter season, with more frequent rain, particularly from October onwards. Early autumn (September) can still be quite mild, but temperatures drop as November approaches Oxfordshire experiences moderate rainfall throughout the year, with an annual average of 600 to 700 mm.

The wettest months are usually October through January, with the driest period typically being April through August. Rainfall is spread evenly, though autumn and winter see more persistent rain. The county gets around 1500 to 1600 hours of sunshine per year. Usually, May to August are the sunniest months, with each month receiving around 180 to 200 hours of sun. December and January are the darkest months, with fewer than 50 hours of sunlight per month. The average relative humidity tends to be moderate, ranging between 75% and 85% throughout the year, and slightly higher in winter. Table 3.2 illustrates the average values for the four main climate factors (Min. temperature, Max. temperature, rainfall, and sunshine hours for the period 1980-2022).

**Table 3.2** Average values for four mains climate factors for Oxfordshire (Metrological office UK)

| Months | Av. Tmax. ( °C) | Av. Tmin. ( °C) | Av. Rainfall (mm) | Av. SSH (hours) |
|---|---|---|---|---|
| J | 1.18 | 11.27 | 53.88 | 59.1 |
| F | 7.70 | 0.83 | 75.89 | 76.42 |
| M | 10.59 | 2.55 | 111.93 | 117.16 |
| A | 13.37 | 3.81 | 164.74 | 168.29 |
| M | 16.85 | 6.84 | 199.47 | 208.48 |
| J | 19.98 | 9.71 | 203.18 | 208.44 |
| J | 22.55 | 11.91 | 225.74 | 228.11 |
| A | 22.13 | 11.76 | 203.09 | 201.43 |
| S | 18.95 | 9.59 | 144.44 | 148.69 |
| O | 14.61 | 6.91 | 109.71 | 108.5 |
| N | 10.34 | 3.60 | 66.55 | 66.4 |
| D | 7.54 | 1.29 | 50.60 | **61.3** |

## 3.3 Data Set for the Studied Areas

### 3.3.1 Climatic Data

This study employs climatic historical climate data for the period of (1980-2022) and it contains the main climatic factors such as (rainfall in mm, minimum and maximum temperatures in °C, and sunshine hours SSH). These data were collected from the Iraqi Metrological Department and the Official website of the Ministry of Agriculture as well as daily data for the Kirkuk governorate. These data were utilized to develop and downscale GCMs and evaporation models. For Oxford Shire County the climatic data were collected from the National Metrological Library and Archive in the UK as daily data. These daily climate factors were employed to predict and simulate the future climate projection for both studied regions. To determine the measured climate from which to compute any hypothetical changes in climate, a reference baseline period is required. The selection of the baseline period will be determined by the accessibility of the necessary data for rainwater harvesting suitable site selection. Consequently, the years 1980–2010 were utilized. According to Semenov et al. (2013), 1980–2010 can be used as minimum a baseline to create climate parameters for the future projection.
The distribution of a quantitative variable can be effectively visualized using a box and whisker plot. This graphical representation is based on the five-number summary, offering a concise numerical description of the dataset. The five key statistics included are the minimum, first quartile (Q1), median, third quartile (Q3), and maximum value. Figures (3.1) through (3.4) illustrate the distributions for the selected variables, providing insights into their spread, central tendency, and potential outliers. Figure 3.3 illustrates the average monthly maximum temperature for both studied regions. There is a big difference in mean and median in both values for the two studied regions as it is higher in Kirkuk than in the Oxford Shire region.

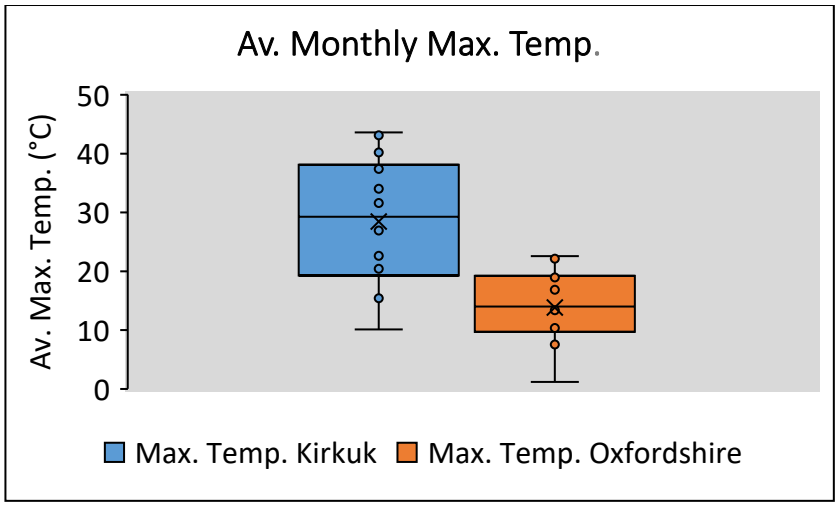


**Figure 3.3** Box Plot of Average Monthly Maximum Temperature for Both Areas

Figure (3.4) shows the average minimum temperature for both studied regions and it is obvious there are differences in mean and median values in both studied regions as it is higher in Kirkuk governorate than in Oxfordshire county and the average minimum temperature in Oxfordshire is less and near to lower values.

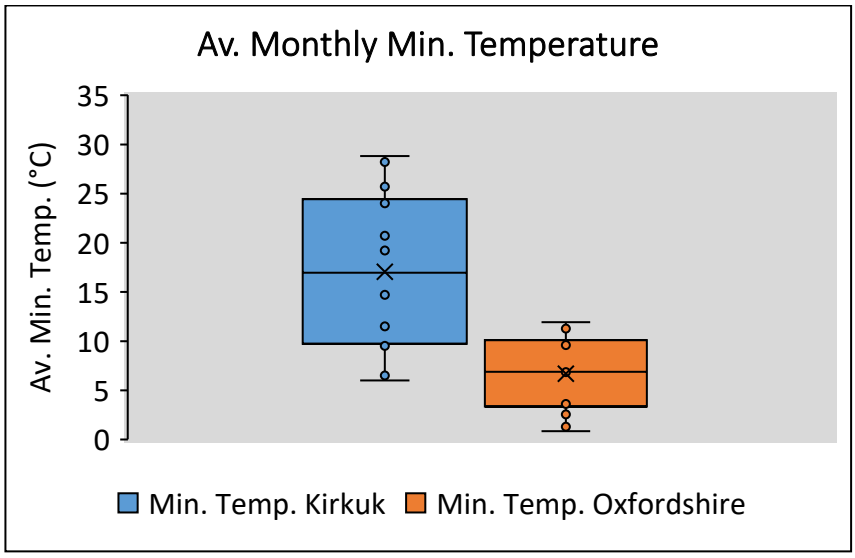


**Figure 3.4** Box Plot of Average Monthly Minimum Temperature for Both Areas

As shown in Figure 3.5, the median value of rainfall in Oxfordshire is about 128.1 mm compared to the median value of Kirkuk governorate which is about 50.9 mm and there is a big difference in average monthly rainfall both both studied regions.

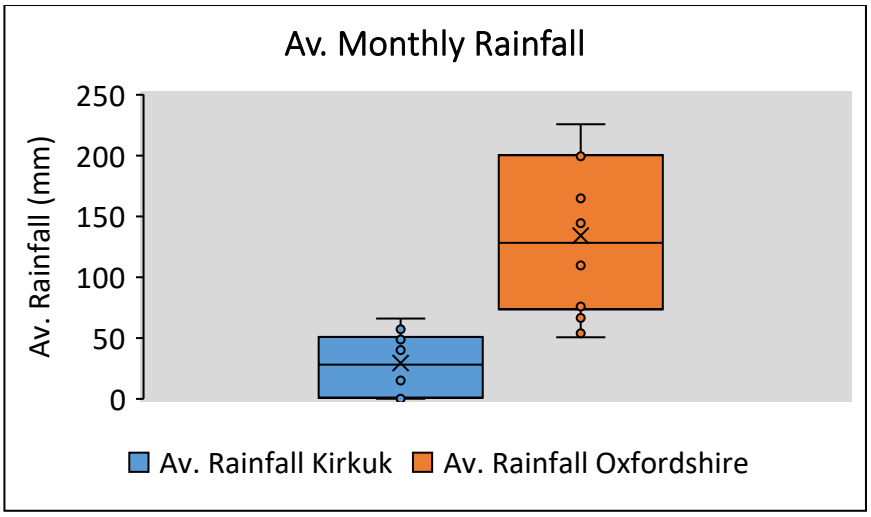


**Figure 3.5** Box Plot of Average Monthly Rainfall for Both Areas

Figure 3.6 shows the average monthly values for both studied regions for sunshine hours (SSH) and it is clear there are differences in mean and median values for both studied regions.

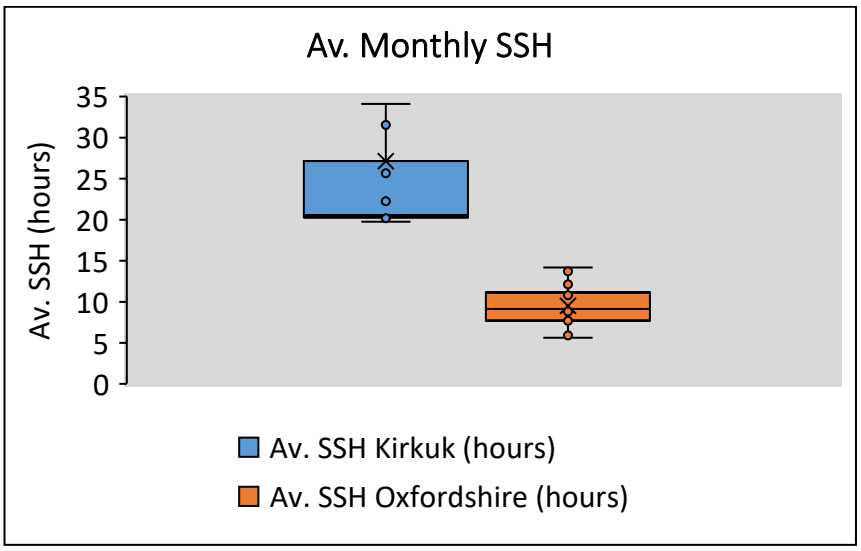


**Figure 3.6** Box Plot of Average Monthly Sunshine Hours for both Areas

### 3.3.2 Data Cleaning and Processing

Data cleaning techniques involve detecting and addressing irrelevant, erroneous, or outlier data to improve the quality of analysis (Wand and Wang 2019). When datasets contain extreme values or noise, they can distort regression models and reduce the

accuracy of predictive outcomes. Specifically, extreme data points, such as outliers, can bias the regression solution, leading to poor model performance. Therefore, removing or adjusting these anomalies is crucial for building more reliable models and achieving more accurate results in data analysis. Cleaned data ensures that climate models are correct, leading to more reliable predictions of weather patterns, global warming trends, or extreme climate events. Cleaning data leads to removing any noise or errors or biases in that data such as those caused by outdated or faulty equipment, ensuring that the analysis reflects true climate phenomena.

To ensure the data cleaning process, the Adjacent Average process is a specific case of a moving average, often used in time series data to smooth out noise by taking the average of each data point and its adjacent neighbors. It's a simple technique that operates similarly to a simple moving average (SMA) but typically uses only the immediate neighbors rather than a larger window of surrounding points. The adjacent average involves calculating a new value for each data point by averaging it with its direct neighbors. For time series data, where there is an ordered sequence of observations (e.g., Max. and Min temperature, sunshine hours (SSH) and rainfall), this smoothing technique helps reduce high-frequency noise while maintaining the overall trend and ensures to removal of all missing and duplicated data.

Formula for Adjacent Average

Given a time series X1, X2, X3, Xn the adjacent average for a data point X*t* is calculated as:

$$Yt = \frac{Xt-1+Xt+Xt+1}{3} \quad (3.1)$$

Where: Y*t* is the smoothed value at time *t*, Xt is the original value at time *t,* X*t*-1 and X*t*+1 are the adjacent points.

All raw required data were cleaned and adjusted by applying Adjustment Average formula for both studied sites. For Max. temperature trend for Kirkuk study area as shown in Figure 3.7, the data were processed to remove all noise and handling any missing data, as the average T max. trend shows an extreme noise for the raw data and fluctuation and that can affect the quality of the final results if not cleaned and make

the signal clear, so by applying average adjustment technique by using OriginLab Pro, 2025 and four trails were applied as shown in Figure 3.7 and fourth trail shows a smooth trend and all noise, short term extreme temperature data were processed and adjusted as illustrated in Figure 3.7.

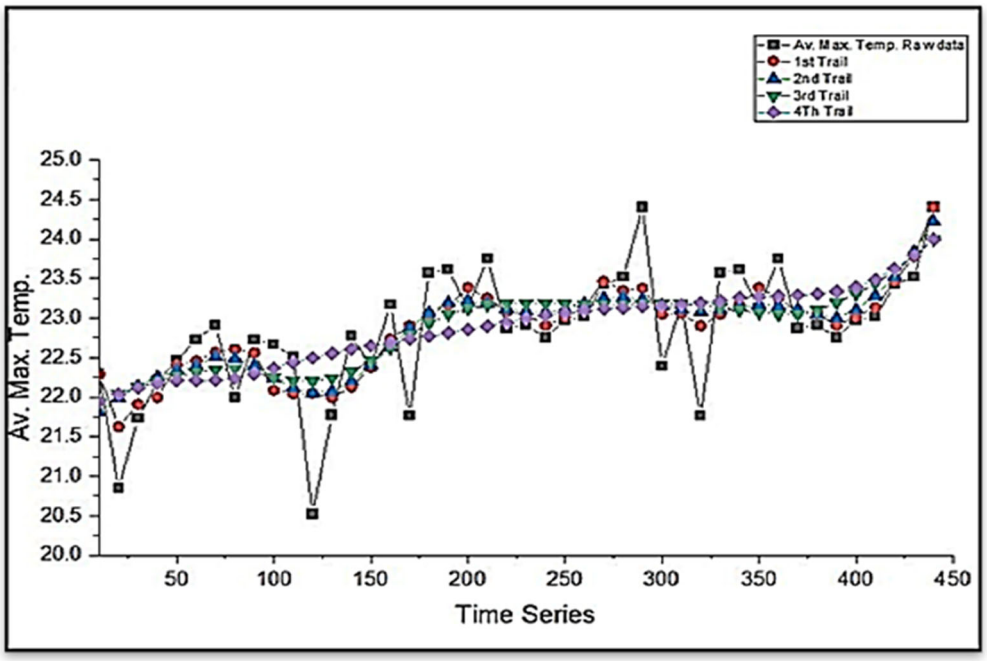


**Figure 3.7** Max. Average T. Monthly Time Series of Kirkuk

The data of min. T. were cleaned and smoothed by using OriginLAB Pro, 2025. The original raw data showed a slight noise and fluctuation in some parts and after applying the average adjustment for $4^{th}$ trails, the data trend is smooth and clean as illustrated in Figure 3.8.

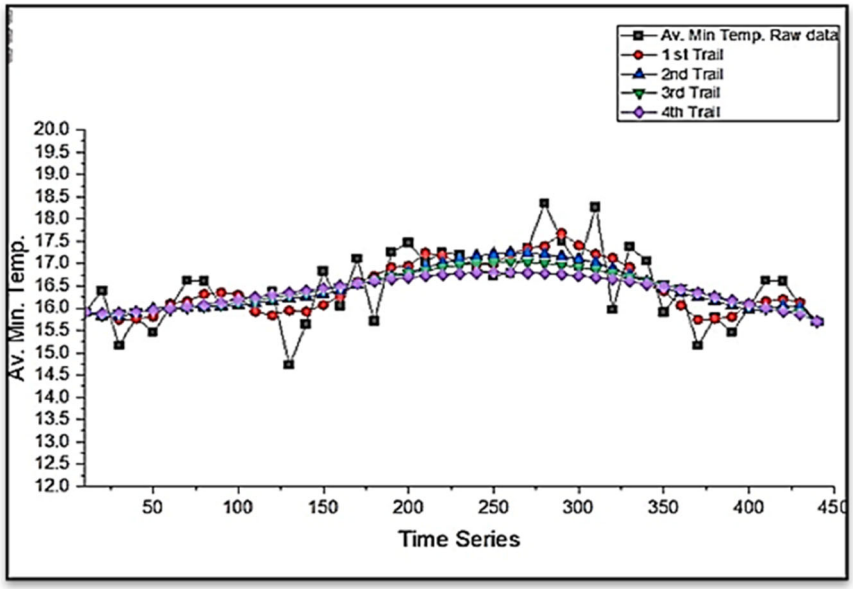


**Figure 3.8** Min. T. Monthly Average Time Series of Kirkuk

Rainfall raw data flacuated as shown in Figure 3.9 and the average raw trend data is not smooth so all data were cleaned accordingely and adjusted by utilizing OriginLab Pro, 2025 and after applying 4$^{th}$ trails the data were smoothed and cleaned ann all missing data were adjusted by applying average adjacent method and filling gaps as shown in Figure 3.9. The sunshine hours raw data were cleaned by applying average adjucement method as the raw trend data was extremely flacuated therfore all data were cleaned by utilizing OriginLab Pro for fourth trails and as shown in Figure 3.9.

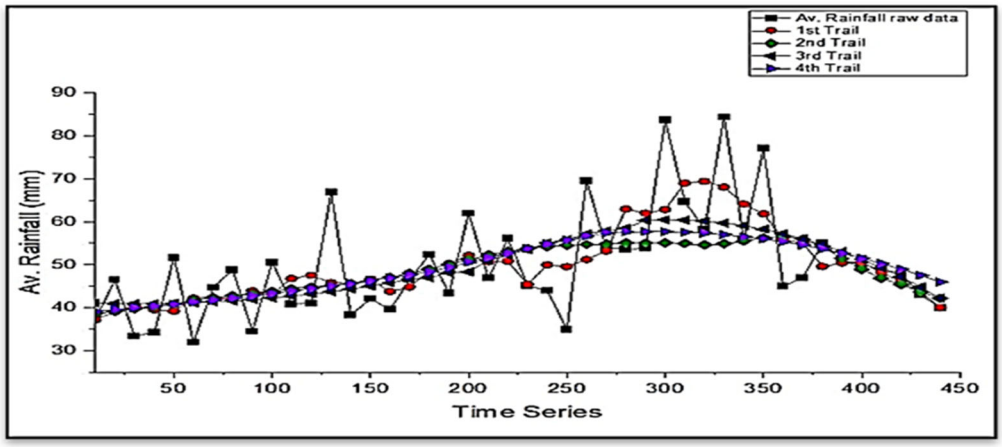


**Figure 3.9** Monthly Average Rainfall of Kirkuk

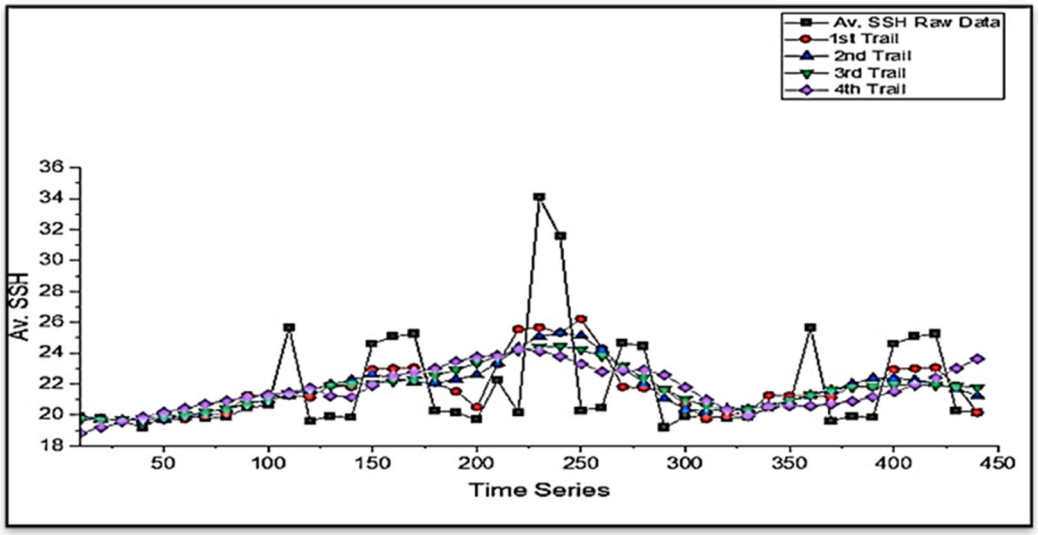


**Figure 3.10** Monthly Average Sunshine Hours of Kirkuk

The average Max. T. raw data for Oxfordshire study area were cleaned as there are few fluctuations as shown for the average raw trend data but by applying average adjustment for four trails the data were cleaned and smooth as shown in the Figure 3.11. For Min T. the raw data were less fluctuated except for some points but to ensure data quality the raw data were also cleaned and smoothed by utilizing OriginLab Pro. 2025 and average adjustment method as shown in Figure 3.12 the data trend is smooth and the noise was reduced.

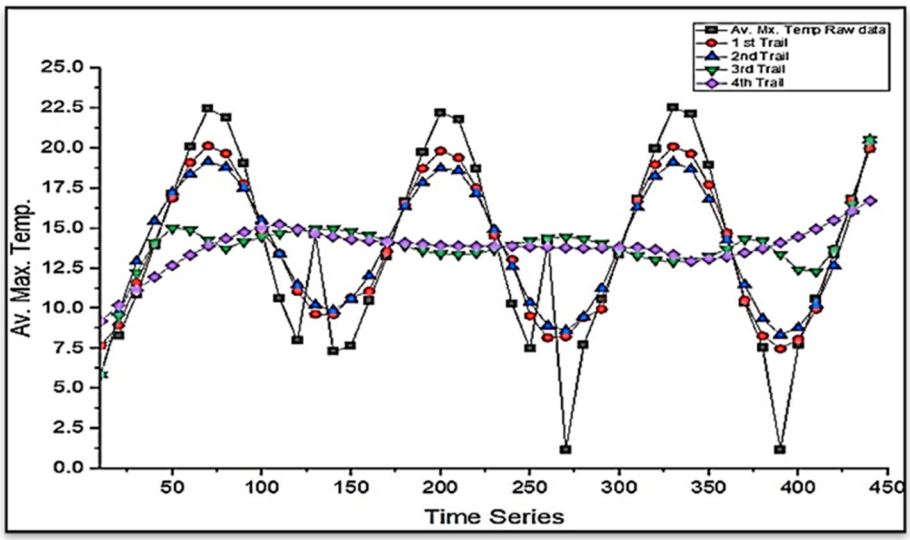


**Figure 3.11** Monthly Av. Max.T Time Series of OxfordShire

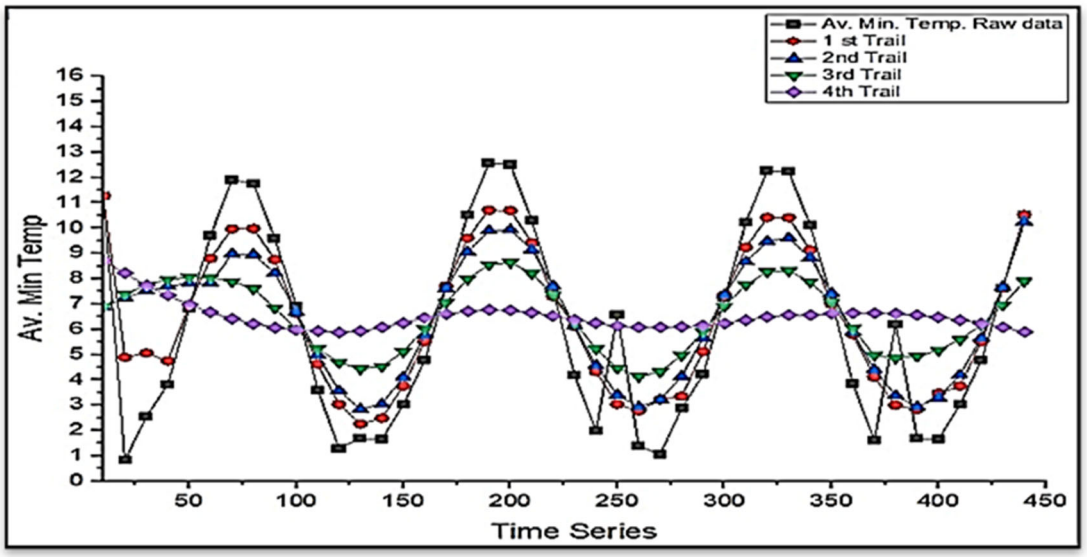


**Figure 3.12** Monthly Av. Min. T. of Oxfordshire

The raw data for rainfall time series for Oxfordshire were cleaned as the raw data fluctuated as shown in Figure 3.13 and there was a noise that removed and cleaned by applying average adjustment method to ensure data quality and clear signal for actual trend. For sunshine hours, raw data were cleaned as well, as the original trend data were fluctuated and the noise is very dominate, therefore fourth trail applied to clean thar data and the fourth trail shows the trend is clear and smooth as shown in Figure 3.14.

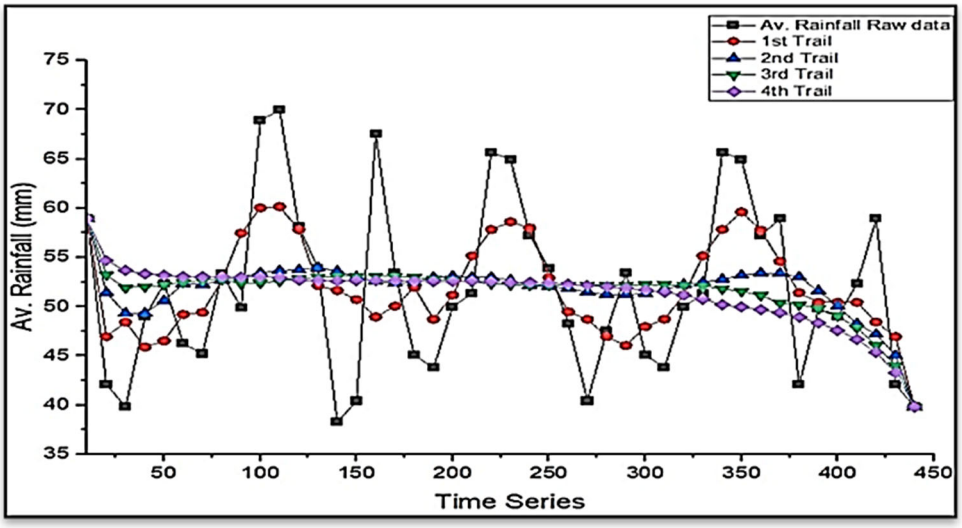


**Figure 3.13** Monthly average rainfall Time Series of Oxford shire

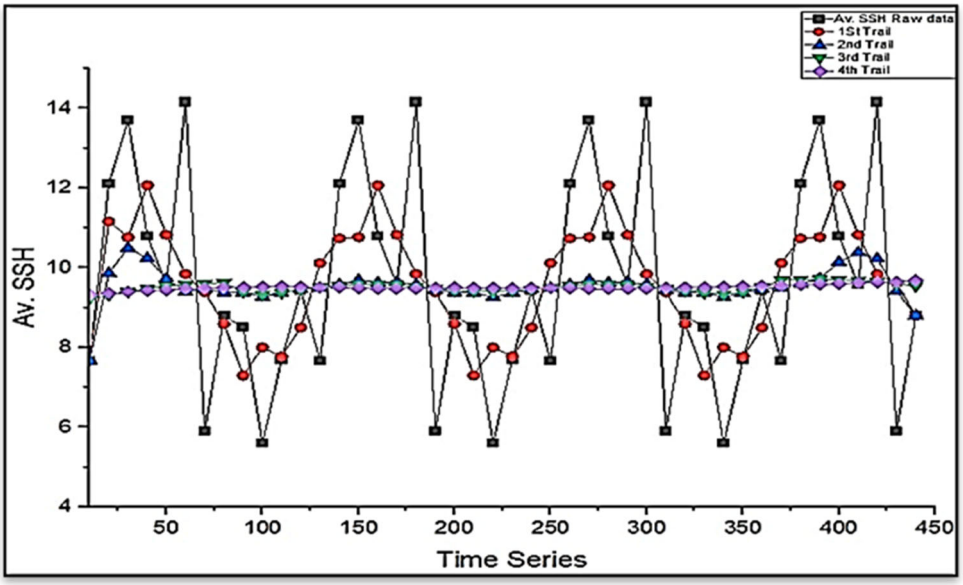


**Figure 3.14** Monthly Average SSH Time Series of Oxford shire3.3.3 Data for RWH Site Selection

The data collection, and processing for preparing the thematic layers to identify RWSH as the below:

### 3.3.3.1 Digital Elevation Model (DEM)

The Digital Elevation Model (DEM) used in this study was downloaded from the United States Geological Survey, (USGS: https://www.earthexplorer.usgs.gov), specifically derived from the Shuttle Radar Topography Mission (SRTM) with a resolution of 30 meters by 30 meters as TIF file. The DEM underwent processing, which included filling any data gaps, mosaicking multiple tiles, and clipping the dataset to fit the boundaries for both of the studied areas of Kirkuk governorate and Oxfordshire County. These steps were performed using various tools in ArcMap software 10.8.2 to produce the final DEM and prepare it as depicted in Figures 3.15 and 3.16 respectively.

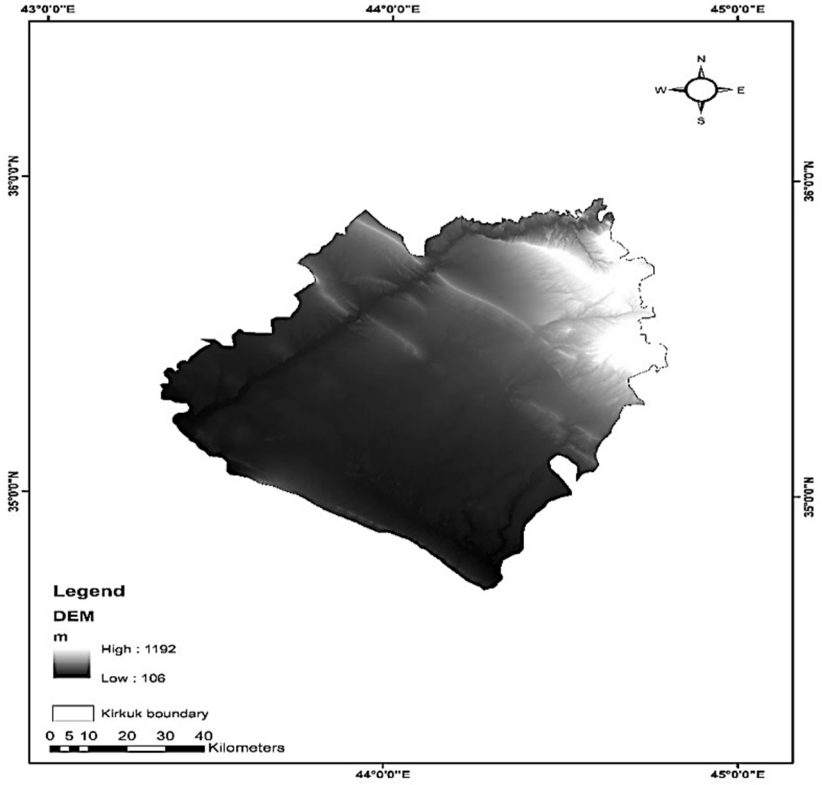


**Figure 3.15** DEM for Kirkuk

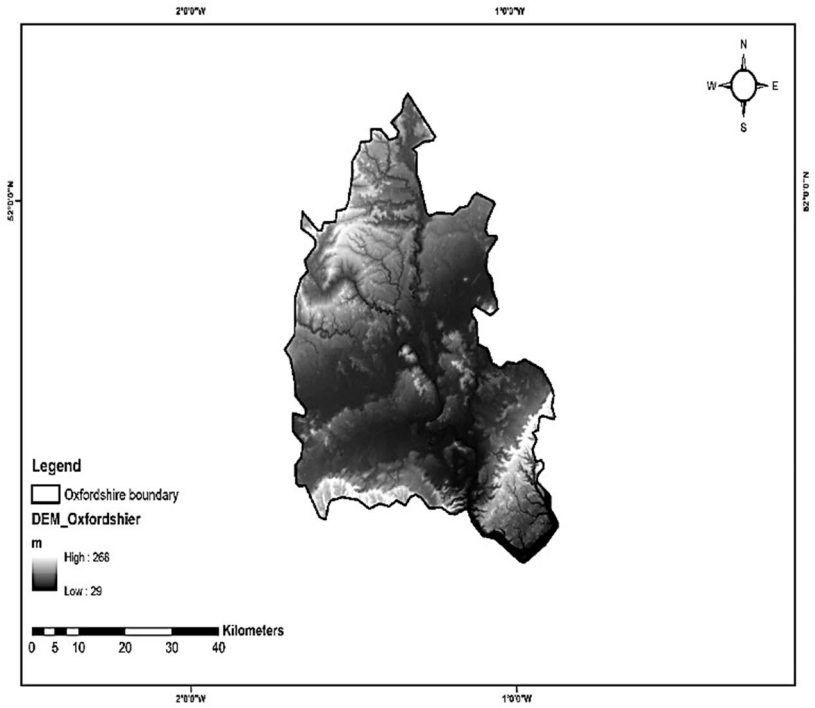


**Figure 3.16** DEM for Oxfordshire

### 3.3.3.2 Hydrological Soil Group (HSG)

The soil maps of Iraq and the United Kingdom were obtained from the Food and Agriculture Organization's official website (FAO, 2021). This map is compared to a previous soil map from the Ministry of Agriculture of the Iraqi government for Kirkuk governorate and with British Geological Survey maps for Oxfordshire County. The downloaded file as a TIF format was processed by using ArcMap, and GIS tools and reclassified according to the hydrological soil types of the study area to produce the hydrological soil map model. The hydrologic soil group model was reclassified into four group types (C, D, C &D, D &C) according to the classification of the United States Department of Agriculture (USDA) and as shown in figures 3.17 and 3.18 respectively for both studied regions. Table 3.3 shows the relationship between soil types, runoff, and HSGs according to USDA classification.


**Figure 3.17** HSGs for Kirkuk

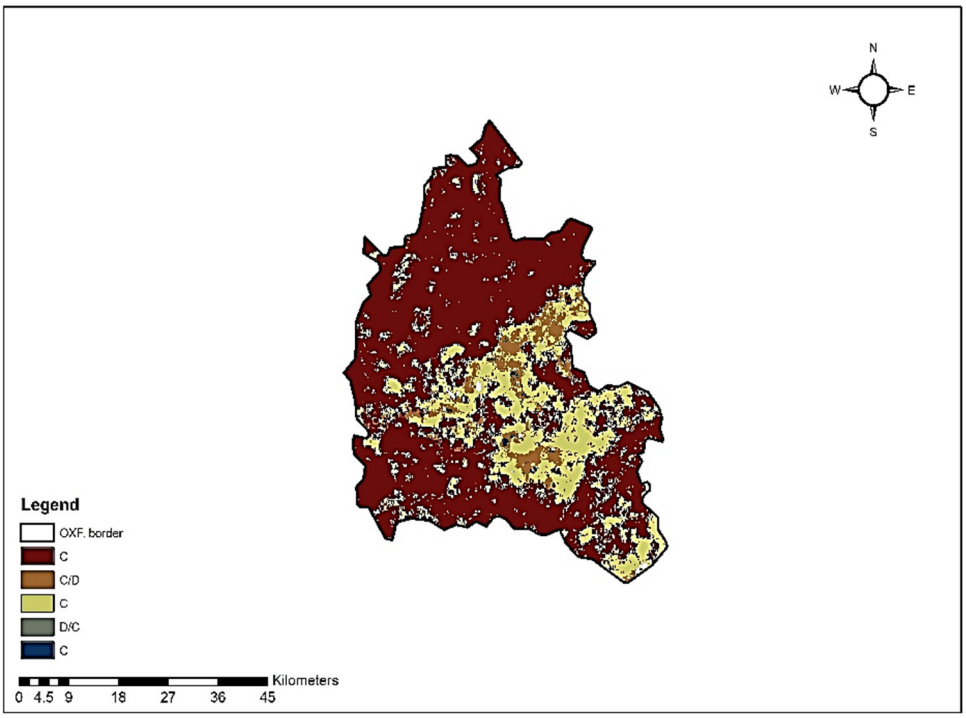


**Figure 3.18** HSGs for Oxfordshire

**Table 3.3** Soil types, runoff, and HSGs

| Soil type | Soil Group and Description |
|---|---|
| Clay | D, Highest runoff potential: Includes mostly clays |
| Clay-Loam | D, Highest runoff potential: Includes mostly clays of the high percentage, but the group also includes some shallow soils with nearly impermeable texture |
| Silty Clay Loam | D, moderately high runoff potential. |
| Sandy-Clay Loam | C, moderately high runoff potential. Comprises shallow soils and soils containing considerable clay though less than those of group D. |
| Silty-Loam | C, moderately high runoff potential |

### 3.3.3.3 Crop Data Set

Four types of data are required for using the CROPWAT 8.0 software, rainfall data, climatic data, soil data, and crop data. The rainfall and climatic data including (min. T, Max. T) for a period 1980-2010 were used and gathered for both studied sites for historical period (1980-2022) and future projection.

The all-soil data were obtained from FAO and assessed by utilizing CROPWAT 8.0 software for both studies sites. Crop data for wheat, barley and sunflower were obtained from FAO manual 56 and were added to CROPWAT software including rooting depth, crop coefficient, critical depletion, yield response factor, and length of plant growth stages and planting dates (Clarke et al, 2001).

### 3.4 Summary

This chapter described the study regions that were chosen to assess the impact of climate change on RWH. It presented the data preprocessing that is employed to prepare raw data before using it in RWH and downscaling models.

**Area of Study**

The availability and reliability of data lead to the selection of Kirkuk governorate as a case study. It is a significant governorate located in the Northern region of Iraq. Rainfall harvesting is the main water resource for agriculture as the region is well-known for crop production like winter wheat, barley, and sunflower. The next selected region was Oxford Shire County. It is a small county located in the Southeast of England in the UK. Oxfordshire county receives a good annual amount of rainfall, and this county is well-known for agriculture for main crops like Wheat, Barley, and Sunflower.

**Data Set**

This part of the chapter presented the type of data and period that will be used to identify RWH and the future prediction model over a specific period and their reliability. These variables comprise maximum temperature, minimum temperature, rainfall, and sunshine hours (i.e. these variables were used in several previous studies for the recommended baseline period of 1980-2010 for climate change assessment).

The period 1980-2022 was used for the purpose of building downscaling climate variables and evaporation models. A correlation test was applied for climate data by applying PCA and results can be found in Appendix A.

**Data Preprocessing**

This part explained the main climate data for both studied areas. For Kirkuk data were obtained from Iraqi metrological department and Ministry of agriculture for seven stations across Kirkuk. Data checked and cleaned for any missing data and reduced the noise to improve the data quality by using average adjustment techniques to maintain clean and good data and reduce errors. For Oxfordshire, data were obtained from metrological department Library for three stations. All data were checked and cleaned buy applying average adjustment techniques to remove any missing and to minimize the error. The DEMs were obtained from USGS official website as a TIF files and processed by using ArcMap software for both studied areas. The HSGs, were obtained as TIF files from FAO official website and compared to local Maps of soils in both studied areas and processed, classified according to study areas soil types of information by applying ArcMap software to obtain the final HSGs maps.

# Chapter 4: Methodology: Climate Downscaling, Integrated Models for Rainwater Harvesting, Evaporation and Crop Water Requirements

## 4.1 Introduction

This chapter outlines the research methodology used to detail the approaches taken to identify suitable rainwater harvesting site selection under climate scenarios' impact on evaporation and crop water requirements. This methodology is based on the integration and combination of multiple models and techniques together to produce the final models. The first stage involves integrating Geographic Information System (GIS) and Remote Sensing (RS) techniques with a hydrologic model using a digital elevation model (DEM) to create thematic layers. This is done to generate and estimate the curve number and runoff depth model using ArcMap 10.8.2 software. All these models and combined thematic layers were utilized by using Multi-Criteria Decision Analysis (MCDA) and applying Analytical Hierarchy Process (AHP) to identify suitable sites for RWH collection by using GIS techniques for both current and future climatic projection. The second stage involves downscaling the climate models using daily climatic data factors for the period (1980-2022). These factors were employed in statistical downscaling models to simulate future climatic data projections. Specifically, the Long Ashton Research Station Weather Generator (LARS-WG 8.0) model is applied to simulate future climate factors for four distinct periods: 2031-2050, 2051-2070, 2071-2090, and 2091-2100. These intervals (2031-2050, 2051-2070, 2071-2090, and 2091-2100) are commonly used in climate research because they capture meaningful, sequential climate patterns over time. Five General Circulation Models (GCMs) are incorporated to address the uncertainty associated with different assumptions. The use of multi-model's approach ensures a more robust and comprehensive understanding of future climatic conditions for both study regions and by applying multi-models can reduce the biases for many signal models. Models assume a certain climate sensitivity and how much the Earth's temperature will rise in response to a doubling of $CO_2$ concentrations which is one of the assumptions used in GCMs that is often incorporate assumptions about future levels of greenhouse gas

emissions based on different socio-economic scenarios for example: (low, medium, or high emissions pathways). The models showed a good performance and validation in both studied areas based on historical climatic factors that have been used to downscale the model.

The third stage is estimating the evaporation by utilizing an Artificial Neural Network (ANN) model utilizing monthly climate data for the seventh climate factor. The artificial neural network model algorithm development, evaluation, performance function, and model prediction of the pan evaporation utilizing the ANN technique are discussed in this chapter.

The fourth stage is the estimation of crop water irrigation requirements for three types of crops for both study areas by utilizing CROPWAT 8.0 software that tool developed by the (FAO). The software is a cornerstone of agricultural water management, offering precise calculations of crop water requirements derived from crop, climate, and soil data. Further details are explained in detail in this chapter. The diagrammatic presentation of the research methodology is presented in Figure 4.1.

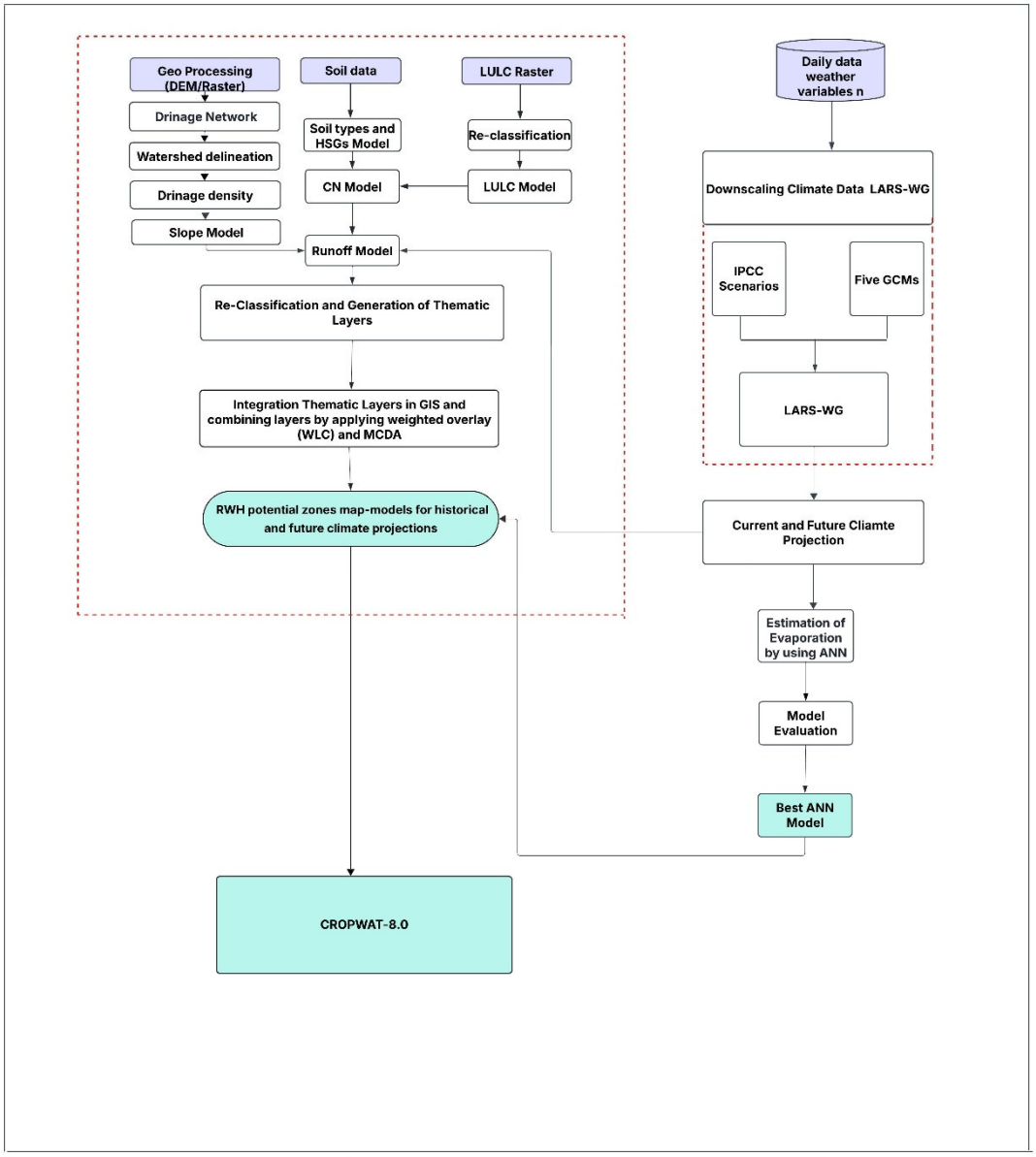


**Figure 4.1** Flow Chart Diagram of Research Methodology

## 4.2 Statistical Downscaling Technique

The statistical downscaling technique employed to simulate future climate factors in this study follows the methodology recommended by Daniels et al. (2012). Trzaska and Schnarr (2014) identified several statistical downscaling models, including the Long Ashton Research Station Weather Generator (LARS-WG), MarkSim GCM, and Nonhomogeneous Hidden Markov Models (NHMM).

However, there are significant caveats associated with both the MarkSim GCM and NHMM models. The MarkSim GCM model, for instance, struggles to accurately

project high rainfall variances. This limitation arises because the model aligns future climate projections with the most similar present climate cluster, rendering it ineffective for simulating future climates that differ significantly from current conditions. The NHMM model also presents challenges, particularly due to its reliance on hidden states, which complicates both the interpretation and the determination of the number of states required.

In contrast, the LARS-WG model has been shown to perform successfully in various regions as reported by Semenov et al. (2013). The LARS-WG model was specifically developed to study the impact of climate change by simulating daily time series data, as noted by Khalaf et al. (2022). Given its demonstrated reliability, LARS-WG (version 8.0) has been selected for use in this thesis.

LARS-WG is a stochastic model capable of statistically downscaling global climate model (GCM) data to generate synthetic weather time series at specific locations under current and future climate scenarios. It works by analysing certain statistical properties of the input observed daily weather data for the chosen site and then by using these properties, along with a pseudo-random number generator, to produce simulated weather data one day at a time. The generator specifies daily probability distributions for each weather variable and certain statistical relationships between the variables. The input observed weather data is used to determine the parameters of the probability distributions and the correlation coefficients between the variables. The parameters for each distribution are varied either on a monthly or a daily basis to express the seasonal component of each weather variable (Semenov et al., 2013).

The WG assume the assumes that the historical climate data used to calibrate the generator is stationary over the period used for model calibration. In other words, the statistical properties of weather variables (like means, variances, and covariances) are assumed to remain constant during the historical calibration period.

This study utilized LARS-WG version 8.0 to downscale precipitation projections, reducing uncertainty in climate change impact analysis. LARS-WG 8.0 incorporates coupled model intercomparison project phase 6 (CMIP6) data from the ensemble of GCMs used in the sixth Assessment Report of the. Intergovernmental Panel on Climate Change (IPCC AR6) (Al-Hasani B., 2024; Semenov et al, 2013). It has been widely tested globally and has shown skill in reproducing historical climate conditions across

diverse environments (Semenov, 2008). Climate prediction and generation scenarios for a certain future period were constructed based on a baseline parameter which is calculated from the observed weather data for Kirkuk Governorate and Oxfordshire for the period (1980-2010) and combined by using Coupled Model Intercomparison Project Phase 6 (CMIP6) used in the IPCC multi-model sixth report and included in version 8.0 of LARSE-WG. Five GCMs were selected for downscaling to drive the rainfall-runoff modeling in this study, as listed in Table 4.1.

**Table 4.1** The global climate models selected from IPCC AR6 incorporated LARS-WG 8.0

| No. | GCM (Global Climate Models) | Research Centre | Spatial resolution |
|---|---|---|---|
| 1 | CSIRO-Mk3.6.0 | Commonwealth Scientific and Industrial Research Organization | 1.8"×1.8" |
| 2 | HadGEM2-ES | Met Office Hadley Center, United Kingdom | 1.2"×1.8" |
| 3 | CanESM2 | Canadian Centre for Climate Modeling and Analysis, Canada | 2.8"×2.8" |
| 4 | MIROC5 | Atmosphere and Ocean Research Institute (The University of Tokyo), National Institute for Environmental Studies, and Japan Agency for Marine-Earth Science and Technology, Japan | 1.4"×1.4" |
| 5 | NorESM1-M | Norwegian Climate Center, Norway | 2.0"×2.0" |

The generation of synthetic weather data using the LARS-WG model can be divided into three stages:

1. Calibration: Daily historical climate data from 1980-2010 was utilized to calibrate the LARS-WG model. This calibration is achieved using the "SITE ANALYSIS" function in LARS-WG, which analyzes measured climate variables such as maximum and minimum temperature, solar radiation, and precipitation to determine their statistical characteristics. These statistical parameters are then stored in files for use in the subsequent stages of synthetic weather data generation.

2. Validation: The parameter files derived from the measured weather data during the calibration stage are then used to generate synthetic weather data with the same statistical characteristics as the original data. A statistical comparison between the historical weather data and the synthetic data generated by the LARS-WG model is conducted to verify the model's accuracy. This comparison ensures that the simulated climate data closely matches the real long-term measured distributions for the selected site. The validation process involves graphical tests based on mean and standard deviation and statistical tests such as the P-value and Kolmogorov-Smirnov (K-S) test to assess the similarity between the measured and synthetic climate data.
3. Generation: After successful calibration and validation, the LARS-WG model is ready to generate synthetic weather data based on the climate scenarios, using five different Global Climate Models (GCMs) over four future periods: 2031-2050, 2051-2070, 2071-2090 and 2091-2100. The generation process begins by selecting the first period (2031-2050) of the climatic scenario and applying the first GCM to simulate the time series for all climate factors.
4. This process is repeated for each of the five GCMs, for SSP2-4.5 and SSP5-8.5 scenarios resulting in five simulated time series for each climate factor, such as rainfall. These five-time series' ensemble means are then calculated to provide a more robust estimate.

### 4.3 Approach and Methods to Identify Suitable Sites Selection for RWH

Determining potential sites for water harvesting requires a fundamental understanding of rainfall characteristics and a detailed assessment of soil properties, topography, and land use in a particular area. Therefore, identifying suitable areas for water harvesting is a multi-objective and multi-criteria process dependent on the physical, socioeconomic, and environmental factors for the location (Oweis, 2004).

The identification of suitable sites for RWH consists of four steps as the following:

1. The appropriate selection of criteria.
2. Classification of suitability for each criterion.

3. Employing GIS, RS, and hydrologic analysis and generation of suitability maps.

4. Identification of suitable sites for RWH by utilizing MCDA and AHP.

The Food and Agriculture Organization (FAO) identifies six key factors for assessing site selection in soil and water conservation projects: climate, hydrology, topography, agronomy, soils, and socioeconomics (Kahinda et al., 2008). These criteria provide a comprehensive framework for evaluating potential sites for rainwater harvesting (RWH).

In this study, five of these factors were utilized to identify suitable RWH sites. The selection was based on a thorough review of relevant literature, expert judgment and crucially the availability of data. Following FAO's guidelines, the assessment included the following parameters:

1. Climate: Evaluated through rainfall and runoff data.
2. Hydrology: Assessed using stream-flow order.
3. Topography: Determined by analyzing the slope of the land.
4. Agronomy: Investigated through land use and cover types.
5. Soils: Evaluated based on soil texture.

While FAO emphasizes the importance of socio-economic criteria, these were not included in the current analysis due to data limitations. The socioeconomic factors such as income levels and population growth can influence the results, the primary focus of this study was on climatic and geospatial data and future projection. The exclusion of these criteria was a deliberate methodological choice aimed at isolating the direct impacts of climate factors. The climatic and geospatial data are robust enough to provide reliable estimates without the need for socioeconomic data. The objective of this research was to assess the direct climatic impacts. While socioeconomic factors could potentially influence broader outcomes, they were beyond the scope of this study, which focused on understanding climate dynamics in isolation. Future work could integrate these variables for a more comprehensive understanding. Nonetheless, the selected parameters offer a robust foundation for identifying potential RWH sites, aligning with established best practices. The criteria of the selection table can be found in Appendix B.

### 4.3.1 Rainfall

According to the Food and Agriculture Organization (FAO), rainfall is a critical factor influencing runoff amounts, especially in arid and semi-arid regions. It is recommended that the minimum average rainfall required for effective rainwater harvesting (RWH) should range between 300 and 600 mm (Zakaria et al., 2014; Oweis, 1999). However, for regions with average rainfall of 150mm, the FAO recommends micro-cathmnet areas and the effective runoff from nearby hills and slope for farming. While the the range of 750 mm, fthe FAO recommended this large scale for RWH to be stored in large pounds, earth damns or it is approprtait to store the runoff during the rainy eason in in large reservioure for sprinkle irrigation.

The rainfall data were collected and processed by using ArcMap 10.8.2 to identify suitable site selection for RWH. These local datasets were compared with NASA meteorological data, spanning 30 years from 1980 to 2022 to ensure accuracy.

To estimate rainfall distribution within the study areas, the Inverse Distance Weighting (IDW) algorithm was employed. This method is recognized for its precision in estimating rainfall distribution in locations where direct measurements are unavailable (Bashir & Fouli, 2015).

The analysis revealed that the annual average rainfall in the study area was 360 mm for the first study areas of Kirkuk governorate. In comparison, the average rainfall of the second study area of Oxford Shire was 667 mm which is within the FAO-recommended range for RWH in both semi-arid and humid regions.

### 4.3.2 Slope

The Slope is a critical factor in runoff generation, influencing sedimentation rates, water flow speed, and the volume of material needed for dam construction (e.g., dyke height) (Adham et al., 2016a). Critchley et al. (1991) advised against water harvesting in areas with slopes exceeding 5%, as these areas are prone to high erosion rates due to uneven runoff distribution, and require significant earthworks (Al-Adamat et al., 2010).To analyze the slope in the study area, a Digital Elevation Model (DEM) with a 30-meter resolution was obtained from the United States Geological Survey (USGS). This DEM was used to create a detailed slope map. Before analysis, sinks and flat

areas were corrected using ArcGIS 10.8.2, ensuring the continuity of water flow toward the catchment outlet. The slope data were then reclassified into five categories, ranging from the lowest (0 meters) to the highest (60.5 meters) for the Kirkuk study region. For the UK study region, the slope data were classified into five categories, ranging from (0 meters) to (30.8meters). These classifications were tailored to the specific topographical characteristics of both study regions, providing a foundation for the final slope model used in this assessment.

### 4.3.3 Runoff depth

Runoff depth is a crucial criterion for selecting suitable sites for rainwater harvesting (RWH), as it helps assess the potential water supply generated during runoff events. To estimate runoff depth, the Curve Number (CN) method provided by the Soil Conservation Service (SCS) was employed (Matomela et al.2020). The CN is a well-established parameter that predicts runoff potential based on the characteristics of soil and land cover.

For this study, CN values were calculated for each pixel within the study areas, using detailed land-cover and soil-texture maps. These maps allowed for precise estimation of runoff depth across the landscape. The runoff depth (Q) can be expressed as the following:

$$Q=\frac{(p-Ia)^2}{(P-Ia)+S} \quad (4.1)$$

Where Q is runoff depth (mm), *P* is precipitation (mm), *S* is potential maximum retention after the onset of runoff (mm) and *Ia* is an initial abstraction (mm) that includes all losses before the onset of runoff, infiltration, evaporation and water interception by vegetation.

Using *Ia* = 0.2S was determined by analyzing the rainfall data for many small agricultural basins (Melesse and Shih, 2002). Equation 4.1 can therefore be expressed as:

$$Q=\frac{(p-0.2S)^2}{(P+0.8S)} \quad (4.2)$$

*S* can be calculated using *CN* as:

$$S = \frac{25400}{CN} - 245 \quad (4.3)$$

Curve Numbers (CNs) are dimensionless values that range from 1 to 100, representing the runoff potential of an area. A CN of 100 indicates low rainfall infiltration and a high runoff value, while a CN of 1 suggests high rainfall infiltration and low runoff. High CNs suggest that a large proportion of rainfall will be converted to surface runoff, as Krois and Schulte (2014) noted. In this study, it was observed that the downstream areas of the watershed experienced more runoff compared to the upstream areas. This variation is likely due to differences in land cover, soil type, and slope, critical factors in determining the CN values. Table 4.2 illustrates the relationship between land cover/land use, hydrologic soil group, and the corresponding Curve Number (CN) values. These values were derived from the Hydrologic Engineering Centre and the United States Department of Agriculture (USDA). The key parameters of soils types as flow, type A: High infiltration rate, type B: moderate infiltration rate, type C: slow infiltration rate and type D: very slow infiltration rate.

**Table 4.2** The relationship between LC/LU, HSG, and the value of the (CN)

| | LU/LC | Hydrologic Soil Group (HSG) | | | |
|---|---|---|---|---|---|
| NO. | | A | B | C | D |
| 1 | Water | 100 | 100 | 100 | 100 |
| 2 | Trees | 43 | 65 | 76 | 82 |
| 3 | Grass | 30 | 58 | 71 | 78 |
| 4 | Flooded vegetarian | 68 | 79 | 86 | 89 |
| 5 | Agriculture | 67 | 77 | 83 | 87 |
| 6 | Scrub/Shrub | 36 | 60 | 73 | 79 |
| 7 | Built up area | 77 | 85 | 90 | 92 |
| 8 | Bare ground | 39 | 61 | 74 | 80 |

### 4.3.4 Soil types and texture

Soil texture plays a critical role in determining both the rate of infiltration and the amount of surface runoff. The relative proportions of sand, silt, and clay define the textural class of soil. According to White (1987), fine- and medium-textured soils are

generally more favorable for rainwater harvesting (RWH) due to their superior water retention capabilities.

Soils with high water-holding capacities are ideal for RWH (Adham et al., 2016a). Specifically, clay soils are considered optimal for water storage because of their low permeability and ability to retain harvested water. Given this, soil texture is a crucial factor when selecting a site for an RWH scheme, particularly when the goal is to conserve water for human, livestock, and agricultural uses (Al-Adamat, 2008).

The soil texture and classification into soil groups were derived from data provided by the FAO website. The model classified soils into hydrologic soil groups (HSG) based on the United States Department of Agriculture (USDA) classification system. For the study area, the soils were categorized into HSG C and D, indicating textures that include clay, clay loam, loam, and sandy loam. Table 4.3 provides a detailed classification of hydrologic soil groups according to USDA standards, alongside their corresponding soil textures.

**Table 4.3** The HSG and soil texture according to USDA classification

| Hydrologic Soil Group (HSG) | Soil Texture |
|---|---|
| A | Sand, loamy sand or sandy loam. |
| B | Silt or loam. |
| C | Sandy clay, loam |
| D | Clay loam, silt clay loam, sandy clay, silty clay, or clay |

### 4.3.5 Land cover and Land use

Land cover significantly influences the runoff generated during rainfall in a given area. Dense vegetation, for instance, tends to intercept more rainfall and promote greater infiltration, thereby reducing surface runoff (Kahinda et al., 2008). To analyze this relationship, a land cover raster for the year 2021 was acquired from the ESRI website. This raster has a spatial resolution of 10 meters, providing detailed information on the land cover types in the area of interest. Using a maximum-likelihood classification algorithm, the raster data was analyzed to categorize the land cover. This algorithm

classifies the land cover based on statistical parameters such as means, variances, and covariance matrices.

The analysis identified eight distinct types of land cover in the model:

This classification provides a detailed understanding of the land cover, which is crucial for modeling the hydrological response of the area to rainfall events:

1. Water
2. Trees
3. Grass
4. Flooded Vegetation
5. Agriculture
6. Scrub/Shrub
7. Built-up Area
8. Bare Ground

### 4.3.6 Stream Order and Drainage Density

The analysis of stream order is crucial for mapping rainwater harvesting (RWH) potential, as it directly influences the permeability and infiltration rates of an area. Generally, lower stream orders are associated with higher permeability and infiltration, making them more suitable for RWH purposes, whereas higher stream orders tend to have lower permeability.

To assess stream order, a Digital Elevation Model (DEM) was utilized, which was downloaded from the USGS website. The DEM had a spatial resolution of 30 meters, providing sufficient detail for hydrological analysis. Using ArcMap 10.8.2, various hydrological processes were applied to the DEM. These included:

- **Fill and Sink:** Prepare the DEM by eliminating depressions that could affect flow direction analysis.
- **Flow Direction and Flow Accumulation:** To determine the direction of water flow across the terrain and the accumulation of flow at different points.
- **Stream Order:** To classify streams based on their hierarchy in the watershed.

- **Drainage Density:** To calculate the density of the drainage network, which influences the runoff potential.

These hydrological tools allowed for a detailed analysis of the stream order, which is essential for identifying optimal sites for RWH.

### 4.4 GIS-RS-based MCDA analysis and generation suitability map models

Remote Sensing (RS) and Geographic Information Systems (GIS) are widely used techniques for identifying suitable sites for rainwater harvesting (RWH) (Buraihi, 2016). In this study, an integrated approach was adopted that combines RS, GIS, and hydrological data with Multi-Criteria Decision Analysis (MCDA) to evaluate parameters critical to site selection.

To determine the most suitable sites for RWH, thematic layers representing key criteria such as slope, land use/land cover, runoff, and drainage density were analyzed. Each thematic layer and its respective features were assigned weights based on their importance in rainwater collection, using Saaty's scale of 1 to 9 (Saaty, 1999). The GIS database was developed using ArcGIS software, incorporating both vector and raster datasets. A suitability model was created using a weighted overlay technique in conjunction with the Analytic Hierarchy Process (AHP) method （Saaty, 2008). ArcGIS 10.8.2 was used to implement all processes necessary for site identification, integrating GIS, RS, and hydrological analyses. The AHP-based MCDA framework involved the creation of pairwise comparison matrices to determine the relative importance of each criterion. The assigned weights were then normalized using the eigenvector method to ensure consistency. The consistency ratio for each criterion was calculated following equation (4.4) as suggested by Saaty (1999), ensuring the reliability of the weighting process.

Once the weights were assigned and validated, thematic layers were reclassified according to the calculated weights. The overlay method tool within the Spatial Analyst module of ArcMap (10.8.2) was then used to combine these layers, resulting in a final suitability map for RWH. This map highlights the zones within the study area that are most suitable for rainwater harvesting, considering all relevant criteria.

$$Consistency\ Ratio(CR) = \frac{CI}{RCI} \tag{4.4}$$

where *CI* is the consistency index and *RCI* is the random consistency index. indicated by Equation (4.5):

$$CI = \lambda max - \frac{n}{n-1} \quad (4.5)$$

n represents the number of criteria, and λmax is the major eigenvalue calculated using the eigenvector approach (factors). Saaty (1999) states that the weights should be retested if the consistency ratio (CR) value exceeds 10%.

To identify RWH-appropriate areas, all thematic layers and their normalized weights were integrated using the ArcMap software. The standardized criteria were combined using the weighted linear combination method. In this approach, each factor was multiplied by its assigned weight, and the results were then summed to derive a multi-criteria solution to identify the suitability of RWH (Chowdhury et al., 2016). Table 4.4 presents the comparative weight matrix values used to determine the best location for the study area. The following equation can calculate the suitability:

$$Suitability\ S = \Sigma\ wf\ xf \quad (4.6)$$

where *S* is the suitability, $wf$ is the weight of factor *f*, and $xf$ is the criterion score of factor *f*.

**Table 4.4** The values of the comparison weight matrix to identify suitable sites selection of RWH

| Criteria | RD | SL | ST | SO | LC |
|---|---|---|---|---|---|
| RD | 1.00 | 2.00 | 3.00 | 4.00 | 5.00 |
| SL | 0.50 | 1.00 | 2.00 | 3.00 | 4.00 |
| ST | 0.33 | 0.50 | 1.00 | 2.00 | 3.00 |
| SO | 0.25 | 0.33 | 0.50 | 1.00 | 2.00 |
| LC | 0.20 | 0.25 | 0.33 | 0.50 | 1.00 |

Where RD= Runoff depth, SL= slope, ST= soil type, SO= stream order, and LC=Lc/Lu.

For GIS and development of RWH suitable site selection model, the assumption of Land cover/Land use, soil types, slope is not changed for future projection. In this study, the assumption that land cover, soil types, and slope remain constant to limit the complexity of the model and focus on climate-driven changes. The focus of this study

is on climate-related variables. While land cover and soil types may change over time, their influence is considered secondary to the primary drivers of interest.

### 4.5Artificial Neural Network Modeling Basis (ANN)

Artificial Neural Networks (ANNs) are composed of layered structures, with Multilayer Perceptrons (MLP) being the most widely utilized type in hydrological engineering applications (Adamowski et al., 2012). These networks consist of several layers, each containing processing units known as neurons or perceptrons. The input layer, located at the front of the network, holds the effective variables pertinent to the problem at hand, while the output layer, situated at the end, represents the objective variables or the model's predictions.

Between the input and output layers lie one or more hidden layers. These hidden layers contain neurons that serve as computational units, often described as the "black box" of the network due to their role in processing and transforming the input data through complex computations. The architecture of an MLP is characterized by the connections between neurons, which are organized into a network of synaptic weights. Each of these weights signifies the strength of the connection between two neurons. A weight of zero indicates the absence of a connection, effectively isolating the neurons from each other.

Notably, connections between neurons are only formed between different layers, there are no intra-layer connections, meaning neurons within the same layer do not directly interact (Sayadi et al., 2013). This organized structure enables the network to learn patterns and make predictions based on the input data.

Each node (neuron) in the network computes an input (Ij), which is the weighted sum of the outputs (Oj) from the nodes in the preceding layer. Mathematically, this can be expressed as:

$$Ij=i\sum Wij \times Oi \tag{4.7}$$

Where: Wij represents the weight connecting node i in the previous layer to node j in the current layer.Oi is the output of node i in the preceding layer. Figure 4.2 illustrates

a classic ANN structure, providing a visual representation of this interconnected architecture.

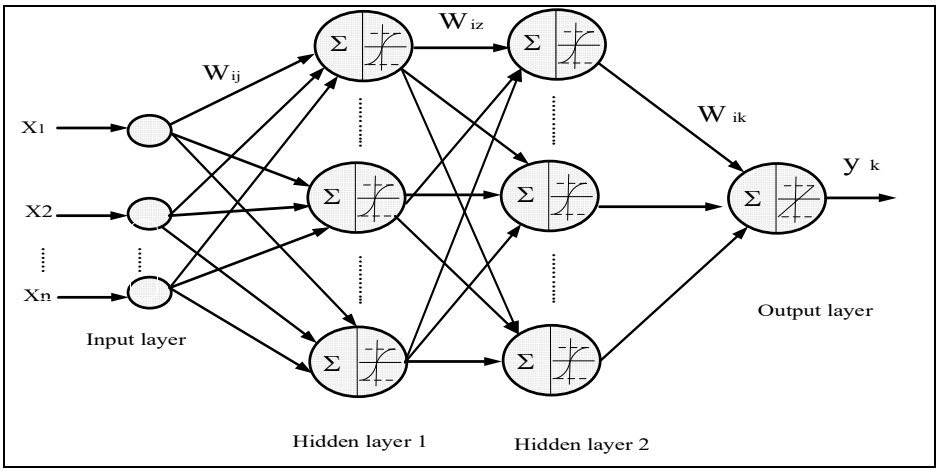


**Figure 4.2** The Classic ANN structure

A neuron in an Artificial Neural Network (ANN) is composed of several key components: input variables (which may include a bias term), synaptic weights associated with these inputs, a summation function, an activation function, and the desired output (Bennett et al., 2013). The synaptic weights are crucial as they determine the strength of the connections between the input variables and the neuron, influencing the output generated by the network.

Training an ANN involves adjusting these synaptic weights to optimize the network's performance, as Hagan et al. (2014) described. This training process typically employs algorithms that iteratively minimize the difference between the network's predicted output and target values, refining the model's ability to learn from data.

Once the learning (or optimization) phase is completed, the model's performance must be validated to ensure its robustness in simulating data or generating accurate forecasts. Kingston et al. (2005) emphasize that this validation step is crucial for confirming that the model can generalize well to new, unseen data, thereby ensuring its reliability and effectiveness in practical applications.

ANN models must be refined to overcome impediments that negatively impact prediction results. This study aims to systematically develop the ANN model to achieve improved performance. This approach involves addressing key factors,

including the activation function, ANN training and learning rate, data division, stopping criteria, and model optimization (Araghinejad, 2014; Hagan et al., 2014).

### 4.5.1 Activation Function

The activation (or transfer) function is used to transform the activation level of a neuron, converting the input summation into an output signal that typically falls within either [0, 1] or [-1, 1], depending on the specific transfer function used. This transformation enables the network to effectively map nonlinear processes (Bennett et al., 2013). According to Jain et al. (2001), the transfer function is generally assumed to be continuous, differentiable, and bounded both above and below. Hagan et al. (2014) noted that the hyperbolic tangent, sigmoid, and linear activation functions are commonly utilized in neural network (NN) models. Typically, the linear activation function is applied in the output layer, while nonlinear activation functions are used in the hidden layers. The input layer, however, does not contain an activation function. It's important to note that noise can adversely affect the performance of activation functions.

In this study, to understand how climate variables influence water consumption, two types of activation functions were employed. The tansigmoidal activation function was used in the hidden layers to account for the full range of negative input values, while the output layer utilized the linear activation function to accommodate the positive values of water demand. Araghinejad (2014) presented the tansigmoidal and linear activation functions as the following equations, respectively.

$$f(x) = \left(\frac{2}{1 + e^{-\alpha x}}\right) - 1 \quad \alpha > 0 \tag{4.8}$$

$$f(x) = x \tag{4.9}$$

### 4.5.2 ANN Training and Learning Rate

The learning rate is a crucial hyperparameter in the training of artificial neural networks (ANNs). It determines the step size at each iteration while moving toward a minimum of the loss function. In essence, the learning rate controls how much to adjust the weights of the network concerning the gradient of the loss function.

Hagan et al. (2014) stated that the learning rate coefficient is a factor used to preserve the learning speed by significantly altering the size of the steps taken in weight space from one cycle to another. It helps prevent the learning process from being trapped at a local minimum instead of reaching the global minimum. Typically, the learning rate coefficient remains constant during the learning process. A small learning rate value will slow the training; in contrast, a large value may cause unstable weights (W) that oscillate around the optimal value (Basheer and Hajmeer, 2000).

Many researchers, such as Jain et al. (2001), Bougadis et al. (2005), and Adamowski et al. (2008), have utilized the trial-and-error technique, which is unsystematic, to locate the optimum learning coefficients.

Choosing the appropriate learning rate is critical. If the learning rate is too small, the training process will be slow. If it is too large, the weights may oscillate, preventing convergence. To mitigate oscillations while using a larger learning rate, a momentum term can be introduced Hagan et al. (2014). This term makes the weight change dependent not only on the current gradient but also on the previous weight change. The update rule with momentum can be expressed as:

$$\Delta wt = -\eta \frac{\partial E}{\partial wt} + \alpha \Delta wt - 1 \qquad (4.10)$$

where: Δwt is the change in weight at iteration t, η is the learning rate, $\frac{\partial E}{\partial wt}$ is the gradient of the error concerning the weight, α is the momentum factor, which determines the influence of the previous weight change Δwt−1.

Training a neural network involves adjusting the interconnecting weights to minimize the overall training error, which is the difference between the network's calculated and desired outputs.

1. Rescaling of Data: Before training, input data is rescaled to ensure that all features receive equal attention. In this study, the data was rescaled to the interval [−1,1].
2. Parameter Vector: The network parameters, including weights and biases, are denoted by a vector.
3. Error Estimator: The error during training is measured using the Sum of Squared Errors (SSE), a common error metric that quantifies the discrepancy between the predicted and actual outputs.

### 4.5.3 Data Division

Data division is a crucial step in the development of an Artificial Neural Network (ANN) model. The available data is typically divided into three subsets: training, testing, and validation. The training data is used to adjust the network's weights, while the testing data assesses the network's performance at various stages of training. The validation data is essential for evaluating the model's generalization capability (Basheer and Hajmeer, 2000).

The training set must be sufficiently large to represent the data and ensure accurate and effective learning. All three data sets, training, testing, and validation, must represent the overall data, as ANNs cannot extrapolate beyond the range of data used during training. Consequently, if the validation data contains values outside the range of the training data, the model may produce poor forecasts (Maier and Dandy, 2000). This study divided the data into training, testing, and validation sets of 70%, 15%, and 15%, respectively.

In this research study, the Artificial Neural Network (ANN) technique has been utilized to predict evaporation, incorporating climatic variables as key model inputs. Critical components of the ANN architecture, such as the number of neurons in the hidden layers and the learning rate coefficient, play a pivotal role in the model's performance. These factors are essential for accurately mapping the relationship

between the input and output variables, ensuring the effective development of the ANN model. Additionally, they help the model avoid becoming trapped in local minima, thereby enhancing its predictive accuracy and robustness. In this study two layers were applied and five population sizes of neurons: 5, 10, 15, 20, 25 to let each algorithm determine the population that could attain the minimal fitness function value. The fitness function for optimising the model minimising was the root-mean-squared error (Wang et al., 2010).

### 4.5.4 Support Vector Machines

SVM is a powerful tool that has been extensively applied to both classification and regression tasks due to its robustness and effectiveness. SVM is not only useful for classification but also highly effective in regression problems, where it is referred to as Support Vector Regression (SVR). The key idea behind SVM is to find a function that best fits the data while maintaining a balance between model complexity and prediction accuracy. This balance is achieved by minimizing a loss function subject to certain constraints, ensuring that the predictions are as accurate as possible while avoiding overfitting (Sadia, 2023). The SVM regression function can be expressed as:

$$f(x) = w.\phi(x) + b \tag{4.11}$$

Where: $w$ is the weight vector that defines the orientation of the hyperplane in the transformed feature space and $\phi(x)$ is a non-linear function that maps the input vector x into a higher-dimensional space, allowing the model to handle non-linear relationships in the data. While $b$ is the bias term that adjusts the output to align with the target values. The objective of SVM in regression is to find the optimal weight vector $w$ and bias $b$ that minimize the prediction error while satisfying the margin constraints. The model tries to fit the best possible hyperplane (or line, in the case of linear regression) that lies within a predefined margin of tolerance for error. This model was developed by using MATLAB software version 23.

### 4.5.5 Model Evaluation and Validation

After calibrating all the model structures using the calibration/training dataset, their performance was evaluated based on several standard statistical criteria. These criteria are essential for quantifying the errors associated with model predictions, providing a

clear measure of prediction accuracy (Adamowski, 2008). The assessment of prediction errors is crucial, as it significantly influences the selection of suitable models and offers insights that can guide adjustments to existing models, aiming to minimize deviations in future predictions (Donkor et al., 2014). Several statistical parameters will be applied in the model's calibration such as Mean Absolute Error (MAE), Mean Squared Error (MSE), Root Mean Squared Error (RMSE), and Correlation Coefficient (R). These indicators are defined in Equations. (4.12) through (4.15).

$$MAE = \frac{\sum_{m=1}^{N}|x_o - x_p|}{N} \tag{4.12}$$

$$MSE = \frac{\sum_{m=1}^{N}(x_o - x_p)^2}{N} \tag{4.13}$$

$$RMSE = \sqrt{\frac{\sum_{m=1}^{N}(x_o - x_p)^2}{N}} \tag{4.14}$$

$$R = \left[\frac{\sum_{m=1}^{N}(x_o - \overline{x_o})(x_p - \overline{x_p})}{\sqrt{\sum(x_o - \overline{x_o})^2 \sum(x_p - \overline{x_p})^2}}\right] \tag{4.15}$$

Where $x_o$= observed water consumption, $x_p$= predicted water demand, N= sample size, $\overline{x_p}$= mean of predicted demand, and $\overline{x_o}$= mean of observed consumption.

To estimating future evaporation, the projected climates from the downscale model have been employed on ANN, and it is assumed that the model parameters (weights, number of ANN neurons) are constant in the future.

### 4.6 Crop Water Requirements

Crop water requirements were estimated by utilizing CROPWAT 8.0 software, the adaptable CROPWAT software (8.0) has proven to be a valuable tool for precisely estimating the referenced evapotranspiration ($ET_0$), crop evapotranspiration (ETc), and irrigation water requirements across a variety of crops. Its effectiveness in this regard

was emphasized by Moseki et al. (2019), who highlighted its successful implementation in a variety of agricultural scenarios.

CROPWAT 8.0, an esteemed software tool developed by the (FAO), is a cornerstone of agricultural water management, offering precise calculations of crop water requirements derived from crop, climate, and soil data (CROPWAT, 2023). Central to its functionality is the estimation of reference evapotranspiration (*ET0*) using the rigorous Penman-Monteith method, as shown in Equation 4.16. To perform *ET0* computations, CROPWAT 8.0 necessitates essential relative humidity, wind speed, and sunshine hours specific to designated climate stations. The crop coefficient (*Kc*) plays a pivotal role in delineating crop developmental stages, serving as a multiplier in the calculation of crop evapotranspiration (*ETc*) alongside (*ET0*), as delineated in Equation 4.17. Moreover, this study incorporated effective rainfall (*Re*) determination, employing the USDA Soil Conservation Service method, as demonstrated in Equation 4.18 (Schaefer et al., 2007).

Furthermore, CROPWAT 8.0 facilitates the calculation of the net irrigation water requirement (NIWR) by deducting Re from *ETc,* as represented in Equation 4.19. This comprehensive approach allows users to ascertain the gross irrigation water requirement (GIWR) in liters per second per hectare, computed using Equation 4.20, based on user-defined soil and crop patterns.

$$ETo = 0.408\Delta\,(Rn - G) + \frac{\frac{900\,\gamma\,U_2(es-ea)}{T+273}}{\gamma(1 + 0.34\,U_2)} \tag{4.16}$$

*ET0* represents the reference evapotranspiration (mm/day), Rn represents the net radiation of the surface crop (MJ.m²/day), and G is the soil heat flux density (MJ/m ²/day). T is the average daily air temperature at 2 m level height, while $U_2$ is the wind speed at 2-meter height (m/s) and es represents the mean saturation vapor pressure (Kpa) while ea is the actual vapor pressure (Kpa), Δ is the slope of saturation vapor pressure curve (KPa/◦C), and γ is the psychrometric constant (KPa/◦C).

$$ETc = ETo \times Kc \tag{4.17}$$

where $ETc$ represents the crop evapotranspiration (mm/day), $ET0$ is the reference evapotranspiration (mm/day), and $Kc$ refers to crop coefficient and it is dimensionless.

$$Re = \frac{R(125-0.2R)}{125} \quad \text{for R} \leq 250 \text{ mm}$$
$$Re = 125 + 0.1R \quad \text{for R} > 250 \text{ mm} \tag{4.18}$$

where $Re$ represents the effective rainfall, and $R$ represents the total rainfall in (mm). The net irrigation water requirement can be calculated using the following equation (4.19):

$$NIWR = ETc - Re \tag{4.19}$$

The gross irrigation water requirements were calculated using Equation 4.20.

$$GIWR = (NIWR + Lr)/Ea \times 100 \tag{4.20}$$

$NIWR$ represents net irrigation water requirements in mm, $Ea$ is the efficiency of application and $Lr$ is the leaching requirements in mm that can be calculated using the following equation 4.21:

$$Lr = f \times NIWR \tag{4.21}$$

as $f$ ranges from 5-12% depending on soil salinity availability.

For purpose of climate change assessment, crop water requirements have been estimated for the reference period (1980-2010) and the projected periods P1 (2031-2050), P2(2051-2070), P3(2071-2090) from downscaling climate models using five Global Circulation Models (GCMs) for both study regions. However, it is assumed that all parameters for the equations used in the calculation are assumed to be constant in the future. Three types of crops were selected for both study regions: Wheat, Barely, and Sunflower.

### 4.7 Summary

This chapter described the methodology to investigate the extent of identifying suitable sites for RWH under the impact of climate change and the influences on crop water requirements. The chapter covered the steps of the research methodology to meet the objectives set out in chapter one based on the literature review of current and previous studies on the GIS, RS, and MCDA, and identifying suitable site selection of RWH.

The utilizing weather downscaling as mentioned in this chapter. Also explained the evaporation techniques by employing ANN, computational intelligence algorithm, and estimation of crop water requirements.

Geographic Information System and utilizing MCDA to identify RWH

Utilizing GIS and remote sensing techniques to identify suitable sites for RWH by combining multiple models and employing multi-criteria decision analysis as an effective methodology. This section explained the procedure and techniques used to select the suitable sites for RWH according to multiple criteria combined to produce the final model. Several studies previously utilized this technique but never considered the impact of climate change. The section explains the methods and techniques that have been used to select suitable sites and the effect of main criteria such as rainfall, soil types, slope, LCLU, and runoff and how to combine these criteria and layers to produce the final model by using GIS, and RS technology.

Weather Downscaling

This section discussed the methodology adopted for weather downscaling. The statistical downscaling approach was employed in this study to simulate future climate variables. Several studies have recommended using the Long Ashton Research Station Weather Generator (LARS-WG) model. Five GCMs were applied to reduce the uncertainty for the climate projection considering two scenarios SSP2-4.5 and SSp5-8.5. Daily data for maximum temperature, minimum temperature, rainfall and solar radiation, which are supported by the LARS-WG model, over the period 1980-2010 were employed.

Artificial Neural Network (ANN)

Several studies recommended using ANN to predict evaporation because it can map the non-linear relation between evaporation and climate factors, and it is also appropriate for long-term prediction.

This section presented a short background about ANN and explored the main components: model architecture, activation function, learning rate, data division, stopping criteria, and model optimization (training and validation). It also discussed its strengths, and how to select better choices.

Crop Water Requirements (CWR)

This section explained the estimation of crop water requirements and water irrigation requirements by employing CROPWAT 8.0. This effective application developed by FAO and utilizing climate data such as rainfall, minimum temperature, maximum temperature, and sunshine hours to estimate the crop water demand under both periods one is as a reference point and for future projection for three main types of crops.

# Chapter 5: Results and Discussion

## 5.1 Introduction

This chapter describes the results and discussion of the thesis, which are divided into four main stages:

The first stage is to simulate future climate factors by utilizing the Long Ashton Research Station Weather Generator (LARS-WG) to downscale models. In addition, five General Circulation Models (GCMs), daily data of climate factors for the baseline period 1980-2010 and of the Intergovernmental Panel on Climate Change (IPCC AR6) scenarios.

The second stage is developing the rainwater harvesting suitable site selection models for historical and future projection of rainfall data by integrating multiple models for both study areas and the implementation focuses on preparing the thematic layer's models by using GIS, RS, and MCDA techniques with a combination of hydrologic model analysis to prepare the multiple models by analysing the raw data that have been obtained from official websites to prepare the main layers after processing and re-classifying the data by using ArcMap 10.8.2 Software to identify the suitable site selection of RWH.

The third stage is estimating the evaporation by employing Artificial Neural Network (ANN) techniques for both studied regions using Neural Network and Support Vector Machine Algorithm (SVM) by employing MATLAB 2023a.

The fourth stage is to estimates the crop water requirements for three types of crops using FAO's CROPWAT 8.0 software under climate change scenarios.

## 5.2 Model Downscale and Future Projection for Kirkuk Study Area

### 5.2.1 LARS-WG Model Calibration and Validation

The model was developed by using LARS-WG 8.0, utilizing daily historical meteorological data for model validation and calibration of the base line period (1980-2010). This involved incorporating data on CO2 levels to generate and validate the necessary files for the upcoming site analysis phase, yielding three distinct site variable files for the study region. These files are categorized into three types:

The data is divided into three files: wgx, stx, and tst. The wgx file contains information about the study region, the stx file provides statistical outcomes, and the tst file compiles statistics for both observed and generated data to facilitate comparison.

Two statistical criteria test and graphics comparisons between observed and synthetic weather data generated by the LARS-WG model were adopted for maximum temperature (Tmax), minimum temperature (T min), rainfall (Rain), and solar radiation (Radi) to assess how well the model performs.

The Kolmogorov-Smirnov (K-S) test was used to assess whether the distributions of daily climate factors from measured and simulated data were statistically equivalent. A p-value was employed to determine whether to accept or reject the hypothesis that both data sets (observed and simulated) originate from the same distribution. A high p-value, paired with a low K-S statistic, indicates that the simulated climate closely resembles the observed climate, supporting the acceptance of the hypothesis (Semenov et al., 2013). Semenov et al. (2013) further recommended using a p-value threshold of 0.01 for greater accuracy, rather than the conventional 0.05, to increase the reliability of the results.

In Table 5.1, an evaluation and validation of the model's performance in simulating seasonal precipitation variations, both in wet and dry conditions. Table 5.2 presents the results of the statistical analysis for model performance in simulating the monthly Tmax., T min., Rain and solar radiation observed from the data. The seasons were defined in Table 5.1 as DJF represents (December, January and February), the MAM represents (March, April and May), while JJA represents (June, July and August) and SON represents (September, October and November). It can be seen from the assessment results in the table that the model's performance in simulating the distribution of the daily Tmax, T min., and solar radiation is perfect while rainfall is not perfectly good in some seasons, especially in summer due to dry and no rainfall during summer season (June, July and August). That can affect the amount of precipitation in future and can be decrease due to dry season during the summer.

**Table 5.1.** K-S test for seasonal wet/dry serious distribution

| Season | Wet/Dry | N | K-S | P-value | Assessment |
|---|---|---|---|---|---|
| DJF | Wet | 12 | 0.062 | 1.0 | Perfect fit |
| | Dry | 12 | 0.069 | 1.0 | Perfect fit |
| MAM | Wet | 12 | 0.053 | 1.0 | Perfect fit |
| | Dry | 12 | 0.205 | 0.745 | Good fit |
| JJA | Wet | 12 | 0.957 | 0.0 | Poor fit |
| | Dry | 12 | 0.137 | 0.971 | Very good fit |
| SON | Wet | 12 | 0.135 | 0.976 | Very good fit |
| | Dry | 12 | 0.072 | 1.0 | Perfect fit |

**Table 5.2:** K-S test for monthly wet/dry serious distribution

| | **Daily Rainfall distributions** | | **Daily T. Max. distributions** | | **Daily T. Min.** | | **Daily solar radiation** | |
|---|---|---|---|---|---|---|---|---|
| Month | K-S | Pvalue | K-S | Pvalue | K-S | Pvalue | K-S | Pvalue |
| J | 0.045 | 1 | 0.053 | 1 | 0.054 | 1 | 0.044 | 1 |
| F | 0.052 | 1 | 0.058 | 1 | 0.057 | 1 | 0.0 | 1 |
| M | 0.064 | 1 | 0.054 | 1 | 0.054 | 1 | 0.044 | 1 |
| A | 0.081 | 1 | 0.051 | 1 | 0.058 | 1 | 0.043 | 1 |
| M | 0.783 | 1 | 0.081 | 1 | 0.058 | 1 | 0.044 | 1 |
| J | 0.048 | 0.0 | 0.055 | 1 | 0.058 | 1 | 0.044 | 1 |
| J | No precip | No precip | 0.059 | 1 | 0.054 | 1 | 0.044 | 1 |
| A | No precip | No precip | 0.056 | 1 | 0.057 | 1 | 0.0 | 1 |
| S | 0.281 | 0.278 | 0.051 | 1 | 0.044 | 1 | 0.044 | 1 |
| O | 0.033 | 1 | 0.041 | 1 | 0.044 | 1 | 0.044 | 1 |
| N | 0.262 | 1 | 0.00 | 1 | 0.053 | 1 | 0.044 | 1 |
| D | 0.281 | 1 | 0.01 | 1 | 0.053 | 1 | 0.044 | 1 |

In addition to the statistical parameters that contain the mean and standard deviation for observed and synthetic data, as shown in Figure 5.18, it is evident that the model successfully captures the behavior of the three variables: maximum temperature (Tmax), minimum temperature (Tmin.), rainfall (Precipitation), and solar radiation.

The figure illustrates that the model achieves an almost accurate fit for maximum, minimum, and SSH as the synthetic data closely matches the observed data for these variables. While the precipitation model shows differences and fluctuations between observed and generated data as shown in Figure 5.1. The LARS-WG model demonstrates adequate performance in replicating observed values of maximum temperature (Tmax), (Tmin.), rainfall (Precipitation), and solar radiation in this study,

highlighting its suitability for this region. This reliable performance underscores the model's capability to simulate climate variables effectively in this specific setting.

Comparable successes with the LARS-WG model in generating climate factors have been reported globally, as Al-Hasani et al. (2024) and Khalaf et al. (2022) noted. These findings increase confidence in the suitability of this downscaling model for the study.

With the model validated for current conditions, it is now prepared to simulate future daily data for Tmax, Tmin, Rain, and solar radiation. This simulation will utilize five General Circulation Models (GCMs) and encompass the IPCC (AR6) scenarios across four future periods: 2031-2050, 2051-2070, 2071-2090, and 2091-2100. The following section will provide insights into the anticipated outcomes based on these projections.

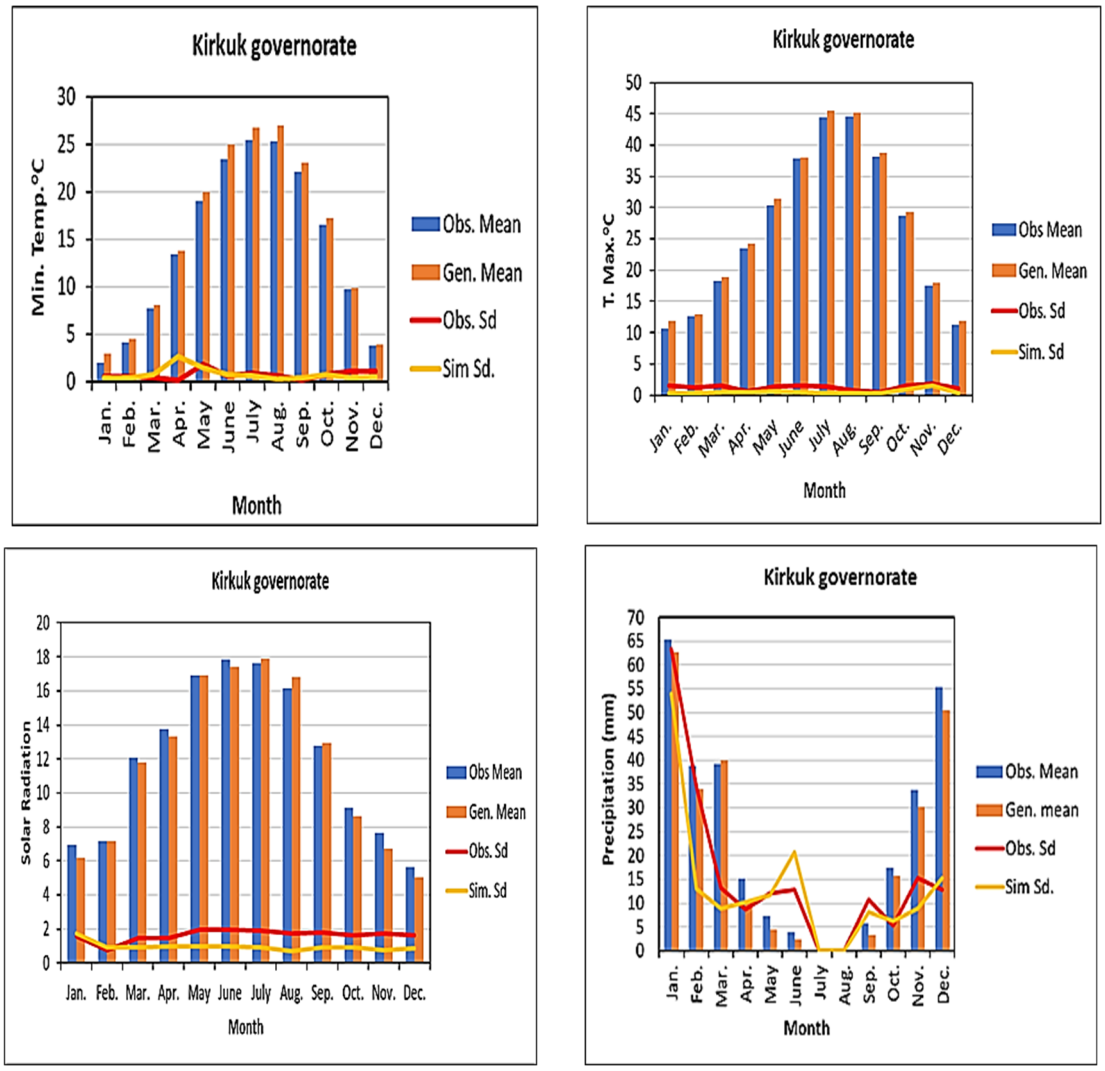


**Figure 5.1:** Calibration and Validation of the LARS-WG

### 5.2.2 Projection of Future Climate Factors

Following the calibration and validation of the LARS-WG model, it was employed to simulate future daily data for maximum temperature (Tmax), minimum temperature (Tmin), precipitation (Rainfall), and solar radiation across three distinct periods: 2031-2050, 2051-2070, 2071-2090 and 2091-2100. These projections were generated based on two emissions scenarios, represented in Shared Socioeconomic Pathways (SSPs) including SSP2-4.5 and SPP5-8.5 and these scenarios were developed to provide a more comprehensive framework for analyzing how societal choices impact emissions, climate adaptation, and mitigation efforts. as outlined in the IPCC's Special Report on Emissions Scenarios (SRES). Each scenario represents a unique pathway of greenhouse gas emissions and corresponding climate response.

The simulations incorporated data from five General Circulation Models (GCMs), providing a diverse range of potential future climates. This approach enhances the projections' robustness, as each GCM reflects varying model structures and parameterizations. Table 4.1 in Chapter 4 details the specific GCMs utilized in this analysis. By examining multiple GCMs across these timeframes and scenarios, the study aims to capture the uncertainties and variations in future climate patterns, offering insights into potential daily changes in temperature, precipitation, and solar radiation.

The comparison results of observed and the projected average monthly precipitation, maximum temperature, minimum temperature, and solar radiation forecasting data for all GCMs, under the SPP2-4.5 and SPP5-8.5 scenarios and their ensemble mean under climate scenarios over (2031-2050, 2051-2070, 2071-2091 and 2091-2100) periods are plotted in Figure 5.2. For precipitation patterns, all projected values for GCMs throughout (2031-2100) fluctuated and got lesser compared to observed values for the study region specifically in the SSP5-8.5 scenario.

**SSP2-4.5** **SSP5-8.5**

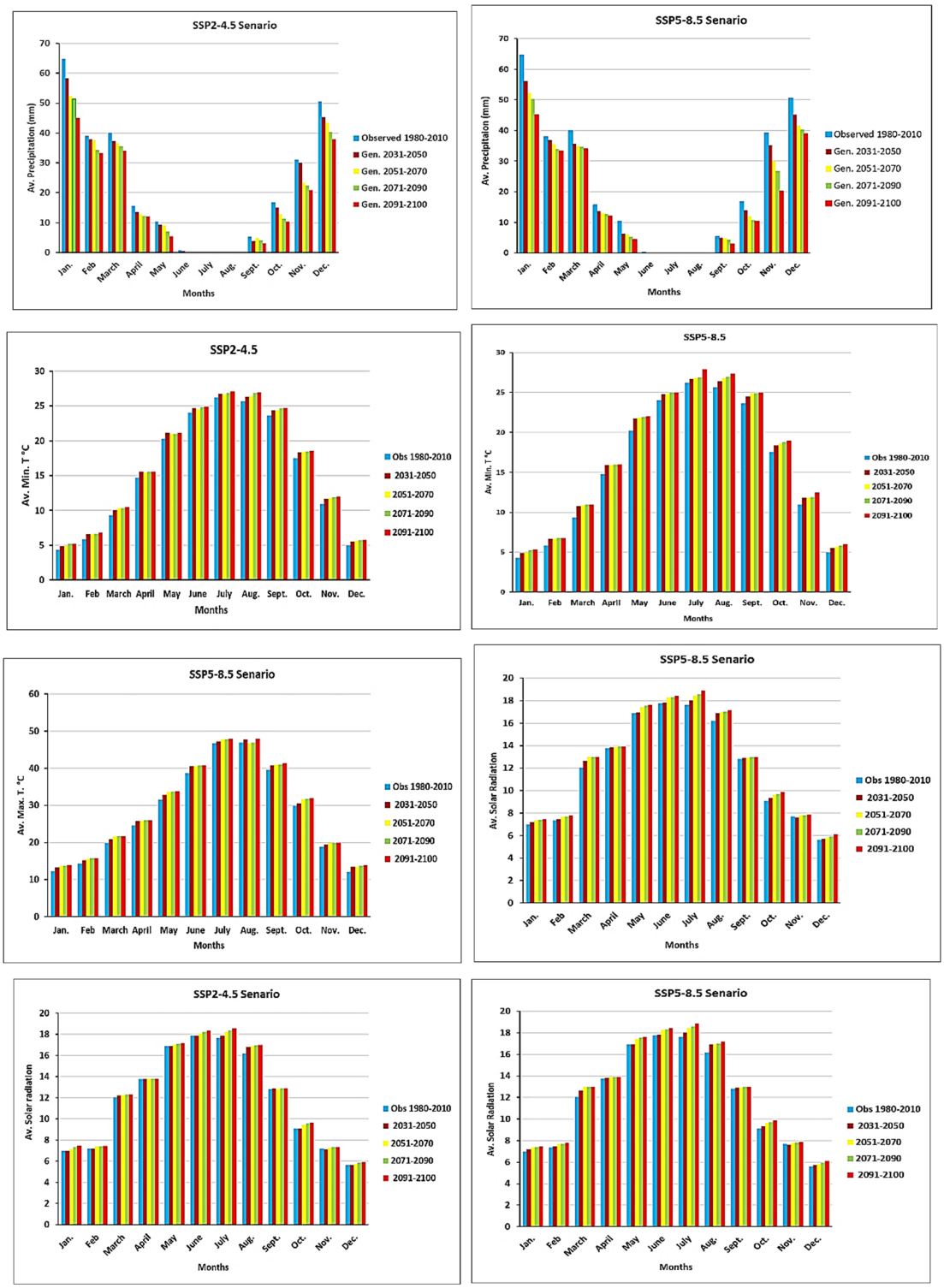


**Figure 5.2.** The Comparison Between Average Monthly Observed and Projected Values under SSP2-4.5 and SSP5-8.5

The minimum and maximum average temperatures show an increase in values through the periods for all GCMs, especially in June, July, August, and September, effect on the SSP5-8.5 scenario is larger than in the SSP2-4.5 scenario as shown in Figure 15.

Average solar radiation showed increasing values for SSp2-4.5 and SSp5-8.5 scenarios and during May, June, July, August, and September for all GCMs compared to the observed values for the Kirkuk study area.

The biggest average change percentage of precipitation under the SSP2-4.5 decreased during January and the values were (6.25, 12.34, 13.38 and 14.61%) for the periods (2031-2050), (2051-2070), (2071-2090) and 2091-2100 respectively. While December and November recorded a decrease in precipitation percentage and the highest values were 10.31 and 12.86 % for periods 2071-2090 and 2091-2100 respectively. For SSP5-8.5 scenario the highest decrease in precipitation percentage was for January for all periods, and the values were 7.52, 13.43, 14.38 and 15.61 % for periods (2031-2100). The second highest decrease was in November and December as the highest values were 10.67 and 12.89 % for periods 2071-2090 and 2091-2100 while for November were 9.76 and 10.25% for periods respectively. The change percent in temperature also increased under SSP2-4.5 and the highest increase was in January, and February for winter season and the values were (14.58 and 15.71 % for periods 2071-2090) and 11.96 and 12.4% for February for same period of time. The summer season also showed an increase in projected min. T specifically in July and August as it reached 17. 97 and 18. 4 % for the periods 2071-2090 and 1091-2100 respectively. Max. temperature also showed an increase in values and the highest change rates were in January and February, the values were 15.79 and 12.79% for periods (2071-2100). Also, August and July showed an increase in percentage and the values were 20, 22.4 % for periods 2071-2090 and 2091-2100 respectively. The max. T also increased under SSP5-8.5 and the highest values were in January and February. The sunshine hours showed a steady values and little increase under both scenarios. Figure 5.3 depicts the change in percentage for precipitation, Min, Max. T and SSH under SSP2-4.5 and SSP5-8.5 scenarios.

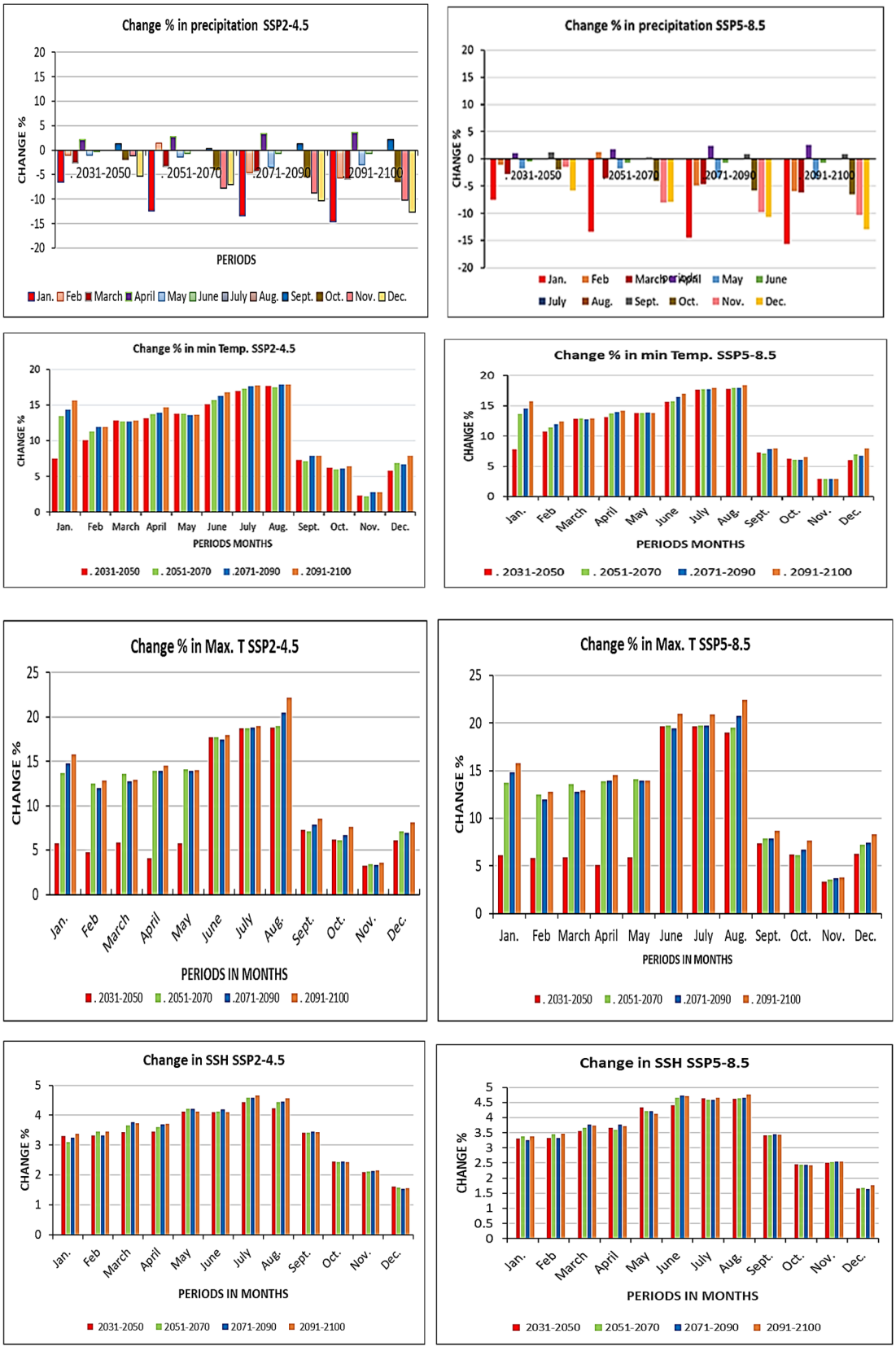


**Figure 5.3** The Change Percentage of Projected Climate Factors

Figure 5.4 depicts the differences in average values of GCM projections for the periods (2031-2050, 2051-2070, and 2091-2100) under the two scenarios (SPP2-4.5 and SSP5-

8.5). Five GCMs were employed to predict and project four climate factors (Max. T, Min. T, precipitation, and solar radiation), as explained in Chapter 4, Table 4.1 The average monthly differences for scenario SPP2-4.5 are better than those for scenario SPP5-8.5. For average precipitation for CanESM2, the average monthly projected value was 58.84 mm for the period (2031-2050) and it is the highest in all GCMs while it was the lowest in the NorESM1-M model and equals 41.676 mm. While in the CSIRO-MK36 model, the monthly projected average precipitation was 56.89 mm close to the CanESM2 model. The HadGEM2-ES and MIROC5 had very close values of monthly average rainfall and were equal to 50.47 and 49.44 mm respectively. The period (2051-2070) for all GCMs showed declining in average monthly projected precipitation specifically for the NorESM1-M model, which equals 42.323 mm. In comparison, the CanESM2 modal showed the highest value equal to 53.75mm. HadGEM2-ES and MIROC5 models were close in values and equal to 47.7 and 46.366 mm respectively. CSIRO-MK36 model had a value of 51.77 mm. All models showed the minimum values for average projected precipitation (2081-2100) compared to previous periods. The highest was equal to 52.61mm for the CanESM2 model and the lowest was equal to 41.676mm for the NorESM1-M model, while HadGEM2-ES and MIROC5 had a small difference, and the values were 45.1mm and 44.123 m respectively. For the SSP5-8.5 scenario, all models showed a sharp decline in average projected monthly precipitation, as for the CanESM2 model the values of average precipitation were 55.84, 50.75, and 49.01 mm for periods (2031-2050, 2051-2070, 2071-2091 and 2091-2100) respectively. The average values for precipitation for the CSIRO-MK36 model showed a decline as they were 53.89, 48.77, and 47.79 mm for periods (2031-2050, 2051-2070, and 2081-2100) respectively. For HadGEM2-ES, MIROC5, and NorESM1-M GC model the average values declined as the lowest was 41 mm for the period (2091-2100) while it was 45.1 and 42.123 mm for HadGEM2-ES and MIROC5 for periods (2081-2100) respectively. While for HadGEM2-ES, MIROC5, and NorESM1-M the values were 51.47, 47.7, 45.44, 43.366, 44.812, and 42.323 mm for periods (2031-2050, 2051-2070) respectively. It is clear that the average monthly precipitation is declining through the two scenarios, and it is getting more declaimed in the SSP5-8.5 scenario. The simulated average minimum temperature for both scenarios showed an increase for all periods as the minimum value was 19.732 °C in the CanESM2 model for the period (2031-2050) while the maximum value reached 21.85 °C for the NorESM1-M model under SSP2-4.5

scenario. For CSIRO-MK36, HadGEM2-ES, and MIROC5 global climate models the average monthly temperature values increased, and the values were (19.811, 19.851, 19.96, 20.19, 20.491, 20.61, 20.822, 21.24 and21.48 °C) respectively for the period (2031-2100). Under the Scenario of SPP5-8.5, the minimum average temperature showed an increasing value during all periods specifically (2081-2100) as the values for all GCMs were very high and reached (19.97, 19.99, 20.91, 21 78, and 21.99 °C) for the (CanESM2, CSIRO-MK36, HadGEM2-ES, MIROC5, and NorESM1-M) respectively.

The maximum average temperature indicated an increase in values for both climate scenarios. The highest values were under NorESM1-M global climate model and showed an increasing value of (31.425, 31.665, and 31.746 °C from 2081 to 2100) under the SSP2-4.5 scenario. While under SSP5-8.5 the average maximum temperature values were higher and indicated 31.95, 31.995, and 32.5 °C under the same period and climate model. While the other GCMs showed an increase in maximum temperature, especially CSIRO-MK36, HadGEM2-ES, MIROC5, and NorESM1-M, the values were 30.68, 31.038, 31.661, and 32.5°C under the SSP5-8.5 scenario respectively. Figure 20 depicts all the differences in maximum temperature values for all GCMs.

The SSH average values showed slightly increasing values for SSP2-4.5 and SSP5-8.5 scenarios and the highest values were under NorESM1-M global climate model as the values were (13.1583, 13.23, 13.43, 13.1593,13.43 and 13.53 for the period 2081-2100) respectively while other GCMs were slightly increased as shown in Figure 5.20.

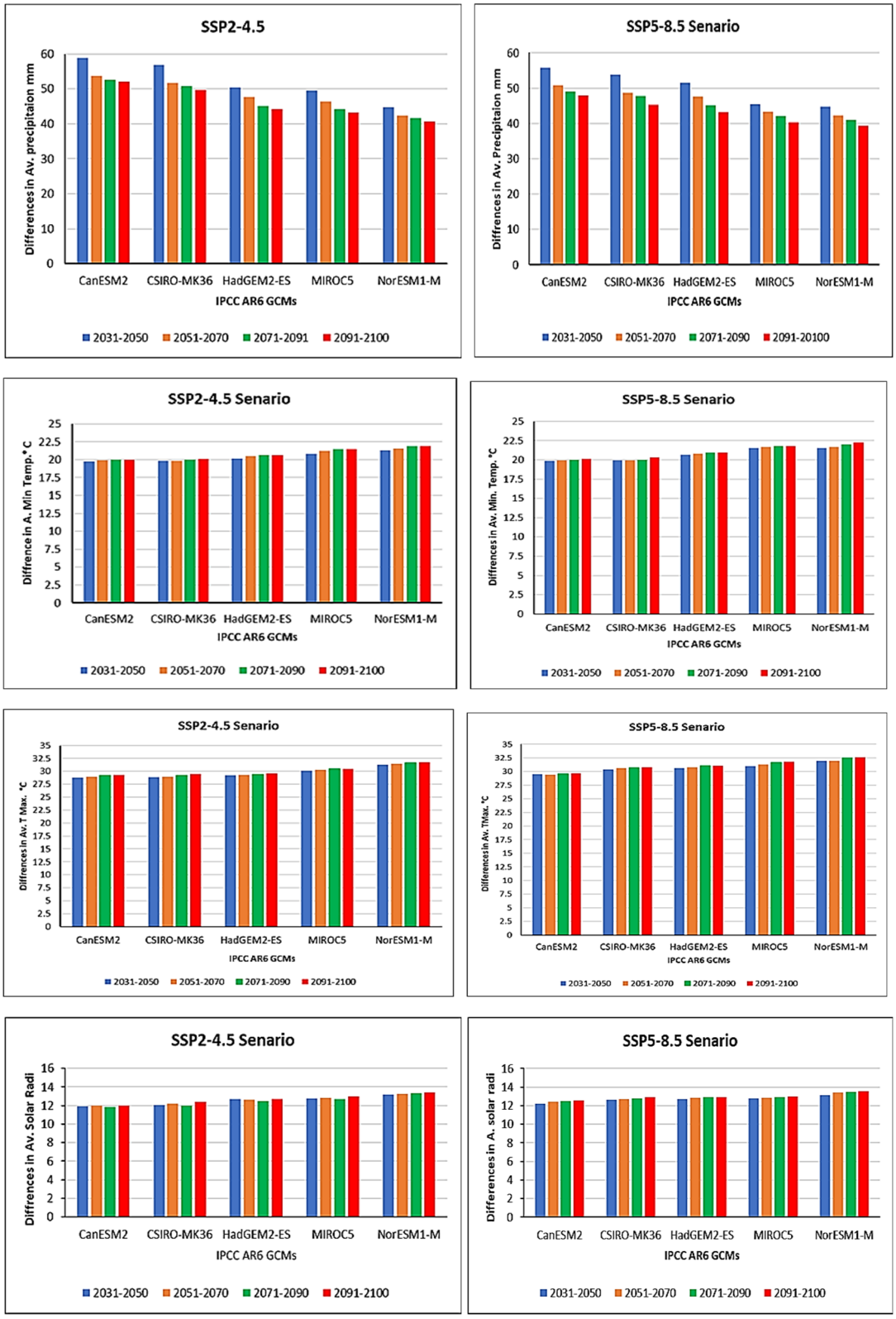


**Figure 5.4** The Differences in Monthly Average Values of Precipitation, T. Max, T. Min, and Solar Radiation under SSP2-4.5 and SSP5-8.5 Scenarios for the Period (2031-2100).

Figure 5.5 shows the percentage change in each GCMs under SSP5-8.5 and SSP5-8.5 scenarios. For precipitation percent under SSp2-4.5, CSIRO-MK36 and HadGEM2-ES global climate models have same percentage of 21%, while MIROC5 and

NorESM1-M have same percent of 18%. The only difference in CanESM2 and the percentage is 22%.

For Min. T, CanESM2 and CSIRO-MK36 have the same percentage of 19% and they are similar. While MIROC5 and NorESM1-M have the same percentage of 21%. The only different GCM is HadGEM2-ES and has 20%. For SSP2-4.5, CSIRO-MK36, HadGEM2-ES and MIROC5 have same percentage of change of 20%. CanESM2 and NorESM1-M have different percentage of 20 and 20% respectively. For Max. T CSIRO-MK36, HadGEM2-ES and MIROC5 have 20% of change while CanESM2and MIROC5 and NorESM1-M have 19, 20 and 21% respectively and are different. CSIRO-MK36, HadGEM2-ES and MIROC5 have same percentage of 20% and similar while CanESM2 and NorESM1-M have 19 and 21% respectively. The GCMs for sunshine hours did not show big differences. Figure 5.6 depicts the different between GCMs in percentage.

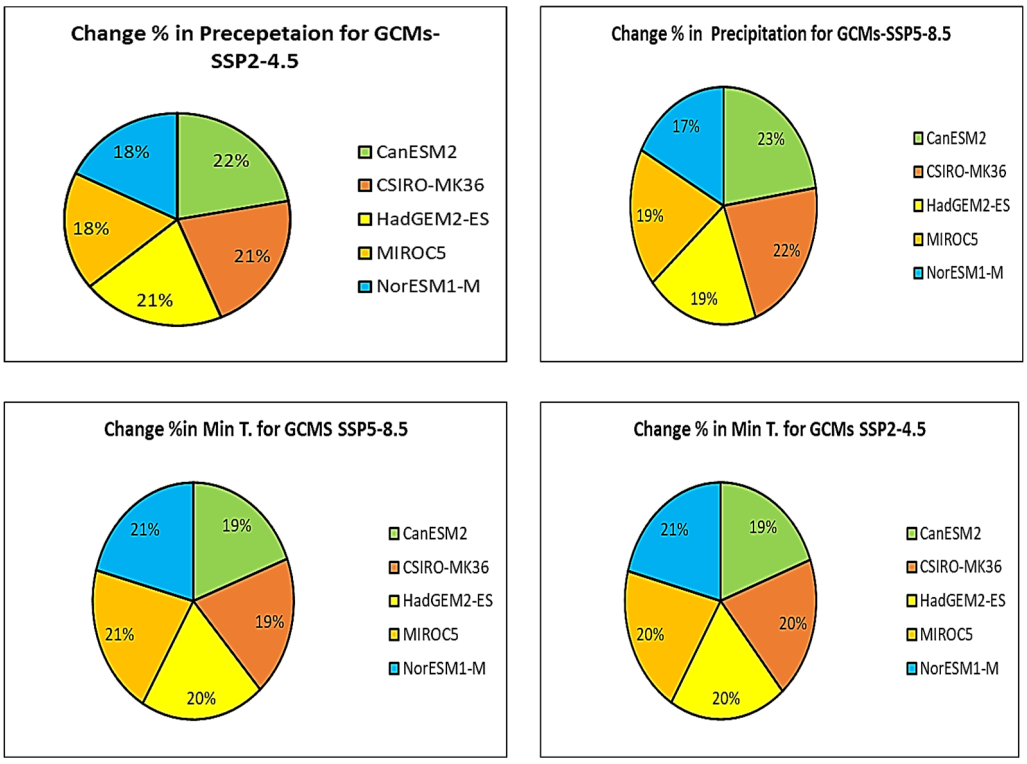

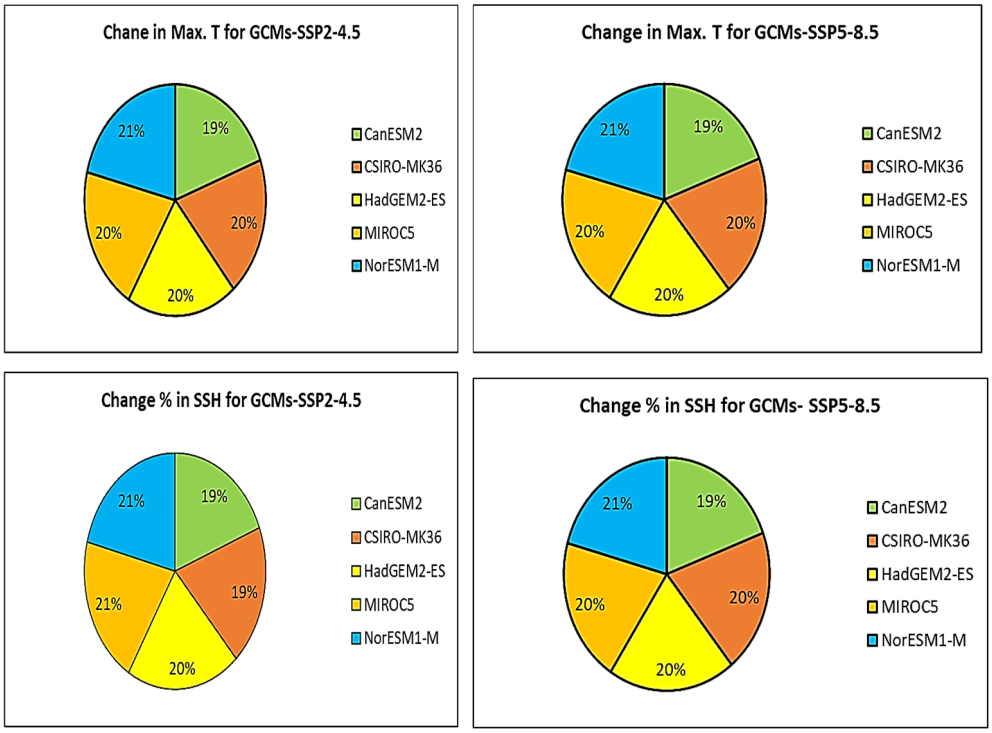


**Figure 5.5** The Difference Percentage Between GCMs

### 5.3 Thematic Layers' Preparation for Identifying RWH Suitable Sites Selection

In this study, several thematic layers were selected to identify suitable sites for Rainwater Harvesting (RWH), based on the availability of data. The following key criteria were used to determine these sites: runoff depth, drainage density, soil texture and group, slope, and land use and land cover (LULC). Among these, runoff depth is the primary factor responsible for generating runoff water. However, drainage density is also crucial in determining RWH suitability (Ramakrishnan et al., 2009).

According to previous studies, land slope significantly influences RWH potential: as slope decreases, the suitability for RWH increases, and vice versa. Soil type remains a key factor in RWH planning. Maps depicting soil types provide essential information about an area's infiltration characteristics and soil texture, which are vital for effective water retention (Mahmoud and Tang, 2015).

Furthermore, LULC is important in surface runoff generation (Kumar et al., 2008). Different LULC categories such as bare soil, farmland, grassland, water bodies, and built-up areas have distinct impacts on runoff depth and the calculation of Curve Numbers (CNs), essential for estimating runoff potential.

### 5.3.1 Input Data and Thematic Layers Analysis for Identifying RWH for Kirkuk Site

#### 5.3.1.1 Historical Rainfall Analysis and Spatial Distribution

The Food and Agriculture Organization (FAO) emphasizes that rainfall is a pivotal factor significantly impacting runoff, particularly in arid and semi-arid regions. For effective rainwater harvesting (RWH) in such areas, the FAO recommends a minimum average annual rainfall ranging from 300 to 600 mm (Zakaria et al., 2012; Oweis, 1999).

Rainfall is related to uncertainty, and probability distributions formally and quantitatively describe the pattern of uncertainty. As shown in Figure 5.1, the mean monthly recorded rainfall data were subjected to a distribution of probability tests using the Anderson-Darling test to remove uncertainties. Figure 5.6 shows skewness in some spots and changes in the spatial pattern of rainfall. The skewness of rainfall data started from 0-30% due to fluctuation in rainfall in the study area. While data above 30% shows better distribution. The rainfall data were cross-referenced with NASA Power Project data and the Ministry of Agriculture in Iraq to minimize any inaccuracy and check missing data and consistency. The rainfall data were checked and cleaned by applying the adjacent average formula which was explained in chapter three previously. Figure 5.9 provides a visual representation of the historical annual average precipitation model in the Governorate of Kirkuk over 42 years. This figure was produced by using ArcMap 10.8.2 software. By applying inverse distance weighting (IDW) to the annual average precipitation, the distribution of precipitation across the study province was calculated and validated. This precipitation map vividly depicts the spatial distribution of rainfall across the first study region.

In this visual representation, high precipitation values are prominently concentrated in the central and western regions of the research area, while lower values are clustered in the northeast. The data from Figure 5.7 indicates that the maximum recorded precipitation value was 490 mm, whereas the minimum recorded was 270 mm.

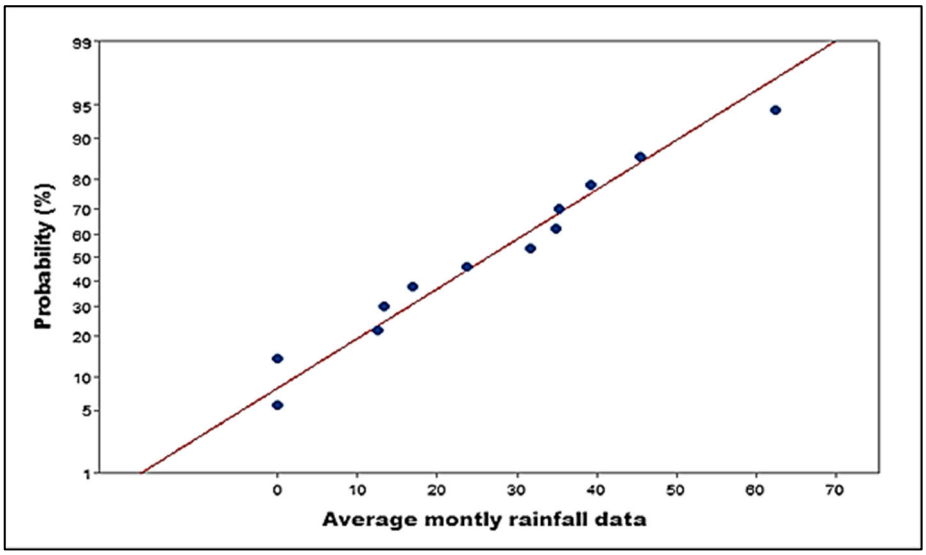


**Figure 5.6** The Probability Percent of Rainfall Data

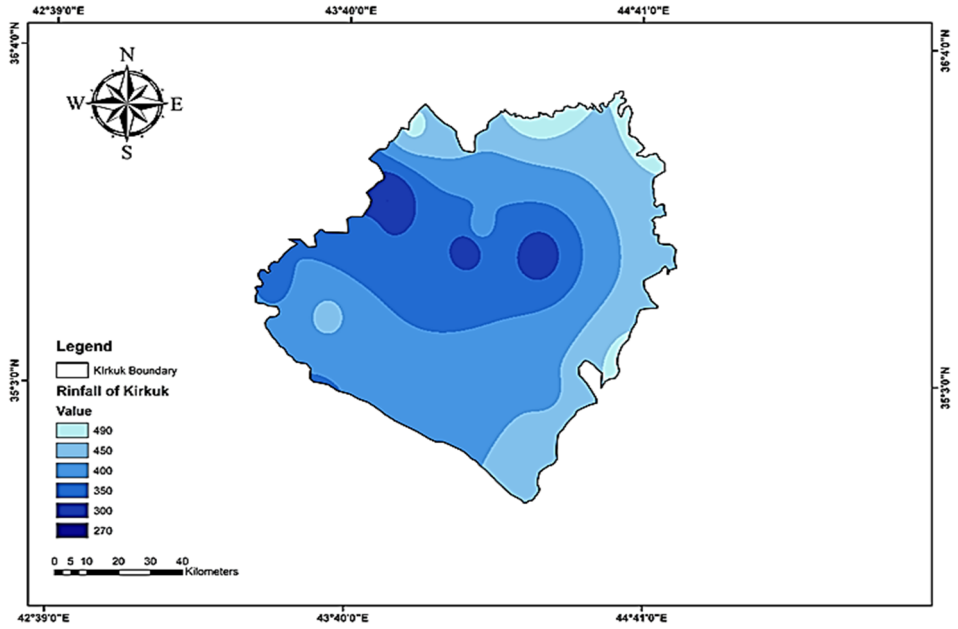


**Figure 5. 7** The Historical Average Precipitation of Kirkuk

### 5.3.1.2 Land use/Land cover model

The land cover within a specific region plays a significant role in influencing the runoff generated by raindrops. Vegetation with higher density exhibits superior interception and infiltration rates, ultimately resulting in reduced runoff (Sameer et al., 2023).

To better understand the dynamics, a maximum-likelihood algorithm technique was utilized to classify the means, variances, and covariance of a land cover raster for the year 2021. This analysis was conducted at a spatial resolution of 10 meters. The land cover was categorized into eight distinct classes, including water, trees, grass, flooded

vegetation, agricultural land, scrub/shrub, built-up areas, and bare terrain. The reclassification of these categories culminated in the creation of the final land cover model. The LC/LU model shows that the agriculture area is the most dominate part in the study area, then the scrub/shrub area. The built-up area is limited to the central of the site and there is a small part of trees and grass covering the site and water body lies in the northwest part. For a visual representation of the land cover and land use within the study region, as shown in Figure 5.8.

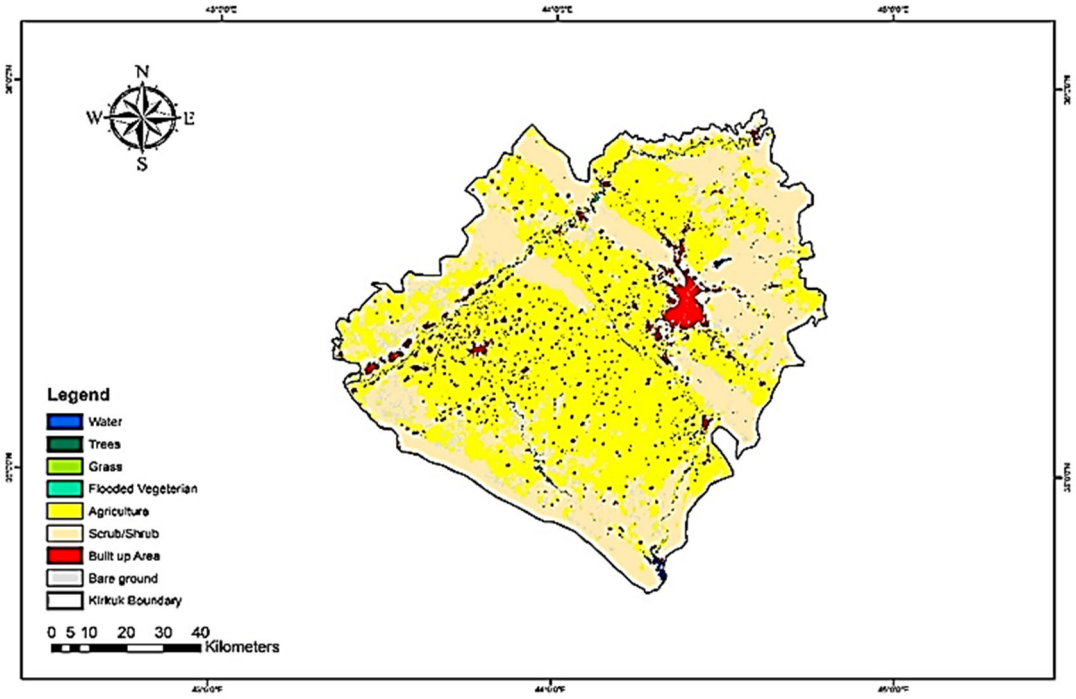


**Figure 5.8** Land use/Land cover of Kirkuk

### 5.3.1.3 Slope Model

The slope model map was constructed using elevation data sourced from a Digital Elevation Model (DEM) with a resolution of 30m × 30ms that was explained in Chapter 3 as DEM was obtained from USGS as a TIF file and processed by utilizing ArcMap 10.8.2 to produce the final model. The slope values were determined within a specified parameter range by employing a filtering technique. Subsequently, a classification process is implemented to identify potential sites suitable for rainwater harvesting (RWH). The slope model was divided into five categories: (0-1.5%) is low, (1.5-2.5%) is mild, (2.5-3.5%) is moderate, (3.5-4.5%) is sharp, and (4.5-60%) is very sharp. Among these classifications, the "low level" and "gentle level" categories are

particularly conducive to RWH, which was uncovered in a substantial portion of the study region. The highest or sharp parts dominant to the northern part of the study area while the further heading to the west south the slope is less and 0-2.5. To provide a visual representation, the Figure 5.9 visually portrays the slope model across the study region within Kirkuk governorate.

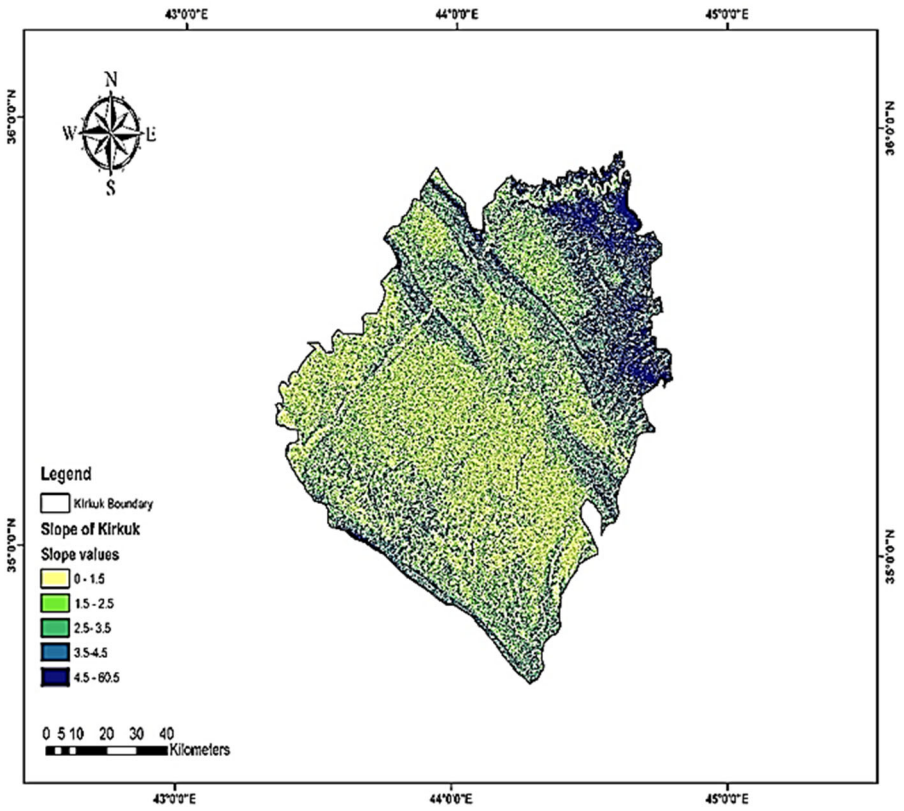


**Figure 5.9** Slope Model of Kirkuk

### 5.3.1.4 Stream Order and Drainage Density Models

The stream order map was prepared through digitization and subsequent reclassification of drainage using ArcMap software. The stream order layer spans from 1 to 6, as visually illustrated in Figure 5.10. Remarkably, (Ammar et al. 2016) propose that higher stream orders are indicative of enhanced suitability for RWH locations. The drainage density within the studied region has been classified into five distinct categories: "very poor," covering an area of 5.34 km²; "poor," spanning around 8.79 km²; "moderately good," encompassing 12.71 km²; "good," occupying 10.03 km², and "very good," with a coverage of 4.75 km². Figure 5.11 visually represents the dominant drainage density groups across provinces. Within this context, the predominant groups were categorized as "moderately good" and "good," which dominate the study area. A

smaller area is covered by the "very good" classification. Conversely, the "very poor" category predominantly encompasses the edges of the study region, while the "poor" classification extends from both the edges and into the interior of the study area.

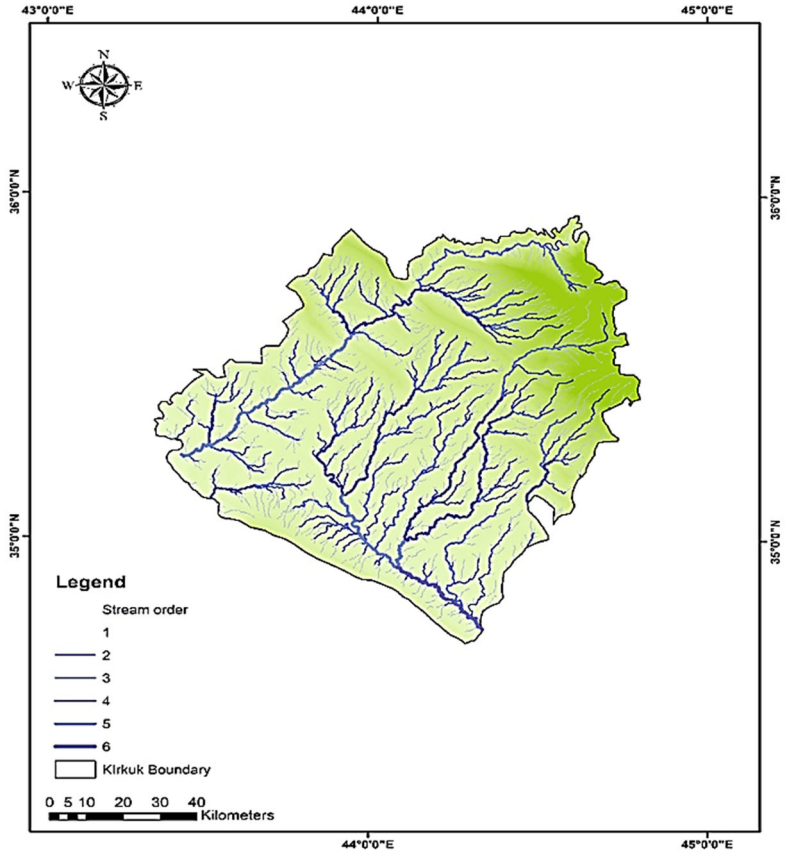


**Figure 5.10** Stream Order of Kirkuk

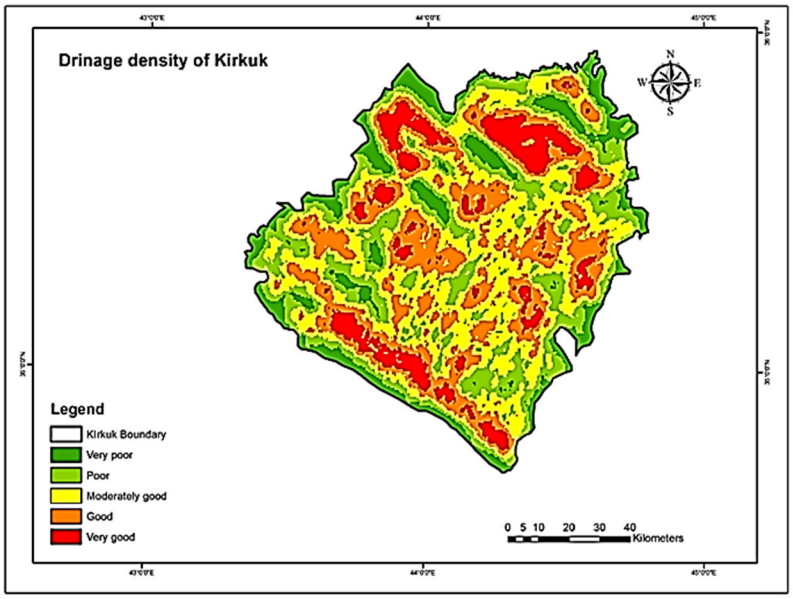


**Figure 5.11**. Drainage Density of Kirkuk

### 5.3.1.5 Hydrologic Soil Groups (HSGs)

The soil texture within Kirkuk Province is divided into two primary types: clay loam and clay. This classification corresponded to two Hydrologic Soil Groups (HSGs), C and, D based on the soil data specific to the study area of Kirkuk governorate as shown in Figure 5.12. Based on the analysis of the study area, it is evident that the predominant soil group, designated Group C, extends over a substantial portion of the landscape and exhibits widespread distribution across the study region. In contrast, soil Group D was confined to smaller patches in the study area. The convergence of climate, hydrology, topography, soil composition, agronomic factors, and land cover/land use (LCLU) renders the research region notably favorable for water retention and substantial generation of runoff, rendering it suitable for the establishment of rainwater harvesting (RWH) zones. This assessment is based on pivotal criteria that warrant meticulous consideration.


**Figure 5.12.** Hydrologic Soil Groups (HSGs) of Kirkuk

### 5.3.1.6 Runoff Potential Depth

Utilizing ArcGIS software, all thematic layers of Hydrologic Soil Groups (HSGs) and land use/cover underwent processing and analysis, culminating in the generation of the curve number model *CN*. This model was constructed based on the standardized values

assigned to each land use/cover category, coupled with the appropriate *CN* value corresponding to the HSG type. The *CN* grid values for the Kirkuk study region were derived using these processes, as illustrated in Figure 8. The computed values ranged from 70 to a maximum mean of 100. A higher *CN* value indicates a reduced infiltration potential and elevated runoff volume, whereas a lower value reflects the opposite scenario. These computations and illustrations were executed using ArcMap software 10.8.2. Figure 5.13 shows CN grid values.

By integrating *CN* grid values with the corresponding land use/cover for each polygon, the application of pixel values was enabled to generate the Rainwater Harvesting (RWH) potential map. This process facilitates the computation of runoff, which subsequently contributes to the construction of the model. A spectrum of five runoff classifications per year was established: "very poor" (190 mm), "poor" (200–250 mm), "moderate" (290–340 mm), "good" (350–400 mm), and "very good" (>400 mm).

The watershed area features locations with "very good" to "moderate" moderate' potential for runoff. This distribution is evident in Figure 5.14 which illustrates the yearly runoff depth model values in millimetres for the Kirkuk governorate. Figure 5.15 shows the validation and correlation and $R^2$ value equals to 95.42 which reflects a good model for rainfall-runoff. The estimated watershed volume is about $8\times10^5$ $m^{3.}$

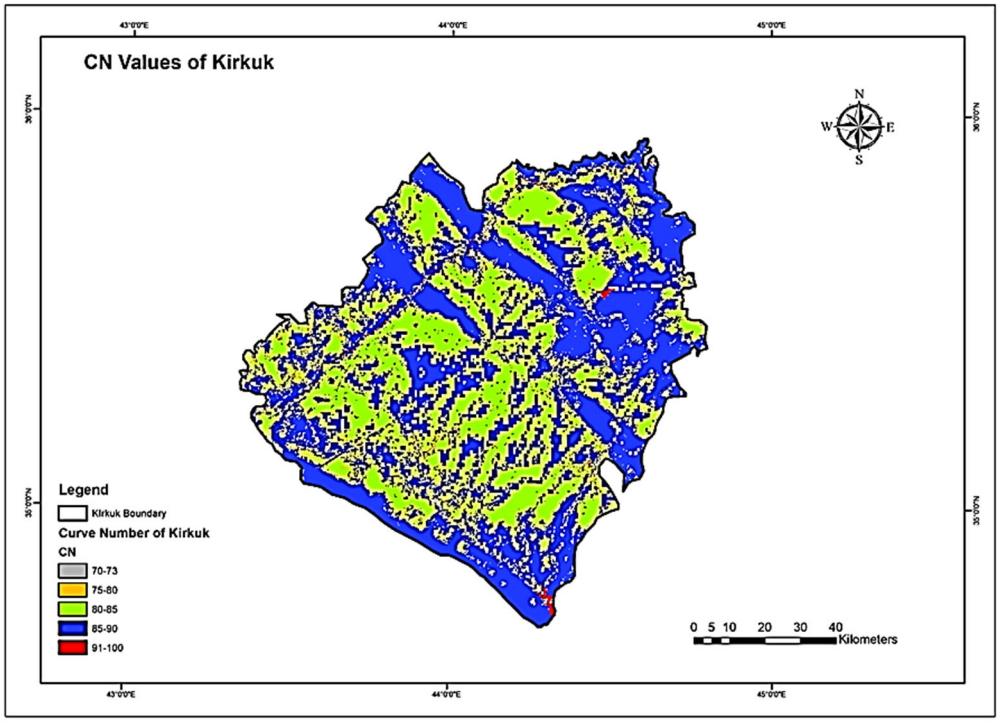


**Figure 5.13** *CN* Grid Values of Kirkuk

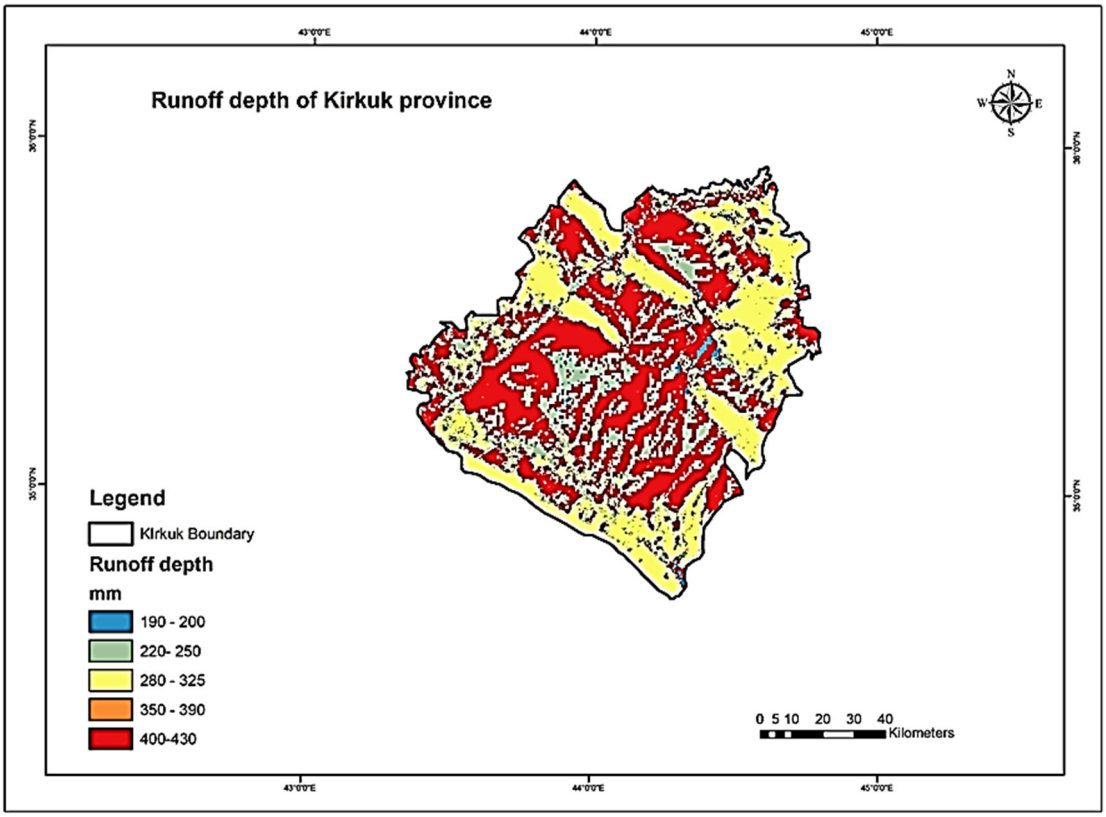


**Figure 5.14.** Runoff Depth of Kirkuk

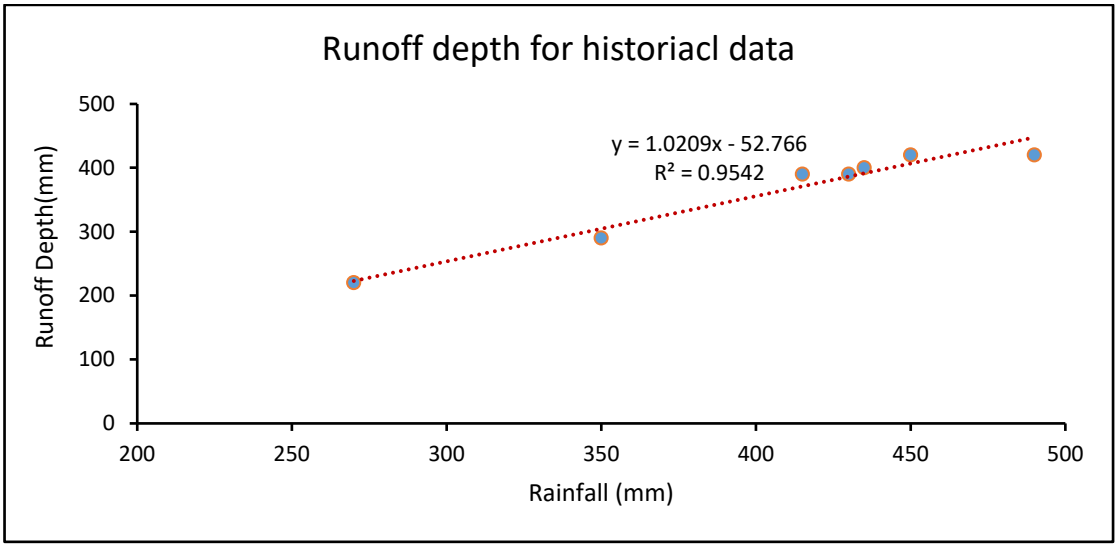


**Figure 5.15.** The Validation of Rainfall-Runoff

#### 5.3.1.7 Sensitivity Analysis

The literature extensively covers several methodologies for sensitivity analysis in geographic information systems, including GIS-MCDA (Hani et al., 2023). One prominent technique involves the reassignment of criterion values, a method employed in the current investigation. In this approach, we systematically adjust the weights of the criteria and explore variations through increments of both +10% and -10%. This deliberate manipulation allowed us to assess the impact of the dynamic interlinkages between the selected criteria. By undertaking this sensitivity analysis, we gain valuable insights into the robustness of our decision-making process, helping us understand how changes in criterion weights influence the overall outcomes of GIS-MCDA. To derive the updated equations for the suitability analysis, we employed a systematic adjustment of the weights assigned to each parameter within the five criteria outlined in our methodology. Each parameter's weight is incrementally increased by 10% in one trial and decreased by 10% in another, ensuring that the total sum of weights in the equation remains constant at one hundred. In each trial, the suitability analysis model was recalculated, allowing us to separate the impact of the individual layers (criteria) on the overall modeling results.

This iterative process, altering the weights of the criteria, positions the sensitivity analysis to treat weights as the primary source of uncertainty. The focus is on a one-dimensional sensitivity analysis if variations in weights significantly influence the model outcomes. The results of this sensitivity analysis can be found in Appendix A2.

#### 5.3.1.8 RWH Potential Site Map Model for Historical and Future Projection

The RWH potential map model for the study area was developed by integrating multiple thematic levels, including drainage density, rainfall, soil texture, land use/cover, slope, and runoff. This integration was facilitated using ArcMap 10.8.2, as shown in Figure 5.12. The ability of each theme layer and its characteristics to collect rainfall efficiently were assessed. Following this assessment, the weights attributed to each thematic layer, along with their essential characteristics, were determined. Pairwise comparison matrices were created using Saaty's Analytic Hierarchy Process (AHP) method (Saaty, 1999). Subsequently, the provided weights were normalized using the eigenvector technique. This process ascertained the consistency of the

weights assigned to each thematic layer and their respective characteristics. Consistency ratios were evaluated using equation (4.6) in the chapter of methodology previously.

The weight of each layer was calculated, and it was clear that the runoff depth had a main effect of 42% of the weight, while the slope had approximately 26% of the effectiveness on the layers, and soil texture had 16% of the total effectiveness weights; hence, stream order and land cover/use had 10% and 6%, respectively. Figure 5.17shows the effective weight percentage distribution according to thematic layer characteristics. Figure 5.16 shows the weight percentages of each thematic layer.

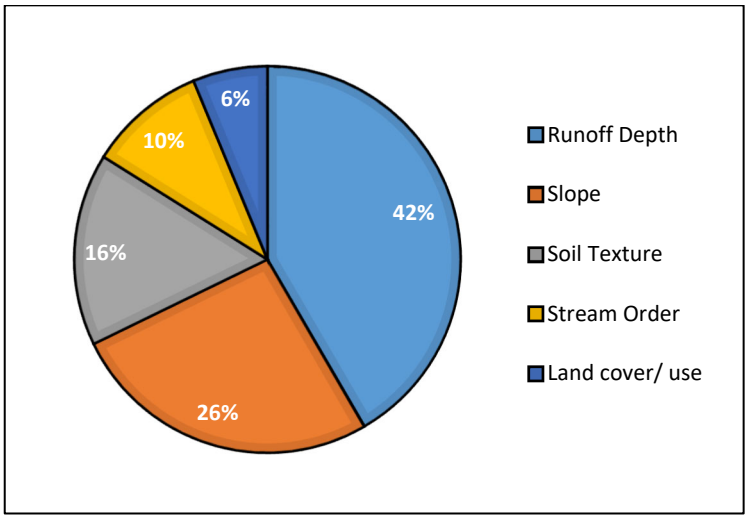


**Figure 5.16.** Percentage Weights of Each Thematic Layer

According to Saaty (1999), the optimal threshold for consistency ratio (CR) values should be less than 10%. If CR exceeds this threshold, reassessment of the weights is warranted. In this case, the CR was below the 10% limit, specifically 0.05. This outcome underscores the reliability of the weight-allocation process for RWH potential mapping. Based on the RWH potential map, four distinct suitability regions can be delineated: (a) Low Suitability: Encompassing approximately 31.8% of the area, (b) Medium Suitability: Spanning around 37.4% of the region, (c) High Suitability: Covering approximately 22.6% of the territory, and (d) Very High Suitability: Extending across approximately 8.2% of the landscape. The spatial distribution is shown in Figure 5.17.

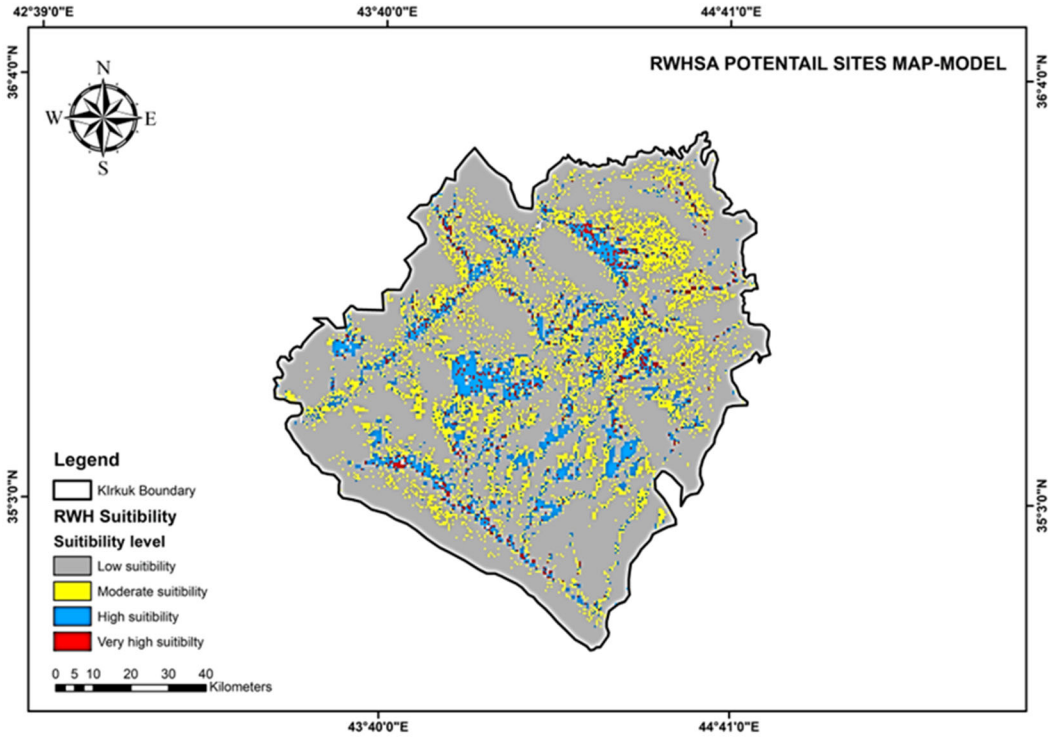


**Figure 5.17**. RWH Potential Site Selection for Historical Rainfall

Notably, the average annual precipitation projection for the future exhibits a distinct spatial distribution under SSP2-4.5 and SSP5-8.5 scenarios. In this projection, for SSP2-4.5 which is represented in Figure 14-B, the maximum values of precipitation are concentrated in the southwest of the study area and the values starts from 335 mm and further goes down to southwest the values of precipitation increasing to reach the highest value of around 400 mm, however, the minimum values found in the northeast part of the study region. These values vary, with the lowest values of precipitation at 255 mm and it is notable that this lowest part is concentrated in circles far to the northeast of the study area. These significant changes and variations in the average annual rainfall values over this extended period underscore the influence of climate change on precipitation levels in the study area. The precipitation values were influenced under SSP5-8.5 scenarios and the annual average amount decreased and the spatial distribution of the precipitation pattern also changed for the study area as shown in Figure 18 A.

The annual average precipitation decreased, and the spatial distribution of the higher values squeezed more to the South-West of the study area and the highest values

decreased to less than 390 mm. The minimum values of precipitation concentrated in the North-East of the study area in less circular shapes of spatial distribution.

The impact of climate change is clearly affecting the study Area and reflecting a decrease in the average annual amount of rainfall and the spatial distribution of precipitation compared to the historical model which reflects a higher value of average annual precipitation reached to 490 mm. Figure 5.18 (A and B) depicts the future projection spatial distribution for precipitation in Kirkuk study area under two scenarios.

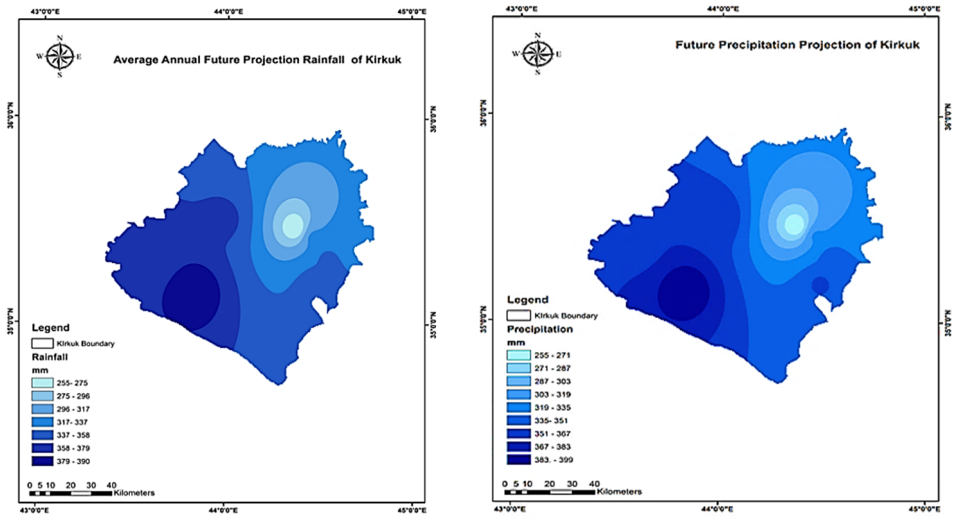


A (SSP5-8.5) B (SSP2-4.5)

**Figure 5.18.** Future Projection Precipitation of Kirkuk

Runoff depth estimation is considered one of the most important factors in identifying suitable site selection of RWH, therefore integrating the Curve number CN grid values with the land use/cover for each polygon. Moreover, the pixel value was applied while generating the RWH potential map, the runoff was computed, and the model was constructed for future runoff estimation models for the study region.

Runoff depth estimation is considered one of the most important factors in identifying suitable site selection of RWH, therefore integrating the Curve number CN grid values with the land use/cover for each polygon. Moreover, the pixel value was applied while generating the RWH potential map, the runoff was computed, and the model was constructed for future runoff estimation models for the study region.

The annual runoff was divided into five categories: extremely poor (180-200 mm), poor (210–230 mm), moderate (230–380 mm), good (380–340 mm), and very good (>350 mm). Places with very good to moderate potential runoff make up most of the watershed region. While the forecast future runoff of the study area was calculated based on future precipitation downscaling values and the future runoff model was generated and classified according to the study area into five classes. The amount of rainfall-runoff was estimated under the two scenarios of SSP2-4.5 and SSP5-8.5 respectively. The first model under SSP2-4.5 and estimation of rainfall-runoff as the lowest value was 180 mm and it concentrated in the middle of the study area. At the same time, the highest one was 340-350 mm and varied across the study region. The amount of surface runoff for the future prediction is lesser due to the reduced amount of rainfall that is influenced by climate change and the estimated watershed volume is approximately $7\times10^5$ $m^3$ under SSP2-4.5. The second rainfall-runoff model estimated values under the SSP5-8.5 were less as the lowest estimated value was 130 mm and the highest is 310 mm. The values varied through the study area, and the lower values concentrated in the middle while the moderate values were in the upper part of north-east and the highest values distributed through the study area. The estimated value of rainfall-runoff for second scenario was about $6.35\times 10^5$ $m^{3.}$ Comparing these values to the historical rainfall-runoff estimated value of $8\times 10^5$ $m^3$ shows that there is decreasing in the surface runoff amount and that reflect the impact of climate change in the study area.

The Rainwater Harvesting (RWH) potential map model for the research location was meticulously crafted using ArcMap, utilizing thematic layers encompassing slope, runoff, land use/cover, soil texture, rainfall, and drainage density. Each thematic layer's capacity to retain rainwater was considered during the assessment of their attributes.

The approach employed a combination of methodologies, including the Weight Overlay method, Analytical Hierarchy Process (AHP), and Multi-Criteria Assessment (MCA). Pairwise comparison matrices were established for the assigned weights of each thematic layer, once their weights and essential attributes were determined. The normalization of given weights was accomplished through the eigenvector technique, and the weight for each thematic layer was computed using equation (4.6) in Chapter 4.

For future projections of RWH potential zones, the distribution altered slightly: under the SSP2-4.5 scenario the suitability divided into 'very high suitability' covered approximately 6.1%, 'high suitability' encompassed around 18.3%, 'moderate suitability' extended in the north-east part and cover approximately 31.2%, and 'low suitability' accounted for around 33.4% and very low suitability around 11% of the study area, as visually depicted in Figure 5.20-B. The potential suitable site selection under SSP5-8.5 scenarios showed less values as the study area categorized into four categories: very high suitability counter about 5.12%, high suitability around 17.2%, moderate suitability about 27.23% and very low suitability about 5.45%. The less amount of rainfall will cause less amount of runoff and in results will affect the suitability site selection of RWH due to impact of climate change in the study area as illustrated in Figure 5.20 A.

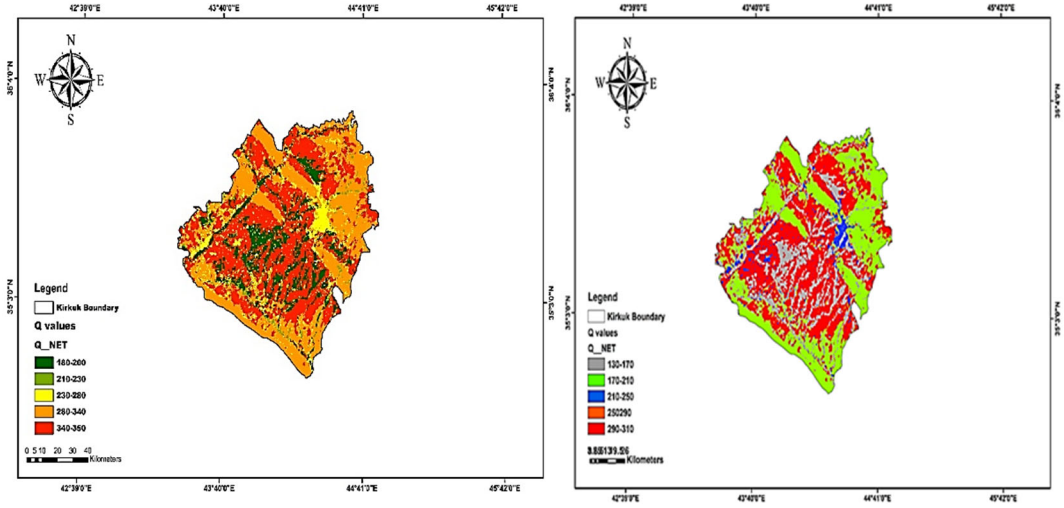


( A ) (B)

**Figure 5.19.** Future Runoff Depth of Kirkuk

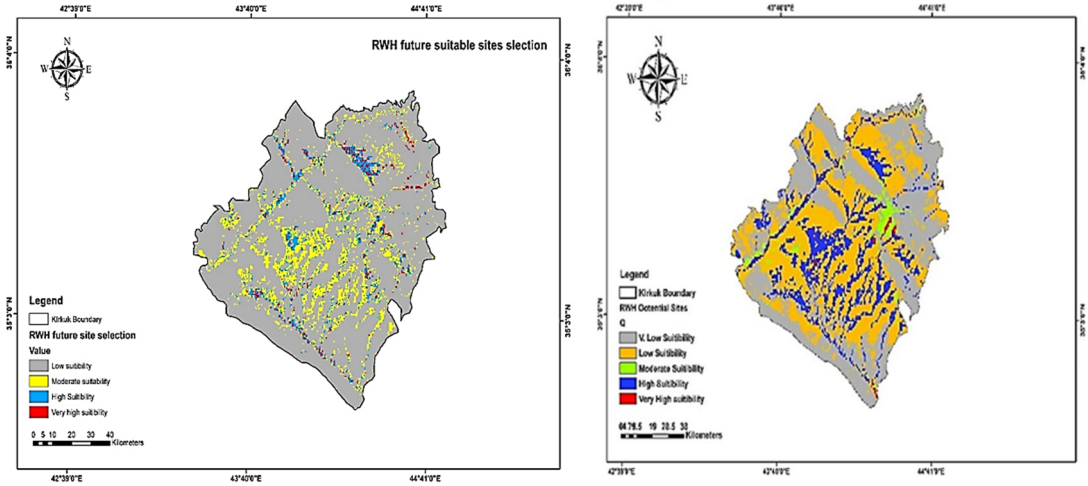


(A ) ( B)

**Figure 5.20** RWH Potential Sites Selection for Future Projection

### 5.3.2 Evaporation Model

In this research study, ANN models were built to predict evaporation using metrological station data employing four predictors: rainfall, minimum temperature, maximum temperature, and sunshine hours. The first ANN model uses MLP multi-layer perception, which consists of three layers (input, middle, and output layer). The second model uses SVM, a support vector machine model. This model was used to compare between two machine learning algorithm models accuracy the ANN and SVM model for estimating the evaporation.

#### 5.3.2.1 Evaporation by Using MLP Model

The ANN model was performed by utilizing MATLAB 2023a to build and train the neural network to find the best neural network architecture to predict the evaporation model. A range of statistical tests was applied to evaluate the model's performance.

To build the ANN model, daily data for rainfall, minimum and maximum temperature, and sunshine hours were input while evaporation data were used as an output. To build the ANN model, the data were divided into three sets: training set, evaluation set, and validation set as a test ratio of 70%, 15%, and 15% respectively. The data divided into 70 % for the learning and 15% for validation and the other 15% for training. By providing a larger portion of the data, 70 % for training, the model can capture more variation in the data, improving its ability to generalize. This helps the model learn complex relationships and reduces the chance of underfitting, where the model fails to capture important patterns. While allocation of 15% for validation provides enough data to give a reliable estimate of model performance during training while ensuring the majority of the data is still used for learning. Using 15 % for testing provides an unbiased estimate of how well the model performs on completely unseen data. The duration of data that have been used (1980-2022). This percentage is good and fast for the model data set. The training set was utilized to train the network, while the validation set monitored and assessed the network's performance at specific intervals during training. Training ceased when the error on the validation set reached its lowest point. Finally, the network's performance was assessed using a test dataset not included in the training phase. Figure 5.21 illustrates the relationship and validation model between the observed and predicted evaporation and the $R^2$ value is 0.955 which means

the accuracy of the model is quite good between observed and predicted values. Figure 5.22 illustrates the time series and relationship between observed and simulated evaporation. The Figure shows the observed simulated results of the evaporation of the study area and the differences are very small around 5% and the model performance is good. The evaporation rate under SSP2-4.5 scenario for the period P1 (2031-2050) increased about 1.5% compared to baseline period while for P2 (2051-2070) the evaporation rate increased by 1.73%. The third period of P3 (2071-2090) showed an increase rate of 1.81% while P4 (2091-2100) was highest, and the rate increased about 2.12 % compared to baseline period. The SSP5-8.5 scenario showed higher increase rates compared to SSP2-4.5. The P1 and P2 increase rate were 1.76 and 1.87 respectively while P3 and P4 rate were 1.92 and 2.23 %. The effect of SSP5-8.5 scenario is higher than SSP2-4.5 scenario on evaporation increasing rate in the study area of Kirkuk. Time series of evaporation of all periods for SSP2-4.5 and SSP5-8.5 depict in Figures 5.23 and 5.24 respectively. The validation, training, and testing model results are presented in Appendix C. Table 5.3 illustrates the validation of MSE, MAE, and RMSE for the evaporation model.

**Table 5.3.** Three statistical criteria for the validation data (MLP)

| Model Input Data | MAE | MSE | RMSE |
|---|---|---|---|
| Rainfall, Tmin, Tmax, SSH | 0.0201 | 0.0112 | 0.1053 |

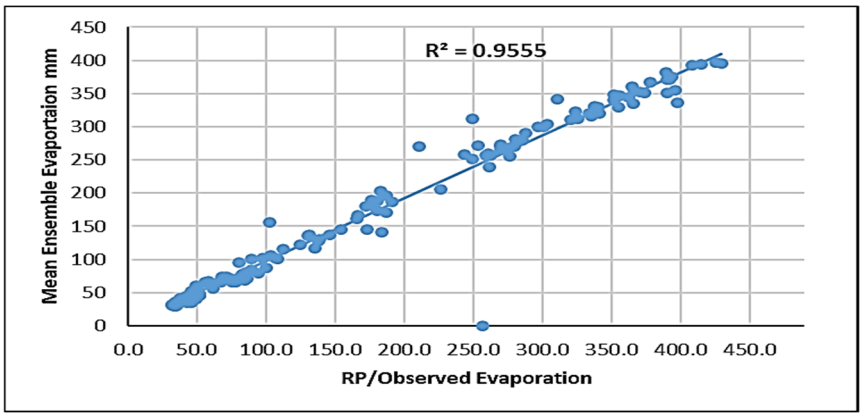


**Figure 5.21.** The Validation Model for Observed and Predicted Evaporation

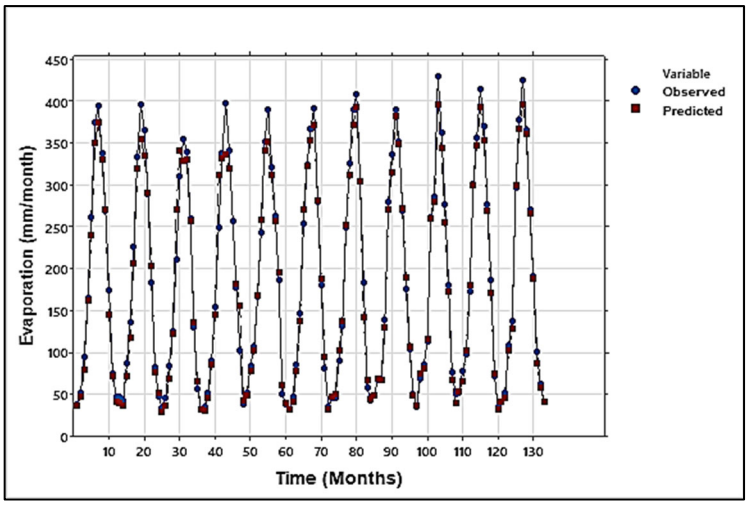


**Figure 5.22** The Relationship Between Observed and Simulated Evaporation

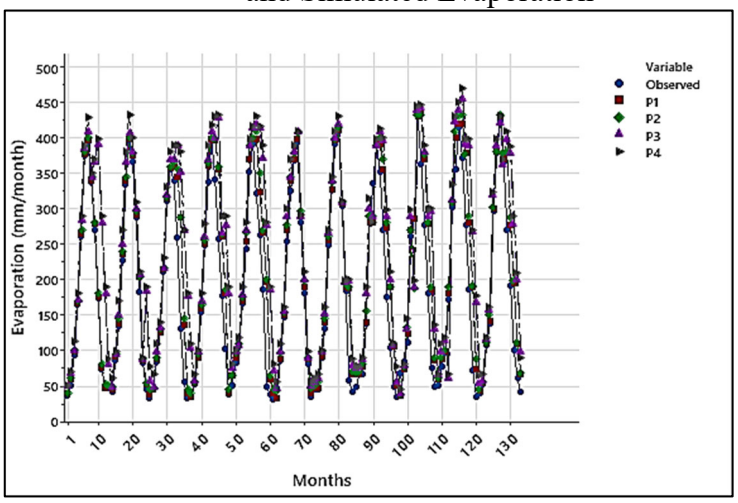


**Figure 5.23.** Time Series of Evaporation for SSP2-4.5 Scenario

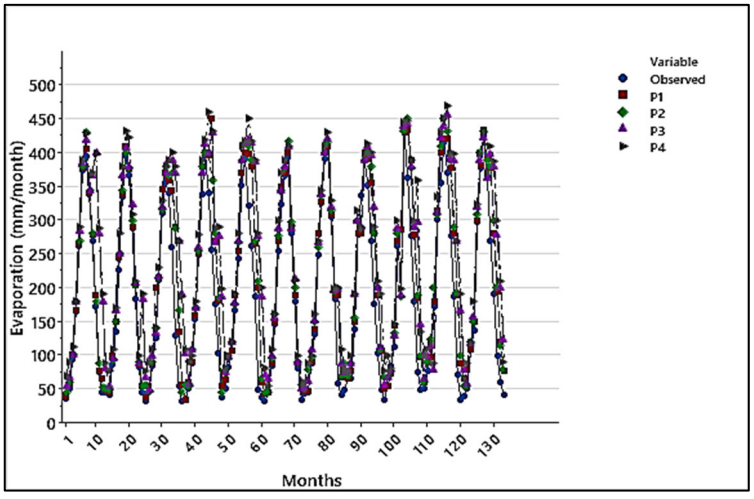


**Figure 5.24.** Time Series of Evaporation of SSP5-8.5 Scenario

### 5.3.3.2 Evaporation by Using SVM Model

The second model was achieved by utilizing SVM techniques to predict and estimate the evaporation. SVM is categorized as a non-statistical binary classification technique; recently, numerous researchers have been interested in this technique (Naggana et al, 2019).

There are two types of SVM models: Support Vector Classification models and Support Vector Regression models. SVM techniques can classify data into different classes, while the SVR framework addresses prediction problems (Abed et al, 2021). This study applied the Support Vector Regression model using four predictors (Rainfall, minT, maxT, and sunshine hours SSH). Table 5.4 demonstrates the MAE, MSE, and RMSE for the SVM best model. Figure 5.25 shows the validation model of mean ensemble evaporation with an $R^2$ value of 0.90 for the best SVM model. The validation and accuracy of the model is good but less than the developed model of Neural Network. Figure 5.26 shows the relationship of observed and predicted values of evaporation time series. The evaporation rate under SSP2-4.5 scenario for period P1(2031-2050) showed a slight increase of 1.59 % while for P2 and P3 (2051-2070, 2071-2090) the difference was little equals 1.87% and1.91% respectively. P4 (2091-2100) showed higher rate vale of 2.67% compared to observed value rate of 1.31%. Figures 5.27 and 5.28 depict the evaporation time series there under SSP2-4.5 and SSP5-8.5 scenarios.

**Table 5.4.** Three statistical criteria for the validation data (SVM)

| Model Input Data | MAE | MSE | RMSE |
|---|---|---|---|
| Rainfall, Tmin, Tmax, SSH | 0.351 | 0.01617 | 0.1323 |

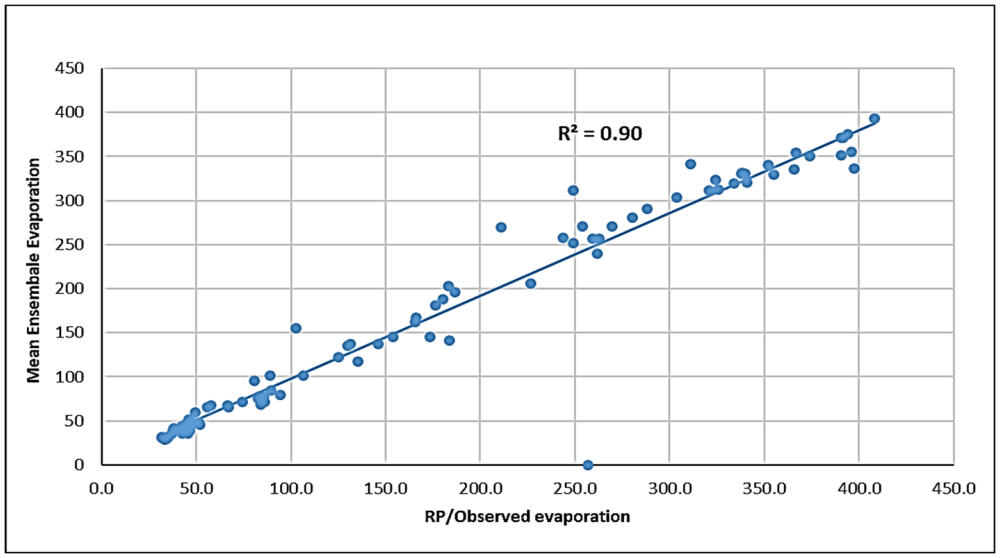


**Figure 5.25.** Validation Model of Mean Ensemble Evaporation for Best SVM

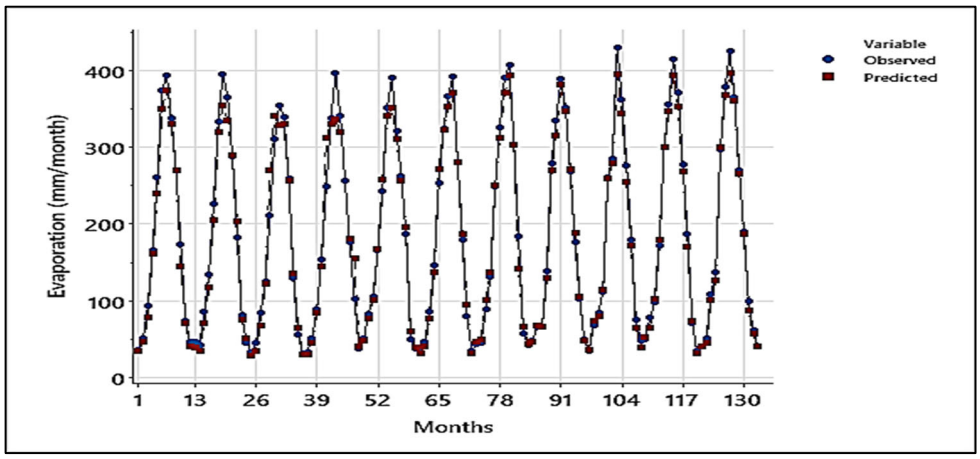


**Figure 5.26** The Relationship Between Observed and Predicted Evaporation

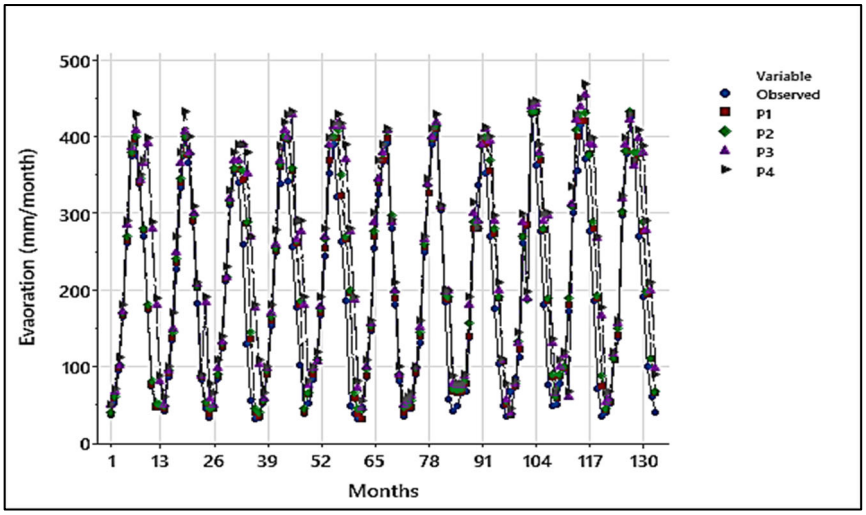


**Figure 5.27.** Time Series of Evaporation for SSP2-4.5 Scenario

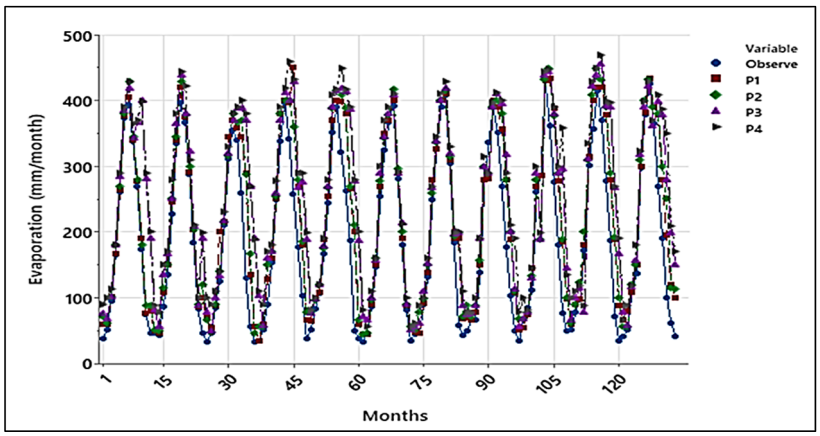


**Figure 5.28.** Time Series of Evaporation for SSP5-8.5 Scenario

The future projection for evaporation is increased for both models MLP and SVM but the MAE, MSE, and RMSE for the MLP model is less than in SVM for all periods and under both climate scenarios. The ensemble validation $R^2$ for MLP is 0.955 and higher than in SVM which is 0.90, the MAE, MSE and RMSE for MLP model values were 0.0201,0.0112 and 0.1053 respectively and less than the validation values of SVM of 0.351, 0.0161and 0.1323 which means that Neural Network model is more accurate and reliable than SVM model. Therefore, the performance of the MLP technique is more adequate than the SVM model. The following Table 5.5 shows the average annual evaporation of baseline compared to future projection evaporation under the SSP2-4.5 and SSP5-8.5 scenarios.

**Table 5.5.** The average annual evaporation of RP/historical compared to future projection evaporation under the SSP2-4.5 and SSP5-8.5 scenarios.

| Scenario | AV. Evaporation mm year$^{-1}$ | | | | Av. Evaporation rate change % |
|---|---|---|---|---|---|
| Baseline period | 1370.9 | | | | - |
| SSP2-4.5 | P1 | P2 | P3 | P4 | 57.2% |
| | 1634.1 | 1651.3 | 1671.8 | 1689.8 | |
| SSP5-8.5 | 1732.2 | 1744.2 | 1753.4 | 1764.3 | 85.9% |

### 5.3.4 Estimation of Crop Water Requirements

In this section, crop and irrigation water requirements Kirkuk were estimated for reference periods and future projections for three types of crops: wheat, barley, and sunflower crops, employing FAO-developed CROPWAT 8.0 software.

#### 5.3.4.1 Reference Period of Precipitation, Evapotranspiration ET0, Minimum and Maximum Temperature

The mean monthly climatic data were input into LARS WG 8.0 to extract the minimum and maximum temperatures and precipitation for the RP. January and December witnessed the highest average monthly precipitation amounts for Reference Period at 63.54 mm and 55.41 mm, respectively. January and December had the lowest monthly average temperatures of 3.06 °C and 3.81 °C, respectively. In contrast, the study region's most significant monthly average temperatures of 44.47 °C and 45.66 °C, respectively, were recorded in July and August. The average annual simulated *ET0* equals 1751.7 mm/year, and the highest and lowest monthly average value rates were 45.3 and 259.5 in January and July, respectively. Figure 5.29 depicts the monthly average values for precipitation, minimum temperature, maximum temperature, and *ET0* for reference period.

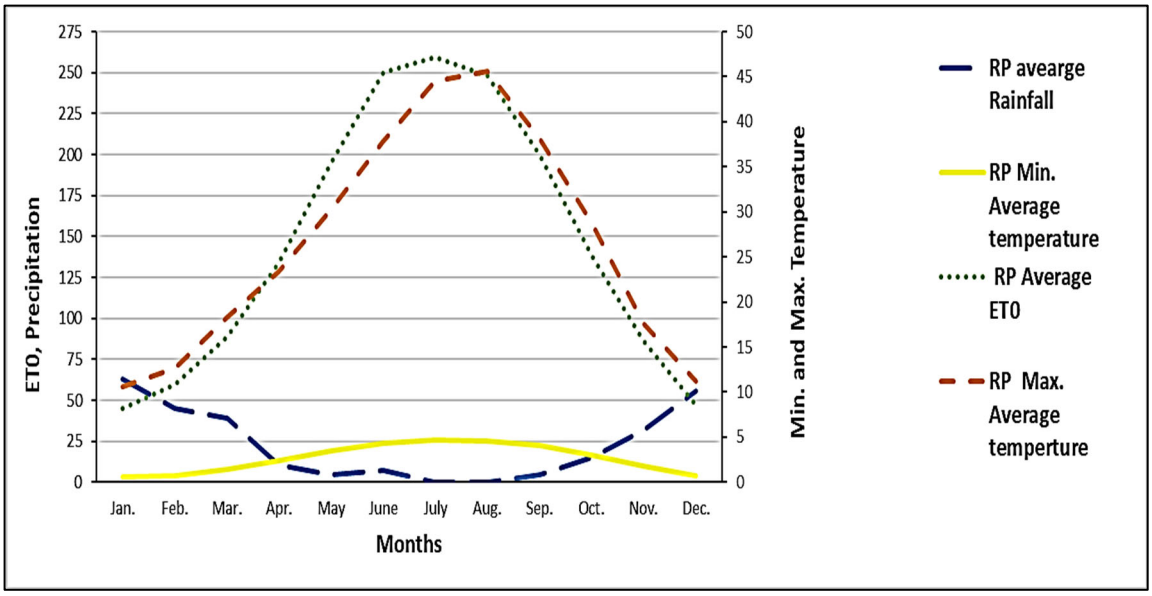


**Figure 5.29.** Monthly Average Values for Precipitation, min T, max. T and *ET0* for RP.

#### 5.3.4.2 Future Projection of Evapotranspiration ($ET_0$)

The future *ET0* projection under the SSP2-4.5 scenario shows that there is an increase in average monthly *ET0* for P1 and P2 as the highest values of ET0 occurred in June, July, and August with 189.86, 268.5 and 254.52, and 182.14, 266.97 and 168.07 mm/month respectively. For P3 and P4, ET0 increased dramatically, and the highest ET0 values occurred in June, July, and August at 206.3, 280.75, 281.02, 232.01, 291.32, and 285.39 mm/month respectively. *ET0* under the SPP5-8.5 scenario for P1 and P2 increased specifically in June, July, August, and September with (254.04, 311.92, 318.97, and 201.59 mm/month) respectively. For P3 and P4, *ET0* continued to increase, with the highest values occurring in May, June, July, August, and September at 223.1, 253.2, 280.66, 273.57, 204.65, 189.25, 233.25,292.25, 287.85 and 180.88 mm/month respectively. Figure 5.30 depicts the average differences in *ET0* for future projections for both the SSP2-4.5 and SSP5-8.5 scenarios compared to baseline period for P1(2031-2050), P2(2051-2071), P3(2071-2090), and P4(2091-2100).

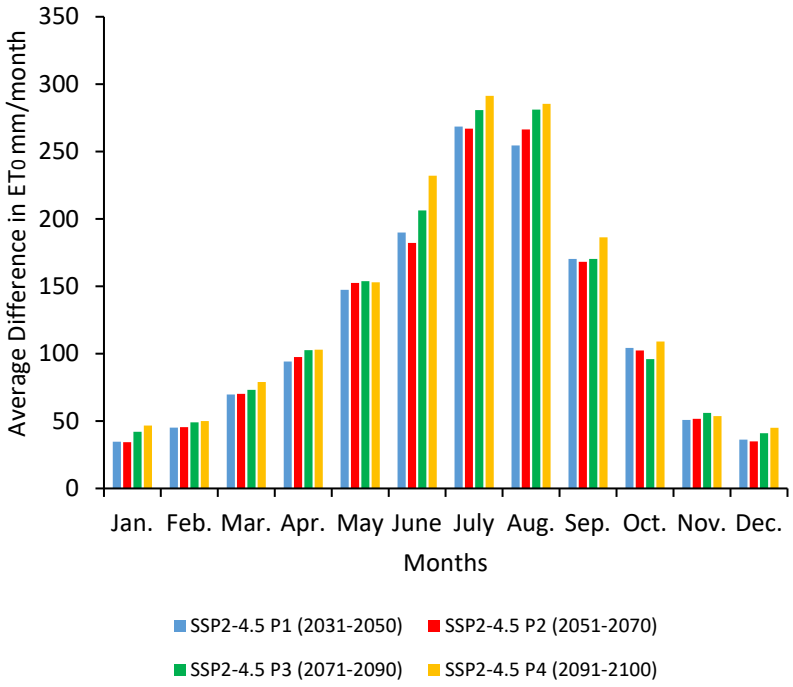


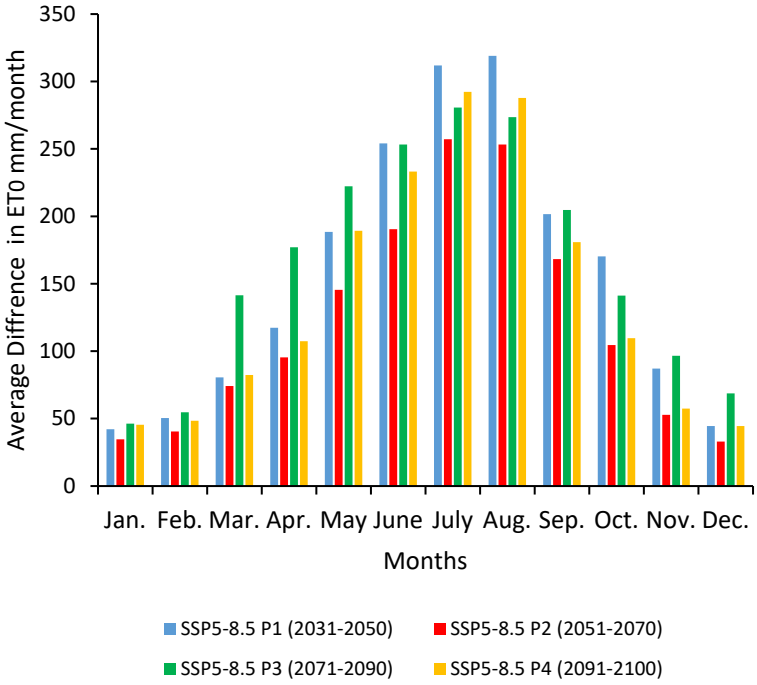


**Figure 5.30** Average Differences in *ET0* for Future Projection Compared to Baseline Period.

### 5.3.4.3 CWR for RP, SSP2-4.5 and SSP5-8.5

Crop water requirements differ and depend on the region's climate, soil type, effective rain, cultivation, and many other factors. The crop water requirements or needs represent the quantity of water that equals the water loss by *ET0*. The amount of water

required for each crop or irrigation water requirement varies with the life span of the crop and is not distributed equally. The irrigation water requirements for the three crops included in this study are (wheat, barley, and sunflower). These crops considered very important for food production, food industry, economic and environment as sunflower improve soil benefits as sunflower known for helping cleaning soil from toxic and prevent soil from erosion due to its deep roots. Table 5.6 illustrates the irrigation and crop water requirements for winter wheat, winter barley, and sunflower for the reference precipitation period and future projected period for the SPP2-4.5 and SSP 5-8.5 scenarios for P1, P2, P3, and P4, respectively, in the study region of Kirkuk.

**Table 5.6.** Crops water requirements for RP and under SSP2-4.5 and SSP5-8.5 Scenarios

| crops | P_H Dates | CWR RP mm/dec | CWR P1-4.5 mm/dec | CWR P2-4.5 mm/dec | CWR P3-4.5 mm/dec | CWR P4-4.5 mm/dec | CWR P1-8.5 mm/dec | CWR P2-8.5 mm/dec | CWR P3-8.5 mm/dec | CWR P4-8.5 mm/dec |
|---|---|---|---|---|---|---|---|---|---|---|
| wheat | 01/11-29/6 | 493.4 | 574.1 | 576.2 | 578.9 | 621.1 | 633.9 | 631.6 | 640.4 | 648.7 |
| barely | 01/11-28/02 | 117.2 | 120.7 | 119.5 | 122.6 | 127.1 | 131.5 | 130.6 | 132.8 | 134.3 |
| Sun flower | 01/03-15/07 | 669.5 | 680.7 | 677.6 | 710.1 | 746.5 | 683.6 | 684.7 | 700.5 | 748.6 |

The CWR increased under the SSP2-4.5 and SSP5-8.5 scenarios respectively. For wheat the percentage increased about 9% for P1 and P2, while for P3 and P4 increased 10 and 13 % respectively. Under SSP5-8.5, the CWR increased 13% for P1, P2 and P3 14% while P3 and P4 15 and 16%. The percentage increased for all periods specifically under SSP5-8.5 for wheat. For Barley, the P1, P2 and P3 showed a slight increase of 4, 2 and 7% respectively. P4 showed a big increase comparing to previous periods and reference period. The SSp5-8.5 showed a sharp increase for CWR for all periods as the percentage was 18, 17, 19 and 21% for P1, P2, P3 and P4 respectively and it is clear there is a big impact of climate change on crop water requirements for Barely. CWR for sunflower increased dramatically specifically for P3 under SSP2-4.5 scenario by 15%, and 28% for P4 respectively. While reached 29% for P4 under SSP5-

8.5. CWR increased for the three types of crops and the biggest increase is for sunflower, wheat and barley has the lowest CWR comparing to them.

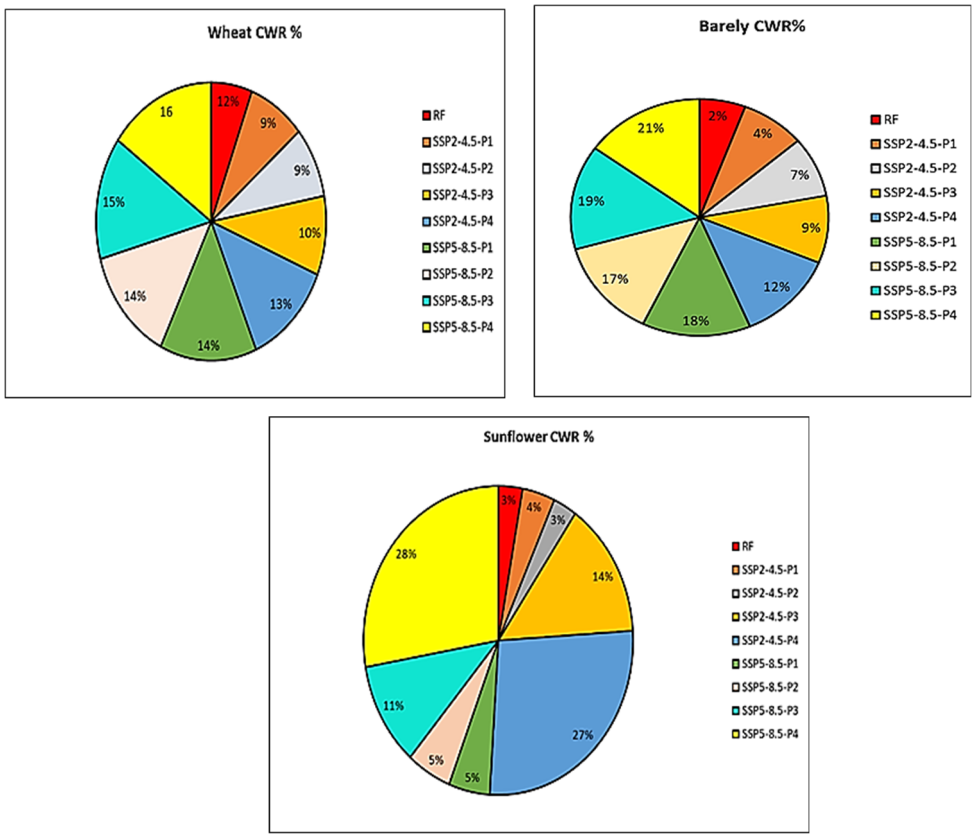


**Figure 5.31** The CWR Percentage under the SSP2-4.5 and SSP5-8.5

### 5.3.4.4 Crops Net Irrigation Water Requirements for RP, under SSP2-4.5, SSP5-8.5 Scenarios

Optimizing crop water requirements and irrigation schedules leads to better irrigation management of major crops. Efficient and purposeful regulation of the irrigation amount, duration, and rate is the aim of utilizing water for cultivation. Tables 5.8 and 5. 9 describe the net irrigation for agriculture requirements for wheat, barley, and sunflower for RP and for (P1, P2, P3, and P4) under the SSP2-4.5, and SSP5-8.5 scenarios.

**Table 5.7.** Net Irrigation agriculture requirements for crops for RP and under SSP2-4.5 scenario

| Crops | Stage | Depl. % | Av. NIWR RP mm | Av. NIWR P1-4.5 mm | Av. NIWR P2-4.5 mm | Av. NIWR P3-4.5 mm | Av. NIWR P4-4.5 mm |
|---|---|---|---|---|---|---|---|
| wheat | Int. | 57 | 127 | 72.4 | 91.2 | 200.6 | 242.3 |
| | DEV | 55 | 225.9 | 241.2 | 241.9 | 228.5 | 236.2 |
| | MID | 56 | 243.4 | 310.4 | 290.1 | 237.5 | 243.2 |
| | END | 52 | **Av.=198.76** | **Av.=208** | **Av.=207.73** | **Av.=222.2** | **Av.=240.56** |
| barely | DEV | 27 | 15 | 20 | 23.7 | 25.8 | 27.9 |
| | END | 20 | 19 | 22.7 | 25.3 | 27.3 | 29.3 |
| | | | **Av.=17** | **Av.=21.35** | **Av.=24.5** | **Av.=26.5** | **Av.=28.6** |
| sunflower | Init | 45 | 50.3 | 55.4 | 58.1 | 59.2 | 58.9 |
| | Dev | 46 | 99.6 | 96.5 | 100.2 | 94.7 | 98.1 |
| | Dev | 50 | 160.8 | 159.2 | 160.9 | 158.1 | 159 |
| | Mid | 51 | 191.7 | 195.7 | 193 | 195.8 | 197 |
| | Mid | 51 | 192.5 | 194.2 | 194.1 | 198.2 | 195.3 |
| | End | 29 | **Av.=138.9** | **Av.=140.2** | **Av.=141.3** | **Av.=141.2** | **Av.=141.7** |

**Table 5.8.** Net Irrigation agriculture requirements for crops for RP and under scenario SSP5-8.5

| Crops | Stage | Depl. % | Av. NIWR RP mm | Av. NIWR P1-8.5 mm | Av. NIWR P2-8.5 mm | Av. NIWR P3-8.5 mm | Av. NIWR P4-8.5 mm |
|---|---|---|---|---|---|---|---|
| wheat | Int. | 56 | 130 | 139.1 | 141.1 | 170.1 | 177.3 |
| | DEV | 56 | 238.9 | 244.4 | 248 | 257.9 | 255.2 |
| | MID | 56 | 246.1 | 249.3 | 255.2 | 261.7 | 267.2 |
| | END | 45 | **Av.=205** | **Av.=210.9** | **Av.=214.7** | **Av.=229.9** | **Av.=233.2** |
| barely | DEV | 29 | 25.5 | 25 | 26.7 | 27.8 | 29.9 |
| | END | 31 | 27.4 | 25.7 | 27.3 | 29.3 | 31.3 |
| | | | **Av.=26.45** | **Av.=25.35** | **Av.=27** | **Av.=28.55** | **Av.=30.6** |
| sunflower | Init | 46 | 55.3 | 56.2 | 64.7 | 67.1 | 68.9 |
| | Dev | 45 | 99.8 | 99.2 | 118.2 | 117.8 | 118.3 |
| | Dev | 50 | 162.8 | 169.9 | 169.5 | 170.8 | 171.9 |
| | Mid | 52 | 192.7 | 200.7 | 200.2 | 211.5 | 213.3 |
| | Mid | 51 | 190.5 | 203.6 | 203.4 | 215.8 | 218.3 |
| | End | 30 | **Av.=140.22** | **Av.=145.92** | **Av.=151.2** | **Av.=156.6** | **Av.=158.1** |

The average net irrigation requirement estimates for wheat, barley, and sunflower for RP and under the SSP2-4.5 scenario for P1, P2, P3, and P4 were 198.76, 208, 207.73, 220.2, and 240.56, 17, 21.35, 24.5, 26.5, 28.6, 138.9, 140.2, 141.3, 141.2 and 141.7 mm respectively. Under SSP5-8.5, the average net irrigation requirement estimations for wheat, barley, and sunflower for P1, P2, P3, and P4 were 205, 210.9, 214.7, 229.9, 233.2, 140.22, 145.92, 151.2, 156.6 and 158.14 mm respectively.

The amount of water required to fill the soil for cultivation and to guarantee adequate moisture for ideal crop development is known as the Net Irrigation Requirement (NIR). Cropping schedules and meteorological variables influence NIR. To accurately determine net irrigation requirements, irrigation efficiency must be considered. When irrigation water is applied and moved, losses such as seepage, evaporation, percolation, and runoff can occur (Azevedo et al., 2007). Soil preparation, transplantation, leaching, and other agricultural operations require water. Model validation was applied for crop water and irrigation requirements for RP, SSP2-4.5, and SSP5-8.5 as shown in Table 5.10. Figures demonstrating the field irrigation schedule for crops (wheat, barley, and sunflower) can be found in Appendix D.

## 5.4 Model Downscale and Future Projection for Oxfordshire Site

This section describes the calibration and developing of downscaling of GCMs by utilizing LARS-WG 8.0

### 5.4.1 LARS-WG Model Calibration and Validation

The model's performance was evaluated using LARS WG 8.0 and historical meteorological data from 1980 to 2010. This analysis integrated $CO_2$ data to produce and validate files for the upcoming site analysis phase, resulting in three distinct site variable files for the study region. These files are categorized as follows:

1. wgx file: Contains metadata and information on the study region.
2. stx file: Includes statistical outcomes of the model.
3. tst file: Compiles statistics for both observed and generated data to enable comparative analysis.

To assess model performance, two statistical tests and graphical comparisons were conducted between observed and synthetic weather data generated by LARS-WG. Key variables analyzed include maximum temperature (Tmax), minimum temperature (Tmin), rainfall (Rain), and solar radiation (Radi).

The Kolmogorov-Smirnov (K-S) test was applied to evaluate whether the distributions of daily climate variables in measured versus simulated data were statistically comparable. The test utilized a p-value to determine acceptance or rejection of the

hypothesis that both datasets (observed and simulated) stem from the same distribution. A high p-value alongside a low K-S statistic indicates that simulated climate conditions closely align with observed conditions, supporting the hypothesis (Semenov et al., 2013).

Table 5.9 provides an evaluation of the model's performance in simulating seasonal precipitation variations across both wet and dry periods. Table 5.10 details the statistical analysis of the model's performance in simulating Tmax, Tmin, Rain, and solar radiation. The assessment shows that the model performs exceptionally well in simulating daily distributions of Tmax, Tmin, and solar radiation. However, rainfall performance is very slightly inaccurate, particularly in the summer and fall seasons due to changing in rainfall through seasons change.

**Table 5.9.** K-S test for seasonal wet/dry serious distribution

| Season | Wet/Dry | N | K-S | P-value | Assessment |
|---|---|---|---|---|---|
| DJF | Wet | 12 | 0.104 | 0.999 | Very good fit |
| | Dry | 12 | 0.103 | 0.999 | Very good fit |
| MAM | Wet | 12 | 0.097 | 1.0 | Perfect fit |
| | Dry | 12 | 0.058 | 1.0 | Perfect fit |
| JJA | Wet | 12 | 0.098 | 0.981 | Very good fit |
| | Dry | 12 | 0.085 | 0.970 | Very good fit |
| SON | Wet | 12 | 0.075 | 1.0 | Perfect fit |
| | Dry | 12 | 0.114 | 0.997 | Very good fit |

DJF: December, January, February; MAM: March, April, May; JJA: June, July, August. SON: September, October, November.

**Table 5.10:** K-S and P-value tests for daily rainfall, Tmax., Tmin. and solar (radi) distributions

| | **Daily Rainfall distributions** | | **Daily T. Max. distributions** | | **Daily T. Min.** | | **Daily solar radiation** | |
|---|---|---|---|---|---|---|---|---|
| Month | K-S | P-Value | K-S | P-Value | K-S | P-Value | K-S | PValue |
| J | 0.035 | 1 | 0.053 | 1 | 0.053 | 1 | 0.044 | 1 |
| F | 0.032 | 1 | 0.008 | 1 | 0.053 | 1 | 0.031 | 1 |
| M | 0.060 | 1 | 0.051 | 1 | 0.054 | 1 | 0.044 | 1 |
| A | 0.066 | 1 | 0.057 | 1 | 0.106 | 0.999 | 0.044 | 1 |
| M | 0.091 | 1 | 0.061 | 1 | 0.054 | 1 | 0.087 | 1 |
| J | 0.050 | 0.940 | 0.065 | 1 | 0.008 | 0.999 | 0.042 | 1 |
| J | 0.023 | 0.991 | 0.051 | 1 | 0.053 | 1 | 0.043 | 1 |
| A | 0.085 | 1 | 0.053 | 1 | 0.054 | 1 | 0.040 | 1 |
| S | 0.234 | 1 | 0.053 | 1 | 0.052 | 1 | 0.044 | 1 |
| O | 0.230 | 0.697 | 0.051 | 1 | 0.053 | 1 | 0.000 | 1 |
| N | 0.066 | 0.520 | 0.052 | 1 | 0.053 | 1 | 0.000 | 1 |
| D | 0.281 | 1 | 0.053 | 1 | 0.016 | 0.999 | 0.034 | 1 |

The model now validated for current conditions can simulate future daily data for Tmax, Tmin, rainfall, and solar radiation. This simulation will employ seven General Circulation Models (GCMs) and integrate IPCC (AR6) scenarios over three future periods: 2031–2050, 2051–2070, 2071-2090 and 2091–2100. The maximum observed average precipitation was in October, November, December and January respectively. There was a slight decrease in generated mean in those months. In January around 2.7%, October 0.68%, November 5.04 % and December round 3.14 %. In June, July and August the decrease percentage was 4.42, 5.15 and 3.28 respectively. The following Figure 5.30 explores projected outcomes based on these scenarios.

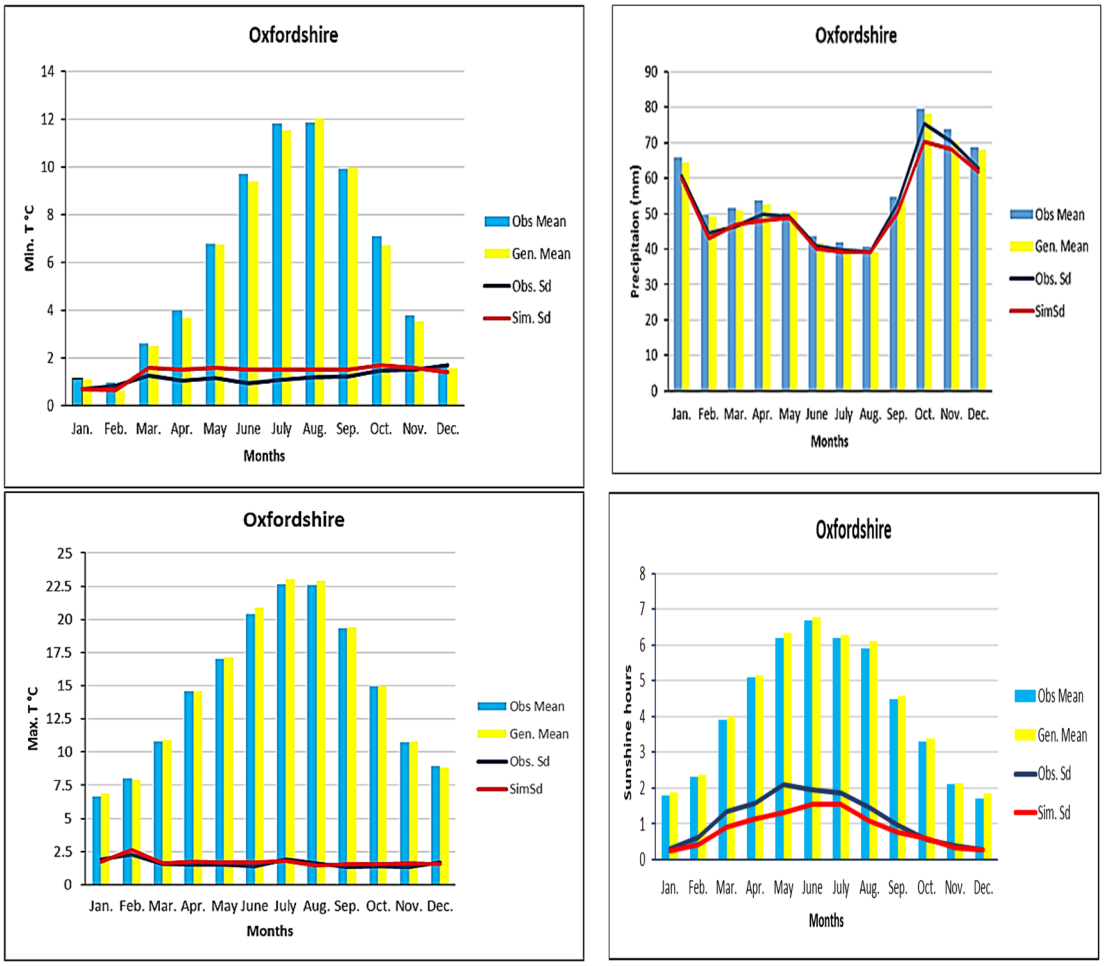


**Figure 5.32**: Calibration and Validation of the LARS-WG Model

### 5.4.2 Projection of Future Climate Factors

Following the calibration and validation of the LARS-WG model, we utilized it to simulate future daily data for maximum temperature (Tmax), minimum temperature (Tmin), precipitation (Rainfall), and solar radiation across three distinct periods: 2031-2050, 2051-2070, 2071-2090 and 2091-2100. These projections were generated based on two emissions scenarios represented in the Shared Socioeconomic Pathways (SSPs): SSP2-4.5 and SSP5-8.5.

These scenarios offer a comprehensive framework for analyzing the impact of societal choices on emissions, as well as on climate adaptation and mitigation efforts, as outlined in the IPCC's Special Report on Emissions Scenarios (SRES). Each scenario reflects a unique pathway of greenhouse gas emissions and its corresponding climate response, providing critical insights into potential future climate conditions.

The simulations incorporated data from five General Circulation Models (GCMs), providing a diverse range of potential future climates. This multi-model approach enhances the robustness of the projections, as each GCM employs varying structures and parameterizations. Detailed information about the specific GCMs used in this analysis can be found in Table 4.1 of Chapter 4. By examining multiple GCMs across different timeframes and scenarios, this study aims to capture the uncertainties and variations in future climate patterns, offering valuable insights into potential daily changes in temperature, precipitation, and solar radiation.

The comparison of observed and projected average monthly data encompassing precipitation, maximum temperature, minimum temperature, and solar radiation for all GCMs under the SSP2-4.5 and SSP5-8.5 scenarios, as well as their ensemble means, is illustrated in Figure 5.43. Notably, the projected precipitation values for all GCMs from 2031 to 2100 exhibited fluctuations and were slightly lower than the observed values for the study region, particularly in summer and Autumn and under the SSP5-8.5 scenario.

The precipitation for periods 2031-2050 for January encounter little decreased by 0.03% comparing to base line period. The precipitation of the periods of 2051-2070 and 2071-2090 has another decreased percent by 0.3 and 0.35 respectively. While the periods 2091-2100 witness a higher percentage of 0.81 and 0.92 % respectively under SSP2-4.5 scenario. For June and July, the percentage increased by 0.95 and 1.05 % respectively. September, October and November witnessed decrease in precipitation by 1.21 and 1.32 and 1.41 % respectively for period 2031-2050. For periods 2051-2070 and 2071-2090 the average precipitation decreased for June, July, September and October by 1.43, 1.49, 1.37 and 1.39 respectively. The other months showed a stabilized amount of precipitation, and the changes were so small. Under SSP5-8.5 scenario, the precipitation has a sharp decrease compared to a base line period by 1.78, 1.81, 1.85, 1.87, 2.23, 1.91 % respectively for June, July, September, October and November for period 2030-2050. For periods 2051-2070, 2071-2090 the percentage increased by 1.85, 1.89, 1.98, 2.38 and 2.01 % respectively. The effect from SSP5-8.5 scenario is bigger than SSP2-2.4.5 in the study area specifically in |Summer, winter and Autumn seasons. The Min. and Max. temperatures fluctuated but showed a slight increase specifically in the summer season. The sunshine hours increased slightly in July, August, and September under the SSP5-8.5 scenario as shown in Figure 5.43.

The results of differences of GCMs for the Oxford Shire study region can be found in Appendix F for both SSP2-4.5 and SSP5-8.5 scenarios.

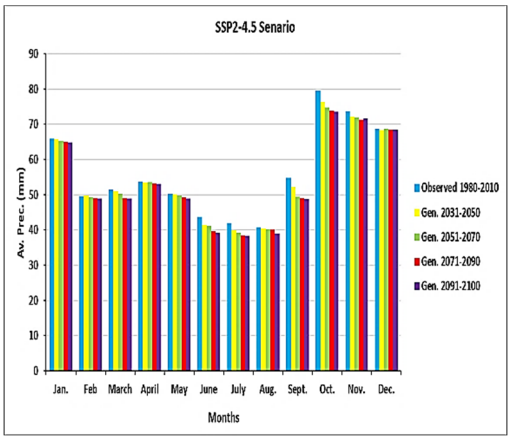


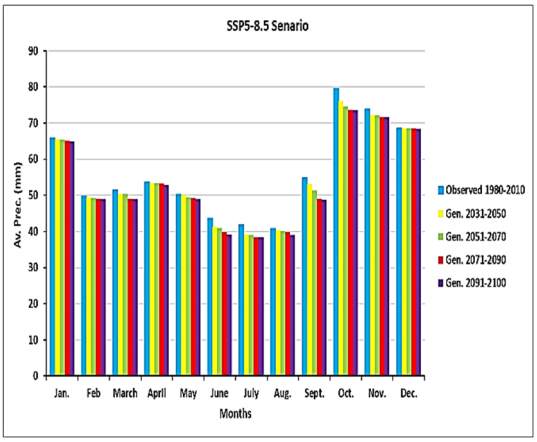


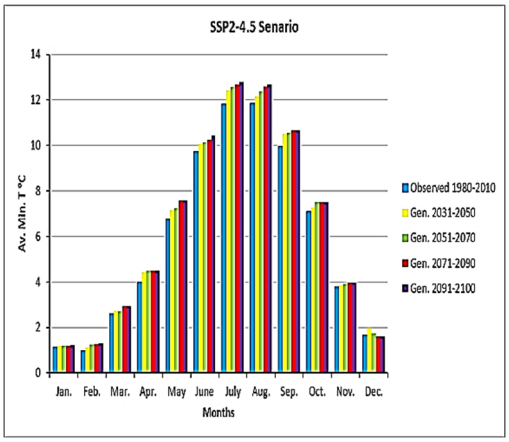


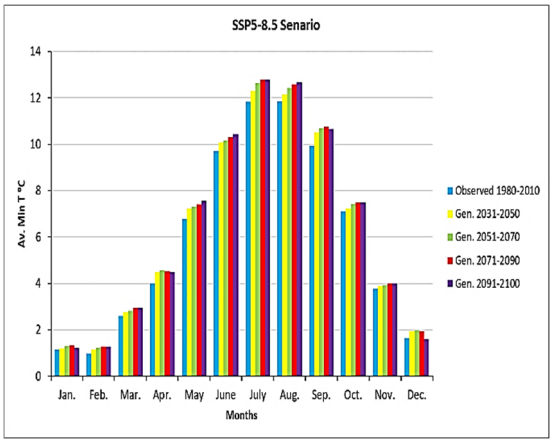


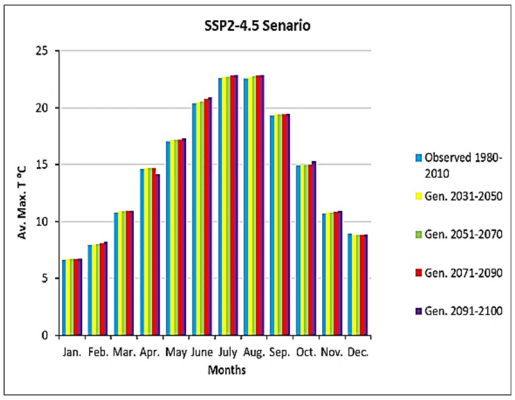


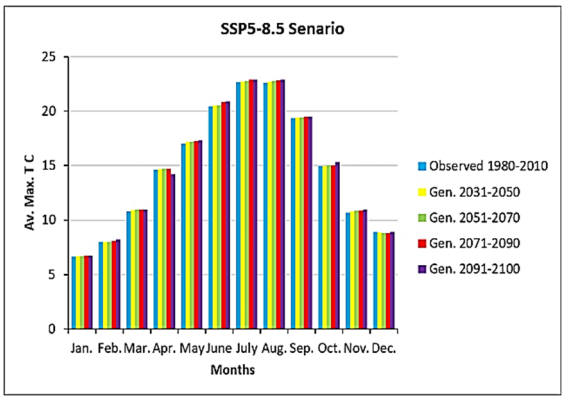

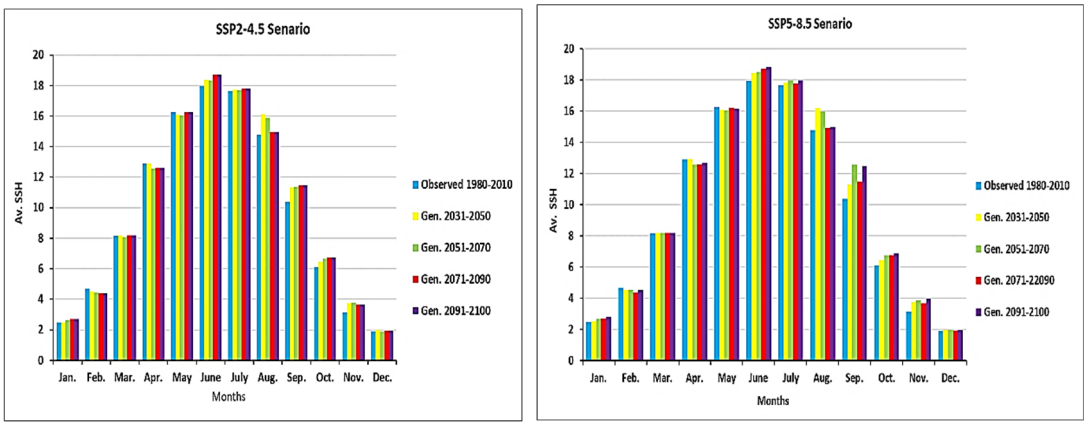


**Figure 5.33.** The Comparison between average monthly observed and projected values under SSP2-4.5 and SSP5-8.5 Scenarios

## 5.5 Required Input Data and Thematic Layers Analysis for Identifying RWH for the Second Study Area in Oxfordshire

In this section the thematic layers will be discussed including spatial distribution of rainfall for historical and future projection, LC/LU, slope, hydrologic soil groups, drainage density, stream order, rainfall-runoff model to produce the final model of RWH suitable site selection.

### 5.5.1 Historical Rainfall Analysis and Spatial Distribution

This study analysed 42 years of rainfall data, covering the period from 1980 to 2022, provided by the UK National Meteorological Library. Since rainfall is subject to uncertainty, probability distributions are used to represent this uncertainty formally and quantitatively. As shown in Figure 5.34, the average monthly rainfall data underwent probability distribution tests, specifically the Anderson-Darling test, to reduce uncertainties. The figure reveals skewness in certain areas and shifts in the spatial rainfall pattern. These skewness in rainfall data appeared below the 50% of probability while above this percent the data distributed normally. The rainfall data were reviewed and cleaned using the adjacent average formula, which was detailed in Chapter Three. Figure 5.35 presents a visual model of the historical annual average rainfall in Oxfordshire site over 42 years. By applying inverse distance weighting (IDW) to the annual average rainfall data, the precipitation distribution across the province was calculated and validated. This precipitation map clearly illustrates the spatial distribution of rainfall, with higher precipitation levels concentrated in the

central and southern regions, and encounter around 60 % of the precipitation while around 40% of lower values in the west. According to Figure 5.32, the highest recorded precipitation was 700 mm, while the lowest was 350 mm.

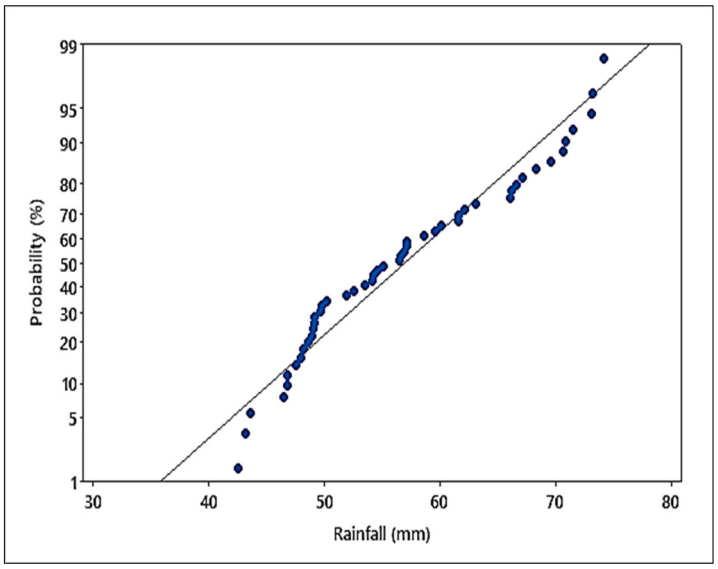


**Figure 5.34** Rainfall Probability Distribution

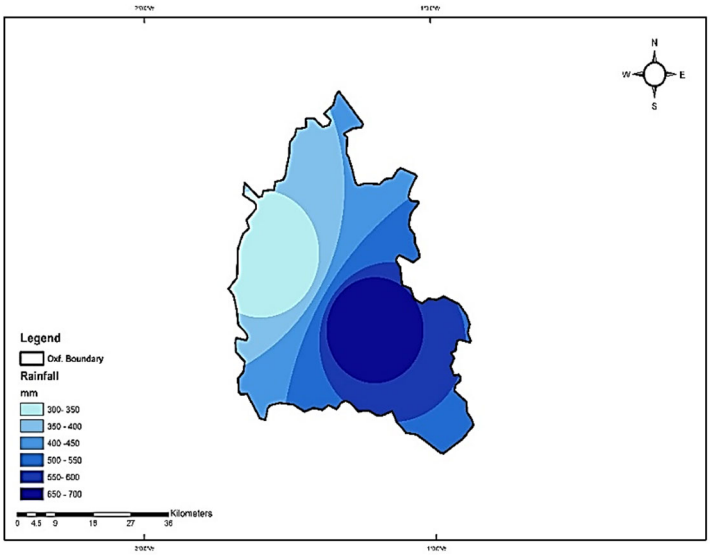


**Figure 5.35.** Rainfall Spatial Distribution of Oxfordshire

### 5.5.2 Land use/Land cover model

The land cover of a region significantly affects the runoff produced by rainfall. Areas with denser vegetation have higher interception and infiltration rates, leading to less runoff. To better understand these dynamics, a maximum-likelihood algorithm was

employed to classify the means, variances, and covariance of a land cover raster for 2021, using a spatial resolution of 10 meters.

The land cover was divided into five categories: water, trees, rangelands, exploded vegetation, crops, and built-up area. Reclassifying these categories led to the development of the final land cover model, as visually represented in Figure 5. 36. Crops dominated the study area by over 60%, while built up area around 18%, trees and extended vegetarian around 10% , water around 8% and 4% rangeland.

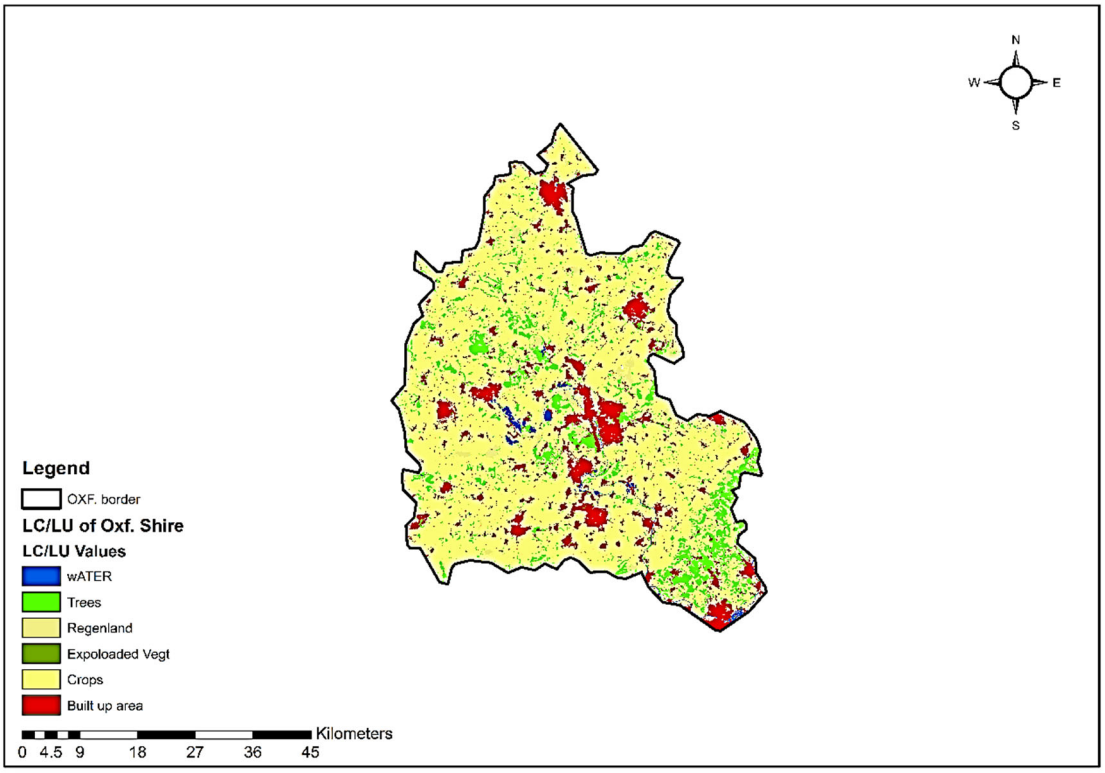


**Figure 5.36.** LC/LU of Oxfordshire

### 5.5.3 Slope

The slope model map was constructed using elevation data sourced from a Digital Elevation Model (DEM) with a resolution of 30m × 30ms that was explained in Chapter 3 as DEM was obtained from USGS as a TIF file and processed by utilizing ArcMap 10.8.2 to produce the final model. The slope values were determined within a specified parameter range by employing a filtering technique. Subsequently, a classification process is implemented to identify potential sites suitable for rainwater harvesting (RWH). The slope model was divided into five categories: (0-1.5%) is low

and it dominates most of the study area by 61.7%, (1.52-3.1%) is mild and dominate 10%, (3.1-5.6%) is moderate dominated around 9 %, (5.6-9.97%) is sharp covers around 8%, and (9.9-30.8 %) is very sharp. Among these classifications, the "low level" and "gentle level" categories are particularly conducive to RWH, which was uncovered in a substantial portion of the study region. To provide a visual representation, Figure 5.37 visually portrays the slope model across the study area within Oxfordshire.

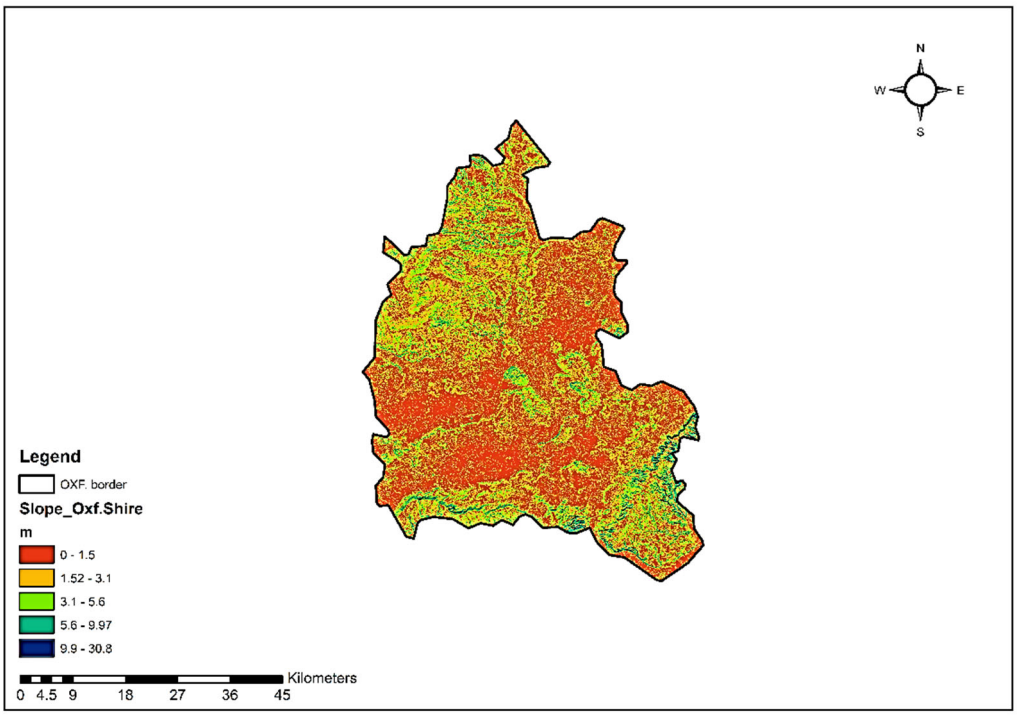


**Figure 5.37.** Slope of Oxfordshire

### 5.5.4 Stream order and Drainage Density Models

The stream order map was prepared through digitization and subsequent reclassification of drainage using ArcMap software. The stream order layer spans from 1 to 7, as visually illustrated in Figure 5.38. The drainage density within the studied region has been classified into five distinct categories: "very poor," covering an area of 5.34 km²; "poor," spanning around 8.79 km²; "moderately good," encompassing 12.71 km²; "good," occupying 10.03 km², and "very good," with a coverage of 4.75 km². Figure 5.39 visually represents the dominant drainage density groups across provinces. Within this context the study area classified into eight groups. As Above poor, moderately good, good, dominated the region. A smaller area is covered by the "very good" and Excellent. Conversely, the "very poor" category predominantly

encompasses the edges of the study region, while the "poor" classification extends from both the edges and into the interior of the study area.

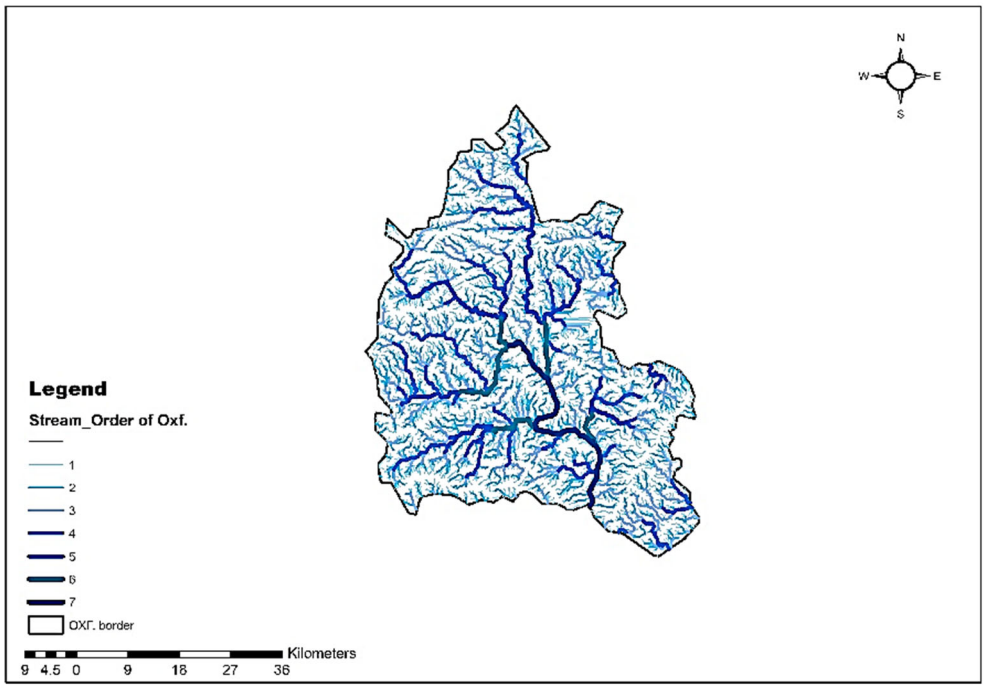


**Figure 5.38** Stream Order of Oxfordshire

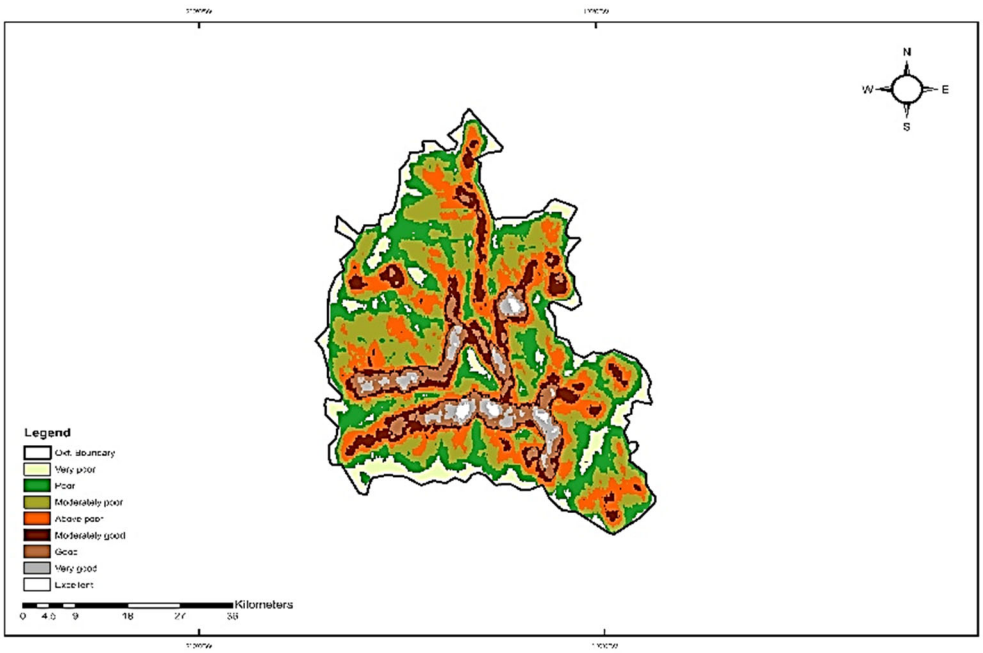


**Figure 5.39.** Drainage Density of Oxfordshire

### 5.5.5 Hydrologic Soil Groups (HSGs)

The soil texture within Oxfordshire is divided into two primary types: loam clay and clay. This classification corresponded to two Hydrologic Soil Groups (HSGs), C, C/D, D/C based on the soil data specific to the study area and as shown in Figure 5.40.

Based on the analysis of the study area, it is evident that the predominant soil group, designated Group C, extends over a substantial portion of the landscape and exhibits widespread distribution across the study region by 73%. In contrast, soil group C/D was confined to smaller patches in the study area around 7%. While D/C group dominate moderately.

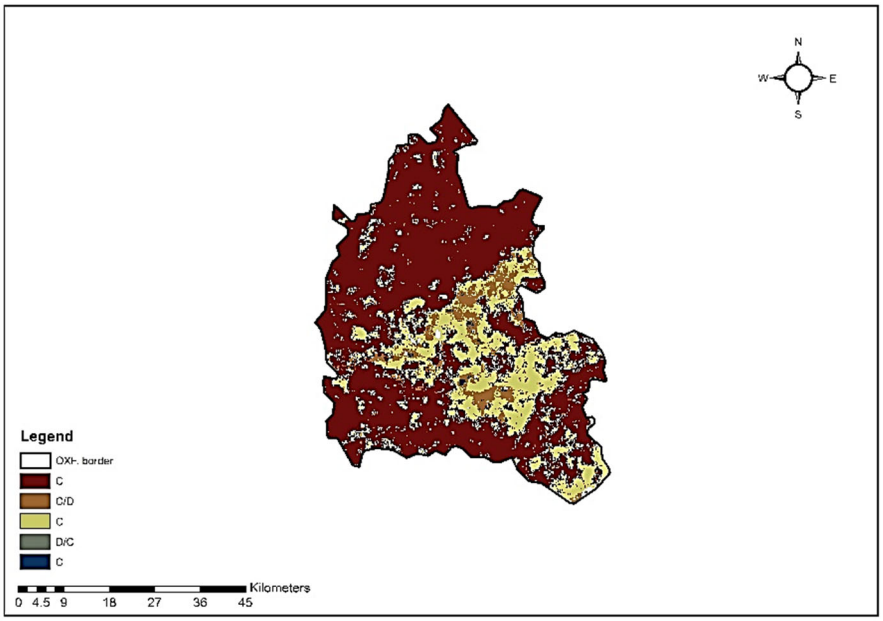


**Figure 5.40.** HSGs of Oxfordshire

### 5.5.6 Runoff potential depth

Utilizing ArcGIS software, all thematic layers of Hydrologic Soil Groups (HSGs) and land use/cover underwent processing and analysis, culminating in the generation of the curve number model *CN*. This model was constructed based on the standardized values assigned to each land use/cover category, coupled with the appropriate *CN* value corresponding to the HSG type. The *CN* grid values for the Kirkuk study area were derived using these processes, as illustrated in Figure 5.41. The computed values ranged from 75 to a maximum mean of 100. A higher *CN* value indicates a reduced

infiltration potential and elevated runoff volume, whereas a lower value reflects the opposite scenario. These computations and illustrations were executed using ArcMap software 10.8.2.

By integrating *CN* grid values with the corresponding land use/cover for each polygon, pixel values were applied to generate the Rainwater Harvesting (RWH) potential map. This process facilitates the computation of runoff, which subsequently contributes to the construction of the model.

A spectrum of five runoff classifications per year was established: “moderate” (300-370 mm), that covers around 4%, "above moderate" (370-380 mm), that dominates the site with about 65%, "good" (380-460 mm), covers around 11% and above good (460-470) and cover 10 % and "very good" (>580 mm) covers approximately 10%. The approximated volume of runoff is about $1\times10^6$ $m^3$.

The watershed area features locations with above moderate to good potential for runoff. This distribution is evident in Figure 5.42, which illustrates the yearly runoff depth model values in millimeters for the Oxfordshire. Figure 5.43 shows the validation and correlation for rainfall-runoff model and $R^2 = 0.977$ that reflects a strong correlation between Rainfall and potential runoff depth and a good model.

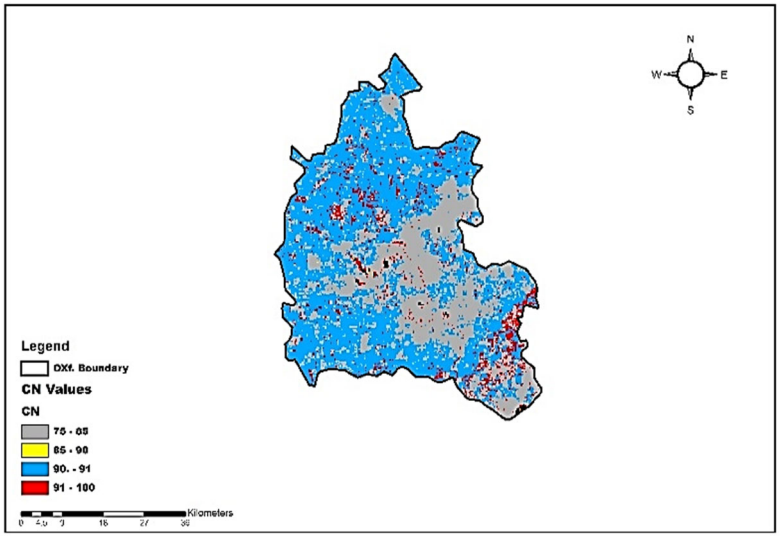


**Figure 5.41.** CN Values of Oxfordshire

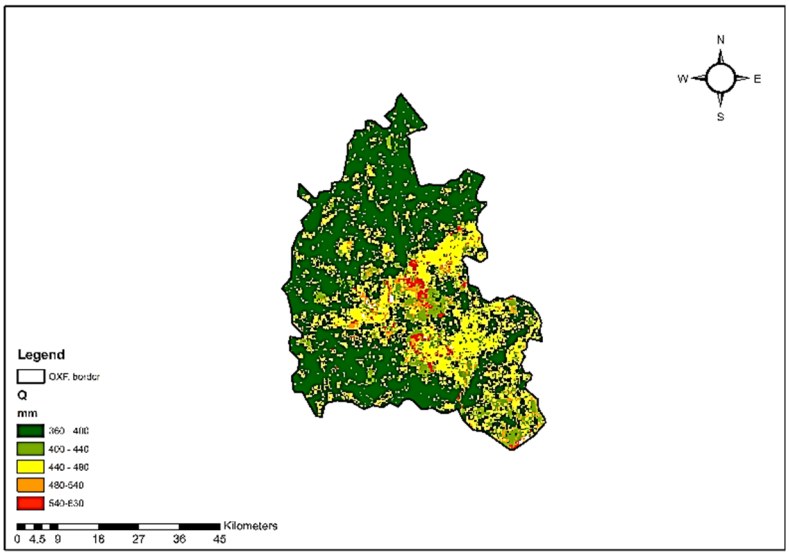


**Figure 5.42.** Runoff Depth

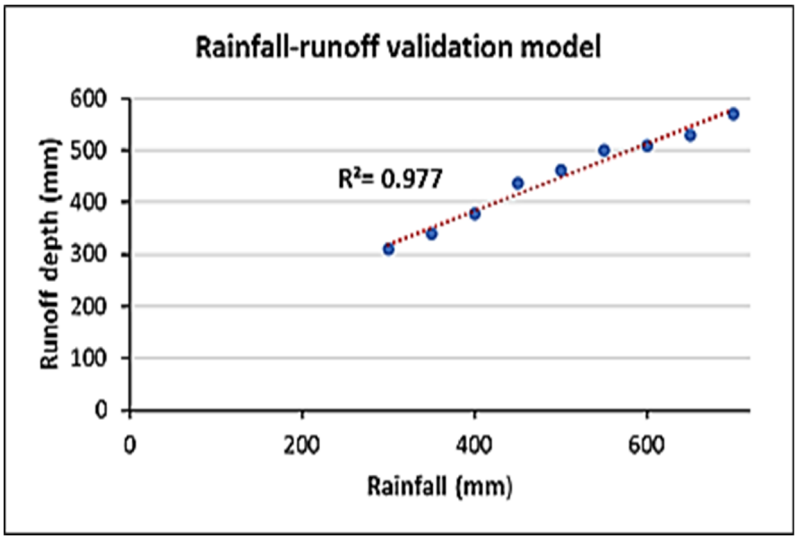


**Figure 5.43.** Rainfall-Runoff Validation Model

### 5.5.7 Sensitivity Analysis

Sensitivity analysis was applied to the Oxfordshire Study region by the weights of the criteria were adjusted and explored through incremental changes of both +10% and -10%. This intentional variation allowed us to evaluate the effects of dynamic relationships between the selected criteria. By performing this sensitivity analysis, we gained important insights into the robustness of the decision-making process, enabling us to understand how altering criterion weights impacts the overall results of the GIS-MCDA. The differences were very slight between the main thematic layers (Runoff, soil, LCLU, and slope). Results can be found in Appendix E.

### 5.5.8 RWH Potential Site Map Model for Historical and Future Projection

The RWH potential map model for the study area was created by combining several thematic layers, such as drainage density, rainfall, soil texture, land use/cover, slope, and runoff. This integration was performed using ArcMap 10.8.2. The future rainfall projection was applied under both scenarios of SSP2-4.5 and SSP5-8.5. The spatial projected distribution of rainfall for SSP2-4.5 varied from 250 as min. to 630 mm as max. In the middle of the study area the amount of rainfall varied from 375-630 mm and covers around 57% of the study area while the other part to the northwest, the projected rainfall varied from 250-350 mm and covers around 45%. The spatial distribution shows a moderate decrease in future projection compared to base line period under SSP2-4.5. The second spatial distribution under the SSP5-8.5 scenario showed a sharp decrease compared to SSP2-4.5 and baseline periods. The rainfall varied from 300-530 mm across the site. The higher values ensemble in the middle and more to the south-east of the site while heading to the north-west the distribution gel lesser. The higher distribution covers around 55% of the study area. Figures 5.44 and 5.45 illustrate the projected spatial distribution under SSP2-4.5 and SSP5-5.8 Scenarios respectively.

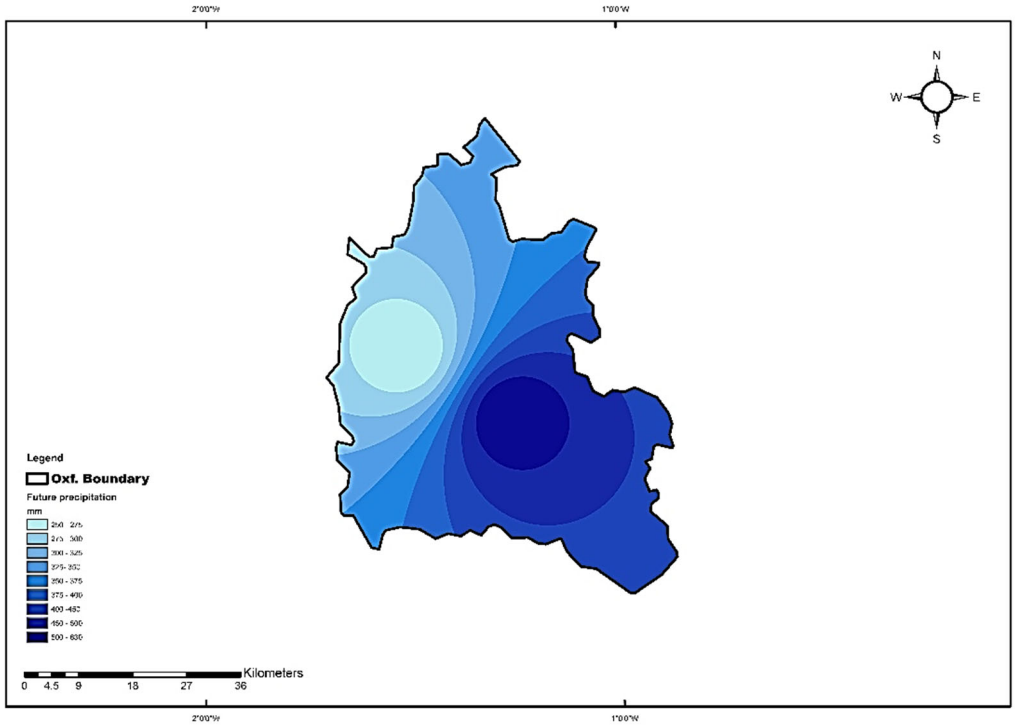


**Figure 5.44** Spatial Distribution of Future Rainfall under SSP2-4.5 Scenario

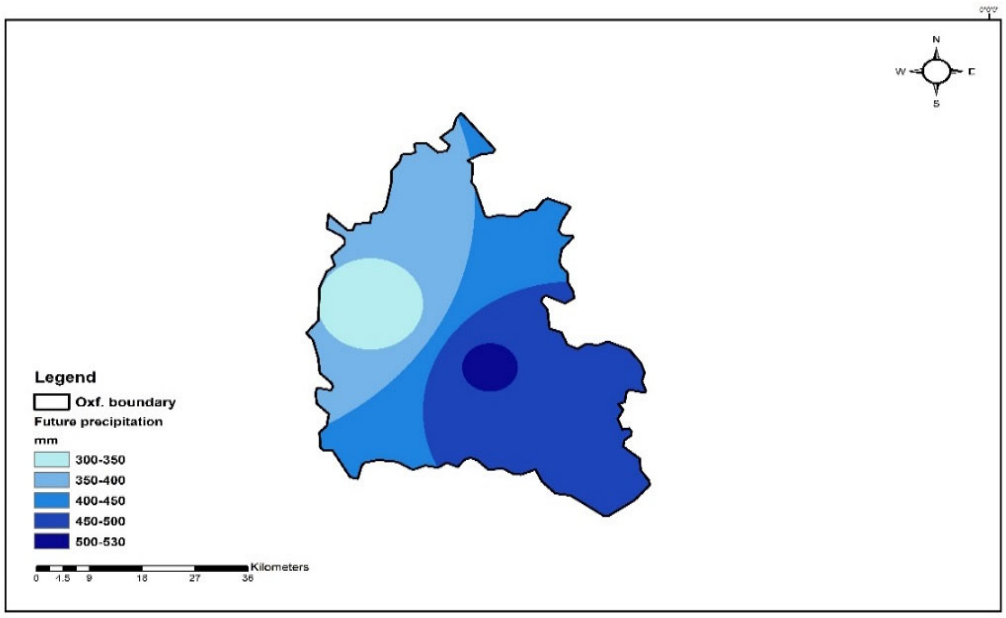


**Figure 5.45** Spatial Distribution of Future Rainfall under SSP5-8.5 Scenario

The runoff values were estimated for both scenarios SSP2-4.5 and SSP5-8.5. The runoff values for SSP2-4.5 values varied from the minimum of 230 to 530 mm. The most dominated estimated values of site varied between 370-380 mm and covers around 65% of the site. The other parts are covered from 380-470 mm by 35% the highest value covers around 10%. The runoff under SSP5-8.5 showed a decrease in values due to decrease in spatiality distribution. The min value was 230 mm and the highest is 530 mm. The dominate part is cover more than 68% of the site and the values 360-400 mm. The second dominate part covers around 20 % and values 430-500 mm. The higher part covers only 8% of the study area. The estimated average volume under SSP2-4.5 is about $0.91\times 10^{6.}$ and $0.79 \times 10^{6}$ under SSP5-8.5. Figures 5.46 and 5.47 demonstrates the future rainfall-runoff models under SSP2-4.4 and SSP5-8.5 respectively.

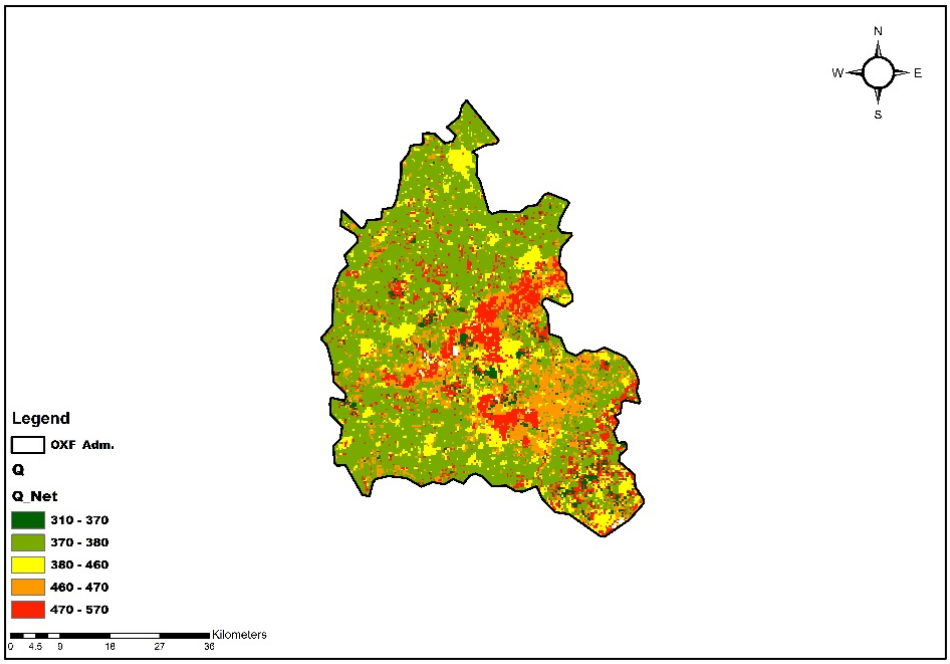


**Figure 5.46** Future Rainfall-runoff under SSP2-4.5

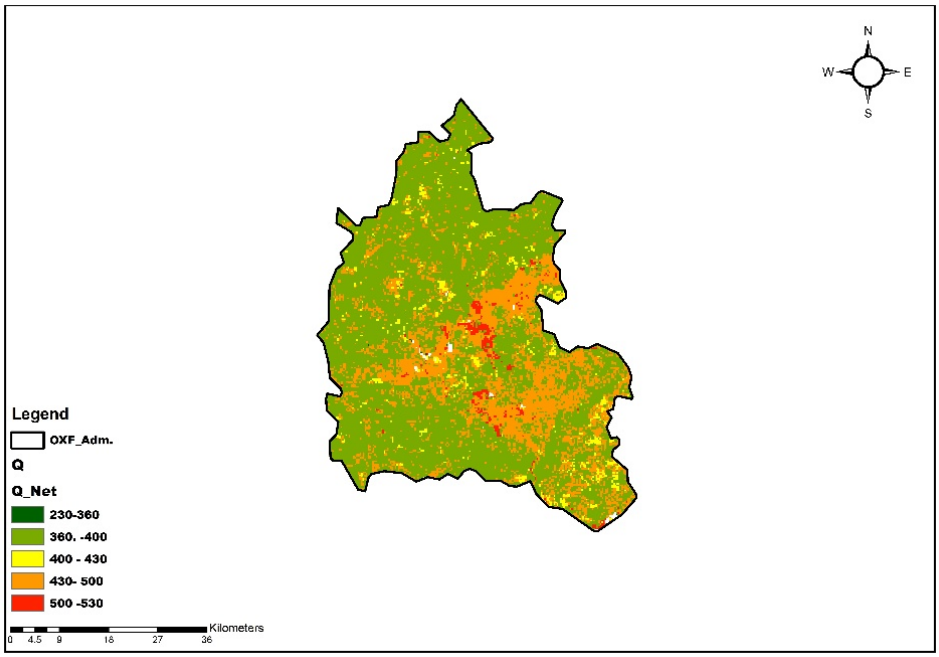


**Figure 5.47** Future Rainfall-runoff under SSP5-8.5

The consistency ratio was calculated (CR) and it was less than 0.05 for the Oxfordshire study region this outcome underscores the reliability of the weight-allocation process for RWH potential mapping for both historical and future projections. Based on the RWH potential map for a historical model, five distinct suitability regions can be delineated: (a) very high suitability: Encompassing approximately 51.3% of the area,

(b) High suitability: Spanning around 29.4% of the region, (c) moderate suitability: Covering approximately 12.6% of the territory, and (d) low suitability: Extending across approximately 4.1% of the landscape and finally very low suitability (e): covering around 2.6% of the study region. The spatial distribution is shown in Figure 41. For Future potential RWH, the results showed a slightly change for SSP2-4.5 as rainfall values fluctuated and there was a slight decrease in rainfall amount in the study area of Oxfordshire, and the very high suitability was affected by this change, and the values as the following; (a) very high suitability: 45.3%, (b) High suitability:33.8%, (c) moderate suitability: covering approximately 16.4% and (d) low suitability: Extending across approximately 2.8% of the landscape and finally very low suitability (e): covering around 1.7% of the study area.

For SSP5-8.5 the potential RWH suitable site selection as the follow: (a) very high suitability: 38.2.%, (b) High suitability:30.8%, (c) moderate suitability: covering approximately 13.4% and (d) low suitability: Extending across approximately 5.02% of the landscape and finally very low suitability (e): covering around 11.7% of the study area. Figures 5.48, 5.49 and 5.50 represents the potential suitable site selection for RWH for historical, future projection under SSP2-4.5 and SSP5-8.5 respectively.

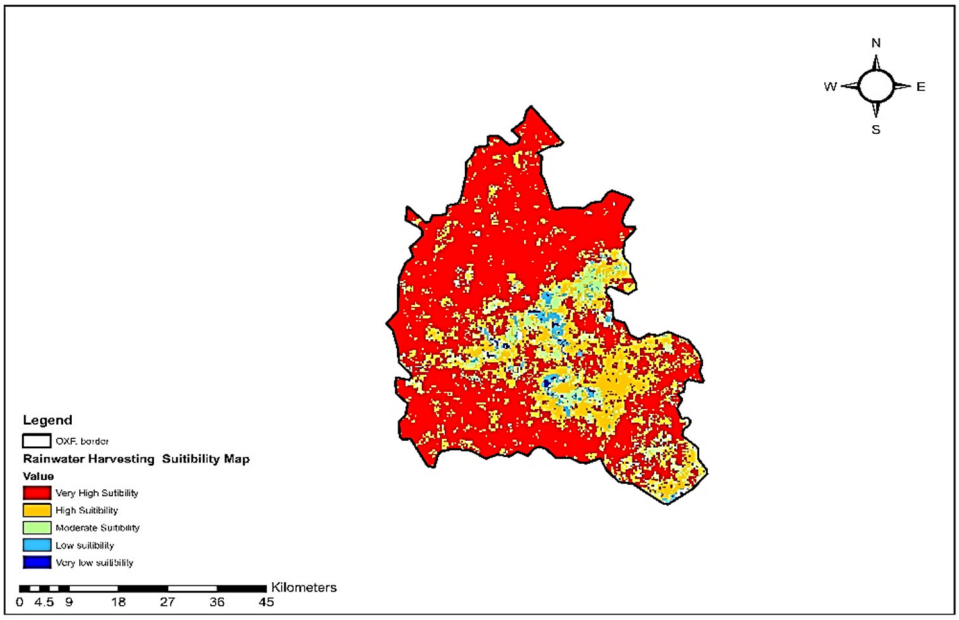


**Figure 5.48** RWH Suitable Site selection for Historical Rainfall

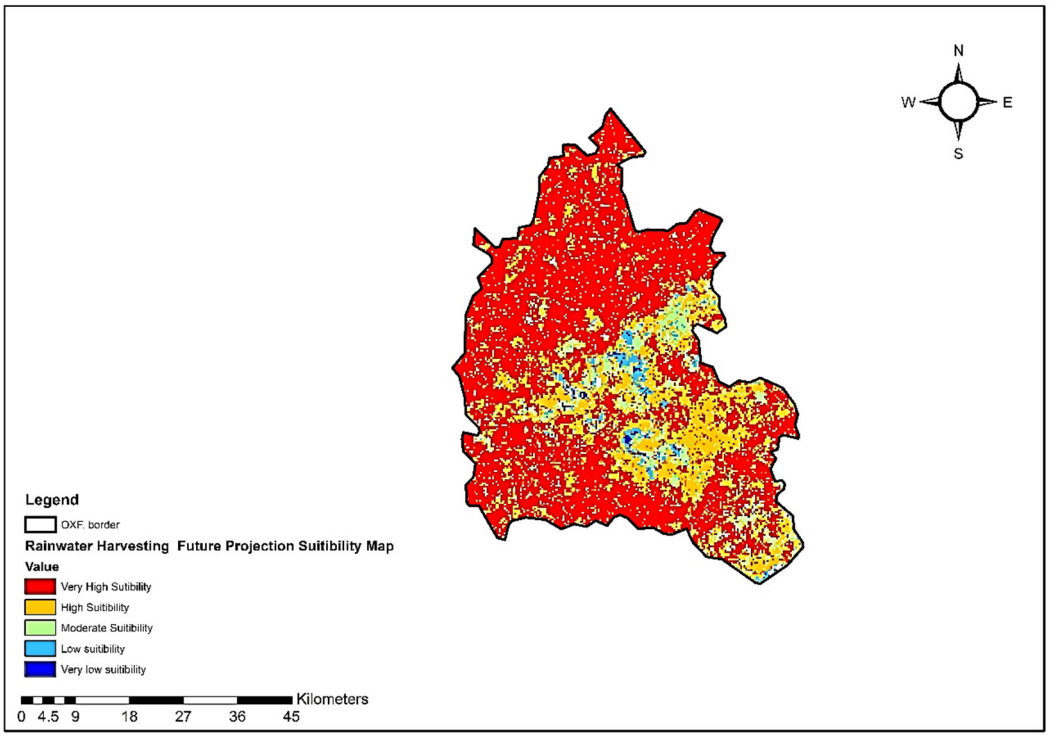


**Figure 5.49** RWH Suitable Site Selection under SSP2-4.5

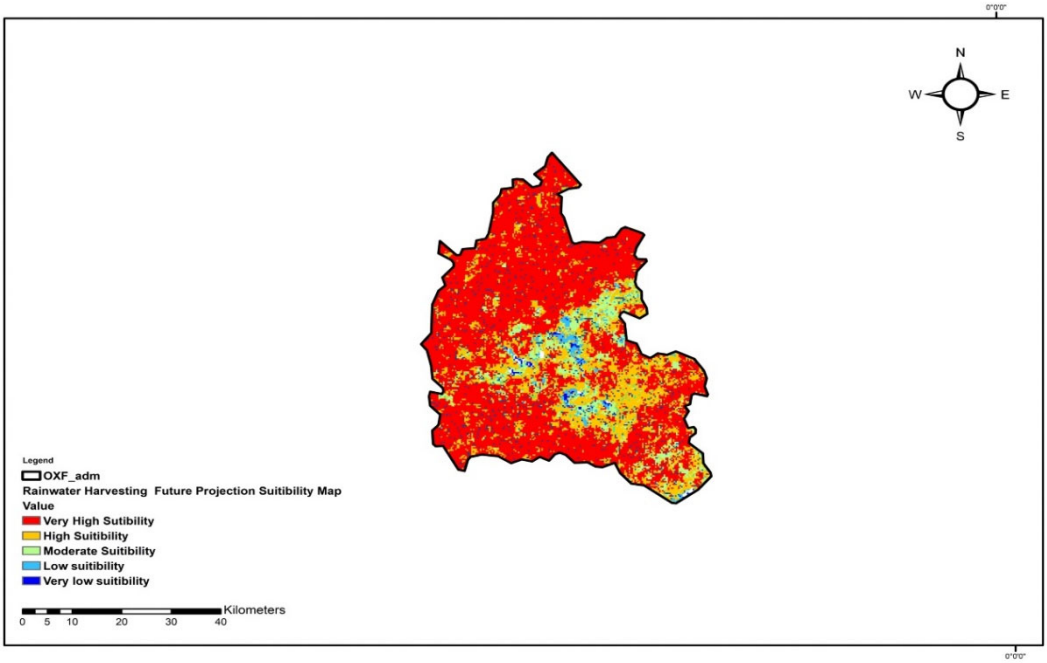


**Figure 5.50** RWH Suitable Site Selection under SSP5-8.5

## 5.6 Evaporation Estimation for Oxfordshire Study Area

### 5.6.1 Estimation Evaporation by Using MLP Model

The Artificial Neural Network (ANN) model was developed and trained using MATLAB 2023a to determine the optimal architecture for predicting evaporation. Several statistical tests were applied to evaluate the model's performance and robustness.

a. **Model Inputs and Structure:** Daily data for rainfall, minimum and maximum temperatures, and sunshine hours were used as inputs, while evaporation data served as the output variable. The dataset was divided into three subsets:

- **Training set** (70%) – used for model training,
- **Validation set** (15%) – employed to monitor performance and prevent overfitting,
- **Test set** (15%) – used to assess the model's generalization to unseen data.

The training process was halted when the error on the validation set reached its minimum to avoid overfitting. After training, the model's performance was evaluated using the unseen test dataset, ensuring its predictive capabilities.

b. **Model Evaluation and Results:** Figure 5.51 presents the relationship and validation model for observed and predicted evaporation, additionally, the figure includes the $R^2$ value for the Oxford Shire, of 0.964 indicating the model's accuracy is very good. Figure 5.52 shows the time series of observed and predicted evaporation relationship between observed and simulated data. The Figure shows the observed simulated results of the evaporation of the study area and the differences are very small less than 4% and the model performance is good. Table 5.12 details the validation metrics Mean Squared Error (MSE), Mean Absolute Error (MAE), and Root Mean Squared Error (RMSE) for ANN model. The ANN technique was used to generate these results, with the best model selected based on performance criteria. Validation, training, and testing results for the ANN model can also be found in Appendix C.

**Table 5.11.** Validation values for the MLP Model

| Model Input Data | MAE | MSE | RMSE |
|---|---|---|---|
| Rainfall, Tmin, Tmax, SSH | 0.0103 | 0.0142 | 0.1123 |

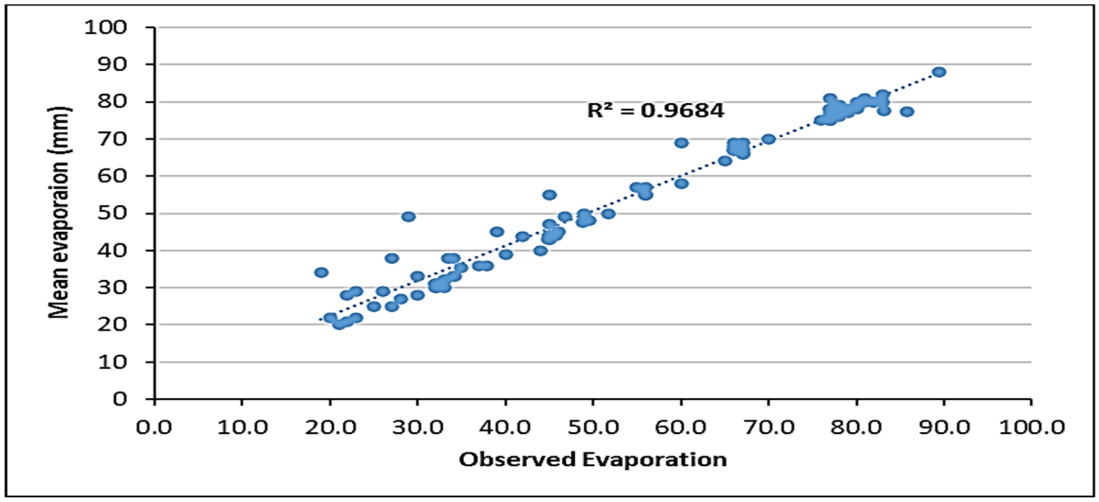


**Figure 5.51** The validation of Evaporation Model

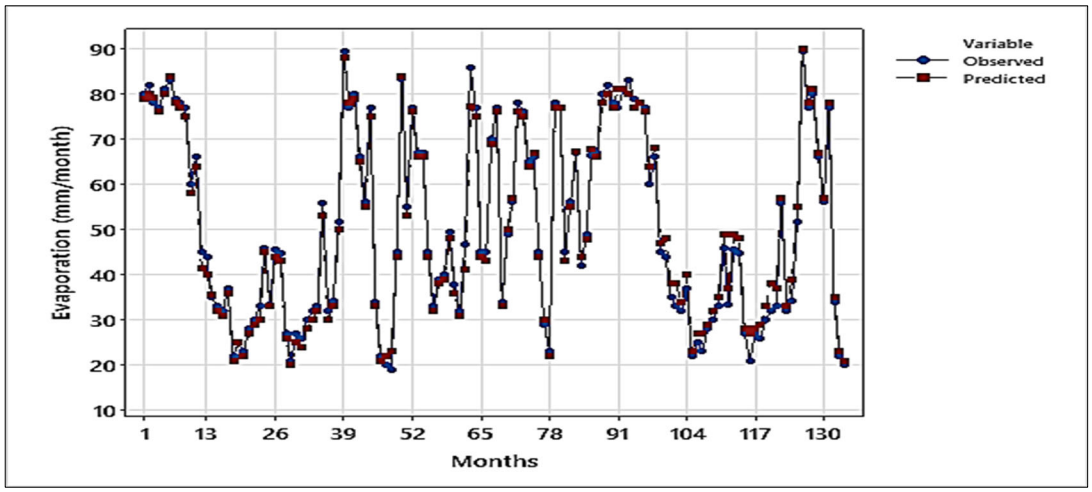


**Figure 5.52** The Time Series of Observed and Predicted Evaporation

The evaporation rate under SSP2-4.5 scenario for the period P1 (2031-2050) increased about 0.64% compared to baseline period while for P2 (2051-2070) the evaporation rate increased by 0.73%. The third period of P3 (2071-2090) showed an increase rate

of 0.81% while P4 (2091-2100) was highest, and the rate increased about 0.92% compared to baseline period. The SSP5-8.5 scenario showed higher increase rates compared to SSP2-4.5. The P1 and P2 increase rate were 0.76 and 0.87 respectively while P3 and P4 rate were 0.96 and 1.05 %. The effect of SSP5-8.5 scenario is higher than SSP2-4.5 scenario on evaporation increasing rate in the study area of Oxfordshire. Time series of evaporation of all periods for SSP2-4.5 and SSP5-8.5 depict in Figures 5.53 and 5.53 respectively.

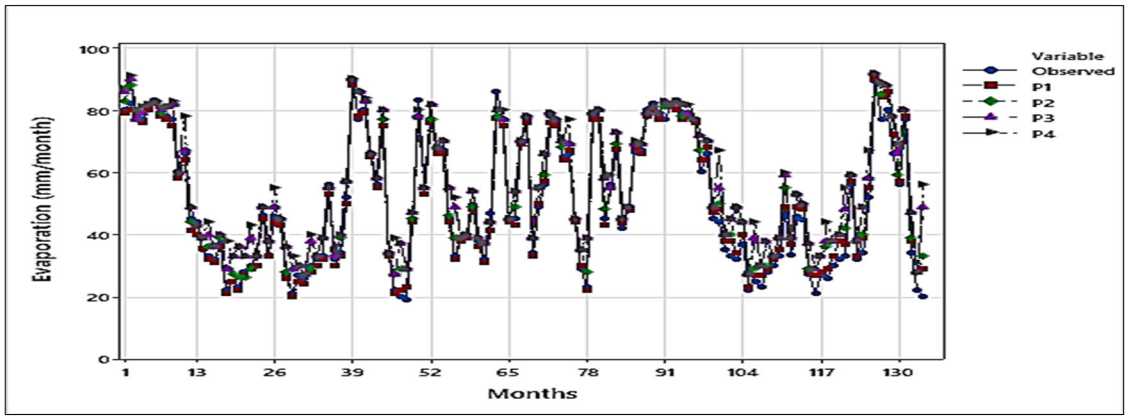


**Figure 5.53.** Time series of evaporation for observed, predicted values of SSP2-4.5

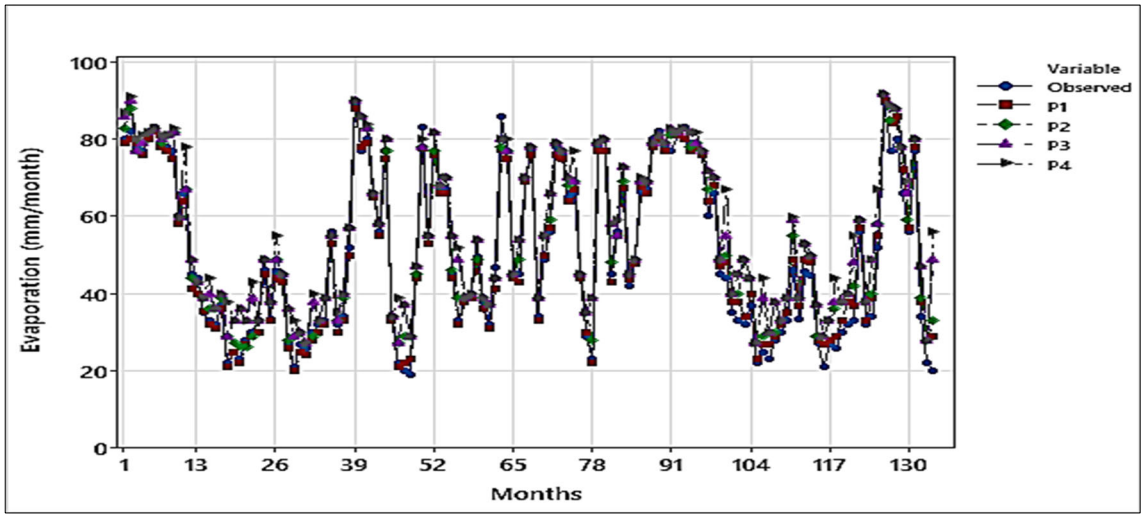


**Figure 5.54.** Time series of evaporation for observed, predicted values of SSP5-8.5

### 5.6.2 Evaporation by using SVM Model

In this study, the SVM model was implemented with four predictors: rainfall, minimum temperature (minT), maximum temperature (maxT), and sunshine hours (SSH). Table 5.12 presents the model's performance, displaying the Mean Absolute Error (MAE), Mean Squared Error (MSE), and Root Mean Squared Error (RMSE) for

the best performing SVM model. Figure 5.55 illustrates the validation process and the correlation between observed and predicted mean ensemble evaporation, achieving an $R^2$ value of 0.90 for the optimal SVM model. Additionally, Figure 5.56 provides time series visualizations of evaporation trends for observed and predicted values. under the SSP2-4.5 and SSP5-8.5 climate scenarios.

The evaporation rate under SSP2-4.5 scenario for period P1(2031-2050) showed a slight increase of 1.64 % while for P2 and P3 (2051-2070, 2071-2090) the difference percentage 1.91% and1.93% respectively. P4 (2091-2100) showed higher rate value of 2.79% compared to observed value rate of 1.31%.

**Table 5.12.** Three statistical criteria for the validation data (SVM)

| Model Input Data | MAE | MSE | RMSE |
|---|---|---|---|
| Rainfall, Tmin, Tmax, SSH | 0.221 | 0.0253 | 0.1153 |

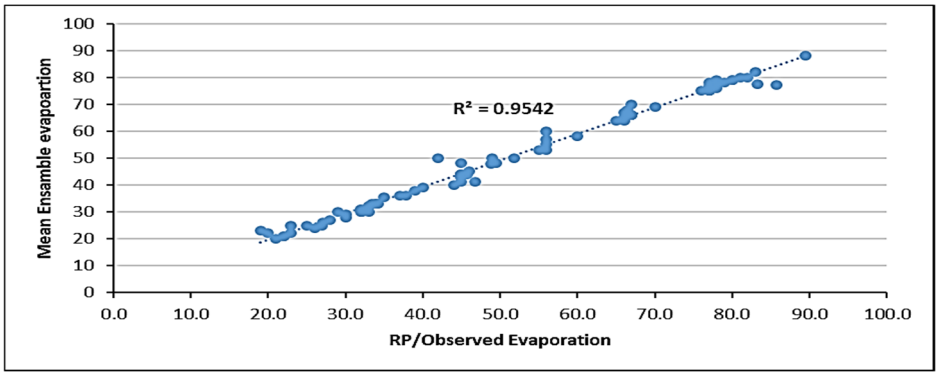


**Figure 5.55.** Validation model

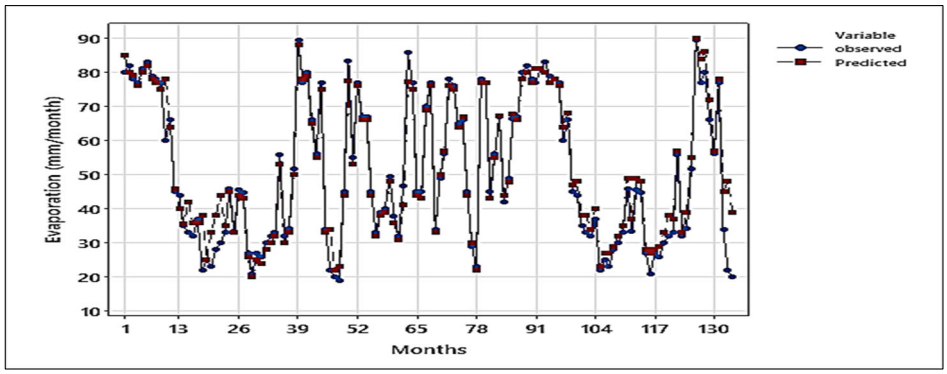


**Figure 5.56.** Time series for predicted and observed evaporation.

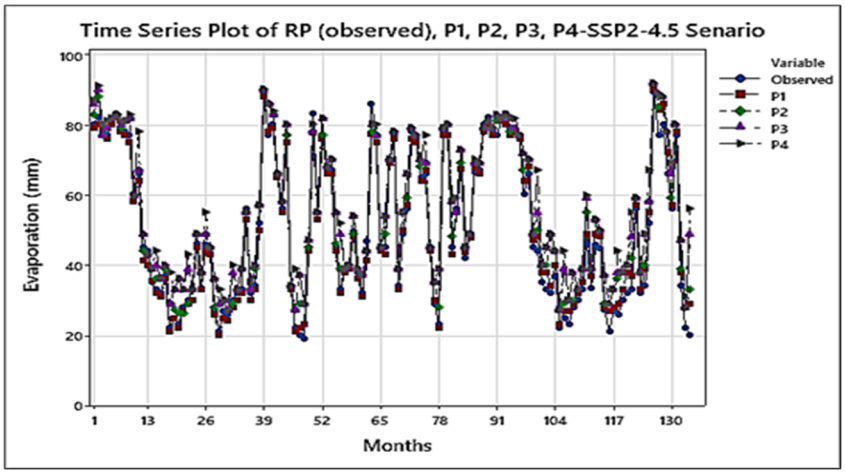


**SSP2-4.5**

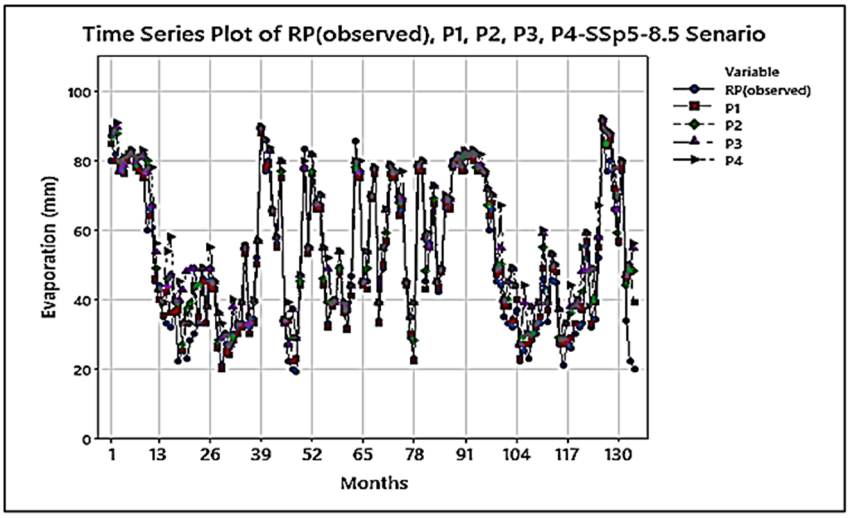


**SSP5-8.5**

**Figure 5.57** Time series of evaporation for observed, predicted values of SSP2-4.5 and SSP5-8.5 scenarios.

The future projections indicate an increase in evaporation for both the MLP (Multilayer Perceptron) and SVM (Support Vector Machine) models. However, the MLP model demonstrates superior performance when compared to the SVM model. This is evident from the lower error metrics MAE (Mean Absolute Error), MSE (Mean Squared Error), and RMSE (Root Mean Squared Error) for the model validation values.

The ensemble validation coefficient of determination ($R^2$) for the MLP model is 0.9684, which is significantly higher than the $R^2$ for the SVM model, which is 0.9542. These results indicate that the MLP model provides a more accurate and reliable prediction of evaporation, outperforming the SVM model in this context.

Table 5.14 below summarizes the average annual evaporation for the reference period (RP/historical) compared to the future projections under the SSP2-4.5 and SSP5-8.5 scenarios, illustrating the increase in evaporation across both models.

**Table 5.13.** The average annual evaporation of baseline compared to future projection evaporation under the SSP2-4.5 and SSP5-8.5 scenarios.

| Scenario | AV. Evaporation mm year$^{-1}$ | | | | Av. Evaporation rate change % |
|---|---|---|---|---|---|
| Baseline period | 577 | | | | - |
| SSP2-4.5 | P1 | P2 | P3 | P4 | 38.1 |
| | 615 | 616.3 | 617.1 | 617.8 | |
| SSP5-8.5 | 647 | 647.7 | 648.5 | 650.4 | 70.3 |

## 5.7 Estimation of Crop Water Requirements

In this section the crop water requirement will be estimated for three types of crops, wheat, sunflower and barley under the effect of two scenarios SPP2-4.5 and ASP5-8.5.

### 5.7.1 Reference period of precipitation, Evapotranspiration ET0, minimum and maximum temperature

The mean monthly climatic data were input into LARS WG 8.0 to extract the minimum and maximum temperatures and precipitation for the RP. January, October, November and December witnessed the highest average monthly precipitation amounts for RP, at 65.83, 79.19, 73.78 and 68.62 mm, respectively. January, February, and December had the lowest monthly average temperatures of 1.15. 0.97 and °C 1.66 °C, respectively. In contrast, the study region's most significant monthly average temperatures of 22.63 °C and 22.53 °C, respectively, were recorded in July and August. The average annual simulated ET0 equals 997.58 mm/year, and the highest and lowest monthly average value rates were 133.64 and 35.79 mm in December and July, respectively. Figure 5.59 depicts the monthly average values for precipitation, minimum temperature, maximum temperature, and ET0 for RP.

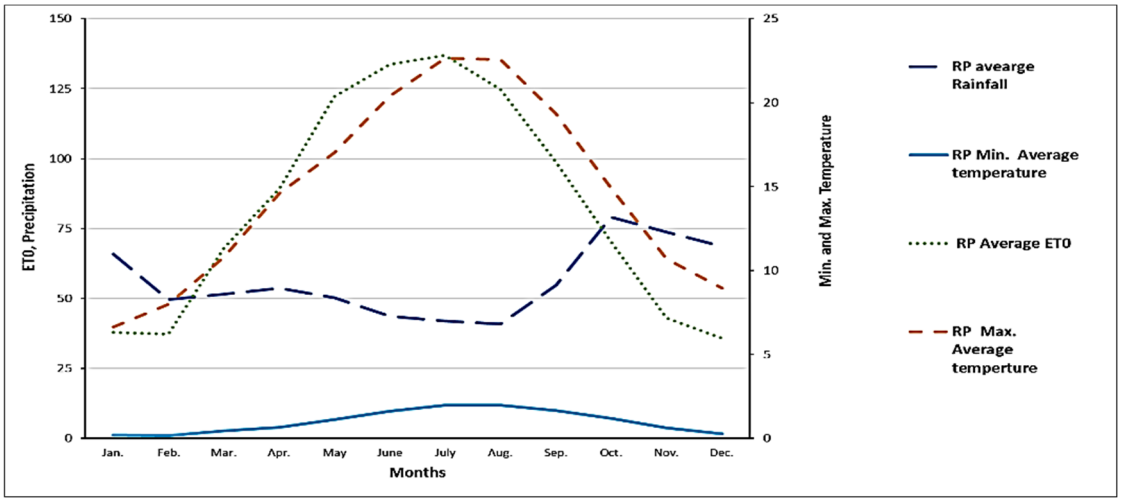


**Figure 5.58.** Monthly average values for precipitation, min, max. temperature, and *ET0* for RP.

### 5.7.2 Future Projection of ET0

The future ET0 projection under the SSP2-4.5 scenario shows that there is a slight increase in average monthly ET0 for P1 and P2 as the highest values of ET0 occurred in June, July, and August with 133.64, 136.98 and 124.76, 133.88, 137.7 and 124 89 mm/month respectively. For P3 and P4, ET0 increased slightly than P1 and P2, and the highest ET0 values occurred in June, July, and August at 133.98, 137.95, 124.99, 134.4, 138.6 and 125.7 mm/month respectively. ET0 under the SPP5-8.5 scenario for all periods increased specifically in June, July, August, and September, as shown in Figure 5.60. The projected effective rain results varied throughout the months, with the highest values occurring in January, May, and December under the SSP2-4.5 and SPP5-8.5 scenarios for P1, P2, P3, and P4, respectively.

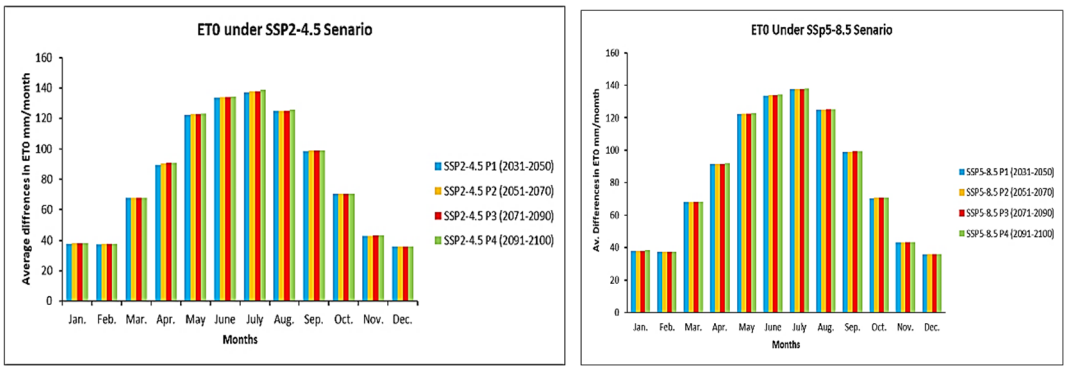


**Figure 5.59.** Differences in average ET0 future projection

### 5.7.3 CWR for RP, SSP2-4.5 and SSP5-8.5

Crop water requirements vary significantly and depend on several factors, including regional climate, soil type, effective rainfall, cultivation practices, and more. These requirements represent the amount of water necessary to compensate for the water lost through evapotranspiration (ET0). The water demand for each crop or its irrigation requirements also changes throughout the crop's life cycle and is not evenly distributed over time.

This study focuses on the irrigation needs of three specific crops: wheat, barley, and sunflower. Table 5.15presents the irrigation and crop water requirements for these crops during the reference precipitation period and future projected periods under climate scenarios SSP2-4.5 and SSP5-8.5. These projections are analyzed for four timeframes: P1(2031-2050), P2 (2051-2070), P3 (2071-2090) and P4 (2091-2100) in the study area of Oxford Shire.

**Table 5.14.** Crops water requirements for RP and under SSP2-4.5 and SSP5-8.5 Scenarios

| crops | P_H Dates | CWR RP mm/dec | CWR P1-4.5 mm/dec | CWR P2-4.5 mm/dec | CWR P3-4.5 mm/dec | CWR P4-4.5 mm/dec | CWR P1-8.5 mm/dec | CWR P2-8.5 mm/dec | CWR P3-8.5 mm/dec | CWR P4-8.5 mm/dec |
|---|---|---|---|---|---|---|---|---|---|---|
| wheat | 01/11-29/7 | 293.4 | 326.1 | 337.2 | 344.5 | 350.3 | 354.9 | 360.6 | 365.4 | 369.7 |
| barely | 01/11-1/07 | 66.2 | 86.7 | 91.5 | 108.6 | 115.1 | 120.5 | 126.6 | 129.8 | 132.3 |
| sun flower | 28/04-01/10 | 358.5 | 370.7 | 379.6 | 387.1 | 395.5 | 401.6 | 415.7 | 421.5 | 434.6 |

The CWR percentage increased under the SSP2-4.5 and SSP5-8.5 scenarios respectively. For wheat the percentage increased about 8% and 11% for P1 and P2, while for P3 and P4 increased 13 and 15 % respectively. Under SSP5-8.5, the CWR increased 15% for P1, P2 and P3 16% while P3 and P4 18 and 19%. The percentage increased for all periods specifically under SSP5-8.5 for wheat. For Barley, the P1, P2 and P3 showed a slight increase of 5, 7 and 11% and 13 % respectively. The SSp5-8.5 showed a slight increase in P1 and P2, 14, 16 % respectively, but increased with a steady percentage for P3 and P4 by 17 %. CWR for sunflower increased steadily specifically for P1 and P2 under SSP2-4.5 scenario by 4%, and 6% respectively. For P3 and P4 the percentage showed a slight increase by 8 and 11%. While under SSP5-

8.5, the CWR increased dramatically compared to SSP2-4.5 and RF by for the three types of crops and the biggest increase is for sunflower, wheat and barley has the lowest CWR compared to them. Figure 5.57 illustrates the increasing difference in percentage for all three types of crops comparing to RF/baseline CWR.

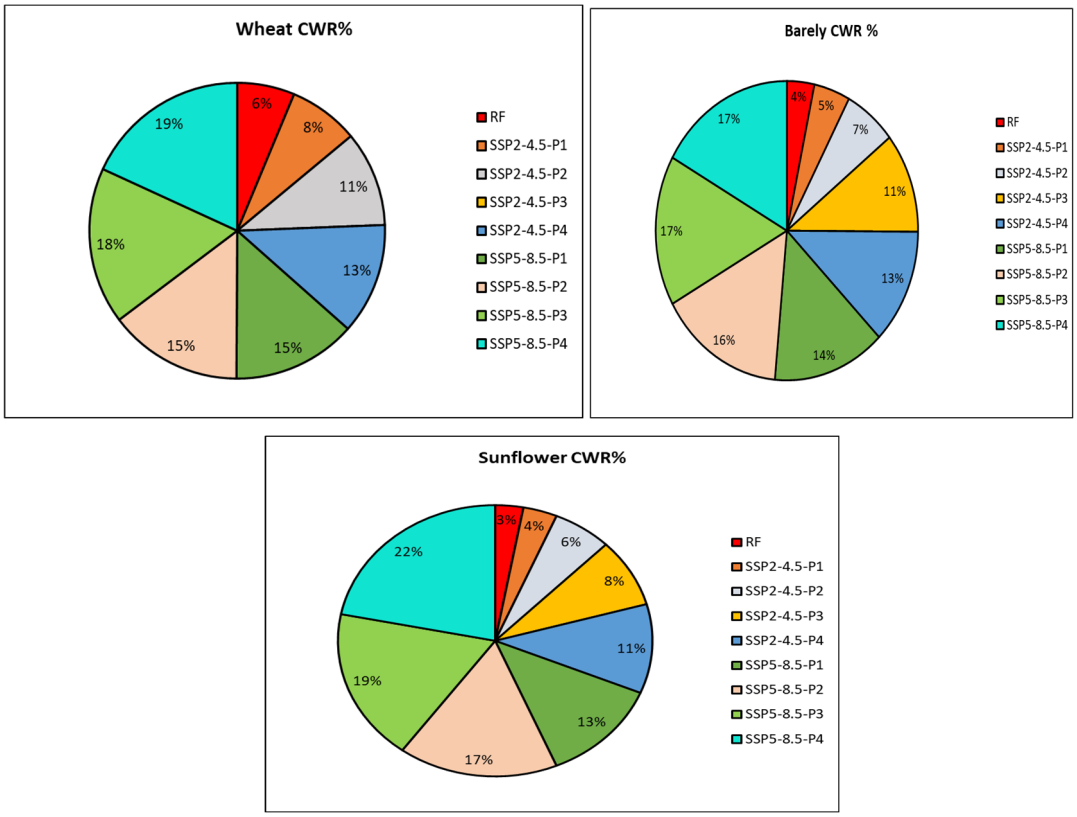


**Figure 5.60** The CWR percentage under the SSP2-4.5 and SSP5-8.55.6.4 Crops Net Irrigation Water Requirements for RP and under SSP2-4.5, SSP5-8.5 Scenarios

Optimizing crop water requirements and irrigation schedules is key to improving irrigation management for major crops. The goal is to efficiently regulate the amount, duration, and rate of irrigation to maximize water use for cultivation. Water resources can be utilized more purposefully by carefully controlling these factors, resulting in better crop yields and sustainable agricultural practices.

Tables 5.16 and 5.17 provide detailed information on the net irrigation requirements for winter wheat, winter barley, and sunflower. These requirements are analyzed for the reference period (RP) as well as for future projections (P1, P2, P3, and P4) under the SSP2-4.5 and SSP5-8.5 climate scenarios.

**Table 5.15.** Net Irrigation agriculture requirements for crops for RP and under scenario SSP2-4.5

| Crops | Stage | Depl. % | Av. NIWR RP mm | Av. NIWR P1-4.5 mm | Av. NIWR P2-4.5 mm | Av. NIWR P3-4.5 mm | Av. NIWR P4-4.5 mm |
|---|---|---|---|---|---|---|---|
| | Int. | 55 | 69.7 | 76.4 | 91.2 | 98.4 | 109.3 |
| wheat | DEV | 60 | 99.4 | 124.2 | 136.9 | 143.6 | 145.7 |
| | MID | 55 | 130.3 | 147.4 | 154.1 | 167.5 | 174.3 |
| | END | 90 | **Av.=99.8** | **Av.=116.8** | **Av.=12** | **Av.=136.5** | **Av.=143.1** |
| | Int. | 55 | 10 | 13 | 16.7 | 20.2 | 21.7 |
| barely | DEV | 60 | 15 | 17 | 20.3 | 22.3 | 24.2 |
| | MID | 55 | 18 | 20 | 22.5 | 24.2 | 26.1 |
| | END | 40 | **Av.=14.3** | **Av.=16.7** | **Av.=24.5** | **Av.=22.3** | **Av.=2** |
| | Int | 45 | 50.3 | 55.4 | 58.1 | 59.2 | 61.9 |
| | Dev | 50 | 140.8 | 159.2 | 165.9 | 168.1 | 171 |
| sunflower | Mid | 80 | 181.7 | 191.7 | 196 | 198.8 | 200 |
| | End | 95 | **Av.=124.2** | **Av.=135.4** | **Av.=140** | **Av.=142** | **Av.=144.3** |

**Table 5.16.** Net Irrigation agriculture requirements for crops for RP and under scenario SSP5-8.5

| Crops | Stage | Depl. % | Av. NIWR RP mm | Av. NIWR P1-8.5 mm | Av. NIWR P2-8.5 mm | Av. NIWR P3-8.5 mm | Av. NIWR P4-8.5 mm |
|---|---|---|---|---|---|---|---|
| | Int. | 55 | 73.4 | 79.1 | 93.7 | 103.1 | 113.7 |
| wheat | DEV | 60 | 109.1 | 128.2 | 141.2 | 147.1 | 149.4 |
| | MID | 55 | 136.2 | 152.2 | 159.2 | 169.8 | 177.8 |
| | END | 90 | **Av.=106.2** | **Av.=119.83** | **Av.=131.4** | **Av.=140** | **Av.=149.96** |
| | Int. | 55 | 12.2 | 14.2 | 16.9 | 21.4 | 21.9 |
| barely | DEV | 60 | 17.5 | 18.8 | 20.8 | 22.8 | 23.9 |
| | MID | 55 | 19.3 | 21.7 | 22.9 | 23.7 | 25.8 |
| | END | 40 | **Av.=16.33** | **Av.=18.23** | **Av.=20.2** | **Av.=22.63** | **Av.=23.86** |
| | Init | 45 | 55.3 | 56.2 | 64.7 | 67.1 | 68.9 |
| | Dev | 50 | 145.3 | 164.1 | 168.1 | 172.2 | 176.2 |
| sunflower | Mid | 80 | 194.1 | 198.2 | 200.2 | 211.5 | 213.3 |
| | End | 95 | **Av.=131.5** | **Av.=139.5** | **Av.=144.3** | **Av.=150.3** | **Av.=152.8** |

The crop water requirements for the SSP5-8.5 scenario have increased compared to the SSP2-4.5 scenario for the three types of crops specifically for sunflowers as it increased in both scenarios. Wheat and the less increasing occurred in barely as shown in tables 5.16 and 5.17 respectively.

## 5.8 Discussion

This study aimed to identify and locate optimal sites for rainwater harvesting (RWH) to enhance water resource management under the impact of climate change in two study areas: a semi-arid environment in Iraq's Kirkuk governorate and Oxfordshire County in the UK. The study compared the two sites for both present conditions and future projections. A comprehensive methodology was adopted to assess potential suitable site selection for RWH in both study areas.

For downscaling climatic models of the first study area of kirkuk located in a semi-arid country, Iraq, under two senarios SSP2-4.5 and SSP 5-8.5 for the periods (2031-2050, 2051-2071, 2071-2090 and 2091-2100). The two statistical tests, namely the Kolmogorov-Smirnov (K-S) test and the p-value analysis, along with graphical comparisons, were conducted to assess the similarity between the distributions of daily climate variables derived from observed and simulated data for the baseline period (1980-2010). The results demonstrate that the LARS-WG model performs satisfactorily in simulating future climate variables, including maximum temperature (Tmax), minimum temperature, (Tmin), precipitation (Rain)**,** and solar radiation (Radi)/SSH, indicating its reliability for climate projections. For precipitation, the P showed significant values specifically in the summer season and months of (June, July, and August). This due to no rainfall during these months in that study location. The assessmnet of of P value for other seasons were perfect, very good and good fit.

The two scenarios showed increasing in minT and, maxT specifically under the SSP5-8.5 scenario, for the periods 2071-2100 during the months, of June July, and August compared to the SSP2-4.5 scenario and historical climate reference. The max average temperature reached 32.5 °C while it reached 31.746 °C under the SSP2-4.5 scenario. While the average min temperature reached 21.85 °C. The precipitation values declined sharply specifically under the SSP5-8.5 scenario and the lowest values equal 41.676mm and 42.123 mm respectively. The annual average precipitation fell in both scenarios compared to reference or historical values, which means climate change impacts the study region. Sunshine hours' results showed a slight increase as well for both scenarios. This indicates that the study region is affected by severe climate change. The biggest average change percentage of precipitation under the SSP2-4.5 decreased during January and the values were (6.25, 12.34, 13.38 and 14.61%) for the

periods (2031-2050), (2051-2070), (2071-2090) and 2091-2100 respectively. While December and November recorded a decrease in precipitation percentage and the highest values were 10.31 and 12.86 % for periods 2071-2090 and 2091-2100 respectively. For SSP5-8.5 scenario the highest decrease in precipitation percentage was for January for all periods, and the values were 7.52, 13.43, 14.38 and 15.61 % for periods (2031-2100). The second highest decrease was in November and December as the highest values were 10.67 and 12.89 % for periods 2071-2090 and 2091-2100 while for November were 9.76 and 10.25% for periods respectively.

For the Kirkuk study area, climate data for 42 years was used to conduct this research study. The study area showed fluctuating rainfall, with a recent decline in average annual precipitation. Historical rainfall ranged from 270 mm to 490 mm annually, while future projections indicate a range of 255 mm to 390 mm and 255-400 mm under SSP2-4.5 ans SSP5-8.5 respectively. Due to the importance of accurate rainfall data, the research addressed associated uncertainties by applying a normality distribution test. Only data with a normality score exceeding 40% were used to ensure accuracy and account for variability in rainfall distribution. Rigorous validation of the rainfall data was also conducted, leading to the discovery of a strong positive rainfall-runoff correlation, with $R^2$ values of 95.42 % emphasizing the crucial link between the two factors in assessing RWH potential site selection.

The study utilized the Weighted Linear Combination (WLC) approach to assign importance to various thematic layers, offering flexibility in weight allocation. Consistency checks were performed to enhance accuracy in delineating suitable RWH zones. Runoff was given the highest weight at 42%, reflecting its importance in identifying potential RWH sites, followed by runoff slope at 25%, due to its significant impact on site selection. Soil texture (16%) also played an important role. It was particularly relevant in the presence of Hydrologic Soil Groups (HSGs) C and D, which indicate good runoff potential and low infiltration. In contrast, stream order, weighted at 10%, and land cover/use contributed 6% to the overall weighting. The rainfall-runoff values varied according to the study area in Kirkuk and historical rainfall-runoff varied from a minimum of 190 mm to a maximum of 430 mm, while for future projection the values were 180 to 340 mm. The impact of climate change and the decline of rainfall for future projection affected the amount of future runoff

depth as discussed in a case study for rainfall-runoff in the northern region of Iraq and specifically in Kirkuk site (Al-Hasani B. et al., 2024). For historical RWH potential site selection, the results indicated that Low Suitability: Encompassing approximately 31.8% of the area, (b) Medium Suitability: Spanning around 37.4% of the region, (c) High Suitability: Covering approximately 22.6% of the territory, and (d) Very High Suitability: Extending across approximately 8.2% of the landscape compared to future projection the results showed the RWH potential zones distribution under SSP2-4.5 scenario altered slightly: 'low suitability' accounted for around 44.4% of the study area, 'moderate suitability' extended across approximately 31.2%, 'high suitability' encompassed around 18.3%, and 'very high suitability' covered approximately 6.1%. The potential suitable site selection under SSP5-8.5 scenarios showed less values as the study area categorized into four categories: very low suitability about 5.45%, moderate suitability about 27.23%, high suitability around 17.2% and very high suitability counter about 5.12% which means that there is an effect of climate change on rainfall distribution and amount of Kirkuk site as it affected the average annual rainfall-runoff. The reduction in rainfall due to climate change will lead to a corresponding decrease in surface runoff, which in turn will significantly affect the suitability of sites for rainwater harvesting (RWH). As rainfall becomes less frequent or less intense, especially in regions or months projected to experience significant declines The study highlights the effective integration of AHP/MCDA, remote sensing, GIS technologies, and climate models for future projections using LARS-WG to project suitable site selection for future rainwater harvesting. This integrated approach successfully identified potential sites for RWH in the study area. Compared to other results (Khan et al, 2022) used GEO-HEC and GIS techniques to identify suitable locations for structures for RWH in their study, which was conducted in Pakistan's semi-arid areas. Suni, Sujono, and Istiarto (2023) used satellite imagery and combined GIS techniques to define rainwater harvesting pounds in Indonesia as a semi-arid zone. However, none of these studies have focused on the importance of RWH for agricultural use or under the impact of climate change.

The evaporation values for MLP and SVM showed increasing values in average evaporation of the Kirkuk study area. The MLP model was more accurate than the SVM, and the $R^2$ was equal to 0.955, MAE, MSE and RMSE values were 0.0201, 0.0122 and 0.1053 respectively For SVM the evaporation values fluctuated for all

periods and the $R^2$ is 0.90. The MAE, MSE and RMSE values were higher than the MLP model and equals to 0.351, 0.01617 and 0.1323 respectively. The average evaporation rate change under SSP2-4.5was 57.2% and 85.9 % under SSP2-4.5 AND SSP5-8.5 respectively The MLP model has been approved and validated as the best model for evaporation prediction for this study.

The crop water requirements for three types of crops were estimated based on RP and future projection scenarios for SSP2-4.5 and SSP5-8.5. The water crop requirements varied based on the season, type of crop, and ET0. Based on the result scenarios, the water requirement for Sunflower was the highest under both scenarios than that for wheat and barley. As the CWR for Sunflower for RP was 669.5 mm/dec compared to wheat 493.2 mm/dec and barley 117.2 mm/dec. These results compared to other results that used CROPWAT 8.0 in different environments such as a study by Aydin (2022) showed the water quantification of some major crops in Turkey as a semi-arid region, while another study was conducted in the north-eastern region of India to estimate crop water requirements and irrigation schedule as a semi-arid region (Panme & Sethi, 2023). Zamani et al. (2020) evaluated the climate change effect on agriculture water allocation in Iran by using (CIMP5) scenarios as a semi-arid region. The result of comparison broadly supports the work of other studies in this area downscaling climate factors by the CROPWAT 8.0 and estimating crop water requirements model. Wheat experienced steady increases in CWR under both scenarios, with a 13-16% rise by the later periods under SSP5-8.5. Barley showed a relatively moderate rise in the early periods, but saw a significant jump in the later stages, with increases of up to 21% under SSP5-8.5. Sunflower had the most dramatic increases in CWR, particularly in P4, reaching 29% under the SSP5-8.5 scenario. This study is combining CWR under impact of climate change integrated with GIS and RS to identifying suitable RWH selection and estimating the water requirements from RWH for crops irrigation.

For Oxfordshire study area, the model downscales performed very good and P value. was perfect. The precipitation for periods 2031-2050 for January encounter little decreased by 0.03% comparing to base line period. The precipitation of the periods of 2051-2070 and 2071-2090 has another decreased percent by 0.3 and 0.35 respectively. While the periods 2091-2100 witness a higher percentage of 0.81 and 0.92 % respectively under SSP2-4.5 scenario. For June and July, the percentage increased by

0.95 and 1.05 % respectively. September, October and November witnessed decrease in precipitation by 1.21 and 1.32 and 1.41 % respectively for period 2031-2050. For periods 2051-2070 and 2071-2090 the average precipitation decreased for June, July, September and October by 1.43, 1.49, 1.37 and 1.39 respectively. The other months showed a stabilized amount of precipitation, and the changes were so small. Under SSP5-8.5 scenario, the precipitation has a sharp decrease compared to a base line period by 1.78, 1.81, 1.85, 1.87, 2.23, 1.91 % respectively for June, July, September, October and November for period 2030-2050. For periods 2051-2070, 2071-2090 the percentage increased by 1.85, 1.89, 1.98, 2.38 and 2.01 % respectively. The effect from SSP5-8.5 scenario is bigger than SSP2-2.4.5 in the study area specifically in Summer, winter, and Autumn seasons. For the Oxford shire study area the suitable site selection for RWH, based on the RWH potential map for a historical model, five distinct suitability regions can be delineated: (a) very high suitability: Encompassing approximately 51.3% of the area, (b) High suitability: Spanning around 29.4% of the region, (c) moderate suitability: Covering approximately 12.6% of the territory, and (d) low suitability: Extending across approximately 4.1% of the landscape and finally very low suitability (e): covering around 2.6% of the study region . While for future projection the percentages of suitability slightly changed and varied as the precipitation also slightly decreases and ranged from 350 to 640 mm/year as an average and the suitability percent also varied according to that as (a) very high suitability: 45.3%, (b) High suitability:33.8%, (c) moderate suitability: covering approximately 16.4% and (d) low suitability: Extending across approximately 2.8% of the landscape and finally very low suitability (e): covering around 1.7% of the study region. The downscaling model showed a slightly effect on climate variables specifically rainfall as decreased specifically in summer season compared to historical records. The min, max temperatures also increased especially in summer season. The annual evaporation values fluctuated for SSP2-4.5 and SSP5-8.5 scenarios and indicated an increase in evaporation rate by 38 and 70 % respectively and the MLP model was more accurate than SVM model. The crop water requirements result for Sunflower was higher than Wheat and Barley under the and SSP2-4.5 and SSP5-8.5 respectively. The CWR showed an increase under the two scenarios as wheat was the highest then sunflower and barely. Wheat: Increased by 8-19% across different periods, with the largest increase under SSP5-8.5. Barley: Showed moderate increases ranging from 5-17% under SSP2-4.5 and SSP5-8.5.

Sunflower had the largest CWR increase more than 22%, especially under SSP5-8.5, with a steady rise across all periods, showing the greatest sensitivity to climate change. The climate change projections are associated with uncertainty specifically the rainfall therefore a normality test has been applied to rainfall data for both study regions to ensure the projection for GCMs reflect accurate results. Despite the uncertainty, both study areas showed decreased in precipitation and increases in min and max. temperatures, but Kirkuk governorate showed an extreme increase in temperature and decrees in average annual precipitation. The RWH suitable site selection also changed according to the decrease in rainfall spatial distribution but the effect of climate change on Kirkuk site was greater than in Oxfordshire site. The crop water requirements also increased due to change in effective rain in both regions. Despite this climate change effect, the average runoff in both regions varied for Kirkuk governorate approximately $8\times 10^5$ $m^3$ and for Oxfordshire approximately, $1\times10^6$ $m^3$. This amount of runoff can be harvested and use for irrigation for different types of crops by encouraging farmers to adopt the innovative methods of harvesting rainwater to be utilized for cultivation. This study could reduce design costs and enhance water resource management in the future.

### 5.9 Summary

This chapter highlighted the process of assessing and identifying suitable site selection of rainwater harvesting for two study regions, the first one in Kirkuk, in northern region of Iraq and the second one in Oxfordshire, in the southeast of the UK, under five various GCMs scenarios from IPCC. Four climate variables were considered in this study for 42 years span period. The chapter also considered the estimation of evaporation by utilizing two methods and estimating crop water requirements for three major types of crops under the impact of climate change. The findings are classified into four stages: identifying suitable site selection for RWH by integrating multiple layers for historical climate variables, downscaling climate variables under five GCMs to predict future rainfall and assessing potential suitable site selection for future projection. The third stage is to assess and estimate evaporation for both study regions and finally assess and estimate crop water requirements for three types of crops.

# Chapter 6: Conclusion, Limitations, Recommendations and Future Works

This chapter provides an overview of the main findings related to the research objectives and presents the conclusions drawn from the study. The world is facing an unprecedented challenge: the adverse impacts of global climate change on our precious water resources. This challenge is reflected in shifting annual precipitation patterns and rising temperatures, both of which significantly contribute to the broader crisis of global warming. In response, sustainable water resource management has become critical, particularly in line with one of the United Nations Development Programme's (UNDP) Sustainable Development Goals by integrating water resource management at all levels to improve water sustainability and promote the use of alternative water resources to support sustainable agriculture.

As climate change continues to affect many regions, severely impacting water resources, urgent and sustainable actions are needed to achieve water sustainability. These actions aim to address water scarcity, reduce pressure on existing water resources, and foster improved water conservation practices.

To meet these goals, this study integrates multiple models to identify suitable sites for Rainwater Harvesting (RWH) under the influence of climate change. The research utilizes advanced tools such as Geographic Information Systems (GIS) and Remote Sensing (RS) technologies, combined with Artificial Neural Networks (ANN) and downscaling models. Additionally, CROPWAT 8.0 software is incorporated to enhance the final models, ensuring accurate site selection for potential rainwater harvesting systems, which can be used to meet agricultural water demands.

As part of achieving sustainable development of water resources management, it became evident that there is a significant gap in research on integrated models of rainwater harvesting (RWH) systems within the agricultural sector under the influence of climate change.

Most existing studies have predominantly focused on identifying suitable locations for rainwater catchment areas in specific regions, with little emphasis on the development and implementation of integrated models that consider multiple factors such as rainfall-runoff, evaporation, RWH systems, climate change projections, and their

impacts on different crops. This research addresses this gap by proposing an innovative approach that integrates various models and methodologies. The novelty of the proposed research can be outlined through the following three key points:

- Utilization of GIS to determine optimal RWH sites based on both current and future climate scenarios. Unlike existing studies, which are limited to current climatic conditions, this research extends the scope by incorporating climate change projections, ensuring the adaptability of RWH systems to future environmental conditions.

- Integration of multiple models, including GIS-based hydrological models, evaporation models, climate change projections, and crop optimization. This comprehensive approach allows for a holistic analysis, optimizing crop selection and the allocation of harvested water in specific areas, thereby enhancing water-use efficiency and agricultural productivity under changing climate conditions.

- Application of Artificial Neural Networks (ANN) to develop a modified model capable of forecasting and estimating potential evaporation from RWH systems in two distinct environments: semi-arid Iraq and the wet environment of the UK. This comparative analysis under different climate change scenarios will provide valuable insights into the performance and feasibility of RWH systems in diverse climatic contexts.

This research aims to fill a critical knowledge gap by developing an integrated framework that addresses both the current and future challenges of water scarcity in agriculture, particularly under the influence of climate change. The application of advanced modeling techniques and the comparative analysis across two contrasting regions further emphasize the innovation and relevance of this study.

## 6.1 Conclusion

Rainwater Harvesting (RWH) presents a promising solution to address water scarcity and enhance water supply, particularly in the face of shifting climate patterns. This research tackles the challenge by integrating a Geographic Information System (GIS)-based Multi-Criteria Analysis (MCA/AHP) with a downscaling approach utilizing the Weather Generator, Artificial Neural Networks (ANN), and CROPWAT 8.0. The primary objective was to develop RWH projections and establish a robust

methodology for identifying potential RWH sites, both for current and future agricultural development under the impacts of climate change.

The study focuses on two distinct regions: a semi-arid environment in the Kirkuk site of Iraq and the Oxfordshire site in the UK. These contrasting areas provide valuable insights into RWH's applicability across diverse climatic conditions, supporting sustainable agricultural practices in the face of future climate uncertainties.

This study endeavors to enhance water resource management and promote water sustainability by advancing methodologies that facilitate the utilization of RWH employing the power of Geographic Information Systems (GIS) coupled with MCDA methodologies to address water scarcity issues. Returning to the findings, which were posed in this study, it is now possible to state that:

Identify potential suitable site selection of RWH:

- The integration of multi-criteria evaluation and AHP within the GIS framework, driven by well-defined evaluation criteria, yields a cost-effective and invaluable resource for analytic locations for RWH and regions conducive to sustainable RWH structures.
- This study examines a thorough assessment of several critical parameters, including slope, stream order, soil type, drainage density, land cover, and land use. These factors collectively indicate the suitability of various sites for RWH.
- The research outcomes reveal promising possibilities to identify suitable sites for RWH. These findings have substantial consequences for managing water resource experts and administrators in the region, offering valuable insights for the wise management of constrained water resources.
- Throughout this study, ArcGIS emerged as a pivotal tool for amalgamating data from various thematic layers to pinpoint relevant locations. The process of identifying optimal areas for collecting and storing rainwater demands access to a versatile, efficient, and comprehensive data source, with ArcGIS serving as an exemplar in this regard.
- The success in identifying suitable RWH sites owes much to the adoption of the soil conservation service curve number (*SCS-CN)* approach in conjunction with GIS, remote sensing (RS), and other significant tools are very effective in

estimating rainfall-runoff amount. These integrated methodologies not only navigate agro-climatic and hydrological gaps but also serve as a model applicable to diverse settings worldwide.

Climate downscaling model

- The Long Ashton Research Station Weather Generator (LARS-WG) model provides an excellent performance for generating a maximum temperature, minimum temperature, solar radiation and rainfall, based on statistical tests for the baseline period 1980-2010. Therefore, it is a valid model to simulate the future climate variables under different emission scenarios.
- The maximum temperature, minimum temperature and solar radiation are expected to increase as we move toward the future, in the same context, the rainfall is likely to decline in amount as we a move toward the future that is impacted by $CO_2$ emissions. In addition, the third period and fourth period ( 2071-2090, 2091-2100) of SSP5-8.5 scenario are the worst situations compared with other periods and scenario.
- We calculate the difference between the stochastic signals of (Tmax, Tmin, Radi and Rain) for the expected mean and the baseline period (1980-2010). Then, the results show that the values of Tmax, Tmin and Radi are rising in general in Summer and spring seasons, while they fluctuated in slightly increased in winter and autumn seasons. In the same context, the Rain values have a non-uniform style for all periods and fluctuated specially in Kirkuk study region and under all emission scenarios. In general, the SSP5-8.5 scenario is the hottest and driest scenario especially in the 3$^{rd}$ and fourth period.

Prediction and Estimation of Evaporation

- Utilization ANN method to predict and estimate ensemble evaporation is very effective.
- Two Machine Learning methods have been employed, the first one was ANN (neural network) and the second is SVM, both methods were effective but neural network was more accurate in estimating evaporation.
- The data used in the evaporation model was (Tmin, Tmax, SSH, and rainfall). The evaporation increased under both climate change scenarios (SSP2-4.5 and

SSP5-8.5) but it was the worst under SSP5-8.5 scenario for the two study regions. It increased dramatically in Kirkuk site more than in Oxfordshire.

Estimation of crop water requirements

- Utilizing and integrating LARS-WG 8.0 and CROPWAT 8.0 software to estimate the crop water and irrigation requirements for three types of crops in the northern region of Iraq in Kirkuk governorate and Oxfordshire in southeast of England was conducted successfully. According to our findings, the crop water requirements increased under the effect of two climate scenarios SSP2-4.5 and SSP5-8.5, specifically for the periods (2051-2070, 2071-2090 and 2091 – 2100) respectively. The results showed that crop water requirements CWR for sunflower are higher than winter wheat and barley in both scenarios for both study regions, but the worst case was under the SSP5-8.5 scenario in the period (2091-2100).
- The results for RWH potential site selection showed a promising method by integrating GIS, RS and climate scenarios to predict the potential sites for RWH and rainfall-runoff amount in both regions under the impact of climate change. Despite that Oxfordshire is considered a wet region compared to Kirkuk governorate but the impact of climate change was clear and there was declining in rainfall. Utilizing RWH for irrigation requirements is essential for supporting a sustainable agriculture concept and these findings have substantial consequences for managing water resource experts and administrators in the regions, offering valuable insights for the wise management of constrained water resources specifically in Iraq as a semi-arid region and facing a severe impact of climate change. This novel method can also enhance food security and agriculture productivity.

## 6.2 Limitations, Recommendations and Future Works

There many limitations should be taken in consideration regarding the water harvesting system and the main ones, rainfall variability patterns such as severe droughts, or severe floods can impact the RWH. The regulation and legal challenges such as, local authorities may impose restrictions on water use that could impact the benefits of harvesting. The seasonality issue in some regions, rainfall is seasonal, and

harvesting systems may not provide a consistent water supply throughout the year. This seasonality can create periods of water scarcity during dry months, requiring backup sources such as groundwater or piped water.

Recommendations and future works

- Further work can be conducted on this methodology by testing the impact of applying more climate variables depending on the availability of climatic data and for different locations worldwide.
- Visit the site for near future to do more field investigation regarding the soil layers and location.
- Implementing new guidelines with local authorities and governorates to encourage utilizing RWH for cultivation use and helping the local farmers to implement RWH system in their farms and helping to build RWH structures like small barriers or pounds depending on the location of the farm and the suitability of these structures according to study area.
- Investing in RWH as an alternative water resource for agriculture and implementing the concept of sustainable water resources for farmers and local councils and governorate.
- Considering the future changes to all model parameters in the future studies regarding soil changes, landcover and land use for study areas to be included for further extended research.

**Publications:**

***International Conference and workshops:***

AL-Hasani, B., Abdellatif, M, Harris, C., Carnacina, I. & S. Zubaidi," Criteria for Selection of Suitable Sites for Rainwater Harvesting in The Middle East for Agriculture Use: A review study. (2022). SICET (2022), 1st SLIIT International Conference on Engineering and Technology, Sri Lanka.

AL-Hasani, B., Abdellatif, M, Harris, C., Carnacina, I. (2022), Integrated Models Layers for Identifying Suitability Sites for Rainwater Harvesting by using Geographic Information System Technique. Faculty Of Engineering and Technology Research Day Conference, Liverpool John Moores University,UK.

AL-Hasani, B., Abdellatif, M, Harris, C., Carnacina, I.(2023), Geospatial Approach Techniques for Rainwater Harvesting Suitable Sites Selection for Sustainable Agriculture Use. (Faculty of Engineering and Technology Research Day Conference, Liverpool John Moores University, UK. Winner of best People's choice Prize for a Poster)

AL-Hasani, B., Abdellatif, M, Harris, C., Carnacina, I.(2024), Integrating Geospatial Techniques to Select Suitable Sites for Rainwater Harvesting for Sustainable Agriculture.Faculty of Engineering and Technology Research Day, Liverpool John Moores University,UK.

AL-Hasani, B., Abdellatif, M, Harris, C., Carnacina, I. (2024), Optimizing Rainwater Harvesting: Geospatial Site Selection Strategies for Climate-Resilient Solutions. (People's Choice poster vote for the mid and later stage category prize winner). PGR Festival Day Conference, Liverpool John Moores University,UK.

***Journal papers:***

Al-Hasani, B., Abdellatif, M., Carnacina, I., Harris, C., Al-Quraishi, A., Maaroof, B. F., & Zubaidi, S. L. (2024). Integrated geospatial approach for adaptive rainwater harvesting site selection under the impact of climate change. Stochastic Environmental Research and Risk Assessment, 38(3), 1009-1033.

Al-Hasani, B., Abdellatif, M., Carnacina, I., Harris, C., Al-Quraishi, A., Maaroof, B. F., & Zubaidi, S. L. (2024), "Geospatial Analysis for Optimal Rainwater Harvesting Site Selection in a Semi-arid Environment. *Journal of Advances in Civil Engineering* **(Under review).**

***Book Chapters:***

Al-Hasani, B., Abdellatif, M., Carnacina, I., Harris, C., Al-Quraishi, A.M.F., Maaroof, B.F. (2024). Assessing Climate Change Impacts on Rainfall-Runoff in Northern Iraq: A Case Study of Kirkuk Governorate, a Semi-Arid Region. In: The Handbook of Environmental Chemistry. Springer, Berlin, Heidelberg. https://doi.org/10.1007/698_2024_1154.

## References


Al-Adamat, R. (2008). GIS as a decision support system for siting water harvesting ponds in theBasalt Aquifer/NE Jordan. *Journal of Environmental Assessment Policy and Management*, *10*(02), 189-206.

Al-Adamat, R., Diabat, A., & Shatnawi, G. (2010). Combining GIS with multicriteria decision making for siting water harvesting ponds in Northern Jordan. *Journal of Arid Environments*, *74*(11), 1471-1477.

Al-Adamat, R., AlAyyash, S., Al-Amoush, H., Al-Meshan, O., Rawajfih, Z., Shdeifat, A., & Al-Farajat, M. (2012). The combination of indigenous knowledge and geo-informatics for water harvesting siting in the Jordanian Badia.

Al-Hasani, B., Abdellatif, M., Carnacina, I., Harris, C., Al-Quraishi, A., Maaroof, B. F.& Zubaidi, S. L. (2024). Integrated geospatial approach for adaptive rainwater harvesting site selection under the impact of climate change. Stochastic Environmental Research and Risk Assessment, 38(3), 1009-1033.

Al-Hasani, B., Abdellatif, M., Carnacina, I., Harris, C., Al-Quraishi, A.M.F., Maaroof, B.F. (2024). Assessing Climate Change Impacts on Rainfall-Runoff in Northern Iraq: A Case Study of Kirkuk Governorate, a Semi-Arid Region. In: The Handbook of Environmental Chemistry. Springer, Berlin, Heidelberg. https://doi.org/10.1007/698_2024_1154

Al-Amri, H. S. M. N. (2021). *Evaluation of Rainwater Harvesting Systems in the Western Desert of Iraq* (Doctoral dissertation).

Al-Ansari, N., Adamo, N., Hachem, A. H., Sissakian, V., Laue, J., & Abed, S. A. (2023). Causes of Water Resources Scarcity in Iraq and Possible Solutions. Engineering, 15(9), 467-496.

Al-Daghastani(2010).WaterharvestingsearchinNinevahgovernmentusingre-IraqiJournalofDesertStudies, 2(1), 1–15.

Al-Shamiri, A., & Ziadat, F. M. (2012). Soil-landscape modeling and land suitability evaluation: thecase of rainwater harvesting in a dry rangeland environment. *International journal of applied earth observation and geoinformation*, *18*, 157-164.

Al Sudani, Z. A., & Salem, G. S. A. (2022). Evaporation rate prediction using advanced machinelearning models: a comparative study. *Advances in Meteorology*, *2022*(1), 1433835.

Al-Obaidy, A. H. M. J., & Al-Khateeb, M. (2013). The challenges of water sustainability in Iraq. *Engineering and Technology Journal*, *31*(5), 828-840.

Abdullah, A., Sudin, S., Ahmad, Z., Saad, F., Ahmad, I., Abdullah, F., ... & Romle, S. R.(2021). Intelligent Irrigation System Using Rain Water Harvesting System and Fuzzy Interface System. *International Journal of Nanoelectronics & Materials*, *14*.

Abdulrahman, S. A. (2018). The drying up of the Lower Zab River and future water disputes between Iran, Kurdistan Region, and Iraq. *International Journal of Environmental Studies*, *75*(1), 29-44.

Abed, M., Imteaz, M., Ahmed, A. N., & Huang, Y. F. (2021, December). Improved prediction of monthly pan evaporation utilising support vector machine technique. In 2021 IEEE Asia-Pacific Conference on Computer Science and Data Engineering (CSDE) (pp. 1-5). IEEE.Abtew, W., & Melesse, A. (2012). *Evaporation and evapotranspiration: measurementand estimations*. Springer Science & Business Media.*Research*, *4*(2), 108-120.

Adamowski, J., Fung Chan, H., Prasher, S. O., Ozga-Zielinski, B. & Sliusarieva, A. 2012. Comparison of multiple linear and nonlinear regression, autoregressive integrated moving average, artificial neural network, and wavelet artificial neural network methods for urban water demand forecasting in Montreal, Canada. *Water Resources Research,* 48**,** 1-14.

Adamowski, J. F. 2008. Peak daily water demand forecast modeling using artificial neural networks. *Journal of Water Resources Planing and Management,* 134**,** 119-128.

Adham, A., Riksen, M., Ouessar, M., Ritsema, C.J. 2016a. A Methodology to assess and evaluate rainwater harvesting techniques in (semi-) arid regions. Water, 8(5), p. 198.

Ammar, A. A. (2017). *Evaluating rainwater harvesting systems in arid and semi-arid regions* (Doctoral dissertation, Wageningen University and Research).

Ammar, A., Riksen, M., Ouessar, M., & Ritsema, C. (2016). Identification of suitable sites for rainwater harvesting structures in arid and semi-arid regions: review. *International Soil and Water Conservation* Ammar, A., Riksen, M., Ouessar, M., & Ritsema, C. (2016). Identification of suitable sites for rainwater harvesting structures in arid and semi-arid regions: A review. *International Soil and Water Conservation Research*, *4*(2), 108-120.

Aznar-Sánchez, J. A., Belmonte-Ureña, L. J., Velasco-Muñoz, J. F., & Valera, D. L. (2019). Aquifer sustainability and the use of desalinated seawater for greenhouse irrigation in the Campo de Níjar, Southeast Spain. *International journal of environmental research and public health, 16*(5), 898.

Arunima, D., Dhinwa, P. S., & Rajawat, A. S. (2015). Monitoring implementation of desertification combating plan using geomatics–A case study, districts Dhar and Jhabua, Madhya Pradesh. Journal of Earth System Science, 124, 87-99.

Araghinejad, S. 2014. Data-Driven Modeling: Using MATLAB® in Water Resources and Environmental Engineering. USA. Springer.

Ashley, R., Blackwood, D., Butler, D., Jowitt, P., Davies, J., Smith, H., ... & Oltean-Dumbrava, C. (2008). Making asset investment decisions for wastewater systems that include sustainability. *Journal of Environmental Engineering*, *134*(3), 200-209.

Aydın, Y. (2022). Quantification of water requirement of some major crops under semi-arid climate in Turkey. PeerJ, 10, e13696.

Bakir, M., & Xingnan, Z. (2008, March). GIS and Remote Sensing applications for rain water harvesting in the Syrian Desert (Al-Badia). In *Proceedings of the 12th International Water Technology Conference* (pp. 73-82).

Basheer, I. A. & Hajmeer, M. 2000. Artificial neural networks: fundamentals, computing, design, and application. *Journal of Microbiological Methods,* 43**,** 3-31.

Bashir, B., & Fouli, H. (2015). Studying the spatial distribution of maximum monthly rainfall in selected regions of Saudi Arabia using geographic information systems. *Arabian Journal of Geosciences*, *8*(11), 9929-9943.

Ben Mechlia,N.,Oweis,T.,Masmoudi,M.,Khatteli,H.,Ouessar,M.,Sghaier,N. Sghaier, M.(2009).*Assessment of supplemental irrigation and water harvesting potential: Methodologies and case studies from Tunisia*. ICARDA.

Bennett, C., Stewart, R. A. & Beal, C. D. 2013. ANN-based residential water end-use demand forecasting model. *Expert Systems with Applications,* 40**,** 1014-1023.

Benzaghta, M. A. (2014). Estimation of Evaporation from a Reservoir in Semi arid Environments Using Artificial Neural. *British Journal of Applied Science & Technology*, *4*(24), 3501-3518.

Buraihi, F. H., & Shariff, A. R. M. (2015). Selection of rainwater harvesting sites by using remote sensing and GIS techniques: a case study of Kirkuk, Iraq. *Jurnal Teknologi*, *76*(15).

Bougadis, J., Adamowski, K. & Diduch, R. 2005. Short-term municipal water demand forecasting. *Hydrological Processes,* 19**,** 137-148.

Clarke, D., Smith, M., & El-Askari, K. (2001). CropWat for Windows: user guide. Oak Brook, IL, USA: IHE.

Cosgrove, W. J., & Rijsberman, F. R. (2014). *World water vision: making water everybody's business*: Routledge.

Cosgrove, W.J. and Loucks, D.P., 2015. Water management: Current and future challenges and research directions. *Water Resources Research*, *51*(6), pp.4823-4839.

Chowdhury, S., Al-Zahrani, M., & Abbas, A. (2016). Implications of climate change on crop water requirements in arid region: an example of Al-Jouf, Saudi Arabia. *Journal of King Saud University-Engineering Sciences*, *28*(1), 21-31.

Cho, G. H., Ahmad, M. J., Lee, S., Choi, K. S., Nam, W. H., & Kwon, H. J. (2019). Influence mechanism of climate change on paddy farming practices and irrigation water demand. *Paddy and water environment*, *17*(3), 359-371.

Darabi, H., Moradi, E., Davudirad, A. A., Ehteram, M., Cerda, A., & Haghighi, A. T. (2021). Efficient rainwater harvesting planning using socio-environmental variables and data-driven geospatial techniques. *Journal of Cleaner Production*, *311*, 127706.

Damkjaer, S., & Taylor, R. (2017). The measurement of water scarcity: Defining a meaningful indicator. *Ambio*, *46*(5), 513-531.

Daniels, A. E., Morrison, J. F., Joyce, L. A., Crookston, N. L., Chen, S. C., & McNulty, S. G. (2012). *Climate projections FAQ*. United States Department of Agriculture, Forest Service, Rocky Mountain Research Station.

Deswal, S., & Pal, M. (2008). Artificial neural network based modeling of evaporation losses in reservoirs. *International Journal of Civil and Environmental Engineering*, *2*(3), 18-22.

Dixon, A., Butler, D., & Fewkes, A. (1999). Water saving potential of domestic water reuse systems using greywater and rainwater in combination. *Water science and technology*, *39*(5), 25-32.

Diaz et al. (2007) forecasted future irrigation water requirements in the Guadalquivir River basin, Spain by applying projected temperature and precipitation data to the CROPWAT model.

Dobrowsky, P., De Kwaadsteniet, M., Cloete, T., & Khan, W. (2014). Distribution of indigenous bacterial pathogens and potential pathogens associated with roof-harvested rainwater. *Applied and environmental microbiology, 80*(7), 2307-2316.

Domènech, L., & Saurí, D. (2011). A comparative appraisal of the use of rainwater harvesting in single and multi-family buildings of the Metropolitan Area of Barcelona (Spain): social experience, drinking water savings and economic costs. *Journal of Cleaner production*, *19*(6-7), 598-608.

Donkor, E. A., Mazzuchi, T. H., Soyer, R. & Roberson, J. A. 2014. Urban water demand forecasting: review of methods and models. *Journal of Water Resources Planing and Management,* 140**,** 146-159.

Doria, R. O., & Madramootoo, C. A. (2012). Retracted: estimation of irrigation requirements for some crops in southern Quebec using CROPWAT. *Irrigation and Drainage*, *61*(4), i-xi.

Elewa,H.H.,Qaddah,A.A.,&El-Feel,A.A.(2012). Determining potential sites for runoff water harvesting using remote sensing and geographic information systems-based modeling in Sinai. *Am. J. Environ. Sci*, *8*, 42-55.

FAO, 2003. Land and water digital media series, 26. Training Course on RWH (CDROM). Planning of water harvesting schemes, Unit 22. Food and Agriculture Organization of the United Nations, Rome, FAO.

Fatima, K. (2023). *Rainwater Harvesting Strategy for Water Sustainability Applications*.Libertatem Media Private Limited.

Fenta Mekonnen, D., & Disse, M. (2018). Analyzing the future climate change of Upper Blue Nile River basin using statistical downscaling techniques. *Hydrology and Earth System Sciences*, *22*(4), 2391-2408.

Fernandes, L. F. S., Terêncio, D. P., & Pacheco, F. A. (2015). Rainwater harvesting systems for low demanding applications. *Science of the Total Environment*, *529*, 91-100.

Fewkes, A. (2012). A review of rainwater harvesting in the UK. *Structural Survey*, *30*(2), 174-194.

Firat, M., Turan, M. E. & Yurdusev, M. A. 2010. Comparative analysis of neural network techniques for predicting water consumption time series. *Journal of Hydrology,* 384**,** 46-51.

Fritsch, O. (2017). Integrated and adaptive water resources management: exploring public participation in the UK. *Regional Environmental Change*, *17*, 1933-1944.

Forzieri, G., Gardenti, M., Caparrini, F., & Castelli, F. (2008). A methodology for the pre-selection ofsuitable sites for surface and underground small dams in arid areas: A case study in the region of Kidal, Mali. *Physics and Chemistry of the Earth, Parts A/B/C*, *33*(1-2), 74-85.

Garg, K. K., Akuraju, V., Anantha, K. H., Singh, R., Whitbread, A. M., & Dixit, S. (2022).Identifying potential zones for rainwater harvesting interventions for sustainable intensification in the semi-arid tropics. *Scientific Reports*, *12*(1), 3882.

Ghorbani, M. A., Deo, R. C., Kashani, M. H., Shahabi, M., & Ghorbani, S. (2019). Artificial intelligence-based fast and efficient hybrid approach for spatial modelling of soil electrical conductivity. *Soil and Tillage Research*, *186*, 152-164.

Ghorbani, M. A., Deo, R. C., Yaseen, Z. M., H. Kashani, M., & Mohammadi, B. (2018).Pan evaporation prediction using a hybrid multilayer perceptron-firefly algorithm (MLP-FFA) model: case study in North Iran. Theoretical and applied climatology, 133, 1119-1131.

Gleick, P. H. (2014). *The world's water volume 8: The biennial report on freshwater resources* (Vol. 8): Island Press.

Gorguner, M., & Kavvas, M. L. (2020). Modeling impacts of future climate change on reservoir storages and irrigation water demands in a Mediterranean basin. *Science of the Total Environment*, *748*, 141246.

Hagan, M. T., Demuth, H. B., Beale, M. H. & Jesús, O. D. 2014. Neural Network Design. 1012.2nd Edtion.

Hameed, H. (2013). Water harvesting in Erbil Governorate, Kurdistan region, Iraq: detection of sites using geographic information system and remote sensing. *StudentthesisseriesINES*.http://www.agromet.gov.iq/station_list.php10.1007/BF03030865.

Hamza, Z. A. H. (2024). Predicted evaporation in Basrah using artificial neural networks. Open Engineering, 14(1), 20220590.

Hanson, L. S., & Vogel, R. M. (2014). Generalized storage–reliability–yield relationships for rainwater harvesting systems. *Environmental Research Letters*, *9*(7), 075007.

Hassan, S. T., Lubczynski, M. W., Niswonger, R. G., & Su, Z. (2014). Surface–groundwater interactions in hard rocks in Sardon Catchment of western Spain: An integrated modeling approach. *Journal of hydrology*, *517*, 390-410.

Hassan, W. H. (2020). Climate change impact on groundwater recharge of Umm er Radhuma unconfined aquifer Western Desert, Iraq. *International Journal of Hydrology Science and Technology*, *10*(4), 392-412.

Hasan, K., Tanaka, T. S., Alam, M., Ali, R., & Saha, C. K. (2020). Impact of modern rice harvesting practices over traditional ones. *Reviews in Agricultural Science*, *8*, 89-108.

Hassan, W. H., & Nile, B. K. (2021). Climate change and predicting future temperature in Iraq using CanESM2 and HadCM3 modeling. *Modeling Earth Systems and Environment*, *7*, 737-748.

Hoegh Guldberg, O., Jacob, D., Taylor, M., Bindi, M., Brown, S., Camilloni, I. A., . . . Engelbrecht, F. (2018). Impacts of 1.5 C global warming on natural and human systems.

Huang, Z., Yang, W. J., Liu, Y., Shen, W., López-Vicente, M., & Wu, G. L. (2020). Belowground soil water response in the afforestation-cropland interface under semi-arid conditions. *Catena*, *193*, 104660.

Ibrahim, G.R.F., Rasul, A., Ali Hamid, A., Ali, Z.F. and Dewana, A.A., 2019. Suitable site selection for rainwater harvesting and storage case study using Dohuk Governorate. *Water*, *11*(4), p.864.

IMSD, 1995. Integrated Mission for Sustainable Development: Technical Guidelines, NRSA, Hyderabad, India, 127 pp.

IPCC, 2013. In: Stocker, T.F., Qin, D., Plattner, G.-K., Tignor, M., Allen, S.K., Boschung, J., Nauels, A., Xia, Y., Bex, V., Midgley, P.M. (Eds.), Climate Change 2013: the Physical Science Basis: Contribution of Working Group I to the Fifth Assessment Report of the Intergovermental Panel on Climate Change. Cambridge University Press, Cambridge, UK; New York, NY, USA, 2013; p. Isioye, O.A., Shebe, M.W., Momoh, U.O., Bako, C.N. 2012. A Multi criteria decision support system (MDSS) for identifying rainwater harvesting site(s) in Jabr, W.M., El-Awar, F.A. 2005. GIS and analytic hierarchy process for siting water harvesting reservoirs, Beirut, Lebanon. Journal of Environmental Engineering, 122 (6), 515-523.

Jain, A., Varshney, A. K. & Joshi, U. C. 2001. Short-term water demand forecast modelling at IIT Kanpur using artificial neural networks. *Water Resources Management,* 15**,** 299–321.

Jung, C., Lee, J., Lee, Y., & Kim, S. (2019). Quantification of stream drying phenomena using grid-based hydrological modeling via long-term data mining throughout South Korea including ungauged areas. *Water*, *11*(3), 477.

Kahinda, J. M., Taigbenu, A. E., Sejamoholo, B. B. P., Lillie, E. S. B., & Boroto, R. J. (2009). A GIS-based decision support system for rainwater harvesting (RHADESS). *Physics and Chemistry of the Earth, Parts A/B/C*, *34*(13-16), 767-775.

Kamel, A., & Mohammed, A. (2010). Determination of water harvesting regions in Iraqi western desert using GIS system. Iraqi Journal of Desert Studies Vol, 2(2). Khudhair, M. A., Sayl, K. N., & Darama, Y. (2020, July). Locating site selection for rainwater harvesting.

Khan, D., Raziq, A., Young, H. W. V., Sardar, T., & Liou, Y. A. (2022). Identifying Potential Sites for Rainwater Harvesting Structures in Ghazi Tehsil, Khyber Pakhtunkhwa, Pakistan, Using Geospatial Approach. *Remote Sensing*, *14*(19), 5008.

Khan, D., Raziq, A., Young, H. W. V., Sardar, T., & Liou, Y. A. (2022). Identifying Potential Sites for Rainwater Harvesting Structures in Ghazi Tehsil, Khyber Pakhtunkhwa, Pakistan, Using Geospatial Approach. *Remote Sensing*, *14*(19), 5008.

Khalaf et al. (2022), employed LARS-WG, and CIMP5 with five GCMs to project precipitation and maximum temperature in the southern region of Iraq for the period (2021- 2100) and the models showed high performance in predicting climatic parameters.

Khudhair, M. A., Sayl, K. N., & Darama, Y. (2020, July). Locating site selection for rainwater harvesting structure using remote sensing and GIS. In *IOP Conference series: Materials science and engineering* (Vol. 881, No. 1, p. 012170). IOP Publishing.

Kim, R. H., Lee, S., Lee, J. H., & Kim, Y. M. (2007). Design of rainwater management system for eco-housing complex. In *Rainwater and Urban Design 2007* (pp. 634-639). [Barton, ACT]: Engineers Australia.

Kim, J., Lee, J., Song, Y., Han, H., & Joo, J. (2018). Modeling the runoff reduction effect of low impact development installations in an industrial area, South Korea. *Water*, *10*(8), 967.

Kingston, G. B., Maier, H. R. & Lambert, M. F. 2005. Calibration and validation of neural networks to ensure physically plausible hydrological modeling. *Journal of Hydrology,* 314**,** 158-176.

Knox, J. W., Rodriguez-Diaz, J. A., Weatherhead, E. K., & Kay, M. G. (2010). Development of a water-use strategy for horticulture in England and Wales–a case study. *The Journal of Horticultural Science and Biotechnology*, *85*(2), 89-93.

Kopittke, P. M., Menzies, N. W., Wang, P., McKenna, B. A., & Lombi, E. (2019). Soil and the intensification of agriculture for global food security. *Environment international*, *132*, 105078.

Konzmann, M., Gerten, D., & Heinke, J. (2013). Climate impacts on global irrigation requirements under 19 GCMs, simulated with a vegetation and hydrology model. *Hydrological Sciences Journal*, *58*(1), 88-105.

Krois and Schulte, 2014Prinz, D., 1998. Rainwater harvesting for dry land agriculture-Developing a methodology based on remote sensing and GIS. In *Proceeding XIII.International Congress Agricultural engineering, 02.-06. 02. 1998. Rabat, Morocco*.

Kumar, M.G., Agarwal, A.K., Bali, R. 2008. Delineation of potential sites for water harvesting structures using remote sensing and GIS. Journal of the Indian Society of Remote Sensing, 36(4), 323-334.

Kumar, P. A. N. K. A. J., Kumar, D., & Panwar, R. (2016). Evaporation estimation from climatic factors. *Mausam*, *67*(4), 897-902.

La Fuente, S., Jennings, E., Gal, G., Kirillin, G., Shatwell, T., Ladwig, R., ... & Woolway, R. I. (2022). Multi-model projections of future evaporation in a sub-tropical lake. Journalof Hydrology, 615, 128729.

Lee, H., Calvin, K., Dasgupta, D., Krinmer, G., Mukherji, A., Thorne, P., ... & Zommers, Z. (2023). Synthesis report of the IPCC Sixth Assessment Report (AR6), Longer report. IPCC.

Lupia, F., Baiocchi, V., Lelo, K., & Pulighe, G. (2017). Exploring rooftop rainwater harvesting potential for food production in urban areas. *Agriculture*, *7*(6), 46.

Mahmoud, S. H., & Tang, X. (2015**).** Monitoring prospective sites for rainwater harvesting and stormwater management in the United Kingdom using a GIS-based decision support system. Environmental Earth Sciences, 1-18.

Mahmoud, S.H., Alazba, A.A. 2014. The potential of in situ rainwater harvesting in arid regions: developing a methodology to identify suitable areas using GIS-based decision support system. Arabian Journal of Geosciences, 8(7), 5167-5179.

Mahmoud, S. H., & Tang, X. (2015**).** Monitoring prospective sites for rainwater harvesting and stormwater management in the United Kingdom using a GIS-based decision support system. Environmental Earth Sciences, 1-18.

Masanganise, J., Mapuwei, T. W., Magodora, M., & Basira, K. (2014). Multi-model projections of temperature and rainfall under representative concentration pathways in Zimbabwe.

Mati,B.,DeBock,T.,Malesu,M.,Khaka,E.,Oduor,A.,Nyabenge,M.,&Oduor,V. (2006). Mapping thepotential of rainwater harvesting technologies in Africa. AGIS over view on development domains for the continent and ten selected countries. Technical Manual. 6 126.

Mekdaschi-Studer, R. and Liniger, H., 2013. Water Harvesting. *Guidelines to Good Practices*.

Mekdaschi, S., Liniger, H. 2013. Water Harvesting: Guidelines to Good Practice. Centre for Development and Environment (CDE), Bern; Rainwater Harvesting Implementation Network (RAIN), Amsterdam; MetaMeta, Wageningen; The International Fund for Agricultural Development (IFAD), Rome, 210 pp.

Melville-Shreeve, P., Ward, S., & Butler, D. (2016). Rainwater harvesting typologies for UK houses: A multi criteria analysis of system configurations. *Water*, *8*(4), 129.

Melenti, I. L., Keri, A. A., & Rusu, T. (2011). Soil Conservation Service Curve Number Method for Surface Runoff Estimation Using GIS Techniques, in Rosia Poieni Mining Area (Romania). *ProEnvironment Promediu*, *4*(8).

Misra, A. K. (2013). Climate change impact, mitigation and adaptation strategies for agricultural and water resources, in Ganga Plain (India). *Mitigation and Adaptation Strategies for Global Change*, *18*, 673-689.

Moges, G. 2009. Identification of potential rainwater harvesting areas in the central Rift Valley of Ethiopia using a GIS based approach (Doctoral dissertation) Wageningen University, the Netherlands, 83 pp.

Mohammed, A. S., Almawla, A. S., & Thameel, S. S. (2022). Prediction of Monthly Evaporation Model Using Artificial Intelligent Techniques in the Western Desert of Iraq-Al-Ghadaf Valley. *Mathematical Modelling of Engineering Problems*, *9*(5).

Nabit, B. I., Al-Anbari, R. H., & Alwan, I. A. (2023, April). Identifying Suitability Rainwater Harvesting Zones in Diyala Watershed, Iraq, Using Multi-Criteria Analysis and GIS Modelling. In *IOP Conference Series: Earth and Environmental Science* (Vol. 1158, No. 2, p. 022036). IOP Publishing.

Orsini, F., Kahane, R., Nono-Womdim, R. and Gianquinto, G., 2013. Urban Agriculture in the developing world: a review. *Agronomy for sustainable development*, *33*(4), pp.695-720.

Osman, Y., Al-Ansari, N., Abdellatif, M., Aljawad, S. B., & Knutsson, S. (2014). Expected future precipitation in central Iraq using LARS-WG stochastic weather generator. *Engineering*, *6*(13), 948-959.

Ouessar, M., 2007. *Hydrological impacts of rainwater harvesting in wadi Oum Zessar watershed (Southern Tunisia)*. Ghent University.

Oweis, T. and Hachum, A., 2006. Water harvesting and supplemental irrigation for improved water productivity of dry farming systems in West Asia and North Africa. *Agricultural water management*, *80*(1-3), pp.57-73.

Oweis, T.Y. 2004. Rainwater harvesting for alleviating water scarcity in the Drier environments of West Asia and North Africa, in: International Workshop on Water Harvesting and Sustainable Agriculture Moscow, Russia. 182 pp.

Oweis, T. Y., Prinz, D., & Hachum, A. Y. (2012). *Rainwater harvesting for agriculture in the dry areas*. CRC press.

Oweis, T., Oberle, A., & Prinz, D. (1998). Determination of potential sites and methods for water harvesting in central Syria. *Advances in GeoEcology*, *31*, 83-88.

Oweis, T., Hachum, A., & Kijne, J. (1999). *Water harvesting and supplemental irrigation for improved water use efficiency in dry areas* (Vol. 7). IWMI.

Oweis, T.Y. 2004. Rainwater harvesting for alleviating water scarcity in the Drier environments of West Asia and North Africa, in: International Workshop on Water Harvesting and Sustainable Agriculture Moscow, Russia. 182 pp.

Oxford Plan 2040:https://www.oxford.gov.uk/local-plan/oxford-local-plan-2040/Accessed on June 2023

Pachauri, R. K., Allen, M. R., Barros, V. R., Broome, J., Cramer, W., Christ, R., ... & van Ypserle, J. P. (2014). *Climate change 2014: synthesis report. Contribution of Working Groups I, II and III to the fifth assessment report of the Intergovernmental Panel on Climate Change* (p. 151). Ipcc.

Panme, F. A., & Sethi, L. N. (2023). Estimation of Crop Water Requirements and Irrigation Scheduling for Major Crops Grown in India's North-Eastern Region. CURRENT APPLIED SCIENCE AND TECHNOLOGY, 10.55003/cast. 52022.55004. 55023.55011 (55011 pages)-55010.55003/cast. 52022.55004. 55023.55011 (55011 pages).

Räisänen, J. (2016). Twenty-first century changes in snowfall climate in Northern Europe in ENSEMBLES regional climate models. *Climate dynamics*, *46*, 339-353.

Riedel, T., & Weber, T. K. (2020). The influence of global change on Europe's water cycle and groundwater recharge. *Hydrogeology Journal*, *28*(6), 1939-1959.

Roy, U., & Majumder, M. (2015). *Vulnerability of watersheds to climate change assessed by neural network and analytical hierarchy process*. Springer.

Sadia, M. (2023). Application of machine learning in analyzing severities of double vehicle crashes in Bangladesh.

Saeed, F. H., Saleh, M., & Al-Faraj, F. A. (2022). Forecasting of future irrigation water demand for salah-addin governorate under various scenarios of climate change. *Journal of Water Resources and Geosciences*, *1*(1), 102-116.

Saaty, T. L. (1999). Comment by Thomas L. Saaty. *Journal of Multicriteria Decisi Analysis*, *8*(1), 23.

Saaty, T.L. 2008. Decision making with the analytic hierarchy process. International journal of services sciences, 1(1), 83-98.

Salman, S. A., Shahid, S., Afan, H. A., Shiru, M. S., Al-Ansari, N., & Yaseen, Z. M. (2020). Changes in climatic water availability and crop water demand for Iraq region. *Sustainability*, *12*(8), 3437.

Salih, S.A., Al-Tarif, A.S.M. 2012. Using of GIS spatial analyses to study the selected location for dam reservoir on wadi Al-Jirnaf, west of Shirqat area, Iraq. Journal of Geographic Information System, 4, 117 pp.

Sayadi, A., Monjezi, M., Talebi, N. & Khandelwal, M. 2013. A comparative study on the application of various artificial neural networks to simultaneous prediction of rock fragmentation and backbreak. *Journal of Rock Mechanics and Geotechnical Engineering,* 5**,** 318-324.

Semenov, M. A., Pilkington-Bennett, S., & Calanca, P. (2013). Validation of ELPIS 1980- 2010 baseline scenarios using the observed European Climate Assessment data set. *Climate Research*, *57*(1), 1-9.

Silva, C. M., Sousa, V., & Carvalho, N. V. (2015). Evaluation of rainwater harvesting in Portugal: Application to single-family residences. *Resources, Conservation and Recycling*, *94*, 21-34.

Shadeed, S., Judeh, T., & Riksen, M. (2020). Rainwater harvesting for sustainable agriculture in high water-poor areas in the West Bank, Palestine. *Water*, *12*(2), 380.

Shahin, M. A., Jaksa, M. B. & Maier, H. R. 2008. State of the Art of Artificial Neural Networks in Geotechnical Engineering. *Electronic Journal of Geotechnical Engineering,* 13**,** 1-26.

Shahid, S. (2012). Vulnerability of the power sector of Bangladesh to climate change and extreme weather events. *Regional Environmental Change*, *12*, 595-606.

Shahid, S. (2012). Vulnerability of the power sector of Bangladesh to climate change and extreme weather events. *Regional Environmental Change*, *12*, 595-606.

Shirgure, P. S., and G. S. Rajput. "Evaporation modeling with neural networks–A Research review." *Int J Res Rev Soft Intell Comput* 1, no. 2 (2011): 37-47.

Trzaska, S., & Schnarr, E. (2014). A review of downscaling methods for climate change projections. *United States Agency for International Development by Tetra Tech ARD*, *2014*, 1-42.

UNESCO.(2008). *Water for People, Water for Life: A Joint Report by the Twenty-three UN Agencies Concerned with Freshwater*: UNESCO.

USGS: https://www.earthexplorer.usgs.gov.

Vaes, G., & Berlamont, J. (2001). The effect of rainwater storage tanks on design storms. *Urban water*, *3*(4), 303-307.

Wang, X., & Wang, C. (2019). Time series data cleaning: A survey. *Ieee Access*, *8*, 1866- 1881.

Ward, S., & Butler, D. (2016). Rainwater harvesting and social networks: Visualising interactions for niche governance, resilience and sustainability. *Water*, *8*(11),526.

Weerasinghe, H., Schneider, U.A., Löw, A. 2011. Water harvest-and storage-location assessment model using GIS and remote sensing. Hydrology and Earth System Sciences Discussions, 8(2), 3353-3381.

Wang, Y., Niu, D. & Ma, X. 2010. Optimizing of SVM with hybrid PSO and genetic algorithm in power load forecasting. *Journal of Networks,* 5**,** 1192-1200.

Yalew, S. G., Pilz, T., Schweitzer, C., Liersch, S., van der Kwast, J., Van Griensven, A., ... & van der Zaag, P. (2018). Coupling land-use change and hydrologic models for quantification of catchment ecosystem services. *Environmental Modelling & Software*, *109*, 315-328.

Zaria, Kaduna state, Nigeria. International Journal of Advanced Scientific Engineering and Technological Research, 1(1), 53-71.

Zakaria, S., Al-Ansari, N. A., Knutsson, S., & Ezz-Aldeen, M. (2012). Rain water harvesting and supplemental irrigation at Northern Sinjar Mountain, Iraq.Journal of Purity, Utility Reaction and Environment, 1(3), 121-141.

Zamani, R., Ali, A. M. A., & Roozbahani, A. (2020). Evaluation of Adaptation Scenarios for Climate Change Impacts on Agricultural Water Allocation Using Fuzzy MCDM Methods. Water resources management, 34(3), 1093-1110. doi:10.1007/s11269-020-02486-8.

Ziadat, F., Bruggeman, A., Oweis, T., Haddad, N., Mazahreh, S., Sartawi, W., Syuof, M. 2012. A Participatory GIS approach for assessing land suitability for rainwater harvesting in an arid rangeland environment. Arid Land Research and Management, 26(4), 297–311. DOI: 10.1080/15324982.2012.709214.

Ziadat, F., Oweis, T., Mazahreh, S., Bruggeman, A., Haddad, N., Karablieh, E., Benli, B., Zanat, M.A., Al-Bakri, J., Ali, A. 2006. Selection and characterization of badia watershed research sites. Int. Cent. Agric. Res. Dry Areas (ICARDA), Aleppo, Syria. 111 pp.

Zubaidi, S. L., Dooley, J., Alkhaddar, R. M., Abdellatif, M., Al-Bugharbee, H. & Ortega-Martorell, S. 2018. A Novel approach for predicting monthly water demand by combining singular spectrum analysis with neural networks. *Journal of Hydrology,* 561**,** 136-145.

Zhu, X., Zhao, A., Li, Y., & Liu, X. (2015). Agricultural irrigation requirements under future climate scenarios in China. *Journal of Arid Land*, *7*, 224-237.

# Appendices

## Appendix A1

The PCA Correlation for The Four climate factors for 1st Study Region of Kirkuk:

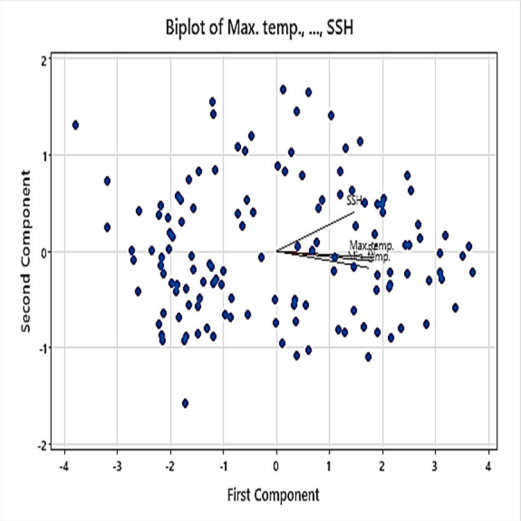


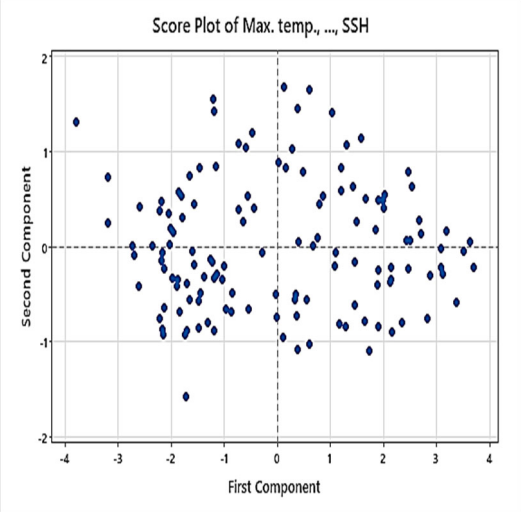


The PCA Correlation for The Four Climate Factors for 2nd Study Region of Oxfordshire:

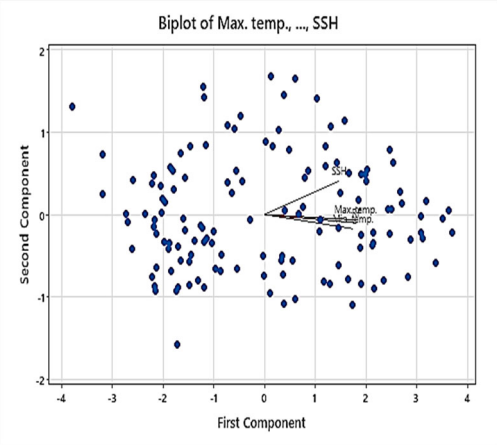


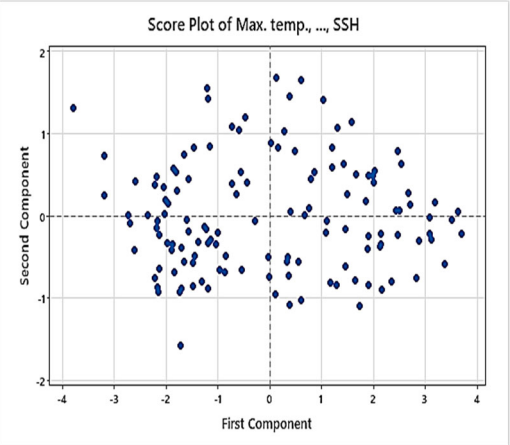

## Appendix A2

The sensitivity analysis reflecting changes in weights by -10% and +10%

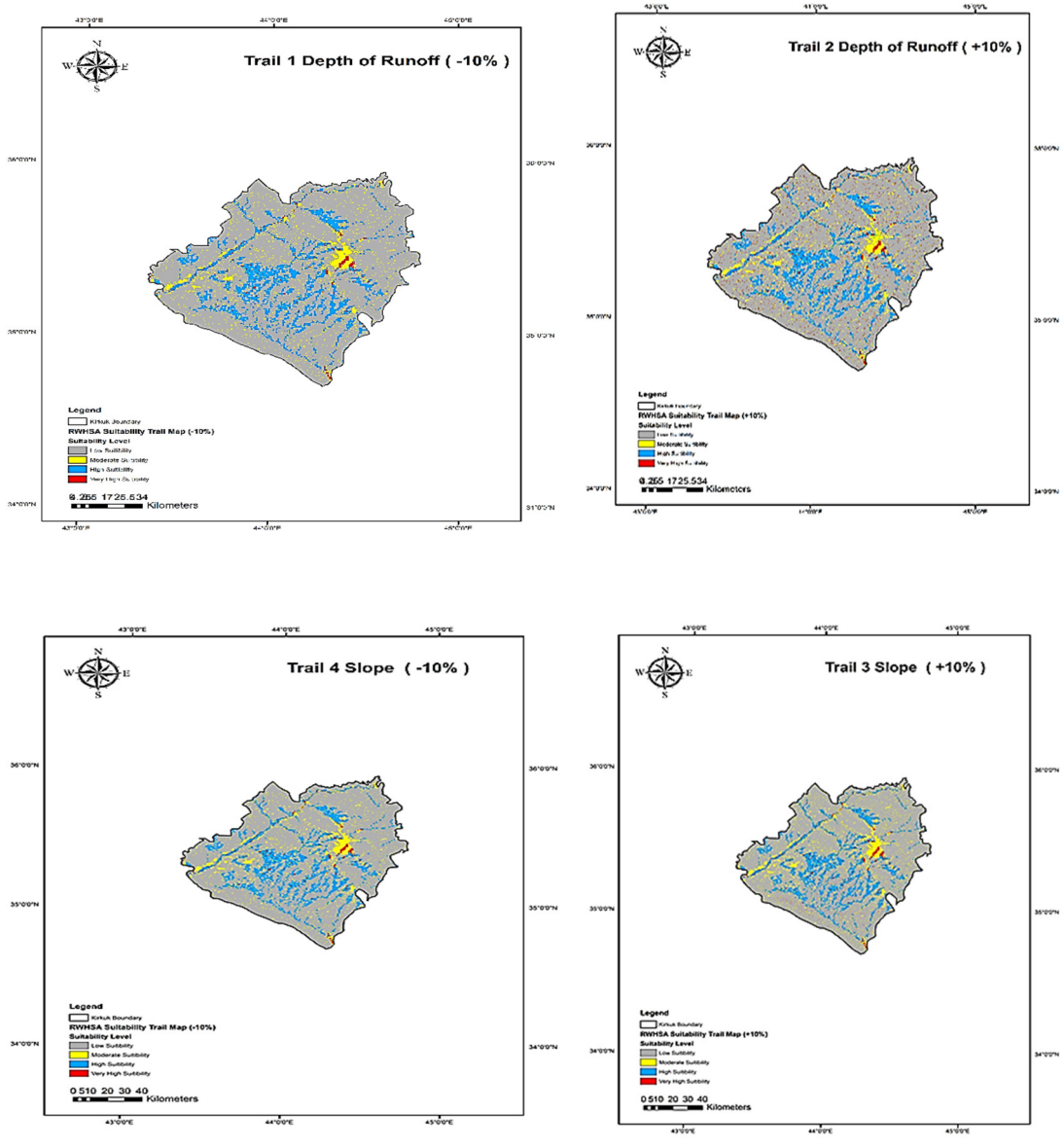

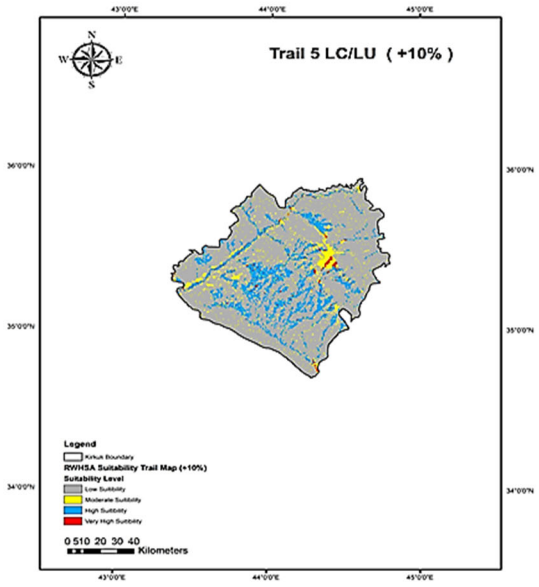
Trail 5 LC/LU ( +10% )
Legend
Kirkuk Boundary
RWHSA Suitability Trail Map (+10%)
Suitability Level
Low Suitibility
Moderate Suitibility
High Suitibility
Very High Suitibility
0 5 10 20 30 40
Kilometers

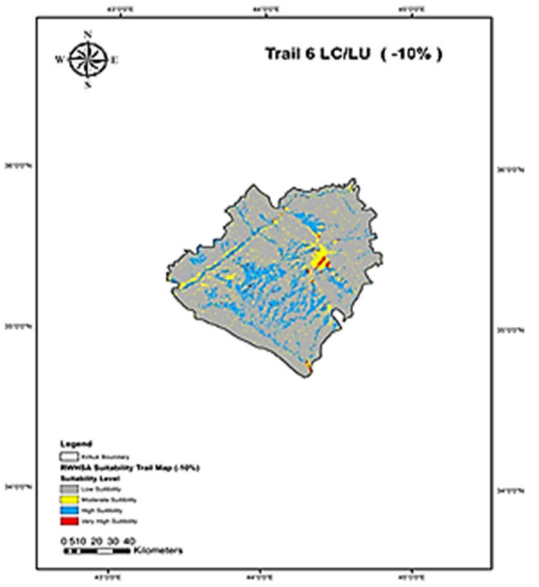
Trail 6 LC/LU ( -10% )
Legend
Kirkuk Boundary
RWHSA Suitability Trail Map (-10%)
Suitability Level
Low Suitibility
Moderate Suitibility
High Suitibility
Very High Suitibility
0 5 10 20 30 40
Kilometers

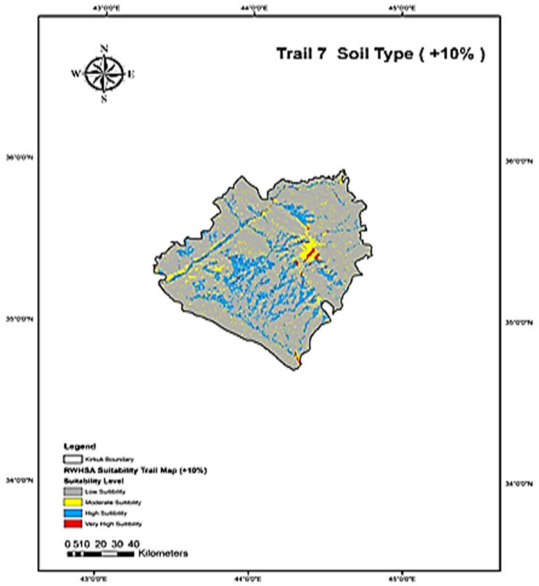
Trail 7 Soil Type ( +10% )
Legend
Kirkuk Boundary
RWHSA Suitability Trail Map (+10%)
Suitability Level
Low Suitibility
Moderate Suitibility
High Suitibility
Very High Suitibility
0 5 10 20 30 40
Kilometers

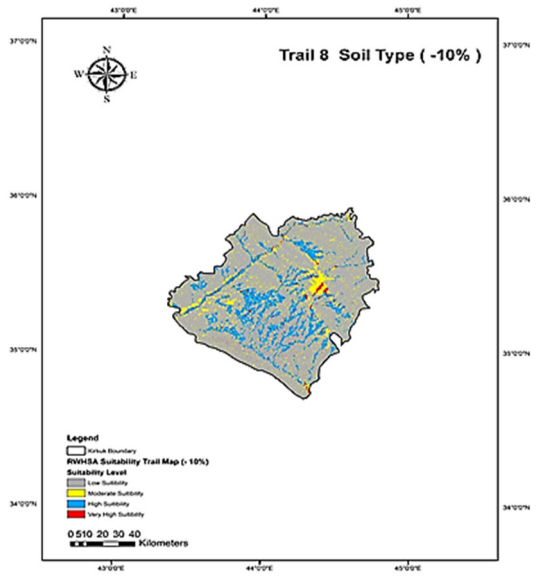
Trail 8 Soil Type ( -10% )
Legend
Kirkuk Boundary
RWHSA Suitability Trail Map (- 10%)
Suitability Level
Low Suitibility
Moderate Suitibility
High Suitibility
Very High Suitibility
0 5 10 20 30 40
Kilometers

## Appendix B

Criteria, categorization, levels of eligibility, and ratings for each factor were used to identify the appropriate location selection for RWH.

| Criterion | Class | Value | Rating |
|---|---|---|---|
| **Depth of runoff** | Very high suitability | 80-90 | 9 |
| | Medium suitability | 70-80 | 8 |
| | Suitable | 60-70 | 4 |
| | Low Suitability | 50-60 | 3 |
| | Very low suitability | <50 | 1 |
| **Slope (%)** | Flat | <1.5 | 3 |
| | Undulating | 1.5-2.5 | 9 |
| | Rolling | 2.5-4.5 | 5 |
| | Hilly | 4.5-7.5 | 2 |
| | Mountainous | >7.5 | 1 |
| **Land cover/Land use** | Trees, grass, and | Very High | 9 |
| | agriculture | High | 8 |
| | Vegetarian flood. | High | 7 |
| | bare ground or soil | Medium | 5 |
| | scrub or shrub | Low | 1 |
| | Mountain | Strictly Limited | Strictly Limited |
| | Urban area and water | Strictly Limited | Strictly Limited |
| | body | | |
| **Soil type** | Clay, very high suitability | >20 | 9 |
| | Silty clay, high suitability | 15-20 | 7 |
| | Sandy clay, medium | 11-15 | 4 |
| | suitability | | |
| | Sandy clayey loam and | 8-11 | 3 |
| | sandy loam, low | | |
| | suitability | <8 | 1 |
| | Other, very low | | |
| | suitability | | |
| **Stream order** | Very high suitability | >7 | 9 |
| | High suitability | 7 | 8 |
| | Medium suitability | 6 | 3 |
| | Low suitability | 5 | 2 |
| | Very low suitability | <4 | 1 |

## Appendix C

## Validation model for evaporation for both study regions by using ANN

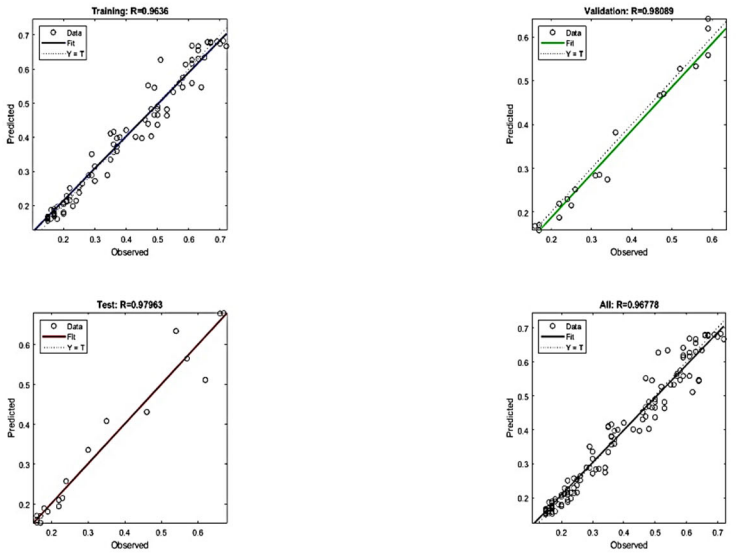


Validation model for Kirkuk region

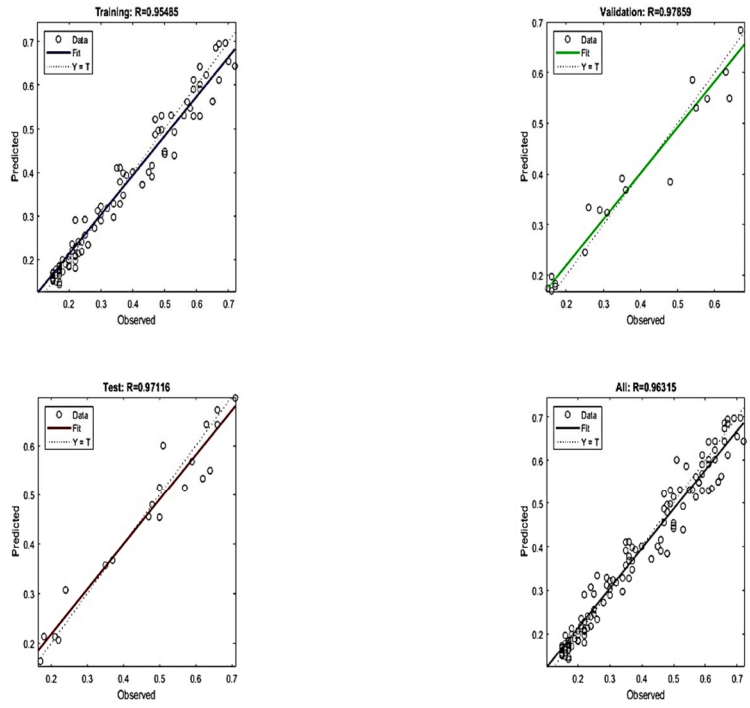


**Validation for Oxfordshire model**

## Appendix D

## Irrigation requirements for Wheat, Barley and Sunflower in Kirkuk Site

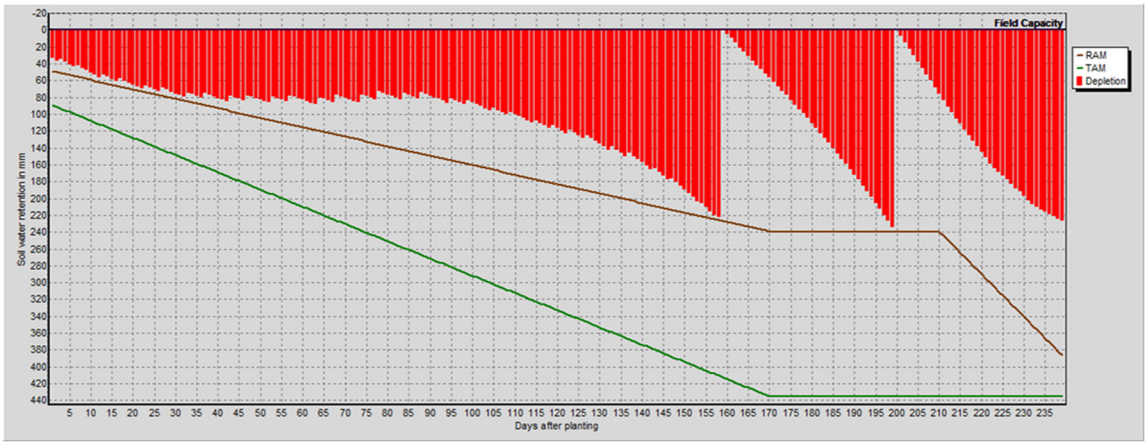


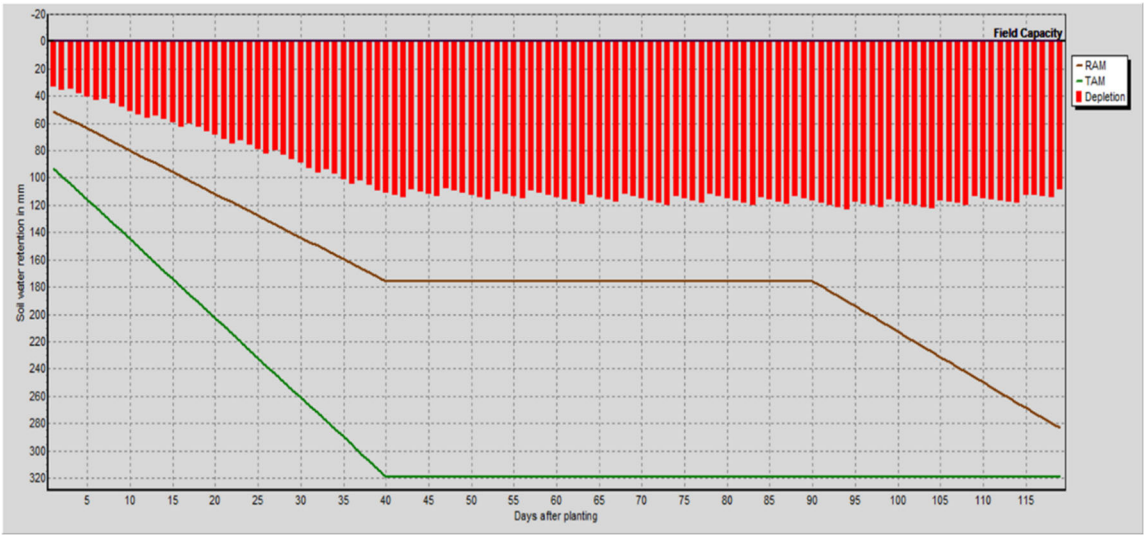


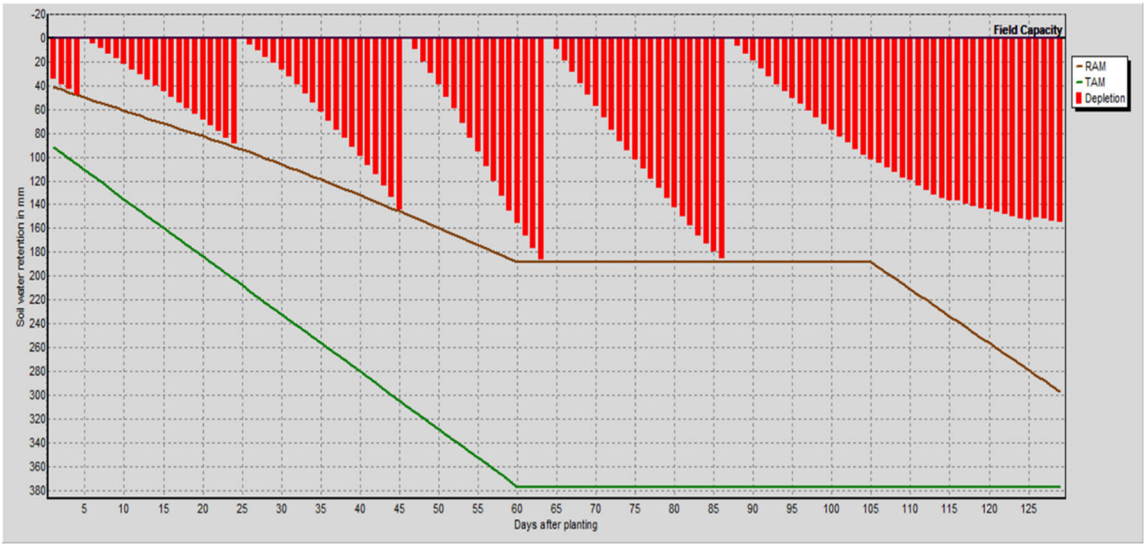

# Appendix E

## Sensitivity Analysis for Oxfordshire Study area

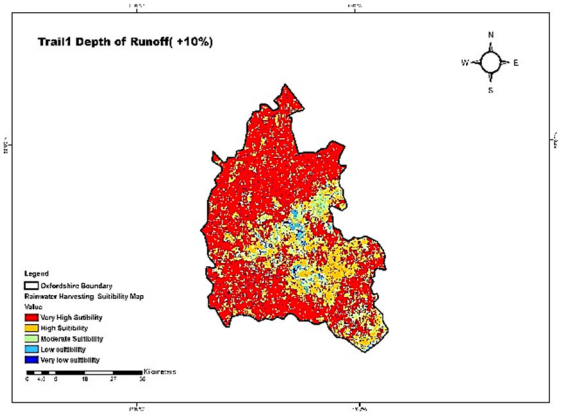


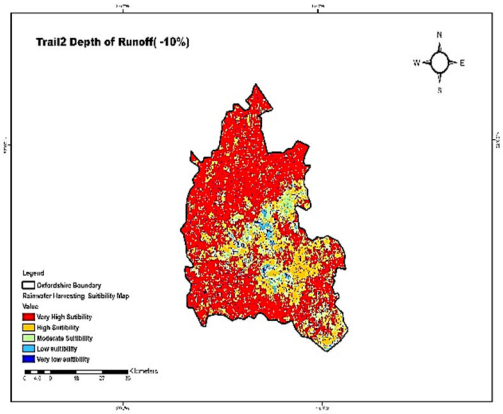


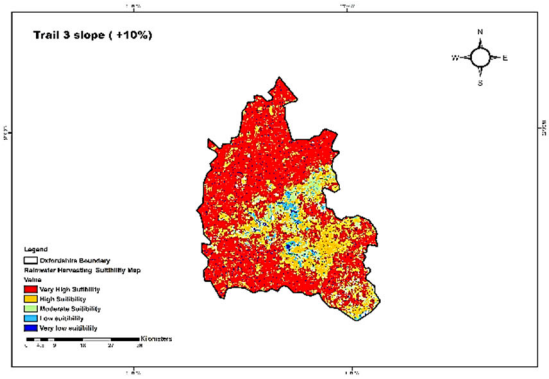


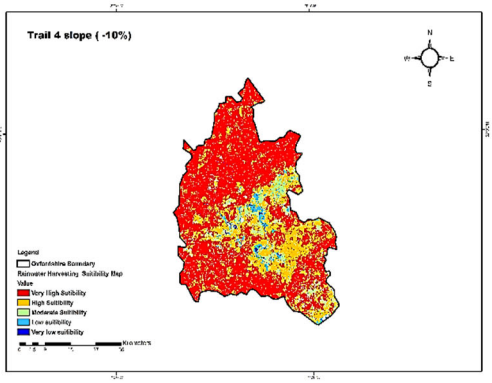

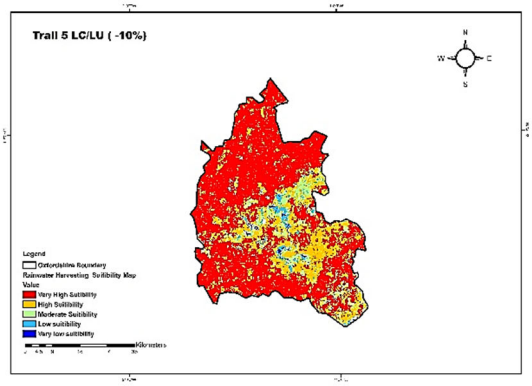
Trail 5 LC/LU ( -10%)
N
W
E
S
Legend
Oxfordshire Boundary
Rainwater Harvesting Suitibility Map
Value
Very High Suitibility
High Suitibility
Moderate Suitibility
Low suitibility
Very low suitibility
Kilometers

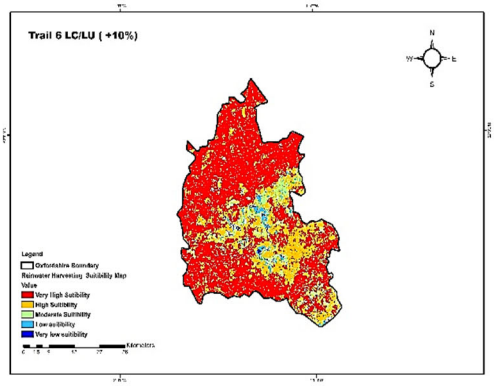
Trail 6 LC/LU ( +10%)
N
W
E
S
Legend
Oxfordshire Boundary
Rainwater Harvesting Suitibility Map
Value
Very High Suitibility
High Suitibility
Moderate Suitibility
Low suitibility
Very low suitibility
Kilometers

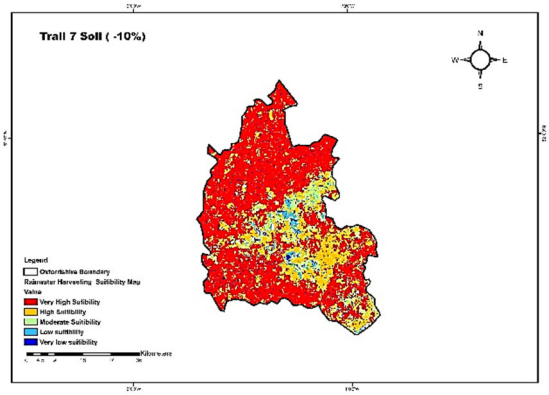
Trail 7 Soil ( -10%)
N
W
E
S
Legend
Oxfordshire Boundary
Rainwater Harvesting Suitibility Map
Value
Very High Suitibility
High Suitibility
Moderate Suitibility
Low suitibility
Very low suitibility
Kilometers

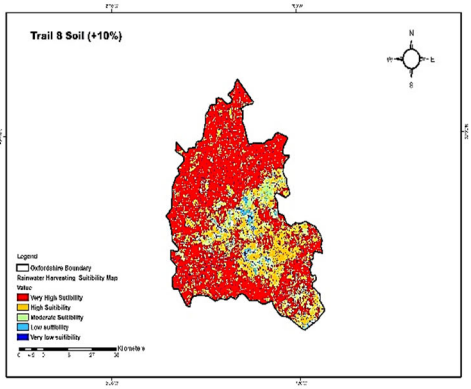
Trail 8 Soil (+10%)
N
W
E
S
Legend
Oxfordshire Boundary
Rainwater Harvesting Suitibility Map
Value
Very High Suitibility
High Suitibility
Moderate Suitibility
Low suitibility
Very low suitibility
Kilometers

## Appendix F1

## Differences in Precipitation, MinT, MaxT and SSH for GCMs for Oxfordshire

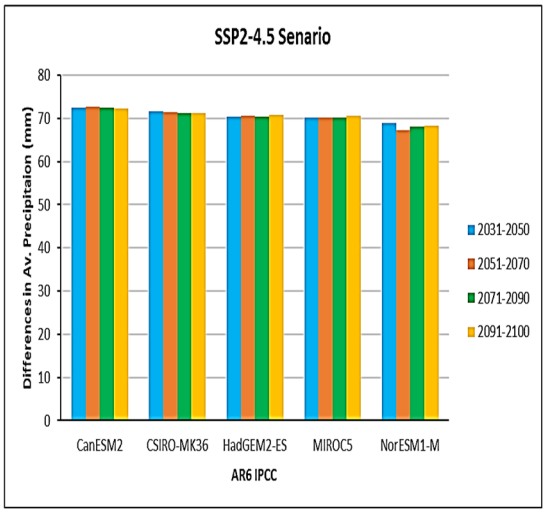


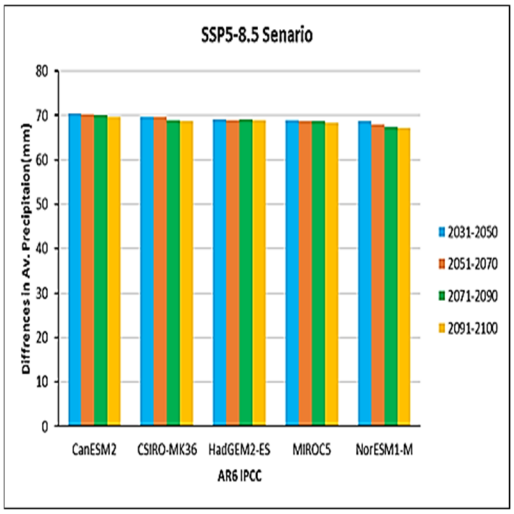


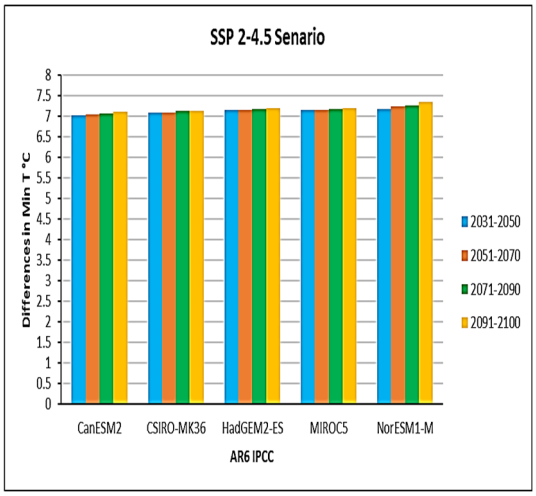


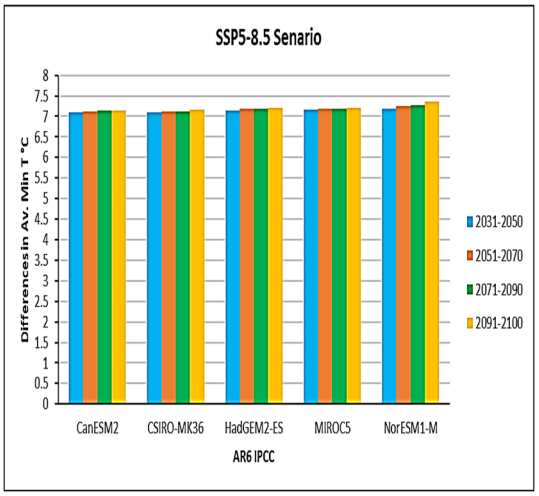

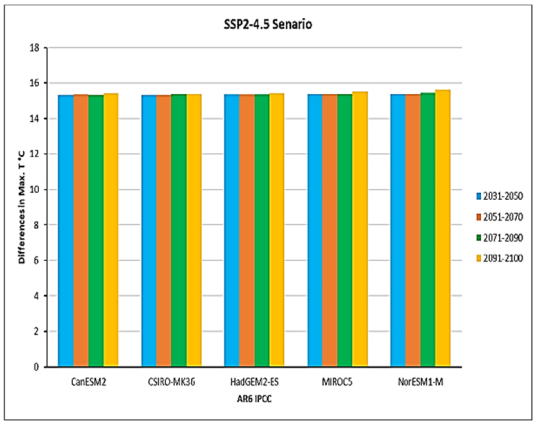
SSP2-4.5 Senario
Diffrences in Max. T °C
18
16
14
12
10
8
6
4
2
0
CanESM2
CSIRO-MK36
HadGEM2-ES
MIROC5
NorESM1-M
AR6 IPCC
2031-2050
2051-2070
2071-2090
2091-2100

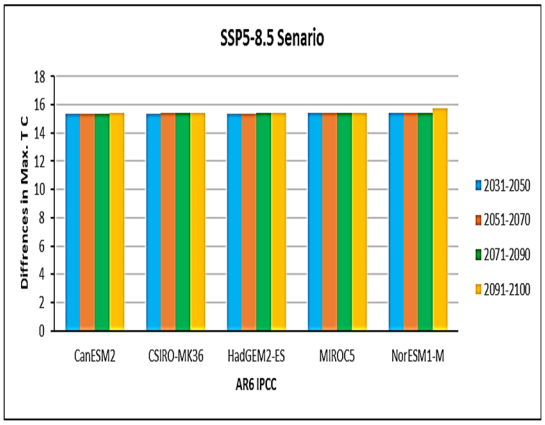
SSP5-8.5 Senario
Diffrences in Max. T C
18
16
14
12
10
8
6
4
2
0
CanESM2
CSIRO-MK36
HadGEM2-ES
MIROC5
NorESM1-M
AR6 IPCC
2031-2050
2051-2070
2071-2090
2091-2100

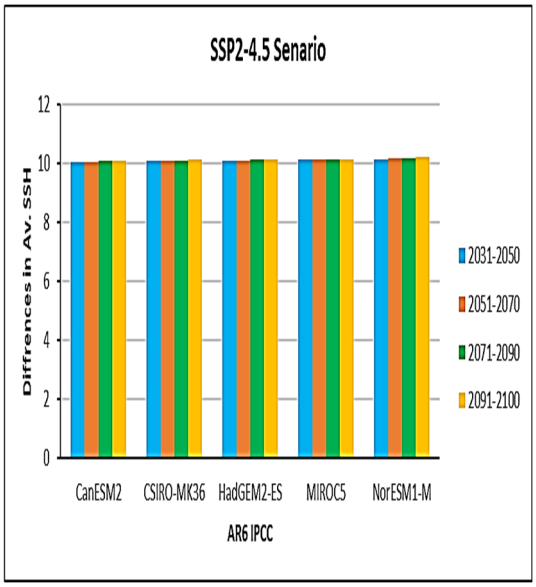
SSP2-4.5 Senario
Diffrences in Av. SSH
12
10
8
6
4
2
0
CanESM2
CSIRO-MK36
HadGEM2-ES
MIROC5
NorESM1-M
AR6 IPCC
2031-2050
2051-2070
2071-2090
2091-2100

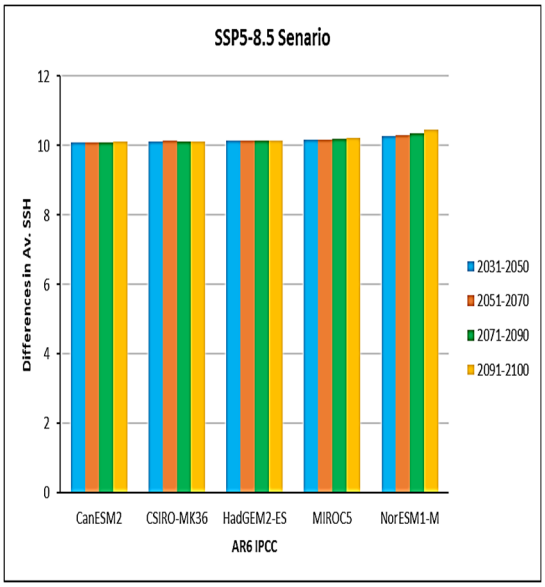
SSP5-8.5 Senario
Diffrences in Av. SSH
12
10
8
6
4
2
0
CanESM2
CSIRO-MK36
HadGEM2-ES
MIROC5
NorESM1-M
AR6 IPCC
2031-2050
2051-2070
2071-2090
2091-2100

## Appendix F2

## % Change in Climatic Factors of Oxfordshire Site

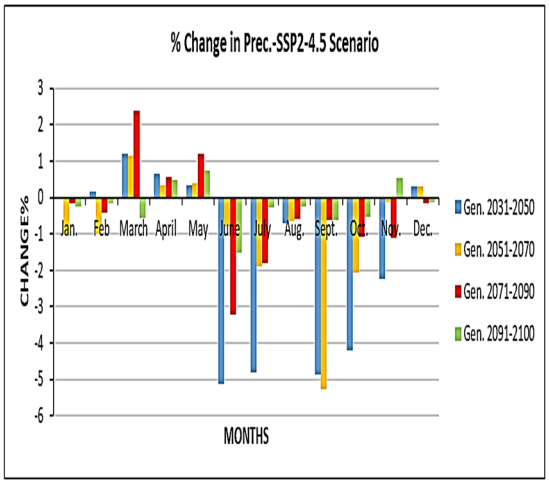


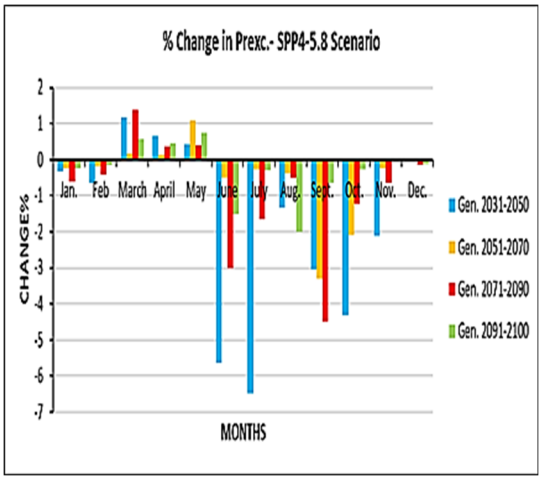


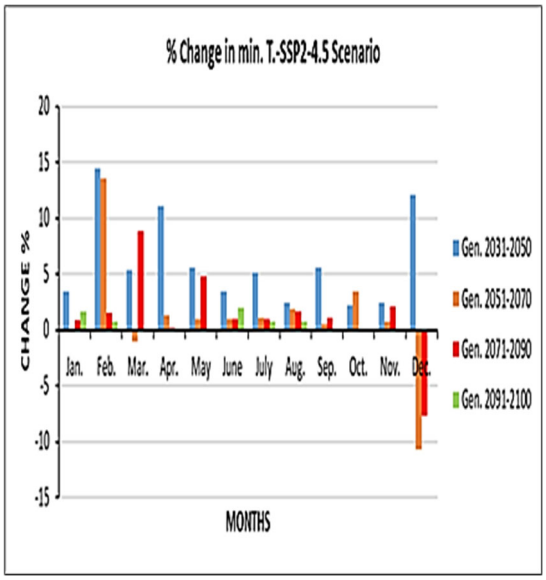


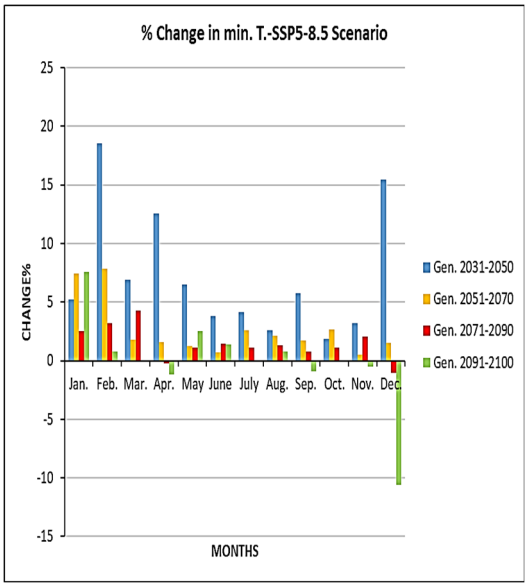

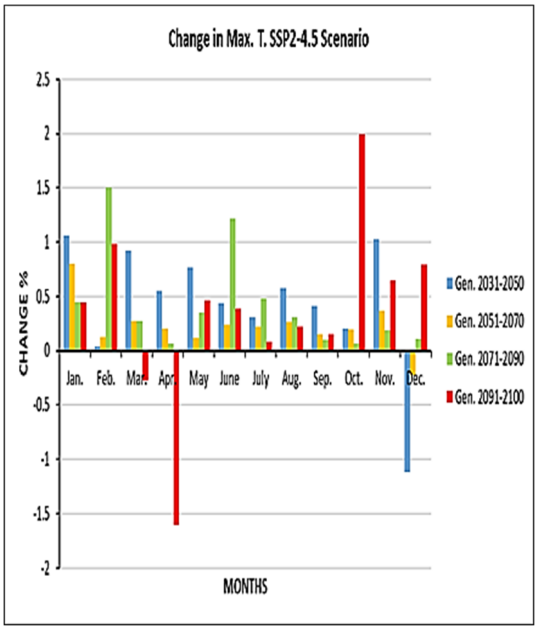
Change in Max. T. SSP2-4.5 Scenario
CHANGE %
MONTHS
Jan. Feb. Mar. Apr. May June July Aug. Sep. Oct. Nov. Dec.
Gen. 2031-2050
Gen. 2051-2070
Gen. 2071-2090
Gen. 2091-2100

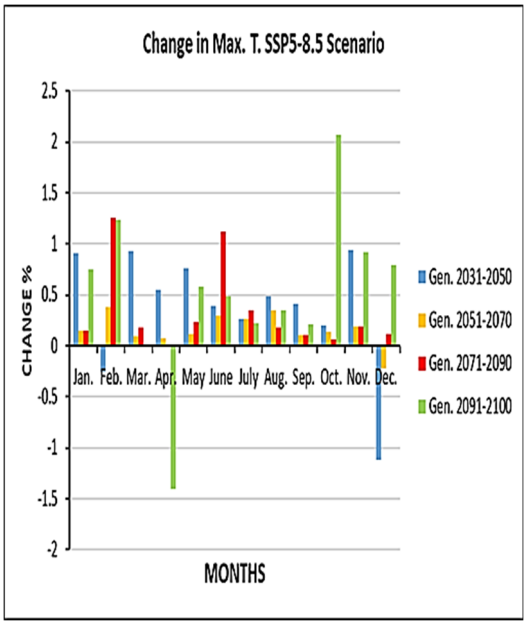
Change in Max. T. SSP5-8.5 Scenario
CHANGE %
MONTHS
Jan. Feb. Mar. Apr. May June July Aug. Sep. Oct. Nov. Dec.
Gen. 2031-2050
Gen. 2051-2070
Gen. 2071-2090
Gen. 2091-2100

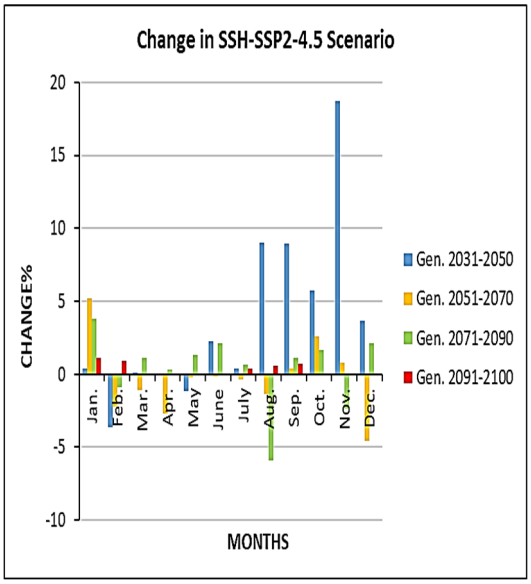
Change in SSH-SSP2-4.5 Scenario
CHANGE%
MONTHS
Jan. Feb. Mar. Apr. May June July Aug. Sep. Oct. Nov. Dec.
Gen. 2031-2050
Gen. 2051-2070
Gen. 2071-2090
Gen. 2091-2100

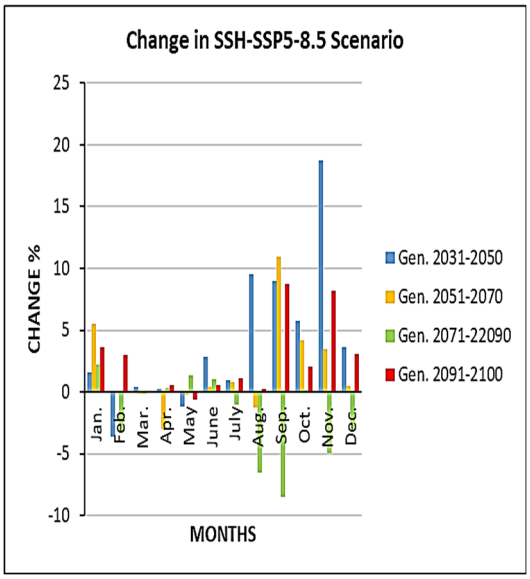
Change in SSH-SSP5-8.5 Scenario
CHANGE %
MONTHS
Jan. Feb. Mar. Apr. May June July Aug. Sep. Oct. Nov. Dec.
Gen. 2031-2050
Gen. 2051-2070
Gen. 2071-22090
Gen. 2091-2100